Origins of foliations and related phenomena in valley glaciers and ice sheets

Stephen J. A. Jennings

Department of Geography and Earth Sciences

Aberystwyth University

A thesis submitted for the degree of

Doctor of Philosophy (PhD)

September 2016

Photograph courtesy of M. J. Hambrey

For my father, Arthur Jennings.

Declaration

Word Count of thesis: 62,098

This work has not previously been accepted in substance for any degree and is not concurrently submitted in candidature for any degree.

Candidate name:

Signature:

Date:

STATEMENT 1

This thesis is the result of my own investigations, except where otherwise stated. Where correction services have been used, the extent and nature of the correction is clearly marked in a footnote(s).

Other sources are acknowledged by footnotes giving explicit references. A bibliography is appended.

Signature:

Date:

STATEMENT 2

I hereby give consent for my thesis, if accepted, to be available for photocopying and for inter-library loan, and for the title and summary to be made available to outside organisations.

Signature:

Date:

Abstract

This study examines how longitudinal foliation develops in glaciers and ice sheets in a wide range of topographic, climatic, and dynamic settings, at a variety of spatial scales. Study locations include four valley glaciers in Svalbard (Austre Brøggerbreen, Midtre Lovénbreen, Austre Lovénbreen, and Pedersenbreen), a valley glacier in Canada (Sermilik Glacier), and seven outlet glaciers in Antarctica (Hatherton Glacier, Taylor Glacier, Ferrar Glacier, Lambert Glacier, Recovery Glacier, Byrd Glacier, and Pine Island Glacier). Detailed structural mapping of the valley glaciers from satellite imagery and field-based measurements were used to document the formation of longitudinal foliation in small-scale ice masses. These findings were 'up-scaled' and applied to much larger glaciers and ice streams. Longitudinal foliation develops in concentrated bands at flow unit boundaries as a result of enhanced simple shear. However, longitudinal foliation is not directly observable from satellite imagery at the surface of larger-scale valley glaciers. The longitudinal structures visible at the surface of larger-scale glaciers form at flow unit boundaries and are composed of bands of steeply dipping longitudinal foliation; however, they appear as individual linear features on satellite imagery as a result of the comparatively low spatial resolution of the imagery. The persistence of flowlines in the Antarctic Ice Sheet through areas of crevassing and net ablation (blue-ice areas) suggests that they are the surface representation of a three-dimensional structure. Flowlines are therefore inferred to be the surface expression of flow unit boundaries composed of bands of steeply dipping longitudinal foliation. The survival and deformation of flowlines in areas of ice flow stagnation indicates that flowlines form in their initiation zones and not along their entire length. Furthermore, these ice stagnation areas indicate that flowlines record past ice dynamics and switches in ice flow.

Acknowledgements

First and foremost, I would like to thank Michael Hambrey and Neil Glasser for providing the vast majority of the support for this project. Their input and encouragement over the years has been truly invaluable. I would also like to thank Bryn Hubbard, Doug Benn, Timothy James, David Rippin, Nicholas Midgley, Toby Tonkin, Simon Cook, Tom Holt, Tristram Irvine-Fynn, Carl Stevenson, Ian Fairchild, and Ian Boomer for friendly advice and scientific help.

I also owe thanks to those who have provided logistical support for fieldwork, as well as laboratory and technical assistance, including Michael Hambrey, Doug Benn, Nick Cox, James Wake, Wynne Ebenezer, Andrew Brown, and Anthony Smith.

Lastly, I would like to thank my family and friends who have provided unwavering support and encouragement. Thanks to Mary, Arthur, and Andrew Jennings for inspiring me, to Jan Roberts and Ann Russell for always being a friendly ear, and to Ottavia Cavalli and Natalie Davies for being there through good times and bad. I thank the many individuals that I have not been able to list above but who have been a significant support.

This work has been funded by a NERC PhD studentship, whose support I gratefully acknowledge.

Contents

Chapter One

Introduction

1.1 Aim

The overall aim of this study is to examine how a common glacier structure, longitudinal foliation, develops in a wide range of topographic, climatic, and dynamic settings. Visible and measurable structures in valley glaciers are first considered, and these observations are then 'up-scaled' by applying them to larger valley glaciers and massive Antarctic ice streams where it is not possible to conduct field-based research. To address this aim, a number of specific objectives have been developed, which are detailed after the literature review (*Chapter Two*) so that they can be viewed in context with current glaciological thinking and knowledge (*see section 2.7*).

1.2 Rationale

Even though structural glaciology shares many principals with structural geology, the development of concepts in structural glaciology have lagged behind those that have been developed in geology. Nevertheless, structural studies of ice masses have a great deal of potential, with wide-ranging applications for both glaciology and geology. Although structural glaciology is an under-represented discipline in glaciology, it has the potential for solving fundamental problems of many other aspects of the subject, such as ice dynamics, glacier hydrology, the entrainment and transport of debris, the formation of glacial landforms, and microbiological investigations.

A large proportion of glaciological structural studies undertaken to date have been conducted on small-scale valley glaciers, which allow easy access for field-based structural mapping and analysis. Observations of structures in these studies have increased our knowledge of how structures form and evolve, especially with regard to cumulative strain (*e.g.* Hambrey, 1976a, b; Milnes and Hambrey, 1976; Hambrey and Milnes, 1977; Hooke and Hudleston, 1978; Hambrey et al., 1980; Hudleston and Hooke, 1980; Hudleston, 1983). More recent work has attempted to combine field-based structural observations with glacier-flow modelling to relate the mapped structures to three-dimensional cumulative strain (*see* Goodsell et al., 2005b; Hambrey et al., 2005). However, the potential for similar techniques to be applied to much larger ice masses, although great, has yet to be achieved. Structural mapping and analysis of ice structures, especially ductile structures such as folds and foliation, are useful tools for inferring the structural evolution and past ice-flow dynamics of smaller ice masses. These techniques enable past ice-flow dynamics to be inferred for periods of time up to the residence time of the ice within the glacier system. As no long-term records of ice sheet dynamics currently exist, it is hoped that similar techniques can be applied to ice sheets to deduce their past dynamics, subsequently aiding the development of more accurate ice-flow models for predicting future ice sheet behaviour under different climate scenarios. To achieve this, a good understanding of ice structures in ice sheets is required; however, only a limited number of structural studies on ice sheets have been conducted (Reynolds, 1988; Reynolds and Hambrey, 1988; Hambrey, 1991; Hambrey and Dowdeswell, 1994; Glasser and Scambos, 2008; Glasser et al., 2011, 2015; Glasser and Gudmundsson, 2012; Ely and Clark, 2015).

One main reason for the lack of structural studies on large-scale ice masses is a result of the logistical challenges associated with the scale and remote locations of the glaciers for undertaking fieldwork. Consequently, structural studies on large ice masses are heavily reliant upon remote sensing techniques with little or no ground-truthing. This study aims to address this challenge by 'up-scaling' the findings of field-based structural studies that have been conducted on small-scale valley glaciers, and attempt to apply their structural conclusions to ice masses that are several orders of magnitude greater in scale. By documenting in detail the formation and evolution of longitudinal

foliation (a ductile ice structure) in small valley glaciers, it is hoped that this information can shed light on whether longitudinal foliation occurs in much larger ice masses. Furthermore, this study aims to determine whether longitudinal structures (flowlines) observed at the surface of fast-flowing ice streams are, in fact, the surface representation of three-dimensional longitudinal foliation. By addressing these questions, it is hoped that the structural analysis of ice sheets using remote sensing techniques that are supplemented by field-based data acquired on small valley glacier, can help to infer the past flow-dynamics of large-scale ice masses.

1.3 Thesis outline

This thesis consists of ten chapters. *Chapter Two* introduces structural glaciology as a sub-discipline of glaciology by providing a broad review of the previous structural glaciological literature that has been conducted in the past century. The chapter concludes by describing the field-study locations investigated in this thesis and reviews the past research that has been conducted on those ice masses, before detailing the specific objectives of this study. *Chapter Three* describes in detail the research methods used for the structural investigation of ice masses in this research. *Chapter Four* describes the characteristics of the different ice facies observed in this study, before interpreting each ice facies and evaluating its glaciological significance. *Chapter Five* provides an in-depth structural investigation of Austre Brøggerbreen, a small cold-based valley glacier in northwest Svalbard. This chapter aims to document the structural characteristics of the glacier at a range of spatial scales, to demonstrate how structural assemblages in individual flow units evolve. *Chapter Six* structurally investigates three further glaciers in Svalbard (Midtre Lovénbreen, Austre Lovénbreen, and Pedersenbreen) at a variety of scales to demonstrate that the formation and evolution of longitudinal foliation is dependent upon the characteristics of the flow units within which they are contained. *Chapter Seven* 'up-scales' the field-based structural findings of the previous two chapters, and applies them to a much larger valley glacier (Sermilik Glacier, Bylot Island, Arctic Canada) through remote sensing techniques. This chapter aims to test the hypotheses of longitudinal foliation

formation that have been developed for small-scale valley glaciers, and determine if they are applicable for an intermediate-sized ice mass. *Chapter Eight* builds on the concepts tested in *Chapter Seven* and applies them to intermediate-scale large valley glaciers and large-scale ice streams in Antarctica, to determine if flowlines present on the surfaces of glaciers and ice streams are related to the formation and evolution of longitudinal foliation. *Chapter Nine* draws on the preceding chapters (*Chapters 4 - 8*) to discuss the formation and evolution of longitudinal foliation in ice masses of various scales from a synthesis of evidence collected for this thesis and from other previous studies. This chapter subsequently identifies areas of future work that would build from work conducted in this thesis. Finally, *Chapter Ten* provides a brief conclusion and summary of the key findings of this study.

Chapter Two

Structural glaciology: a review

2.1 Introduction

Structural glaciology is an important sub-discipline of glaciology, often playing an influential role in other glacial sub-disciplines (*see* Hambrey and Lawson, 2000). Despite often acting as an important controlling factor in other areas of glaciology (*e.g.* glacier hydrology, the entrainment and transport of debris, the formation of glacial landforms, the distribution of microbiota, and interpreting glacier-like features on Mars), structural glaciology is relatively understudied and has been overlooked by many glaciologists. This chapter aims to provide a broad-spanning review of the structural glaciological literature, and present the underpinning principles of the subject.

Structural glaciology and structural geology share several main principles, and analogies between the formation and evolution of structures in glacier ice and in rocks have been made in a number of studies (*e.g.* Wegmann, 1963; Hambrey and Milnes, 1975, 1977; Hudleston, 1977, 1992; Kamb et al., 1985; Lawson et al., 1994). However, structural glaciology and structural geology differ greatly in a number of key aspects. A deformation cycle (ice flowing from the accumulation area of a glacier to the terminus while undergoing deformation) in a typical Alpine valley glacier occurs at a rate that is six orders of magnitude faster than is experienced in compressive mountain belts (*e.g.* the Alps) (Hambrey and Milnes, 1977; Hambrey and Lawson, 2000). Consequently, glaciers provide a unique opportunity for geologists/glaciologists to measure

deformation that is analogous to that occurring in orogenic belts, but on human time-scales (Hambrey and Lawson, 2000). Even though glaciers enable real-time measurements of deformation to be monitored, the preservation potential of structures in glacier ice is much less than is observed in rocks. Polyphase deformation (multiple phases of deformation) in rocks is clearly preserved in the resulting structures, allowing the different phases of deformation to be analysed, even at the microscopic scale. However, even though glacier ice is subjected to polyphase deformation, it is common for only several phases of deformation to be preserved as a result of the relatively coarse ice crystal structure, recrystallization of ice undergoing deformation, and the melt-out of structures (Hambrey and Lawson, 2000). The differences between structural glaciology and structural geology provide a unique opportunity for each subject to benefit from the other as concepts in one can occasionally be applied to the other.

2.2 Historical background

A good historical summary of structural glaciology up to and including the start of the 21st century was written by Hambrey and Lawson (2000). Their summary is briefly paraphrased here, with recent structural glaciological research conducted over the past decade and a half reviewed and summarised afterwards.

Interest in glacier structures dates back to the infancy of glaciology where early researchers drew comparisons between layering in glacier ice with structures found in rocks (Tyndall, 1859; Forbes, 1900). This pioneering work used glacier structure as evidence to lay the foundations for the first fundamental principles of glacier flow.

The early twentieth century saw limited significant progress with regard to understanding glacier flow or dynamics. However, the development of a flow law for ice renewed interest in glaciers during the early 1950's culminating in new robust theories for glacier flow (*e.g.* Nye, 1952, 1953, 1957; Glen, 1955). Subsequent notable contributions from Allen et al. (1960) and Meier (1960) on Blue Glacier, Washington, and Saskatchewan Glacier, Alberta, respectively documented the three-dimensional

orientation and dip of all the major structures present on each glacier. Attempts at relating the observed structures to measured strain rates proved on the whole unsuccessful; however, further examination suggested that ductile structures such as folds and foliation were more likely to be related to cumulative strain, reflecting the structure's initial formation and continuing evolution (strain history) (Hambrey and Milnes, 1977; Hudleston and Hooke, 1980; Hudleston, 1983).

More recent research undertaken at the end of the twentieth century focused on the formation and evolution of structures in surge-type glaciers (*e.g.* Sharp et al., 1988; Lawson et al., 1994; Hambrey and Dowdeswell, 1997; Murray et al., 1997), and applying fieldwork derived structural principles developed on respectively small-scale valley glaciers to much larger ice masses using remotely sensed data (*e.g.* Reynolds, 1988; Hambrey and Dowdeswell, 1994; Dowdeswell and Williams, 1997).

Throughout the last half century there have also been continuous attempts to examine the relationship between glacier structures and debris features. Early researchers primarily focused on individual structure-debris feature relationships (*e.g.* Goldthwait, 1951; Souchez, 1967, 1971) culminating with Boulton's (1967, 1970, 1978) pioneering work that laid the foundations for our understanding of debris-entrainment and depositional processes in a geological context. Nevertheless, an in-depth study examining structure-debris relationships on a glacier-wide scale had yet to be undertaken. Subsequent studies regarding debris transport as part of a larger scale glacial system (*e.g.* Drewry, 1972; Boulton and Eyles, 1979; Small, 1987; Kirkbride, 1995; Evans, 2003) quickly improved our knowledge of structure-debris relationships. More recent research has focused primarily on structural controls of debris transport in high-Arctic polythermal and cold-based glaciers, particularly in Svalbard (*e.g.* Bennett et al., 1996; Hambrey et al. 1996, 1999, 2005; Boulton et al., 1999; Hambrey and Glasser, 2003; Hubbard et al., 2004). Only during the last decade have a few studies started to address whole-glacier structure and structural controls over debris processes in detail for temperate alpine valley glaciers (*e.g.* Goodsell et al., 2005a, b; Roberson, 2008; Appleby et al., 2010; Jennings et al., 2014).

2.3 Deformation in glaciers

Deformation in glaciers occurs as a result of gravity-induced ice creep, combined with the superimposed effects of basal sliding or movement over a deformable bed (Hambrey and Lawson, 2000; Hudleston, 2015). The rate at which ice flows was summarised by Glen's Flow Law (1955), which was subsequently generalised for glaciers by Nye (1957):

$$\dot{\varepsilon} = A\,\tau^{n} \qquad \textit{(Equation 2.1)}$$

where $\dot{\varepsilon}$ is the shear strain rate, τ is the shear stress, n is the creep exponent and A is the flow parameter. The typical value for n in glaciers is approximately 3, but can vary between 1.5 to 4.2, and the parameter A depends on temperature and ice fabric (*see* Cuffey and Paterson (2010) for a review of subsequent refinements of these concepts).

Stress and strain are important concepts for understanding deformation in glaciers. Stress, the force applied per unit area, results in strain, the change in a body's shape and dimensions as a consequence of stress. Stress acting on a surface can be separated in to two basic components; stress acting perpendicular to a surface (normal stress, σ), and stress acting parallel to a surface (shear stress, τ). In each case the stress acting on the surface comprises two equal and opposite tractions. Normal stresses have opposing tractions acting at right-angles to a surface, either pulling in opposite directions (tensile stress) or acting towards one-another (compressive stress). Shear stresses are orientated parallel to one-another along a plane and have tractions that act in opposite directions. Stress at a specific point can be described using a stress element that shows the normal and shear stresses acting on an infinitesimal cube. Parallel faces of the cube are paired with one-another as they experience equal but opposing stresses; therefore, the stress at a point can be described by three perpendicular planes. Each plane has three stress components comprising one normal and two shear stresses (Figure 2.1). Therefore, nine stress components can be used to

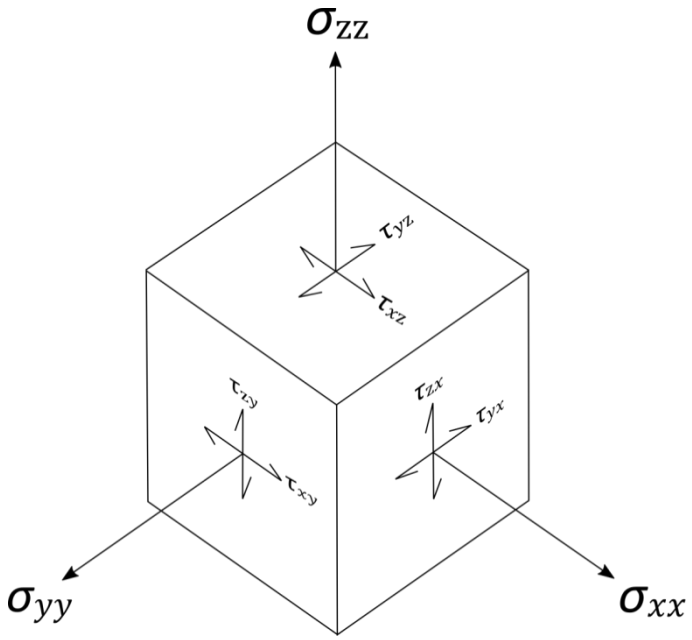

Figure 2.1. An infinitesimal cube showing the normal (σ) and shear (τ) stresses acting on three perpendicular planes that can be used to describe stress at any given point. Note that a Cartesian coordinate system is used, with the first subscript letter indicating the direction in which the stress is acting, and the second denoting the direction perpendicular to the plane on which the stress is acting.

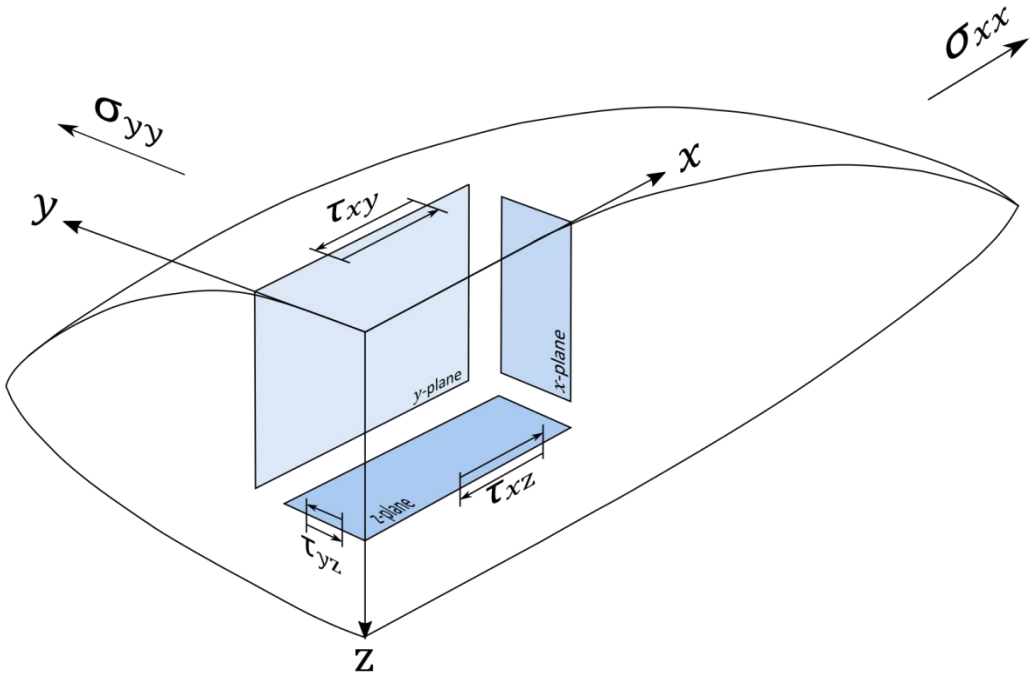

Figure 2.2. A conceptual diagram illustrating the normal (σ) and shear (τ) stress that can be used to describe stress in a glacier. Note that a Cartesian coordinate system is used, with the first subscript letter indicating the direction in which the stress is acting, and the second denoting the direction perpendicular to the plane on which the stress is acting.

describe the state of stress at any point (three normal, six shear). However, moment equilibrium conditions on a stress cube (known as shear stress reciprocity) dictates that there are only six independent components (three normal, three shear) as pairs of shear stresses must be in equilibrium so there is no rotational acceleration of the stress element (Figure 2.1). When describing stresses acting in an ice mass a rectangular Cartesian coordinate system is used to identify the stress type and direction, with the x-axis orientated longitudinally along the glacier, the y-axis orientated transverse, and the z-axis in the vertical (Figure 2.2). Stress type is identified by either σ or τ for normal or shear stresses respectively, each followed by two subscript letters, the first of which (i) indicates the direction in which the stress is acting, and the second (j) denotes the direction perpendicular to the plane on which the stress acts (note that this is the standard convention for describing stress in glaciology (*see* Benn and Evans, 2010); however, some authors use different methods or letters, as is the case in structural geology) (Figure 2.2).Therefore, a normal stress acting in the x direction is denoted σ_{xx}, whereas a shear stress acting in the x direction on a plane orientated perpendicular to the y-axis would be denoted τ_{xy}. Within an ice mass normal stresses tend to act in all directions as a consequence of the weight of the overlying ice causing the ice to spread. The mean normal stress (cryostatic pressure) is given by Equation 2.2:

$$\sigma_{zz} = \rho_i g H \qquad \textit{(Equation 2.2)}$$

where σ_{zz} is the normal stress acting in the vertical direction, ρ_i is the density of the ice, g is gravitational acceleration, and H is the thickness of the ice. In certain circumstances all normal stresses in a glacier may equal the cryostatic pressure, thus no deformation occurs. Any difference between a normal stress and the cryostatic pressure is known as the deviatoric stress (*i.e.* it deviates from the mean) (Equation 2.3):

$$\sigma'_{xx} = \sigma_{xx} - 1/3(\sigma_{xx} + \sigma_{yy} + \sigma_{zz}) \qquad \textit{(Equation 2.3)}$$

where σ'_{xx} is the deviatoric stress in the x direction, and σ_{xx}, σ_{yy}, σ_{zz}, are the normal stresses in the x, y, and z directions respectively. Tensile deviatoric stresses occur when a normal stress is less than the cryostatic pressure; furthermore compressive deviatoric stresses arise when a normal stress is greater than the cryostatic pressure. Interestingly, it is possible for a deviatoric stress to be tensile even if all normal stresses are compressive, providing a compressive stress in one direction is weaker than the remaining compressive stresses. Normal and shear stresses, despite being portrayed as individual processes, are not mutually exclusive, but are fundamentally linked. In situations where ice is undergoing shear stress, normal stresses are acting at 45˚ to the shear plane (Figure 2.3). Similarly, ice subjected to normal stress experiences shear stresses that are initially orientated at 45˚ to the normal stress axes (Figure 2.3). In reality ice is subjected to a combination of normal and shear stresses

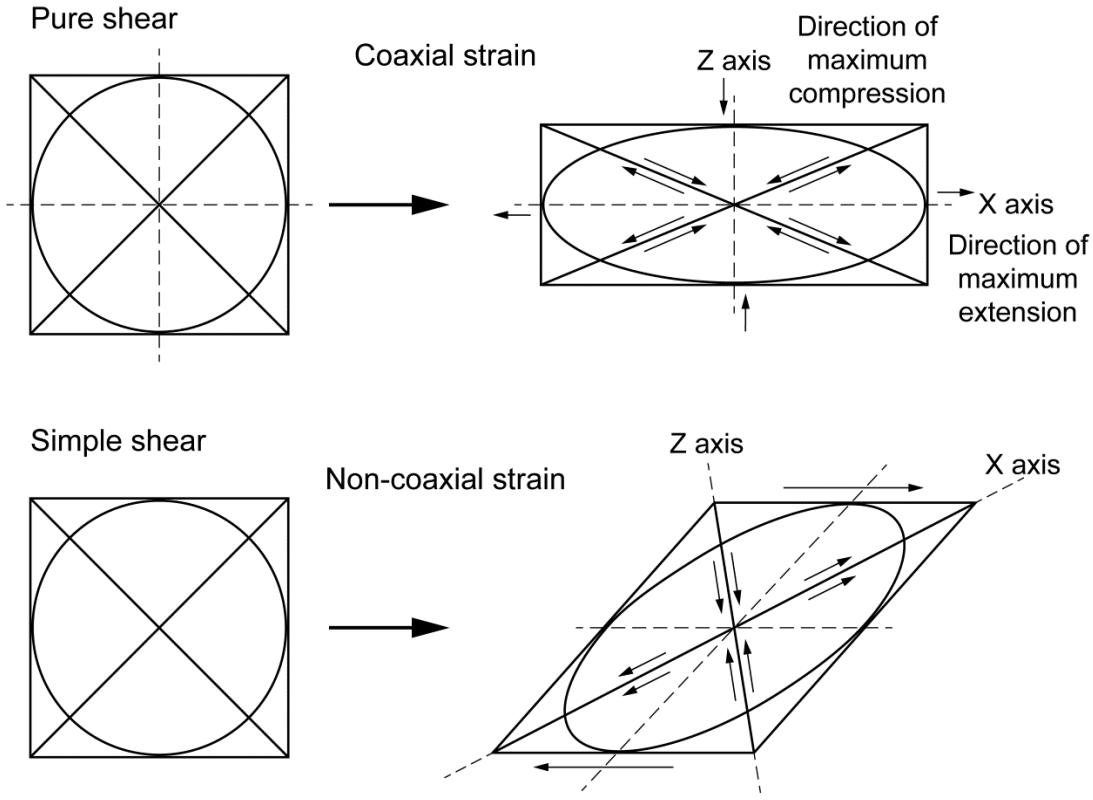

Figure 2.3. The evolution of circular passive markers (strain ellipses) in a deforming body when undergoing pure shear (experiencing normal stress) and simple shear (experiencing shear stress). Direction of maximum extension (x-axis) and maximum compression (z -axis) indicated by dashed lines. Note that when undergoing pure shear the dashed axes remain stationary (coaxial strain), whereas when undergoing simple shear the axes rotate (non-coaxial strain). Small arrows indicate pure and simple shear acting within the deforming bodies.

which coalesce to form a new set of deviatoric and shear stresses. The values of the new set of stresses can be resolved into three mutually exclusive component parts (maximum, intermediate, and minimum values) orientated perpendicular to one-another termed σ_1, σ_2, and σ_3 where $\sigma_1 > \sigma_2 > \sigma_3$ (known as principal stress tensors). It is especially useful to deduce the principal stress tensors when considering the formation of glaciological structures. When studying the initiation of crevassing, it is beneficial to simplify the process by only considering stress components found at the surface of the glacier. Three stress components are active in the surface plane of a glacier (σ_{xx}, σ_{yy}, τ_{xy}) (Figure 2.2) (Nye, 1952), and by looking at the relationship between these three components it is possible to describe stress for a point and deduce the orientation of the principal stress tensors (Figure 2.4).

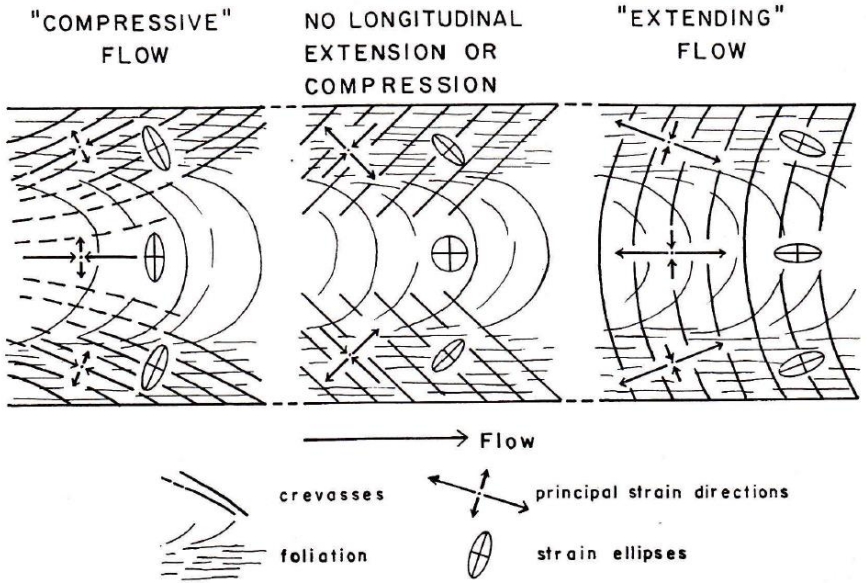

Figure 2.4. The orientation of strain ellipses and principal strain directions at the surface of an idealised valley glacier when experiencing different flow conditions (Hambrey and Milnes, 1975).

Strain (ε) is the change in a material's shape and dimensions resulting from applied stress. The type of strain experienced can be separated into two basic categories, pure shear and simple shear. Both categories of shear are idealistic and in a glaciological setting a combination of the two is required to describe deformation at

any one point; however, the concept of mutually exclusive pure and simple shear is useful for describing the formation and evolution of structures. It is often useful to visualise strain using a strain ellipse which acts as a passive spherical marker within a deforming material. A strain ellipse has two principal strain axes perpendicular to one another that indicate the direction of maximum (x-axis) and minimum (z-axis) strain, with a third intermediate axis (y-axis) normal to the xz-plane (*i.e.* $x > y > z$) (Figure 2.3). Both pure and simple shear are types of plane strain, therefore no deformation occurs in the y-axis (*i.e.* there is no particle movement perpendicular to the xz-plane), and any shortening in the z-axis must be totally compensated by extension in the x-axis (Fossen, 2010). As a result, both types of shear can be illustrated by an ellipse on a two-dimensional diagram where the y-axis is perpendicular to the page. Pure shear occurs as a result of normal stress causing extension in the x-axis and contraction in the z-axis. Pure shear can be regarded as a coaxial strain because the principal strain axes (x-, y-, and z-axes) remain stationary and do not rotate when undergoing deformation. Simple shear develops under shear stress conditions resulting in the rotation and elongation of the x-axis, hence simple shear can be regarded as a non-coaxial strain. Even though pure shear is the result of normal stresses and not shear stress, the resulting strain is called 'pure shear' because shear strain occurs within the body of the object being deformed (Figure 2.3). The amount of strain experienced by a package of ice can be quantified by comparing the dimensions and shape before and after the application of stress, either by measuring elongation or using quadratic equations when the strains are large. Strain rate ($\dot{\varepsilon}$), the amount of deformation occurring per unit time, is dependent on the rheology of the material and the amount of stress applied. However, in structural glaciology it is often more advantageous to consider cumulative strain (*i.e.* the finite amount of strain experience over a set period of time) (Hambrey, 1977a; Hambrey and Lawson, 2000; Hudleston, 2015).

2.4 Classification of glacier structures

Glacier ice can be treated as a geological material. As is the case for rocks, strata systematically build up and subsequently become progressively deformed to produce a

wide range of structures (Hambrey, 1994). As a result, structures that form in glaciers can be broadly classified as 'primary' or 'secondary' (Hambrey, 1994; Hambrey and Lawson, 2000). Primary structures form by the accumulation or accretion of new material, while secondary structures result from ice deformation (Hambrey, 1994; Hambrey and Lawson, 2000). Secondary ice structures can be further generalised into two categories; the product of 'plastic (ductile) deformation', or 'brittle deformation'. Ductile features form as primary structures are altered to varying degrees by ice creep, primarily resulting in folding and foliation. Brittle structures, resulting from the brittle failure of ice, form a wide range of fractures including open fractures (crevasses), closed fractures (crevasse traces), and faults (Hambrey, 1994; Hambrey and Lawson, 2000).

Glacier structures are usually described in relation to the structural evolution of the whole glacier in an attempt to distinguish different phases of deformation and the sequential development of structures. Structural geological conventions are therefore adopted (Hambrey and Milnes, 1977) to describe structures in order of formation, as indicated by cross-cutting relationships. Planar structures are usually labelled S_0, S_1, S_2, … S_n in ascending order of formation, using criteria outlined by Hambrey and Lawson (2000), Goodsell et al. (2005b), and Cuffey and Paterson (2010), with identifiable fold phases termed F_1, F_2, ... F_n indicating major phases of deformation. As is the case for rocks, glacier ice undergoes polyphase deformation (*i.e.* is subjected to several phases of deformation). However, polyphase deformation suggests that deformation phases are temporally separated. In glaciers, phases of deformation sometimes merge into one another to form continuous phases, whereas in some cases phases are totally separate. As the whole ice mass is deforming at the same time, separate deformation phases occur simultaneously (*i.e.* S_0 formation in the accumulation area may be occurring at the same time as S_3 formation lower down the glacier), thus temporal separation of deformation phases is impossible (Hambrey and Milnes, 1977; Hambrey and Lawson, 2000), a concept that has tentatively been adopted into geology (*e.g.* Gray and Mitra, 1993). Therefore, deformation phases in glaciers are not related to a temporal time scale, but are related to the passage of a parcel of ice through the ice mass (Hambrey and Lawson, 2000). Lesser glaciological structures such as crystal

quirks and unconformities are usually excluded from the sequential description of structure formation because they are regarded as unimportant with regard to the structural evolution of a whole ice mass (Goodsell et al., 2005b).

2.5 Glacier structures and their kinematic significance

This section provides a systematic description of the main structures found in glacier ice, beginning with primary structures and then covering secondary structures (ductile and brittle). Key structures are interpreted in terms of their kinematic significance in the context of a flowing ice mass.

2.5.1 Primary structures

The dominant primary structure found in glaciers is primary stratification; generally sub-horizontal ice layers differentiated from one another by varying ice crystal size, bubble content, and dirt content. The stratified nature of the ice represents the annual layering of snowfall deposited parallel to the glacier surface, preserved during firnification (Lewis, 1960; Shumskii, 1964; Hambrey, 1976b, 1994; Hambrey and Lawson, 2000). Boundaries between strata represent surfaces of uniform age or isochrones (Cuffey and Paterson, 2010). The different ice facies reflect seasonal variations in initial snowpack formation (Wadham and Nuttall, 2002; Wadham et al., 2006). Relatively thick layers of low-density coarse bubbly ice represent winter snow accumulation that has undergone partial melt and refreezing. High-density coarse clear ice is the result of meltwater and slush accumulation refreezing at the base of the snowpack (Wadham et al., 2006). Respectively thinner strata consisting of fine ice crystals represents summer snow accumulation (Jennings et al., 2014). Summer layers often contain aeolian-derived dust and organic material which becomes trapped in surface ice (Hambrey, 1994; Goodsell et al., 2005b; Oerlemans et al., 2009; Cuffey and Paterson, 2010; Jennings et al., 2014). Periods of excessive surface ablation can remove many previous layers producing an unconformity, which represents a hiatus in the systematic deposition of snow layers (Hambrey, 1994; Goodsell et al., 2005a, b).

Less important primary structures form as summer meltwater percolates down through the snowpack, refreezing as spatially limited ice layers, lenses, or glands (Hambrey, 1994; Hambrey and Lawson, 2000).

Other less important primary structures include regelation layering, ice breccias, and overridden and incorporated frontal aprons. Regelation layering forms as pressure melting and subsequent regelation at the ice-bed interface produces parallel-laminated ice layers that can have varying amounts of basal debris incorporated (Hambrey, 1994). Ice breccias occur primarily at the glacier margins where the glacier is susceptible to collapse. Ice debris accumulates near ice cliffs or in crevasses, reconsolidating into a breccia. Trapped snow or refreezing of interstitial meltwater between ice debris particles can often fuse the breccia together (Hambrey, 1994), forming an aggregate with randomly orientated veins (Benn and Evans, 2010). In cold regions, frontal aprons composed of ice blocks and debris commonly form below advancing glaciers that terminate in steep ice cliffs. When overridden and incorporated, frontal aprons are visible in basal ice as mosaics of individual ice blocks that become increasingly attenuated by ice deformation. Continuing deformation of entrained frontal aprons eventually forms complex alternating layers of debris-rich and debris-poor ice (Evans, 1989; Fitzsimons et al., 2008; Benn and Evans, 2010).

2.5.2 Ductile structures

Note: In this text the words ductile and plastic are used interchangeably; however, it is worth noting that especially in geological literature the two words have different meanings. In geological texts plastic deformation refers to a permanent change of a body's shape and size without fracture, whereas ductile deformation indicates deformation that preserves the continuity of passive layers and structures yet can occur by a number of different deformation mechanisms. This is a scale-dependent differentiation as a structure that appears to have undergone plastic deformation when viewed in the mesoscopic-scale may have actually deformed by multiple small fractures when viewed in the microscopic-scale (Figure 2.5) (Fossen, 2010). In this text, the words ductile and plastic refer to materials that accumulate strain with no

macroscopically visible fracturing. Even though this convention would be considered erroneous in geology, because of the comparatively large crystal size and poor preservation of deformation phases in glacier ice, it is generally not possible to differentiate between the two phrases in glaciology.

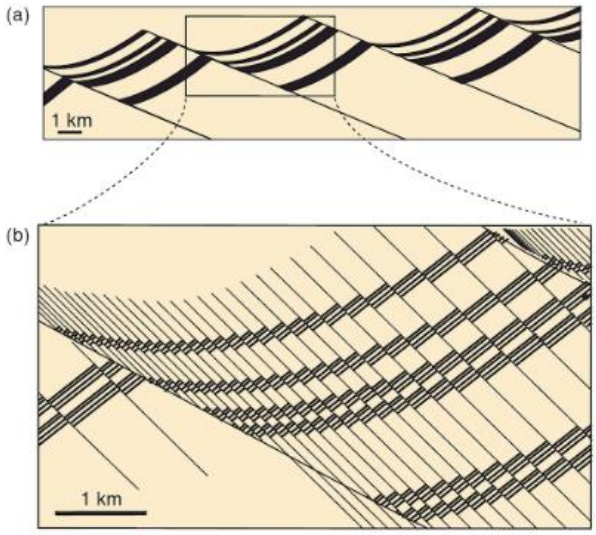

Figure 2.5. An illustration demonstrating the scale-dependent differentiation between ductile and plastic deformation in rocks. (a) When viewed in large-scale layers appear to have undergone plastic deformation; (b) however, when viewed at a smaller scale, layers have actually been deformed by multiple small fractures (Fossen, 2010).

2.5.2.1 Folding

Folding of glacier ice occurs in most ice masses at a range of different scales (Hambrey, 1977a; Hambrey, 1994; Lawson et al., 1994; Hambrey and Lawson, 2000; Cuffey and Patterson, 2010), resulting from changes in valley geometry and flow variations (Hambrey and Lawson, 2000). It is common in many glaciers for primary stratification to become folded by a combination of lateral compression and simple shear as ice flows from a respectively broad accumulation area into a narrow tongue (Lawson et al., 1994; Hambrey et al., 1999; Goodsell et al., 2005b). Folds can form in a range of different styles (Hambrey, 1977a), and can have amplitudes ranging from centimetres through to hundreds of metres. The most common types of fold observed on the surface of a glacier (fold amplitudes ranging from centimetre- to metre-scales) are 'similar' (with thickened fold hinges and attenuated limbs) (Figure 2.6) and 'isoclinal'

(with parallel attenuated limbs) folds (Figure 2.7). However, other fold styles such as 'parallel' (with fold hinge and limbs of a uniform thickness), 'chevron' (zig-zag shaped), and 'intrafolial' (isolated fold hinges severed from fold limbs, often associated with

Figure 2.6. An isolated similar fold hinge composed of coarse bubbly ice surrounding by fine-grained ice on the surface of Vadrec del Forno. Note the thickened fold hinge with attenuated limbs. Ice axe for scale.

foliation) folds can also be observed (Hambrey and Lawson, 2000). Fold axes tend to plunge up-glacier with angles that range from shallow to steep, often with the fold's axial plane parallel to flow direction. Parasitic minor folds are common on larger scale fold structures. However, large-scale features can rarely be observed from the surface of the glacier, yet are usually apparent in aerial photography or satellite imagery.

Folds with axial planes orientated transverse to flow occur less frequently in most ice masses but often form in areas of strong lateral compression. Minor folds with transverse to flow axial planes are common below icefalls, especially if a pre-existing longitudinal structure (*e.g.* longitudinal foliation) exists.

Piedmont glaciers are unique when compared to other ice masses because they experience strongly pronounced longitudinal compression. As a result, longitudinal foliation and medial moraines become folded with axial planes transverse to flow, attaining amplitudes of several kilometres. However, the pattern of folding found in piedmont glaciers is often complicated by surges (Sharp, 1958; Post, 1972; Hambrey and Lawson, 2000).

Figure 2.7. An isoclinal fold with parallel attenuated limbs on the surface of Vadrec del Forno. Photograph courtesy of M. J. Hambrey.

Looped medial moraines are distinctive tear-drop-shaped fold structures that result from surge-type behaviour (Meier and Post, 1969; Rutishauser, 1971; Post, 1972; Driscoll, 1980; Lawson, 1996; Hambrey and Lawson, 2000). Surge-type glaciers experience short-lived periods of enhanced ice flow during their active phase, separated by extended periods of comparative inactivity during their quiescent phase (Lawson et al., 1994). Increased ice discharge from a surging tributary flow unit into

neighbouring less active ice often deforms the medial moraine between the two, resulting in a bulbous shaped medial moraine (Dowdeswell and Williams, 1997; Hambrey and Lawson, 2000). Looped medial moraine structures are useful for identifying surge-type glaciers that have not previously been observed to surge (Dowdeswell and Williams, 1997; Hambrey and Lawson, 2000).

2.5.2.2 Foliation

Foliation is the pervasive planar structure found in most, if not all glaciers, and develops in two main categories: longitudinal and transverse (or arcuate) (Hambrey, 1977a; Hambrey and Lawson, 2000). Longitudinal foliation can be further separated into transposition and axial planar foliation. Foliation mainly comprises anastomosing layers (layers are often discontinuous and can only be traced for a few metres, but on occasion can be followed for hundreds of metres) of coarse clear, coarse bubbly, and fine grained ice, with individual layers rarely exceeding tens of centimetres in thickness. Different formation processes have been suggested for the various types of foliation.

Similarities between the ice facies composition of primary stratification and longitudinal foliation suggests that the latter is inherited from the former (*e.g.* Ragan, 1969; Hambrey, 1975, 1976a, Hambrey and Milnes, 1977; Hooke and Hudleston, 1978; Lawson et al., 1994; Goodsell et al., 2005b; Roberson, 2008; Appleby et al., 2010; Jennings et al., 2014, 2015; Hudleston, 2015). As ice flows from a respectively broad accumulation basin and converges into a narrow tongue, ductile deformation of primary stratification in pure and simple shear regimes gradually folds the initially horizontal layers. Transposition occurs as continued folding and eventual attenuation of fold limbs re-orientates layers until they are parallel to flow (longitudinally orientated) (Figure 2.8); a comparable mechanism to that observed in metamorphic rocks (Hobbs et al., 1976; Hambrey and Lawson, 2000). It is common for fold hinges to become severed from their limbs and isolated during this process, leaving remnant fold hinges (Hambrey, 1977a). Foliation formation is most pronounced where folding is tightest. This primarily occurs in areas dominated by simple shear regimes and

longitudinal extension, such as at the confluence of flow units and at the glacier margins (Hambrey, 1977a; Hambrey and Lawson, 2000). Less frequent sub-centimetre thick layers of fine white ice that are not found in primary stratification are often observed at flow unit boundaries. It has been suggested that these layers are the product of crystallographic modification of ice layers when experiencing simple shear (Hambrey and Milnes, 1977; Jennings et al., 2014), a process similar to cataclasis in metamorphic rocks (Shumskii, 1964).

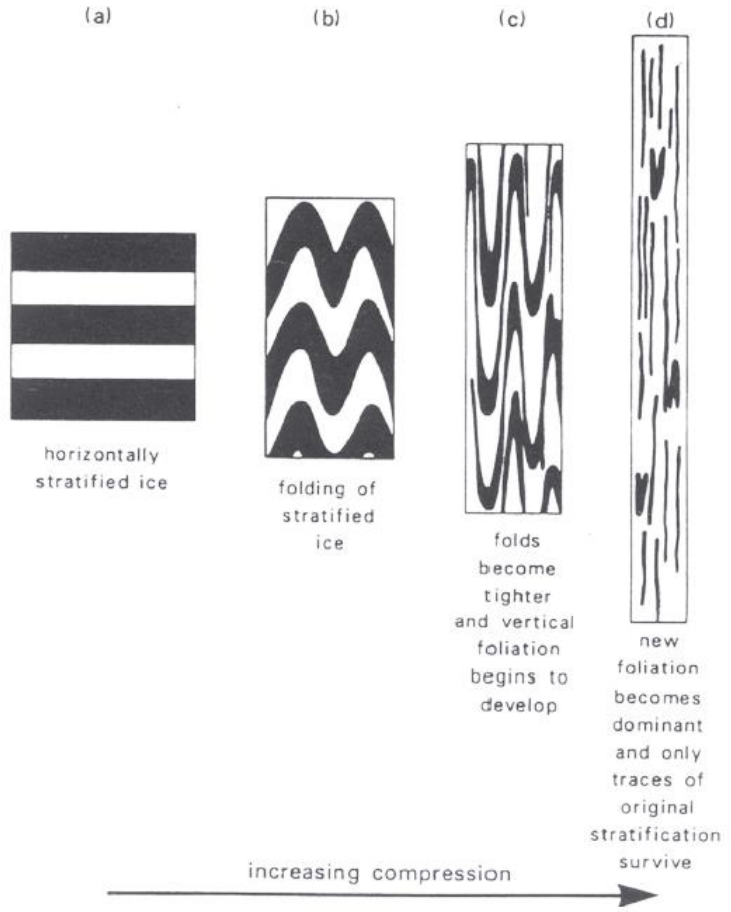

Figure 2.8. Conceptual diagram showing the transposition of initially horizontal primary stratification into longitudinal foliation when experiencing lateral compression and longitudinal extension (Hambrey, 1994).

Not all longitudinal foliation is inherited from pre-existing structures, and it has been documented as a completely new structure (*e.g.* Allen et al., 1960; Lawson, 1990; Pfeffer, 1992; Lawson et al., 1994; Hambrey et al., 1999, 2005; Hambrey and Glasser, 2003; Jennings et al., 2014). This type of foliation has a clear axial planar relationship. The foliation cross-cuts primary stratification in a geometrically similar fashion to the folding/slaty cleavage observed in low grade metamorphic rocks such as mudstones (Hambrey and Lawson, 2000; Hambrey et al., 2005; Jennings et al., 2014). However, the exact formation process for axial planar foliation is currently unknown (Hambrey and Lawson, 2000; Jennings et al., 2014).

Individual flow units, and in many cases whole glaciers, tend to be dominated by one type of longitudinal foliation (*e.g.* axial planar foliation: Hambrey et al., 2005, transposition foliation: Roberson, 2008). It has been suggested that the dominance of axial planar or transposition foliation is location-dependent (Jennings et al., 2014). Comparison of flow units that are dominated by different types of longitudinal foliation on Vadrec del Forno, a temperate Alpine valley glacier, suggested that flow unit characteristics dictate what foliation preferentially forms. It is inferred that in flow units that have pronounced lateral narrowing that there are higher rates of simple shear. As a result, primary stratification is quickly transposed into a transposition foliation relatively high up the glacier. In flow units with less pronounce lateral narrowing, cumulative strain values are inferred to be lower, therefore allowing primary stratification to be preserved further down-glacier. When primary stratification is preserved relatively far down-glacier an axial planar foliation is allowed to develop (Jennings et al., 2014).

A number of studies have attempted to reveal the relationship between longitudinal foliation and incremental strain (often referred to as ‘strain-rate tensors’) (Hambrey and Milnes, 1977). Despite demonstrating that longitudinal foliation forms approximately parallel to the maximum shear strain-rate tensor, the relationship between the two at different points of measurement along a glacier is often unclear (Hambrey and Milnes, 1977; Hambrey and Lawson, 2000). The main reason for this is, once developed, longitudinal foliation can be transported down-glacier as a passive marker (*e.g.* Lawson, 1996), becoming deformed in stress regimes that it subsequently

passes through. Therefore, the orientation of the foliation will no longer have any relation to the incremental strain. Only studies that can measure incremental strain in regions where foliation is actively forming will be able to produce meaningful results (*e.g.* Hambrey and Milnes, 1977). It is often more advantageous to consider the formation and subsequent evolution of longitudinal foliation in relation to cumulative (finite) strain (*i.e.* the strain history). This method recognises that in reality longitudinal foliation is the product of continuous and often multiple phases of deformation (Hambrey et al., 1980). When a longitudinal foliation first forms, a cumulative strain ellipse is initially orientated at 45˚ to the longitudinal axis of the foliation. If the foliation remains in a simple shear regime, the long axis (x-axis) of the strain ellipse will rotate towards parallelism with the long axis of the foliation (Hambrey and Milnes, 1977; Hambrey et al., 1980; Hambrey and Lawson, 2000).

Unlike longitudinal foliation, transverse foliation is primarily derived from crevasse traces (Hambrey and Lawson, 2000). As crevasse traces flow into a longitudinally compressive stress regime (*e.g.* below an icefall) the transverse layering is amplified (Hambrey and Milnes, 1977; Lawson, 1996; Hambrey and Lawson, 2000). Transverse foliation therefore develops in pure shear regimes where the foliation forms normal to the maximum compressive strain-rate. In this case, transverse foliation forms perpendicular to the short axis (z-axis) of the strain ellipse, remaining perpendicular throughout the development of the foliation (Hambrey and Lawson, 2000). It is worth noting that in the case of transverse foliation, the magnitude of cumulative strain and subsequent strength of the foliation are substantially less than for longitudinal foliation (Hambrey and Milnes, 1977; Hambrey et al., 1980; Hambrey and Lawson, 2000).

Longitudinal and transverse foliation have both been observed in surge-type glaciers (*e.g.* Lawson et al., 1994). It has been suggested that longitudinal foliation forms during the quiescent (relatively inactive) phase, in much the same way as it forms in non-surge-type glaciers. However, formation of local transverse foliation is probably related to intense surge-related thrusting and longitudinal shortening (Lawson et al., 1994; Hambrey and Lawson, 2000).

2.5.2.3 Boudins

Boudin structures form as ice layers with different rheologies undergo layer-parallel extension, a process known as boudinage (Fossen, 2010). Classic boudinaged layers when viewed in cross-section look like strings of sausages (hence the derivation of the term boudin from the French word for blood sausage); however, a range of boudin geometries exist depending on the ice layer properties and the specific deformation environment (Hambrey and Milnes, 1975; Hambrey and Lawson, 2000; Fossen, 2010). Boudin shapes vary from rectangular through to pinch-and-swell structures depending upon the viscosity contrast between the ice layers (Figure 2.9). Strongly competent layers (layers that are relatively more resistant to flow than the surrounding matrix or layers) form uniform rectangular boudins by brittle deformation, while the surrounding less competent materials deforms by plastic deformation (Hambrey and Milnes, 1975). As the competence of the boudinaged layer decreases the corners of the boudins become more rounded or pulled out by plastic deformation. Less competent layers that have a low viscosity contrast between adjacent ice types go through a process known as necking, resulting in regularly spaced thinning of the boudinaged layer forming pinch-and-swell structures (Fossen, 2010). Two main types of boudinage are found in glaciers: competence contrast and foliation boudinage. Both types have been observed in temperate glaciers with scales ranging from centimetres through to several metres (Hambrey and Milnes, 1975; Hambrey and Lawson, 2000). However, more complex yet uncommon boudinage geometries such as chocolate tablet boudinage can sometimes develop in non-plane strain deformation regimes (Passchier and Druguet, 2002).

Competence contrast boudins form where a competent layer is extended, separating the layer into regularly spaced and shaped sections by plastic deformation, brittle deformation, or a combination of the two (Fossen, 2010). Examples of competence contrast boudinage have been observed in Swiss glaciers where packages of clear ice have become isolated in bands of debris rich basal ice or in foliation where fine ice layers that are surrounded by coarse bubbly ice become attenuated (Hambrey and Milnes, 1975; Hambrey and Lawson, 2000; Hudleston, 2015).

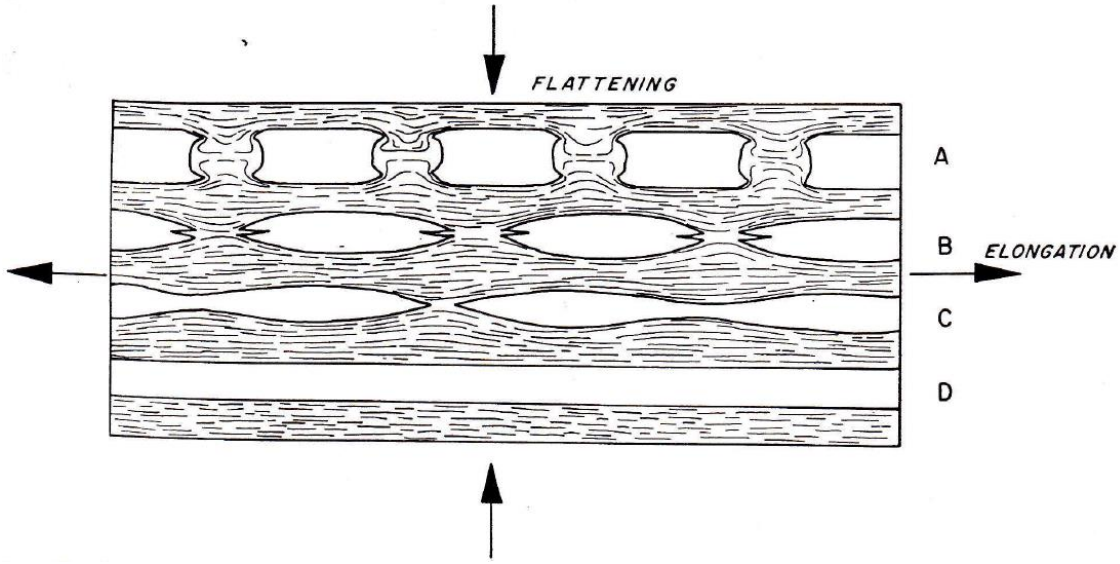

Figure 2.9. Boudinage and pinch-and-swell structures in layers with varying degrees of competence with respect to the surrounding matrix. Layer A is much more competent than the matrix, with layers B and C decreasing in competence. Layer D is the same as the matrix (Hambrey and Milnes, 1975).

Foliation boudinage can be classified into two subcategories: symmetric or asymmetric. Both varieties are found in areas of strong longitudinal foliation such as at the glacier margins or at the confluence of flow units; however, the latter is most common (Hambrey and Milnes, 1975, 1977; Hambrey and Lawson, 2000). Unlike competence contrast boudinage that develops in individual ice layers, foliation boudinage forms in laminated or multi-layered ice. Despite individual ice layers being structurally anisotropic, because the boudins form across a number of layers the laminated ice structure is the same inside and outside of the boudin (Hambrey and Milnes, 1975; Fossen, 2010). As a result, the boudinaged layer as a whole can be regarded as having no competence contrast with the surrounding ice (Hambrey and Milnes, 1975). Symmetrical foliation boudinage forms between tensile fractures. As the fractures open, the foliated ice gets pinched towards the fracture and a void develops between boudins. Observations of symmetrical foliation boudinage has

shown that void structures between boudins become water-filled and subsequently freeze to produce large clear ice crystals that grow perpendicular to the void's edge (Hambrey and Milnes, 1975). Asymmetric foliation boudinage is strongly related to brittle shear fractures or ductile shear zones that crosscut longitudinal foliation obliquely. Displacement along the shear fractures rotates the foliation forming the boudin neck (Hambrey and Lawson, 2000; Fossen, 2010). Two different processes have been suggested for the formation of these structures.

i. Boudin formation in response to longitudinal extension and simple shear occurring in unison. Such conditions can be found on the outside of a bend, and it has been suggested that fractures initially formed up-glacier may act as planes of weakness that can be reactivated in these sorts of stress regimes (Lawson et al., 1994; Hambrey and Lawson, 2000).

ii. Boudin-like features can result from two separate phases of deformation. Tensile fractures develop in areas experiencing extension. Subsequent transport into a non-coaxial strain regime closes and rotates the fracture, also deforming the foliation lying perpendicular to the fracture (boudin neck) to form hook folds (Hudleston, 1989; Hambrey and Lawson, 2000).

2.5.3 Brittle structures

2.5.3.1 Crevasses

Crevasses are a common structure found in almost all ice masses that result from the brittle fracture of glacier ice in response to deformation (Harper et al., 1998; van der Veen, 1998a; Nath and Vaughan, 2003; Benn and Evans, 2010; Hudleston, 2015). Fracture propagation can occur in three basic ways (fracture modes) depending on the

orientation of the applied stress (Figure 2.10) (van der Veen, 1998a; Benn et al., 2007; Benn and Evans, 2010; Hudleston, 2015).

i. Mode I (opening mode): Tensile stresses applied normal to the fracture plane pulls the sides of the crevasse apart. Crack propagation occurs perpendicular to the direction of maximum extension.

ii. Mode II (sliding mode): The fracture walls remain in contact while shear stress is applied parallel along the fracture plane. Crack propagation occurs in the same direction as the applied shear stress.

iii. Mode III (tearing mode): As for above, shear stress is applied parallel along the fracture plane; however, crack propagation occurs at right angles to the applied shear stress.

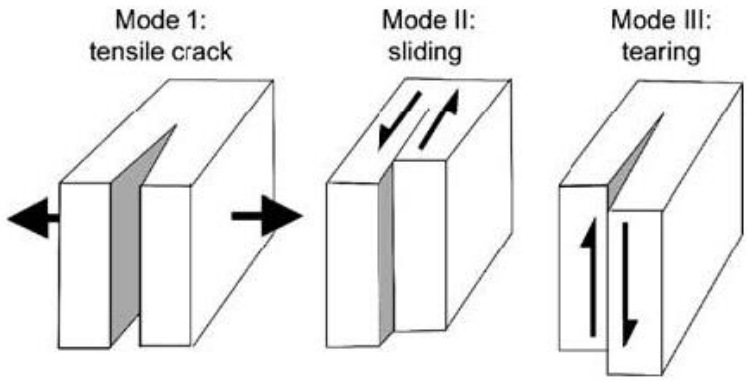

Figure 2.10. Schematic diagram illustrating the three basic modes of fracture propagation (Benn et al., 2007).

A combination of fracture modes can occur simultaneously (mixed-mode fracture) (van der Veen, 1998a; Benn et al., 2007; Benn and Evans, 2010; Hudleston, 2015); however, it is often assumed that surface crevasses primarily form in response to tensile

deformation (fracture mode I), developing normal to the maximum extending strain-rate. A range of crevasse orientations can exist depending on the morphology of the glacier trough and the strain regimes present (Harper et al., 1998; Hambrey and Lawson, 2000; Benn et al., 2007); nonetheless, surface fracturing is primarily associated with areas of fast and extending flow (such as in ice falls) (Harper et al., 1998; Hambrey and Lawson, 2000). Despite the widespread nature of the structure, crevasse formation is relatively poorly understood (van der Veen, 1998a; Nath and Vaughan, 2003; Benn and Evans, 2010).

The presence of a crevasse on a glacier surface suggests that a fracture criterion must have been met or exceeded to induce fracturing (Vaughan, 1993; Campbell et al., 2013). A variety of studies have attempted to identify the criterion required to initiate crevasse formation, yet this has proved to be a complicated problem to resolve, primarily because the tensile strength of ice can be highly variable depending on different ice properties (Benn and Evans, 2010; Campbell et al., 2013). A number of studies have suggested that fracturing occurs once a critical strain-rate value has been exceeded (*e.g.* Meier, 1958; Vornberger and Whillans, 1990). However, field observations by Hambrey and Müller (1978) suggest that this is not the case, concluding that there is not a simple relationship between principal tensile strain-rate and crevasse initiation. Other authors propose that a critical tensile stress must be met to induce crevassing (*e.g.* Kehle, 1964). Vaughan (1993) further developed this idea producing stress failure envelopes for 17 polar and alpine glaciers. This data suggests that the tensile stress required for the fracture of glacier ice is variable, but generally lies in the range of 90 - 320 kPa (Vaughan, 1993; van der Veen, 1998a, b; Benn and Evans, 2010; Campbell et al., 2013), whereas Forster et al. (1999) found that tensile stresses in the range of 169 - 224 kPa is sufficient for crevasse formation in temperate ice. Vaughan (1993) also found no systematic relationship between tensile strength and temperature, in contrast to Meier's (1958) assumption that cold ice has a greater tensile strength than warm ice. Vaughan (1993) suggested that variations in tensile strength could be explained by differences in ice rheology (*e.g.* ice crystal size, orientation, impurity content, or density) (Vaughan, 1993; van der Veen, 1998a; Campbell et al., 2013), a conclusion reiterated by Whillans et al. (1993) who suggested

that surface crevasses preferentially form in veins of recrystallized ice with a softer rheology to the surrounding ice (van der Veen, 1998a).

The depth to which crevasses propagate has also been an area of debate. Applied tensile stress often exceeds the tensile strength of the ice throughout the full thickness of the ice mass; however, crevasses tend to be confined to a shallow surface layer (Benn and Evans, 2010). As crevasse penetration depth increases the deviatoric tensile stress that pulls the walls of the crevasse apart become increasingly offset by the compressive stress exerted by the overburden pressure of the overlying ice (Benn and Evans, 2010). Nye (1955) therefore concluded that for closely spaced crevasses the maximum fracture depth can be defined as the point where the tensile stress equals the overburden compressive stress (Nye, 1955; 1957; van der Veen, 1998a; Benn et al., 2007; Benn and Evans, 2010). Even though this is a good model for crevasse penetration depths in areas of closely spaced crevasses, Weertman (1973) argued that single crevasses could penetrate to a much greater depth. For an isolated fracture in a stressed material, stress concentrates at the crack tip, amplifying the applied stress at that point. As a result, crevasse depth may be significantly increased. However, the effect of stress concentration is comparatively small in highly crevassed areas (van der Veen, 1998a; Benn and Evans, 2010). The presence of water in a crevasse can also have a large influence over the depth to which the fracture can penetrate (Weertman, 1973; Robin, 1974; van der Veen, 1998a; Boon and Sharp, 2003; Alley et al., 2005; Fountain et al., 2005a, b; Benn et al., 2007; Benn and Evans, 2010). In a water-filled crevasse, the pressure exerted by the weight of the water (as water is slightly more dense than ice) acts in the same direction as the deviatoric tensile stress, forcing the crevasse walls apart. As the crevasse propagates deeper the pressure exerted by the increasing water column (provided there is a sufficient supply of water) enables the fracture to penetrate further, eventually reaching the bed (van der Veen, 1998a, 2007; Alley et al., 2005; Benn et al., 2007, 2009; Benn and Evans, 2010). Crevasse propagation to the bed has important implications for meltwater drainage in Arctic glaciers (*e.g.* Boon and Sharp, 2003; Benn et al., 2009), temperate glaciers (*e.g.* Fountain et al., 2005a, b; Benn et al., 2009; Gulley, 2009), ice sheets (*e.g.* Alley et al.,

2005; Das et al., 2008; Doyle et al., 2013), and for ice shelf break-up (*e.g.* Scambos et al., 2000).

Basal crevasses are fractures that propagate from the bed of a glacier or base of an ice shelf up into the ice mass. Originally suggested by Weertman (1973), van der Veen (1998b) demonstrated that basal crevasses could only exist under specific circumstances. To overcome the high overburden compressive stresses present at the base of an ice mass, large tensile stresses and very high basal water pressure is required (van der Veen, 1998b; Benn et al., 2007; Benn and Evans, 2010). It is likely that these conditions are almost exclusively met when ice is rapidly extending and near flotation (or floating) (Benn and Evans, 2010), primarily associated with tidewater glaciers (Mickelson and Berkson, 1974). Very little data has been collected on basal crevasses; however, it has been suggested that they play a role in ice calving processes (*e.g.* Venteris, 1997; Benn et al., 2007). Formation of basal crevasses in valley glaciers is very unlikely except in exceptional circumstances. Crevasse-squeeze ridges in glacier fore-fields suggests that there could be sufficiently high basal water pressures to develop basal crevasses during a surge phase (*e.g.* Kamb et al., 1985; Sharp, 1985; Lawson, 1996; Evans and Rea, 1999; 2003; Evans et al., 2007; Benn and Evans, 2010; Rea and Evans, 2011), a jökulhlaup (*e.g.* Kozarski and Szupryczynski, 1973), or in glaciers with an overdeepening (*e.g.* Ensminger et al., 2001).

Studies of buried crevasses in Antarctica have been used to estimate the amount of time since the fractured ice had been exposed to areas of high stress (*e.g.* Shabtaie and Bentley, 1987; Retzlaff and Bentley, 1993; Clarke et al., 2000). This technique assumes that crevasses only develop at the ice surface and subsequently become buried when passively transported down-glacier. The depth of crevasse burial is then used to estimate the amount of time elapsed since that area of ice was exposed to sufficiently high stresses to initiate crevassing. However, it has been suggested that this assumption may be incorrect and subsurface as well as surface crevasse formation may be possible (Nath and Vaughan, 2003). Nath and Vaughan (2003) found that crevasse formation could occur at depths of several metres in areas absent from surface crevassing, also demonstrating that starter cracks could form not only at the surface, but also at depths of 10 - 30 metres (Nath and Vaughan, 2003).

Crevasse patterns vary greatly depending on the spatial distribution of the factures on the glacier and the strain regime present during formation; therefore, they can be useful indicators of the ice-dynamics experienced within an ice mass (Harper et al., 1998; Herzfeld et al., 2004; Hudleston, 2015). It is common to assume that crevasses are Mode I fractures that develop normal to the principal tensile stress direction (Nye, 1952; van der Veen, 1998a; Benn et al., 2007); thus, by observing different crevasse patterns it is possible to deduce the stress configuration required for their initial formation (Nye, 1952; Benn and Evans, 2010; Cuffey and Paterson, 2010). This assumption is not perfect as field measurements have found that crevasses do not always perfectly align with the principal stress axes (Kehle, 1964; Whillans et al., 1993). van der Veen (1998a, b) suggested this was probably a result of mixed mode fracture with Mode II fractures superimposed on Mode I fractures. A further complicating factor is the deformation and rotation of crevasses subsequent to formation (Benn et al., 2007). Nevertheless, crevasses patterns are useful for inferring surface strain and consequently stress configurations when detailed ice flow data is not available. When considering crevasse formation at the surface of a glacier, the maximum principal tensile stress direction is determined by the relationship between three strain-rate components (σ_{xx}, σ_{yy}, τ_{xy}: explained in detail in *section 2.3*) (Benn et al., 2007). The origin of common crevasse patterns is discussed in turn below:

Chevron crevasses: are linear fractures orientated obliquely up-glacier that form as a result of simple shear (τ_{xy}) derived from lateral drag at the glacier margins. The direction of maximum extension in simple shear regimes is orientated down-glacier at 45° to the direction of flow (x-axis). Chevron crevasses open perpendicular to the plane of maximum extension thus form obliquely up-glacier intersecting the glacier margins at 45°. Primarily associated with valley glacier margins, chevron crevasses can also form at the boundary between fast flowing and relatively immobile ice, often observed at the margins of ice streams.

Transverse crevasses: develop in areas primarily experiencing longitudinal extension (pure shear in the x-direction: σ_{xx}). The principal tensile stress is

longitudinal, therefore linear crevasses develop normal to the direction of maximum extension (Benn et al., 2007; Benn and Evans, 2010; Cuffey and Paterson, 2010). Transverse crevasses typically develop near the centreline of extending valley glaciers or in icefalls where pure shear dominates. However, they can extend towards the glacier margins where the crevasses become increasingly rotated as a result of simple shear at the glacier margins (Benn and Evans, 2010).

Longitudinal crevasses: form in areas dominated by transverse extension (pure shear in the y-direction: σ_{yy}), developing linear fractures orientated normal to the principal stress tensor (parallel to the x-direction). Longitudinal crevasses are primarily found in areas where the glacier tongue broadens, such as in a widening valley or after a constriction in the glacier trough (*e.g.* Meier, 1960).

Splaying crevasses: develop in areas of longitudinally compressive flow. Near the centreline of the glacier where the effects of laterally induced simple shear is negligible, linear longitudinal crevasses develop resulting from transverse extension (in the y-direction: σ_{yy}). However, towards the glacier margins a combination of longitudinal compression (σ_{xx}) and simple shear (τ_{xy}) rotates the principal tensile stress so that it is orientated at more than 45° to the x-axis, bending the crevasses so that they meet the glacier sides at less than 45°.

Radial crevasses: result from the unconfined lateral spreading of ice, primarily associated with piedmont glaciers; yet are commonly observed at the snout of valley glaciers that are no longer confined by its valley sides or lateral moraines. Divergence of flow at the glacier terminus causes margin-parallel extension, thus crevasses develop at right angles to the glacier margin forming a radial pattern (Cuffey and Paterson, 2010).

En-echelon crevasses: develop in response to simple shear and rotation, conditions usually found on the outside of a bend at the glacier margin. Typically found in extensional regimes with lateral velocity gradients perpendicular to flow, en-echelon crevasses initially form offset chains of comparatively short linear fractures normal to flow direction, analogous to tension gashes in geology (Hambrey and Lawson, 2000; Herbst and Neubauer, 2000; Hudleston, 2015). However, continuing ductile

deformation can rotate the central section of the crevasses, altering the fracture into a sigmoidal shape. It is therefore possible to differentiate between different generations of en-echelon fracture by observing the differing amounts of rotation (Benn and Evans, 2010).

Inter-crevasse blocks: develop in highly crevassed areas where pinnacles of ice (also known as seracs) remain between crevasses. Usually found in icefalls, irregular bed topography combined with extensional flow is necessary for inter-crevasse block formation. Block collapse is common as seracs become unstable as a result of glacial movement and surface ablation (Benn and Evans, 2010). Accumulation of ice debris from block collapses often forms an ice breccia (previously discussed in *section 2.5.1*).

Once formed, crevasses get passively transported down-glacier into different stress regimes where crevasse shape, orientation, and dip are modified. It is common for crevasse patterns to completely change when entering new stress regimes (Hambrey and Lawson, 2000; Benn and Evans, 2010; Hudleston, 2015). Crevasses often cease to remain as open fractures during this process and close to form crevasse traces. This is especially evident at the glacier margins where simple shear rotates and closes crevasses, often opening new crevasses that are orientated in a more favourable direction for the new stress regime (Benn and Evans, 2010). Chevron crevasses that initially form obliquely up-glacier gradually rotate down-glacier as a result of simple shear (Cuffey and Paterson, 2010); whereas initially concave down-glacier transverse crevasses become increasingly arcuate down-glacier resulting from pure shear in the middle reaches of the glacier and simple shear at the margins. Observations of deformed crevasses and crevasse traces can prove useful for inferring ice flow velocities and changing stress regimes (Vornberger and Whillans, 1990; Hambrey and Lawson, 2000; Herzfeld et al., 2004; Benn and Evans, 2010; Cuffey and Paterson, 2010; Jennings et al., 2015; Hudleston, 2015).

2.5.3.2 Faults

A number of different types of fault have been observed in glaciers. The types of fault that develop are dependent on the stress regimes present and the geometry of the glacier trough (Hambrey and Lawson, 2000; Herbst and Neubauer, 2000; Cuffey and Paterson, 2010; Hudleston, 2015).

Normal faults: are predominantly found along or near the lateral margins of glaciers, resulting from horizontal extension perpendicular to the margin (Herbst et al., 2006). Ablation induces slumping or relaxation of ice that is no longer constrained by the valley walls. Fault planes predominantly plunge steeply towards the glacier margin, displaying downward displacement in the direction of dip. Normal faults have also been observed at the glacier snout where the ice mass is no longer confined by its lateral moraines (Herbst and Neubauer, 2000), where subglacial cavities have collapsed (*e.g.* Herbst et al., 2006; Jennings et al., 2014), in relation to a glacial depression (*e.g.* Herbst et al., 2006), as a result of a glacier downwasting into a subglacial overdeepening (Phillips et al., 2014), or in icefalls where the downstream walls of crevasses collapse under their own weight (Cuffey and Paterson, 2010).

Strike-slip faults: develop where horizontal tension and compression are orientated perpendicular to one another (Cuffey and Paterson, 2010), in stress regimes where the maximum and minimum principal stresses (σ_1 and σ_3 respectively) reside in the horizontal plane and the intermediate principal stress (σ_2) is vertically orientated (fracture mode II). Also referred to as 'tear faults', strike-slip faulting is relatively uncommon in glacier ice, but can be seen on a small scale when they cross-cut and offset crevasses and crevasse traces (Hambrey, 1976b; Cuffey and Paterson, 2010). In their own right, strike-slip faults are usually linear vertical fractures; however, it is more common for structural weaknesses such as crevasse traces to be reorientated and reactivated as strike-slip faults. Transverse crevasse traces become increasingly convex down-glacier over time, reorientating the limbs of the crevasse trace parallel to flow. Simple shear acting along the crevasse trace's limbs reactivates it as a strike-slip fault, displacing the ice on either side of the fracture (Hambrey, 1976b; Cuffey and Paterson, 2010).

Thrust faults: occur where there is longitudinal compression, usually at or near the glacier snout in relation to rapid advances, slow moving ice obstructing flow, or where there is a topographic obstruction (Hambrey and Lawson, 2000; Herbst and Neubauer, 2000; Herbst et al., 2006; Benn and Evans, 2010; Cuffey and Paterson, 2010; Phillips et al., 2014; Hudleston, 2015). Slow moving or stagnant ice at the glacier terminus can act as an obstacle to faster moving ice up-glacier; therefore the faster moving ice overrides the slower by way of a thrust fault (Sharp et al., 1988; Clarke and Blake, 1991; Hambrey et al., 1996, 1997; Hambrey and Lawson, 2000; Phillips et al., 2014). This process is particularly common in land-based polythermal glaciers where the margins of the glacier are frozen to the bed, acting as an obstacle for the interior zone of temperate sliding ice (Figure 2.11) (*e.g.* Clarke and Blake, 1991; Hambrey and Dowdeswell, 1997; Hambrey et al., 1996, 1997, 1999, 2005;

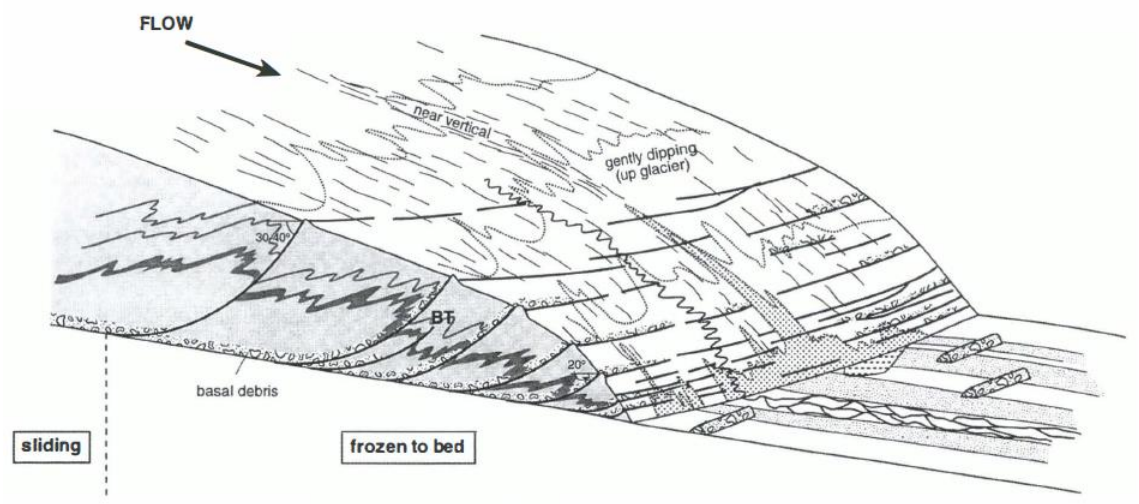

Figure 2.11. A three-dimensional schematic diagram showing the formation of thrusts in the snout of a typical polythermal Svalbard valley glacier (Hambrey et al., 1999).

Glasser et al., 1998; Murray et al., 2000; Glasser et al., 2003; Swift et al., 2006); however, thrust faults have also been observed in Alpine valley glaciers where crevasse traces have been reactivated against a reverse bed slope (*e.g.* Herbst and Neubauer, 2000; Goodsell et al., 2005b; Herbst et al., 2006). Thrusts often form small steps at the surface of the glacier (Cuffey and Paterson, 2010) with the thrust plane

dipping up-flow. Dip angles are generally shallow, although some observations of over-steepened thrusts have been documented (Herbst and Neubauer, 2000). Mapping of thrust planes indicate that they are arcuate at the surface of the glacier suggesting a spoon-shaped plane; however, this geometry may be amplified by greater ice flow velocities in the centre of the glacier (Herbst and Neubauer, 2000; Herbst et al., 2006). Thrust faults do not always reach the surface of the glacier, and may die out within the body of the glacier to develop 'blind thrusts' (Hambrey and Lawson, 2000). However, the conditions required for any type of thrust fault to develop as a new structure has been questioned by Moore et al. (2010) who concluded that the criterion required for compressive fractures in ice is rarely met, suggesting that thrusting in glacier ice is only plausible if a pre-existing structural weakness or fracture is already present. It has been suggested that thrust faulting is likely to occur where the lower limb of recumbent folds in basal ice become attenuated, eventually developing a narrow shear zone or discrete thrust fault (Hambrey and Lawson, 2000). Alternatively, favourably-orientated crevasse traces (*e.g.* Hambrey and Müller, 1978; Goodsell et al., 2005b) or previously existing thrust faults (*e.g.* Lawson et al., 1994; Hudleston, 2015) have been identified as planes of weakness that may be exploited by thrust faults. Despite the debate about thrust fault formation, observations have convinced many researchers that thrusting is an active process in many glaciers that can play an important role in debris entrainment. Basal debris can often be englacially incorporated or elevated to the surface of the glacier along thrust faults (Hambrey et al., 1999, 2005; Herbst and Neubauer, 2000; Glasser and Hambrey, 2002; Glasser et al., 2003; Herbst et al., 2006; Benn and Evans, 2010; Hudleston, 2015). Basal debris can be elevated as slabs of debris laden basal ice are overthrust stagnant or slower moving ice. Alternatively, subglacial debris can be transported along thrust planes by simple shear, water flow, or sediment injection (Benn and Evans, 2010). The resulting debris-filled structures have been highly debated, and in some cases interpreted as crevasse fills (*e.g.* Evans and Rea, 1999; Woodward et al., 2002; Glasser et al., 2003); however, the presence of drag folds indicates that thrusting was active during the formation of many other examples of these structures (Benn and Evans, 2010).

2.5.3.3 Crevasse traces (water-filled crevasses)

Healed water-filled crevasses form planar scars (known as crevasse traces) that comprise relatively thin blue layers of coarse clear ice (Hambrey, 1975, 1994; Hambrey and Lawson, 2000; Benn and Evans, 2010; Jennings et al., 2014). Ice crystals grow perpendicular to the crevasse edges as meltwater refreezes, forming large crystals that join to form a suture that runs along the centre of the fracture. In some cases crevasse traces may comprise thin white bubbly ice where there has been snow infill of the fracture (Benn and Evans, 2010). In both types of crevasse trace, debris may be present where supraglacial debris has fallen into the open crevasse, providing an important source of englacial debris entrainment for some glaciers. In extreme cases, debris-filled crevasse traces can form where a crevasse fills with supraglacial debris and subsequently closes (Gulley and Benn, 2007). This is rarely seen on small valley glaciers; however, it is very common on debris-covered glaciers where the debris-filled crevasse can provide a route for englacial water flow (Benn and Evans, 2010). Crevasse traces are structural weaknesses that can be reactivated and exploited as strike slip or thrust faults. Crevasse traces become increasingly arcuate resulting from rotation and differential flow, re-orientating the fracture into favourable positions for displacement to occur along the weakness (Hambrey and Lawson, 2000).

2.5.4 Combined brittle/ductile structures

2.5.4.1 Basal ice

Basal ice can be separated from other types of glacier ice based on unique physical and/or chemical characteristics that it has acquired at the basal zone of an ice mass (Hubbard et al., 2009). Study of basal ice facies is important for deducing the conditions and processes occurring at or near to the bed that cannot be directly observed. Consequently, a great deal of research has been conducted on basal ice (*see reviews by* Hubbard and Sharp, 1989; Alley et al., 1997; Knight, 1997; Hubbard et al., 2009). Many previous studies have attempted to separate different ice types into discrete classifications, assuming that similar ice facies are derived from the same

formation process or have undergone the same influences post-formation (Hubbard et al., 2009).

2.5.4.2 Shear zones

Shear zones are tabular areas that experience noticeably higher strain than the surrounding area, often associated with thrusting and foliation, but can also be evident in areas of crevasse formation (Hudleston, 1989, 2015; Hambrey and Lawson, 2000). A combination of ductile and brittle deformation is often seen in shear zones with initial ductile deformation becoming superseded by brittle fracture when the brittle strength of the ice is exceeded. Simple shear can also modify ice crystals by breaking down large ice crystals to develop a fine-grained ice in a similar fashion to cataclasis in metamorphic rocks; however, ice crystal growth can also be promoted depending on the balance of constructive and destructive processes active during deformation (Hambrey and Lawson, 2000). Simple shear is an important process for the formation and development of a number of glacier structures (*e.g.* transposition foliation, *see section 5.2*); however, discrete shear zones are primarily observed at flow unit boundaries in areas of strong longitudinal foliation, in areas of active crevasse formation and strike-slip faulting, or parallel to thrust faults (Hambrey and Lawson, 2000).

At the confluence of two flow units, enhanced simple shear tightly folds and transposes primary stratification into a strong longitudinally orientated transposition foliation (*see section 2.5.2*). It is at or near to flow-unit boundaries that shear zones composed of comparatively thin layers (sometimes called shear bands) of fine-grained white ice can often be observed (*e.g.* Hambrey, 1977a; Hambrey and Lawson, 2000; Jennings et al., 2014). The presence of fine-grained ice is evidence of crystallographic modification of pre-existing ice layers (Jennings et al., 2014). Simple shear acting along longitudinally orientated ice layers breaks down large ice crystals forming pronounced bands of fine-grained white ice, analogous with mylonite zones found in rocks that have undergone ductile deformation as large shear strains accumulate (Hambrey and Lawson, 2000).

Shear zones can also be observed where strike-slip faulting occurs in areas of active crevassing, or where crevasse traces are reactivated. Bending of passive marker layers (*e.g.* longitudinal foliation) within the shear zone occurs as a result of ductile deformation, displacing the layering and forming hook folds (sometimes called drag folds) that bend towards the fracture. Ductile deformation continues to displace layering until the brittle strength of the ice is exceeded and brittle fracture is initiated (Hambrey and Lawson, 2000).

Sheared ice is often observed parallel to thrust faults, where ductile deformation deforms englacial layers (*e.g.* longitudinal foliation) before brittle fracture is initiated. Evidence of thrust fault related shear zones has been observed in surge-type glaciers in Svalbard (*e.g.* Hambrey et al., 1996), where shear zones evident on the surface of the glacier reached up to several tens of metres in length. Further evidence of ductile shear zones has been observed in Variegated Glacier with the formation of foliation boudinage following the 1982-83 surge (Lawson, 1990; Hambrey and Lawson, 2000).

2.5.4.3 Ogives

Ogives are alternating arcuate bands or waves occasionally seen below icefalls in valley glaciers. The convex down-glacier nature reflects ice flow differences across the breadth of the glacier. Ogives can be separated into two categories, band ogives (sometimes referred to as Forbes bands) and wave ogives (sometimes referred to as swell and swale ogives); however, they can often be seen simultaneously (Post and LaChapelle, 1971; Waddington, 1986; Hambrey and Lawson, 2000; Goodsell et al., 2002; Benn and Evans, 2010; Cuffey and Paterson, 2010). Band ogives consist of alternating dark bands of highly foliated debris-rich ice and light bands of coarse bubbly ice, whereas wave ogives are arcuate surface undulations which can have a maximum amplitude of *c*. 5 metres directly below an icefall (Goodsell et al., 2002; Herbst et al., 2006; Benn and Evans, 2010). Band ogives have a three-dimensional geometry often compared to stacked spoons with dip orientated up-stream. At present no consensus on ogive formation has been reached, especially with regard to

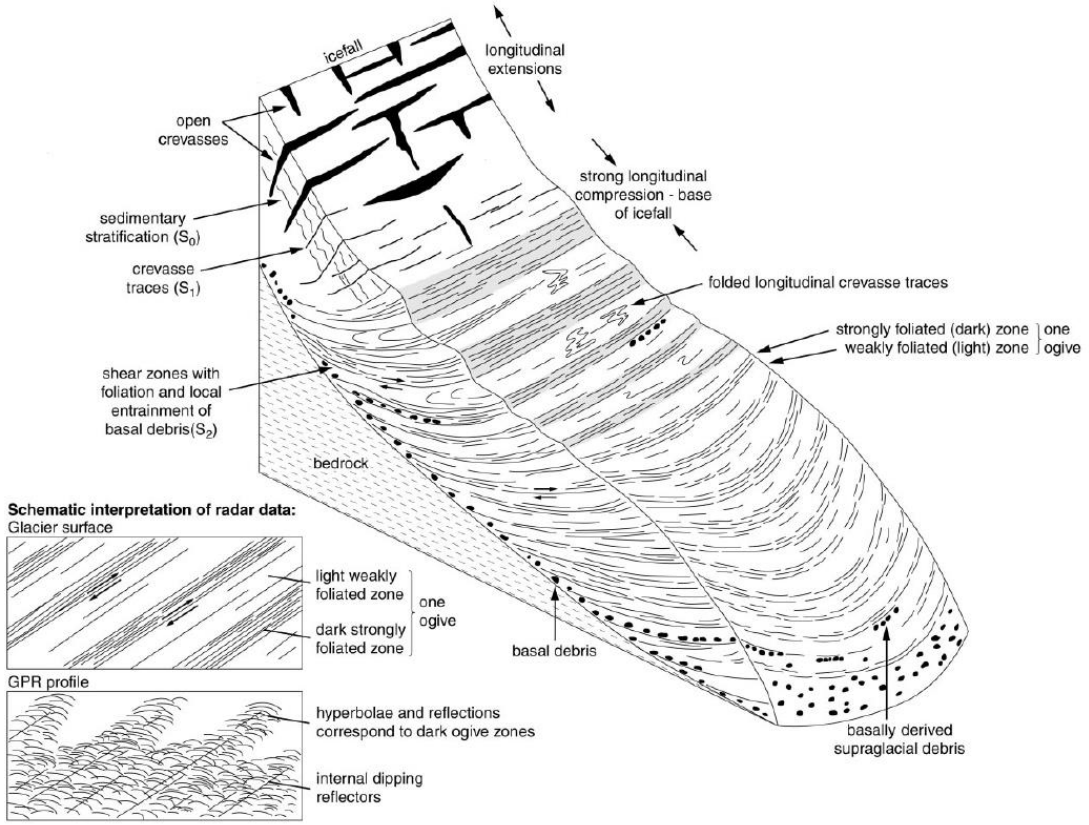

Figure 2.12. A three-dimensional schematic diagram showing the formation of ogives below an icefall (Goodsell et al., 2002).

band ogives. There is general acceptance that wave ogive formation is a result of seasonal variations in ablation as ice velocity increases when entering an icefall, creating a wave and trough morphology for each year's movement of ice through an icefall (Hambrey and Lawson, 2000). Extension and resultant thinning of the ice ensures that ice in the icefall has an increased surface area. Therefore, comparatively more ablation during the summer months is reflected in a surface lowering that forms the wave troughs, whereas ridges reflect ice passage during the winter months when snow accumulates and raises the surface. This model has also been used to explain the formation of band ogives, suggesting that the troughs act as sediment traps during the summer months (Nye, 1958, 1959b; Waddington, 1986; Benn and Evans, 2010).

However, Goodsell et al. (2002) proposed that dark ogive bands were the surface expression of intense up-glacier dipping (transverse) foliation formed in shear zones present at the base of an icefall (Figure 2.12). Intense longitudinal compression found at the base of an icefall forms strongly foliated ice as a result of folding and/or thrusting. Colour variation between ogive bands can be explained by the varying intensity of foliation; however, debris with subglacial characteristics has been found in dark ogive bands in both Alpine and Icelandic glaciers (Goodsell et al., 2002; Spedding and Evans, 2002; Swift et al., 2006).

2.5.4.4 Crevasse traces (tensional veins)

Crevasse traces resulting from the refreezing of meltwater in open crevasses have been discussed in *section 2.5.3*. However, a second form of crevasse trace can also develop as a structure in its own right. Tensional veins are fractures that form as a result of tensile fracturing (fracture Mode I), yet the fracture walls remain in contact. Valley glacier crevasse traces can typically extend for several hundred metres, a distance that is much longer than the majority of open crevasses. As such, it has been suggested that tensional veins can form as lateral and vertical extensions of open crevasses (*e.g.* Hambrey, 1976b; Hambrey and Müller, 1978; Goodsell et al., 2005b; Jennings et al., 2014) in a similar fashion to tensional veins found in deformed rocks (Durney and Ramsay, 1973). The presence of so many crevasse traces in comparison to open fractures, combined with observations of crevasse traces located within or close to areas of open crevasses suggests that many fractures primarily form as tensional veins in their own right and do not experience any opening (*e.g.* Jennings et al., 2014). Additionally, the ubiquitous nature of crevasse traces on many glaciers despite undergoing substantial ablation indicates that fracture propagation must be relatively deep, possibly reaching the bed (*e.g.* Hambrey and Müller, 1978; Goodsell et al., 2005b; Jennings et al., 2014, 2015), a further indication that many fractures experience little if any opening.

2.5.5 Hydrological-derived structures

2.5.5.1 Supraglacial channels

Ice structure combined with glacier surface topography has a very strong influence over the initial formation of supraglacial channels. Glaciers with convex cross-sectional profiles often have marginal streams where supraglacial water has drained to the lateral margins of the glacier, whereas glaciers with concave cross-sections usually develop supraglacial channels in the middle-reaches of the glacier (Hambrey, 1977b). It is common for supraglacial meltwater channels to preferentially form along favourably orientated ice structures such as steeply dipping longitudinal foliation as a result of differential weathering of different ice types (Hambrey, 1977b; Jennings et al., 2014). Structurally controlled channels that develop in strongly foliated areas are often comparatively small and linear in nature (*e.g.* Jennings et al., 2014). As supraglacial channel size increases, the control that ice structure has over channel morphology decreases. Large meandering supraglacial channels are no longer controlled by layered structures such as longitudinal foliation; however, fractures that intersect channels often divert water-flow or develop as moulins (*see* hydrofracturing, *section 2.5.3*) (Stenborg, 1968, 1969, 1973; Hambrey, 1977b; Benn et al., 2009; Gulley et al., 2009b; Benn and Evans, 2010; Jennings et al., 2014).

2.5.5.2 Cut and closure systems

Supraglacial meltwater channels are usually ephemeral features that close as a result of ice creep during the winter months, subsequently reforming in a different location during the following melt-season. However, in certain circumstances, channel incision rates can exceed surface melting of the surrounding ice, allowing perennial supraglacial channels to develop. The development of perennial supraglacial channels is favoured in cool environments where surface ablation is relatively low, yet there is still a high surface discharge (*i.e.* where a channel drains a large catchment) to enable high incision rates (Benn and Evans, 2010). As supraglacial channels deeply incise into

the glacier, the conduit's roof can close as a result of ice creep, or become blocked by drifted snow or refrozen meltwater (Fountain and Walder, 1998; Gulley et al., 2009a, b; Benn and Evans, 2010). Continuing channel incision through the ice mass can eventually reach the glacier bed; however, conduit blockages resulting from the refreezing of meltwater during the winter can divert the channels course. Englacial conduits formed in this fashion are usually highly sinuous with shallow channel gradients separated by steep cliffs (nickpoints) along its length. A prominent suture is usually present running along the roof where the channel walls have closed up in response to ice creep (Gulley et al., 2009a; Benn and Evans, 2010).

2.5.5.3 Crystal quirks

Circular or elliptical void structures (crystal quirks) are commonly observed on the surface of glaciers. Voids are usually water-filled or fully-healed, with a variety of sizes that can attain diameters of up to several metres. Fully-healed crystal quirks rarely exceed *c*. 1 metre in diameter and consist of blue ice crystals that grow parallel to the structure's edge, forming a suture in the centre (Figure 2.13) (*e.g.* Jennings et al., 2014). Crystal quirks are the remnant voids of moulins and englacial conduits which have closed up (Stenborg, 1968; Goodsell et al., 2005b; Jennings et al., 2014). In most glaciers supra- and englacial channels rarely occupy the same course for more than a year, and on glaciers that have sufficiently high ice-flow velocities, old meltwater channels tend to close during the winter as a result of ice deformation (Hambrey, 1977b). However, conduits rarely fully heal and the remaining voids eventually get exposed at the surface of the glacier by ablation. Once at the surface meltwater often accumulates in the crystal quirks, enabling smaller voids to recrystallize. Stagnant pools contained in larger crystal quirks act as sediment traps for aeolion-derived dust. It is common for prominent mounds of silt nodules to remain on the surface of a glacier when ablation of the surrounding ice melts-out a crystal quirk revealing the sediment that has been trapped within it (Jennings et al., 2014).

Figure 2.13. A partially-healed crystal quirk at the surface of Vadrec del Forno. Note the coarse clear ice crystals growing perpendicular to the edge of the structure, and forming a suture where they join in the centre. Photograph courtesy of M. J. Hambrey.

2.5.6 Up-scaling to ice sheets

2.5.6.1 Flowlines

Longitudinal surface structures commonly found in Antarctica and Greenland are most prominent on the surface of fast-flowing ice streams and outlet glaciers; however, their formation and significance is poorly understood (Glasser and Gudmundsson, 2012). A wide range of literature has previously referred to these structures by many names, such as flow stripes (*e.g.* Casassa and Brecher, 1993), flow bands (*e.g.* Swithinbank et al., 1988), flow traces (*e.g.* Merry and Whillans, 1993), or streaklines (*e.g.* Hulbe and Fahnestock, 2004, 2007) to list a few. However, longitudinal surface structures will be subsequently referred to as flowlines in this paper (*following* Crabtree and Doake, 1980). At present there is no consensus on what flowlines are and how they form. Glasser and Gudmundsson (2012) provided a brief summary of

previous literature regarding the formation of flowlines highlighting the wide range of possible formation processes. Glasser and Gudmundsson (2012) also demonstrated that flowlines can develop in two main circumstances: (i) where ice converges around nunataks or at the confluence of flow units and (ii) within glacier flow-units. In the former circumstance, clear and narrow flowlines are defined on the surface of the glacier. A conceptual model developed by Glasser and Gudmundsson (2012) illustrates how flowlines form at the confluence of flow units; however, a consensus on the formation of the second type of flowline has yet to be reached. Two of the leading hypotheses suggest that flowlines are the surface expression of three-dimensional structures, such as macro-scale folds or longitudinal foliation (*e.g.* Reynolds and Hambrey, 1988; Hambrey and Dowdeswell, 1994), or develop as ice flows over irregular features at the bed of the ice sheet (*e.g.* Gudmundsson et al., 1998; Hulbe and Fahnestock, 2004, 2007; Raup et al., 2005). Despite disagreement on a unified formation processes, it seems likely that flowline structures may encompass a number of longitudinal structures that have different formation processes, yet have similar looking surface expressions.

2.5.6.2 Boudins

An in-depth analysis of boudinage formation in valley glaciers has been covered in *section 2.5.2*. However, boudins also develop on a much greater scale in large polar outlet glaciers and ice streams, as well as in the centre of ice sheets (*e.g.* Gow, 1972; Cunningham and Waddington, 1990; Marmo and Wilson, 2000). Understanding boudinage structures on this scale is very important, especially with regard to the stratigraphic disturbances boudins can have on deep ice cores (Staffelbach et al., 1988; Cunningham and Waddington, 1990). It is common to observe folds, kink bands, and shear zones near the lateral margins of ice sheets as a result of basal shear (*e.g.* Hudleston, 1976); however, the majority of ice sheet models predict that the stratigraphic layering near ice divides should be preserved in their correct chronological order (Waddington et al., 2001). Nevertheless, a lack of stratigraphic correlation between two deep ice cores from the centre of the Greenland Ice Sheet

has led some researchers to look at the possibility of folding or boudinage to occur at ice divides. Waddington et al. (2001) demonstrated that it is possible for overturned folds to exist near ice sheet centres, possibly introducing errors into deep ice core stratigraphy. Cunningham and Waddington (1990) also demonstrated that boudin structures can develop at or near ice divides, with the implication that ice layers may be interpreted as erroneously thick or thin depending if the ice core intersects the boudin neck or swell. Therefore, numerical modelling of boudinage occurrence and behaviour (*e.g.* Cunningham and Waddington, 1990; Passchier and Druguet, 2002) is extremely important for identification of areas that should be avoided when coring.

2.6 Study-site descriptions

A wide range of glaciers are investigated in this study to enable the development of longitudinal foliation to be documented at a variety of spatial scales in contrasting topographic, climatic, and dynamic settings. A description of all the studied glaciers, including a review of the previous research conducted on each, can be found below.

2.6.1 Svalbard

Field-based research in this study is focused on four glaciers located in the Norwegian high-Arctic archipelago of Svalbard. All data were collected during a field campaign in the summer of 2013. The research conducted was based out of the settlement of Ny-Ålesund located on Brøggerhalvøya in northwestern Spitsbergen, the largest island in the archipelago of Svalbard. The four glaciers studied were Austre Brøggerbreen, Midtre Lovénbreen, Austre Lovénbreen, and Pedersenbreen, each of which are at an approximate latitude of 79° 55’ N (Figure 2.14) and are described in detail below. As for many glaciers in Svalbard, each of the four studied glaciers has receded and thinned substantially since the Neoglacial maximum *c*. 1900 AD, revealing the internal structure of the glaciers in remarkable detail. The surrounding geology of Brøggerhalvøya can be broadly separated in two groups: rocks of Proterozoic age, and rocks of Carboniferous and Permian age. The cirque headwalls and valley walls of

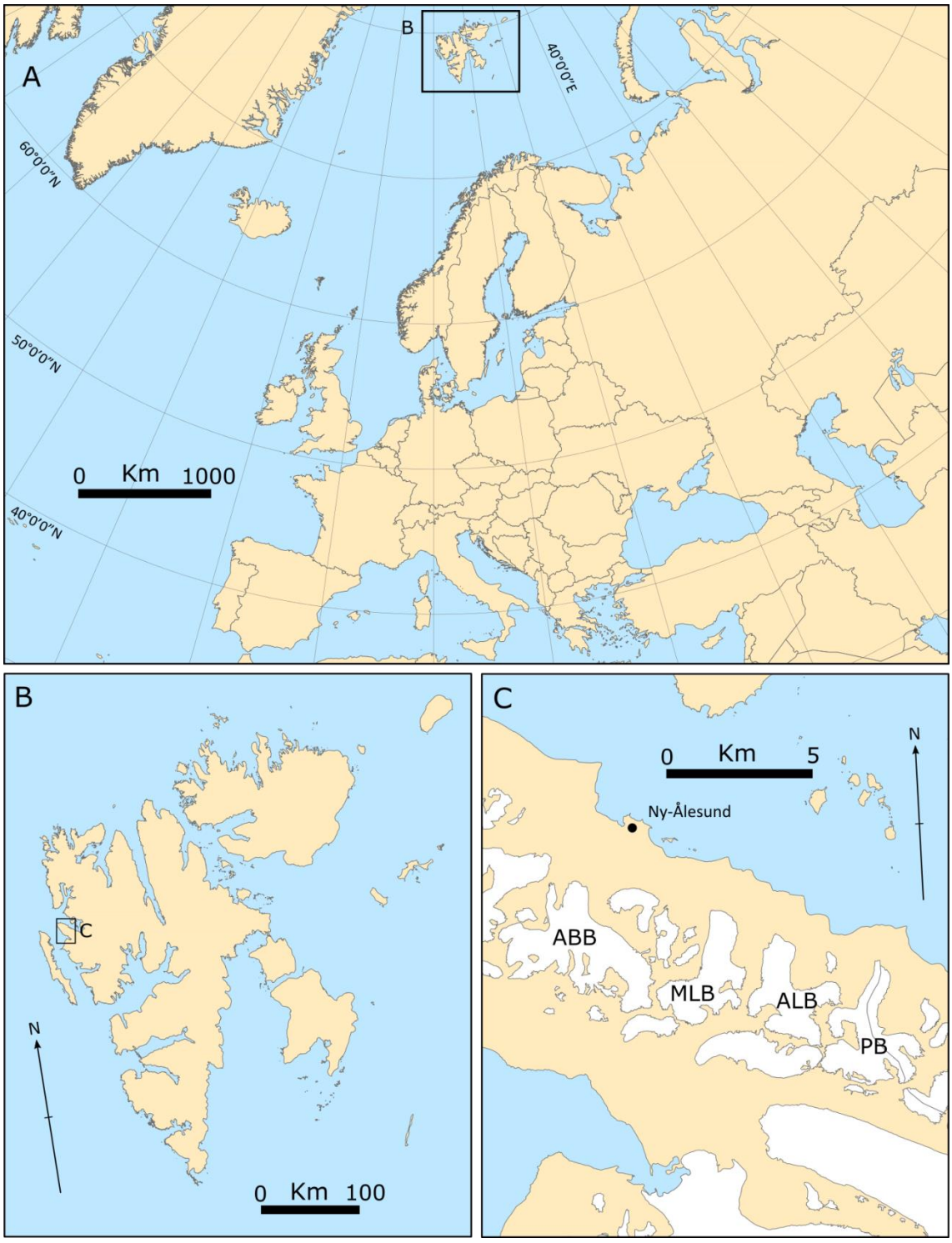

Figure 2.14. Location map: (A) the location of Svalbard in relation to continental Europe; (B) the location of Brøggerhalvøya in north-west Spitsbergen, the largest island in the Norwegian high-Arctic archipelago of Svalbard; (C) the location of Austre Brøggerbreen (ABB), Midtre Lovénbreen (MLB), Austre Lovénbreen (ALB), and Pedersenbreen (PB) in relation to the nearby research settlement of Ny-Ålesund. Map based on the location map in Jennings et al. (2015).

Midtre Lovénbreen, Austre Lovénbreen, and Pedersenbreen consist predominantly of metamorphic rocks of the Proterozoic Kongsvegen Group (Harland, 1997), which include phyllites, quartzite, garnet schist, amphibolite and marble (Glasser and Hambrey, 2001). The proglacial areas of Midtre Lovénbreen and Austre Lovénbreen contain rocks of the Gipsdalen Group, which include Carboniferous and Permian limestone, chert and dolostone. Furthermore, infrequent pockets of Ny-Ålesund Subgroup Palaeocene sandstone and conglomerate can be found in the proglacial zone of Austre Lovénbreen (Glasser and Hambrey, 2001). The surrounding geology of Austre Brøggerbreen is much more complex than for the other glaciers, with Palaeozoic sedimentary rocks having being thrust up and strongly folded with metamorphic rocks during the Palaeocene West Spitsbergen Orogeny (Harland, 1997; Glasser and Hambrey, 2001).

2.6.1.1 Austre Brøggerbreen

Austre Brøggerbreen (Figure 2.14) is a north-flowing valley glacier that comprises multiple accumulation basins that coalesce into a comparatively short and narrow tongue. The glacier had an area of *c*. 12 km^2 during in the 1990s (Hagen et al., 1993; Etzelmüller and Sollid, 1996), and initial ground penetrating radar (GPR) profiles at the thickest localities of the glacier identified areas of the glacier bed that were at the pressure melting point. However, subsequent ablation and surface lowering means that the glacier is now primarily composed of cold ice that is below the pressure melting point (Hagen and Sætrang, 1991), a conclusion that is supported by the lack of aufeis formation in the proglacial zone, suggesting that there is little to no water production at the base of the glacier (Stuart et al., 2003). The subglacial topography of Austre Brøggerbreen has been reconstructed from borehole measurements and radio-echo soundings (Hagen and Sætrang, 1991), and has a maximum thickness in the accumulation area of *c*. 110 metres (Björnsson et al., 1996); however, substantial ablation and surface-lowering over the past two decades has greatly reduced this. The glacier is also relatively inactive, with flow velocities ranging from 0.5 to 3.0 m a^{-1} (Hagen and Liestøl, 1990; Hagen et al., 1993).

2.6.1.2 Midtre Lovénbreen

Midtre Lovénbreen (Figure 2.14) is a north-flowing 4 kilometre-long valley glacier that comprises four accumulation basins feeding into a comparatively narrow tongue. The glacier has an equilibrium-line altitude of *c*. 395 metres above sea level and is known to be polythermal from radio echo soundings (Björnsson et al., 1996). Comparatively thick areas of temperate ice (up to 50 metres) lie beneath the accumulation area, whereas the terminus and lateral margins of the glacier are frozen to the bed (Björnsson et al., 1996; Hambrey et al., 2005). The glacier has had measured velocities taken at the equilibrium line in the centre of the glacier ranging from 4.4 to 7.3 m a^{-1} (Liestøl, 1988; Björnsson et al., 1996). However, records of the net mass balance of the glacier derived from ground surveys have been predominantly negative (Lefauconnier and Hagen, 1990). Complex sediment landforms related to ice structure can be found in the proglacial area of the glacier, plus extensive *Aufeis* (icings) form during the winter as drainage from the glacier persists year-round (Björnsson et al., 1996; Hodson et al., 1997; Hambrey et al., 2005). Midtre Lovénbreen is one of the most studied glaciers in the high-Arctic (only second to White Glacier on Axel Heiberg Island) and has had previous structural studies relating to the relationship between folding, foliation, and medial moraine formation, as well as a comprehensive whole-glacier structural study (Hambrey et al., 1997; Hambrey and Glasser, 2003; Hambrey et al., 2005). There has been a great deal of debate about whether Midtre Lovénbreen is, or was once, a surge-type glacier. Photographs dating from 1982 (*see* Hamberg, 1894) show Midtre Lovénbreen at its Neoglacial maximum with a near vertical ice cliff. Liestøl (1988) interpreted this as evidence that Midtre Lovénbreen was a surge-type glacier, a conclusion that was further supported by Hansen (2003) who suggested that Midtre Lovénbreen had surged in the past, but no longer could be classified as a surge-type glacier. However, work by Jiskoot et al. (2000) disagreed with this conclusion, and later structural glaciological work undertaken by Hambrey et al. (2005) also suggested that Midtre Lovénbreen was not a surge-type glacier, or had not surged in the past several hundred years.

2.6.1.3 Austre Lovénbreen

Austre Lovénbreen (Figure 2.14) is a small north-flowing valley glacier that is currently less than 4 kilometres in length. The glacier has four main accumulation basins that feed into a comparatively narrow tongue. As is the case for Midtre Lovénbreen, Austre Lovénbreen is a polythermal glacier based on the interpretation of a ground-penetrating radar survey conducted in 2010 by Saintenoy et al. (2013) (Midgley et al., 2013). However, the glacier is predominantly frozen to the bed, with only a small region of warm-based ice located at the thickest extent of the glacier. Ground-penetrating radar profiles have also highlighted the presence of an over-deepened basin below the glacier, starting *c*. 250 metres and extending to *c*. 2.7 kilometres up-glacier from the 2010 glacier terminus (Saintenoy et al., 2013). The mass balance of the glacier is likely to be similar to that of adjacent Midtre Lovénbreen, being predominantly negative. Mapping of the terminal position of Austre Lovénbreen in 1962, 1995, and 2009 shows that the glacier receded by *c*. 300 metres during the period 1962 to 1995, and by *c*. 75 metres from 1995 to 2009 (Friedt et al., 2012).

2.6.1.4 Pedersenbreen

Pedersenbreen (Figure 2.14) is a north-flowing valley glacier that is fed by five main accumulation basins. During the 1990s the glacier was 5.4 kilometres long and covered an area of 5.6 km^2 with an altitude range of 90 - 650 metres above sea level (Hagen et al., 1993; Bennett et al., 1996). The thermal regime of the glacier is not directly known; however, it has been suggested that it is likely to be similar to that of Midtre Lovénbreen and Austre Lovénbreen, *i.e.* polythermal with ice frozen to the bed at the glacier margins and temperate ice in the accumulation area (Hagen and Sætrang, 1991; Bennett et al., 1996). This hypothesis is further supported by the presence of *Aufeis* (icings) in the proglacial zone during the winter, indicating that water is discharged from the glacier during the winter months even when atmospheric temperatures are well below zero degrees (Bennett et al., 1996). Despite there being no historical evidence documenting Pedersenbreen as a surge-type glacier, structural evidence, and

the presence of a loop moraine on the glacier suggests that Pedersenbreen, or one of its tributaries, may have surged in the past (Bennett et al., 1996; Glasser et al., 2004).

2.6.2 Bylot Island

Bylot Island [72.5° N to 74° N, 76° E to 81° E] is found in Arctic Canada, located to the northeast of Baffin Island (Andrews, 2002). The island is dominated by the Byam Martin Mountains, which cover the length of the island in a northwest-southeast direction, and primarily consist of igneous and metamorphic rocks of Archaean/Aphebian age (Klassen, 1993). Consequently, central Bylot Island comprises rugged mountains with the highest peaks reaching *c*. 1900 metres above sea level, with elevations decreasing in all directions towards the coast (Dowdeswell et al., 2007). The present configuration of ice on Bylot Island comprises an ice cap that is drained by outlet glaciers that terminate either on land or at the coast, and comparatively small mountain glaciers that have become isolated from the ice cap. The ice extent at the end of 2001 was 4783 km^2, covering 43% of the island's 11,122 km^2 total area (Dowdeswell et al., 2007). Glaciers flowing out from the uplands of Bylot Island do so through a series of valleys, each of which originate from cirque headwalls. Identification of individual glacier basins is possible using nunataks and ridges, a process that is still possible despite there being ice cover over some ridgelines. Glaciers that extend onto the flat coastal plains tend to form piedmont lobes (Dowdeswell et al., 2007). Even though it is recognised that there are large numbers of surge-type glaciers in the Canadian Arctic islands (Copland et al., 2003), few have been positively identified on Bylot Island (Andrews, 2002). Dowdeswell et al. (2007) used high-resolution satellite imagery to identify possible surge-type glaciers, interpreting ten glaciers on Bylot Island to be of possible surge-type. Nevertheless, regardless of glacier type, all large glaciers on Bylot Island have retreated *c*. 0.9 to 1.8 km since their Neoglacial maxima that occurred approximately 120 years ago (Dowdeswell et al., 2007). The Canadian Arctic Archipelago contains one-third of the global terrestrial ice volume outside the ice sheets, and recent research has shown that the area is providing a significant contribution to eustatic sea-level rise (Gardner et al., 2011,

2012; Lenaerts et al., 2013). Recent loss from the area totals 61 ± 7 gigatonnes per year (Gt yr^{-1}) of ice, equating to 0.17 ± 0.02 mm yr^{-1} of sea-level rise (Gardner et al., 2011).

The Quaternary glacial history of Bylot Island has been investigated through stratigraphic relationships and distribution of marine deposits. Chronological evidence from radiocarbon and amino-acid dating have helped identify six Quaternary glacial episodes, three local, and three involving regional ice sheets (Klassen, 1993; Dowdeswell et al., 2007). At present, Bylot Island lies within an area of continuous permafrost (Irvine-Fynn et al., 2006), and Zdanowicz et al. (1996) suggested that many of the island's glaciers are currently polythermal.

2.6.2.1 Sermilik Glacier

Sermilik Glacier is a south-flowing large valley glacier that is located adjacent to Eclipse Sound that separates Bylot Island from its much larger neighbour, Baffin Island. The glacier used to be a marine-terminating glacier; however, as a result of recession it is currently a land-terminating glacier. From the Neoglacial maximum until 2001, Sermilik Glacier decreased in area by 9.3 km^2 and receded 1400 metres, yielding a retreat rate of 11.7 m a^{-1} (Dowdeswell et al., 2007). At present the glacier is *c*. 35 kilometres in length with a maximum glacier snout width of *c*. 4 kilometres.

2.6.3 Antarctica

The Antarctic Ice Sheet covers an area of *c*. 13.5 million km^2 with an ice volume of 25.4 million km^3 when including its fringing ice shelves (Benn and Evans, 2010). The ice sheet is divided into two unequal component parts, the East Antarctic Ice Sheet and the West Antarctic Ice Sheet, by the Transantarctic Mountains which run between the Weddell and Ross Seas. Large amounts of both ice sheets are grounded below sea level (Lythe et al., 2001; Bamber et al., 2007); however, if the remaining ice above sea level

were to melt, there would be the equivalent of 57 metres of sea-level rise (Lythe et al., 2001).

The East Antarctic Ice Sheet is the larger of the two ice sheets, and is composed of a comparatively flat dome. Ice drains from the dome towards the coast and through the Transantarctic Mountains, where it enters the West Antarctic Ice Sheet or the Ross Ice Shelf (Benn and Evans, 2010). Ice flow through the Transantarctic Mountains gets channelled by topography into large ice streams, whereas, ice discharge near the coast becomes focused in outlet glaciers and ice streams that are constrained by local ice domes or mountainous terrain.

The configuration of the West Antarctic Ice Sheet is more complex than the East Antarctic Ice Sheet, as it consists of three major ice domes with numerous other smaller ice domes (Benn and Evans, 2010). Ice discharge is controlled by topographic divides and can be split into three sectors, the Amundsen Sea sector, the Weddell Sea Sector, and the Ross Sea sector (Fahnestock and Bamber, 2001; Bindschadler, 2006; Benn and Evans, 2010).

2.6.3.1 Hatherton Glacier

Hatherton Glacier is a large topographically confined outlet glacier located in the Transantarctic Mountains, situated to the north of Byrd Glacier and bounded by the Ross Ice Shelf to the east and the East Antarctic Ice Sheet to the west (Zawar-Reza et al., 2010). The glacier drains from the Antarctic Polar Plateau in an approximate easterly direction, flowing along the southern side of the Darwin Mountains before entering the Darwin Glacier at Junction Spur.

2.6.3.2 Taylor and Ferrar Glaciers

Both the Taylor and Ferrar Glaciers are located in the McMurdo Dry Valleys, which is the largest ice-free area in Antarctica covering *c*. 4800 km^2 (Drewry et al., 1982). Taylor Glacier is a topographically confined outlet glacier that drains from the East Antarctic

Ice Sheet, terminating into Lake Bonney. The source of the glacier is Taylor Dome and the glacier extends *c*. 90 kilometres from its source to its terminus at the west end of Taylor Valley, *c*. 25 kilometres from the coast of McMurdo Sound. Ferrar Glacier is also a topographically confined outlet glacier that drains the Taylor Dome, flowing along an approximately west-to-east-trending valley that terminates as a floating tongue in McMurdo Sound. The glacier extends for 150 kilometres through the Royal Society Range, and has comparatively slow ice flow velocities, typically less than 20 ma^{-1} (Johnson and Staiger, 2007).

2.6.3.3 Lambert Glacier system

The Lambert Glacier system and adjoining Amery Ice Shelf [68.5° S to 81.0° S, 40.0° E to 95.0° E] is the largest glacier and ice shelf system in East Antarctica (Fricker et al., 2000). The total area covered by the Lambert-Amery Ice Shelf system is 1,550,000 km^2, comprising the Amery Ice Shelf which covers 69,000 km^2 (Phillips, 1999). As a result, the grounded section of the Lambert-Amery Ice Shelf system covers 16% of the grounded East Antarctic Ice Sheet amassing an area of *c*. 9,245,000 km^2 (Drewry et al., 1982). The Lambert-Amery Ice Shelf system comprises eight independent ice streams including the Lambert, Mellor and Fisher Glaciers, with further ice streams joining the system further along its main trunk, including Charybdis Glacier from the west and a large ice stream originating from the Mawson Escarpment joining from the east (Hambrey and Dowdeswell, 1994).

2.6.3.4 Recovery Glacier

Recovery Glacier (sometimes referred to as Recovery Ice Stream) [*c*. 81.0° S, 28.0° W] drains a large section (*c*. 8%) of the East Antarctic Ice Sheet (Joughin and Bamber, 2005) and reaches in excess of 800 kilometres in length (Jezek, 1999). The glacier flows westwards along the southern edge of the Shackleton Range, eventually feeding into the Filchner Ice Shelf and the Weddell Sea.

2.6.3.5 Pine Island Glacier

Pine Island Glacier drains *c*. 175,000 km^2 of the West Antarctic Ice Sheet and comprises several tributaries feeding into the main glacier tongue (Stenoien and Bentley, 2000). Pine Island Glacier has received considerable attention in recent years (*e.g.* Jenkins et al., 2010; Rignot et al., 2014) as ice flow at the grounding line of the glacier is comparatively fast (> 2.5 km a^{-1}) resulting in a flux that is one of the largest in Antarctica (Vaughan et al., 2006).

2.6.3.6 Byrd Glacier

Byrd Glacier (80.3° S, 160.0° W) drains one of the largest ice catchments in Antarctica (*c*. 1,070,400 km^2) delivering approximately 23.6 ± 2 km^3 a^{-1} of ice from the East Antarctic Ice sheet into the Ross Ice Shelf (Hughes, 1998; Rignot and Thomas, 2002; Reusch and Hughes, 2003; Stearns and Hamilton, 2005). Ice from the catchment area strongly converges as it approaches Byrd Glacier, becoming funnelled through a *c*. 100 kilometre long, *c*. 20 kilometre wide fjord that cuts through the Transantarctic Mountains, which subsequently diverges as the ice enters the Ross Ice Shelf (Reusch and Hughes, 2003; Stearns and Hamilton, 2005). Ice flow velocities reach in excess of 650 m a^{-1} (Brecher, 1982) and the ice becomes afloat approximately halfway along the fjord (Reusch and Hughes, 2003). Wind scour and sublimation in the fjord removes the snow cover from the surface of Byrd Glacier, revealing the ice surface (Reusch and Hughes, 2003).

2.7 Specific objectives of this thesis

To address the overall aim of this study (*see section 1.1*), a number of specific objectives have been developed. The specific objectives are listed below, with the relevant hypothesis/hypotheses detailed after each objective in italics. Based on the current glaciological thinking and knowledge as summarised above, the specific objectives are:

i. To map in detail the structures of several polythermal glaciers in Svalbard using aerial photography, satellite imagery, and field-based observations, and to document how ice structures in these glaciers with multiple accumulation basins change through time.

ii. To define the flow units in each glacier, characterise their boundaries, and evaluate the evolution of structures within them.

Hypothesis (for objectives i and ii): *Flow units are mutually exclusive with regard to the structures present, and that each flow unit evolves in a unique manner, as proposed by the author from investigations on a Swiss Alpine glacier (Jennings et al., 2014).*

iii. To determine how longitudinal foliation and associated structures form and evolve in Svalbard valley glaciers.

Hypothesis (for objective iii): *Longitudinal foliation evolves either through the process of transposition from earlier layering (stratification or crevasse traces) or as an axial planar structure related to folding with flow-parallel axes (Hambrey and Lawson, 2000; Hambrey and Glasser, 2003).*

iv. To 'up-scale' the analysis of glacier structure by mapping the longitudinal structures of a typical high-Arctic valley glacier with a large number (n = 45) of accumulation basins (Sermilik Glacier, Bylot Island, Nunavat, Canada). Upscaling at this level is an order of magnitude

greater than for the Svalbard glaciers, and resolves the problem that such glaciers are too large to undertake extensive ground-based observations. A combination of satellite imagery and oblique aerial photography is used for this purpose.

Hypothesis (for objective iv): *Longitudinal flow structures in a large valley glacier containing numerous accumulation basins are dominate by flow-unit boundaries and provide the location for the development of pervasive longitudinal foliation.*

v. To further 'up-scale' the structural observations and interpretation from valley glaciers to much larger ice streams in Antarctica using satellite imagery. This requires evaluation of features typically described as 'flow-lines' or 'flow stripes', the physical characteristics and three-dimensional character of which have not been considered by most authors (*e.g.* Fahnestock et al., 2000; Hulbe and Fahnestock, 2007). This approach considers whether such linear features are, in reality longitudinal foliation as proposed by Hambrey and Dowdeswell (1994) and Ely and Clark (2015), or the product of some other mechanism (Glasser et al., 2015).

Hypothesis (for objective v): *Flowlines are a macro-scale version of longitudinal foliation as can be seen in small valley glaciers and they form in a similar manner. Primary stratification in the interior of the ice sheet becomes folded as it flows from a broad accumulation area into a topographically confined narrow glacier tongue. Flowlines are therefore the surface expression of a three-dimensional structure that forms in response to strong lateral compression and longitudinal extension (Reynolds and Hambrey, 1988; Hambrey and Dowdeswell, 1994). Furthermore, they also develop*

in the lee of nunataks and at the confluence of tributary glaciers where there is strong convergence and longitudinal extension (Glasser and Gudmundsson, 2012). In all the situations above, flowlines represent the surface expression of a three-dimensional structure.

Hypothesis (for objective v): *Flowlines form at the confluence of two flow units that are flowing at different velocities, subsequently forming a shear margin at the boundary between the two. As a result, flowlines mainly form at the confluence of glaciers or flow units. They may also represent the surface expression of vertical sheets of differing ice fabrics that develop as a result of shear. In this case, flowlines represent weak bands in the ice sheet where shear aligns ice crystals (Hulbe and Whillans, 1997; Whillans and Van der Veen, 1997).*

Hypothesis (for objective v): *Flowlines are the surface expression of bed topography that has been transmitted to the ice surface in areas of rapid basal sliding and where bed perturbations have wavelengths of a similar length as the overlying ice thickness (Gudmundsson et al., 1998).*

Chapter Three

Methods

3.1 Introduction

A variety of field-based and remotely sensed techniques were utilised for data collection in this thesis. Techniques described in this chapter include two-dimensional structural mapping at a variety of scales from satellite and aerial photography, field-based three-dimensional structural measurements, detailed logging of surface ice facies, oxygen isotope sampling and analysis, and sediment sampling and analysis. Each method is described in detail below.

3.2 Glacier structural mapping

Structural mapping of glaciers is important for ascertaining the overall structural composition of an ice mass, identifying the different types of structures present, deducing the sequential order in which structures form and evolve, and for inferring the stress regimes present within the ice mass. The two- and three-dimensional structural characteristics of ice masses from different locations (Svalbard, Bylot Island, Antarctica) and at a range of scales (small-scale, intermediate-scale, large-scale) were ascertained through a combination of remotely sensed mapping and field-based structural measurements. The methods for both are further discussed below.

3.2.1 Structural notation

In this study, structural features are described in an interpretive sense following geological convention (Ramsay, 1967; Fossen, 2010). In the physical geographical discipline it is accepted that features are initially non-genetically described before being interpreted. However, in some geology disciplines, the description and interpretation of structures is usually combined. This convention is necessary as deformation structures are usually described in the order in which they form; however, this requires a certain level of interpretation. This study adopts the structural geological approach. However, it embraces where possible the method of separating description and interpretation of features in an attempt to be more objective. Identification of structures from both satellite/aerial imagery and in the field is accomplished using the criteria outlined by Goodsell et al. (2005b) and Jennings et al. (2014) and adapted for this study (Table 3.1). Furthermore, as in structural geology, the sequential order of the formation of structures can be ascertained. Ice undergoes polyphase deformation where structural formation and evolution can derive from several phases of deformation. However, in geology, polyphase deformation implies that each phase of deformation is temporally separated. This is not the case in glaciology as 'early' structures forming in the accumulation area of a glacier can form at the same time as 'later' structures forming further down-glacier. Consequently, glaciological structures are sequentially ordered in relation to a parcel of ice travelling from the accumulation area to the glacier terminus (Hambrey and Milnes, 1977). Planar structures are sequentially labelled from the upper reaches of the glacier to the terminus in order of formation using structural glaciological notation (*e.g.* S_0, S_1, S_2, … S_n), using criterial outlined by Hambrey and Lawson (2000), Goodsell et al. (2005b), Cuffey and Paterson (2010), and Jennings et al. (2014, 2015). Associated phases of deformation or fold phases are termed F_1, F_2, ... F_n in ascending order of occurrence from up-glacier to down-glacier.

TABLE 3.1 - STRUCTURE IDENTIFICATION TABLE – PLEASE SEE APPENDIX

3.3 Satellite image and aerial photograph interpretation

Satellite imagery and aerial photography have been used for structural mapping of ice masses for over half a decade (*e.g.* Allen et al., 1960; Meier, 1960; Hambrey and Milnes, 1977; Hambrey and Müller, 1978; Reynolds, 1988; Reynolds and Hambrey, 1988; Hambrey and Dowdeswell, 1994; Goodsell et al., 2005a; b; Hambrey et al., 2005; Roberson, 2008; Appleby et al., 2010; Jennings et al., 2014; 2015; Glasser et al., 2015). In this study, the two-dimensional structure of ice masses was manually interpreted from a variety of satellite imagery and aerial photography sources, utilising both optical and radar sensors. Identification and mapping of structures was conducted using the criteria outlined by Hambrey and Lawson (2000), Goodsell et al. (2005b), Cuffey and Paterson (2010) and Jennings et al. (2014, 2015) (Table 3.1). Two-dimensional structural mapping of ice masses was undertaken at a range of scales utilising a variety of sources, and digitised on-screen using ESRI ArcMap 10.1 Geographical Information System software. For each field-site, the source of imagery and techniques used for mapping are discussed below.

3.3.1 Svalbard

Detailed structural mapping of Austre Brøggerbreen and Midtre Lovénbreen was undertaken utilising aerial photography collected by the UK NERC (Natural Environment Research Council) Airborne Research and Survey Facility (ARSF) (*after* Jennings et al., 2015). The NERC ARSF campaign in northwest Svalbard attained aerial photographs of Austre Brøggerbreen and Midtre Lovénbreen on 25 July 2004. Photographs were collected at an altitude of 3800 metres above sea level using a calibrated RC-10 aerial camera system yielding images at 1:25 000 scale. Photographs were digitally scanned at a resolution of 10 µm (2540 dpi) resulting in an approximate sea-level pixel size of 25 centimetres. To georeference the imagery and remove any spatial distortions derived from the camera geometry and the variable terrain, photographs were processed in BAE Systems' SOCET SET digital photogrammetry suite. Georeferencing was accomplished for the two-dimensional imagery by linking three-dimensional ground control points extracted from a 2 metre resolution lidar digital

elevation model (DEM) collected by the UK NERC ARSF program in 2005 to the imagery (*following* James et al. (2006)). The DEM was down-sampled to 20 metre resolution so that it could be used for orthorectication of the aerial photographs so that any image distortion from surface relief could be removed. The final product is a high-resolution georectified aerial image with the planimetric correctness of a map (Figure 3.1) (Wolf and Dewitt, 2000; Jennings et al., 2015). The average root mean square (RMS) error for the imagery when compared to the ground control points is 1.27 metres, providing a good estimate of the horizontal accuracy of the final image product (Jennings et al., 2015).

Figure 3.1. The final high-resolution georectified aerial image of Austre Brøggerbreen used for detailed glacier-wide structural mapping.

Detailed structural mapping of Austre Lovénbreen was conducted using a combination of aerial photography collected by the UK NERC ARSF which was

supplemented by Digital Globe satellite imagery sourced from Google Earth (Google Earth, 2016). The NERC ARSF campaign collected imagery of Austre Lovénbreen during summer 2003. A total of 18 individual aerial photographs obtained at an altitude of 1500 metres above sea level were processed using Agisoft PhotoScan Structure-from-Motion software. Ground control points located in the proglacial area of the glacier were used to obtain a single georeferenced orthomosaic. The imagery was processed using high accuracy image alignment, automatic camera optimisation, high-quality dense cloud production, and colour correction enabling settings to ensure a high-resolution final product. The ground resolution of the imagery is 0.174 metres per pixel, with a total reported error of 0.723 metres for the entire coverage area of 19.1 km^2. Digital Globe satellite imagery of Austre Lovénbreen collected on 8 May 2011 was acquired from Google Earth and sourced through QGIS 2.12-Lyon Geographic Information System software.

Structural mapping of Pedersenbreen was undertaken using satellite imagery sourced through Google Earth. Imagery was collected by Digital Globe on 8 May 2011 and acquired using QGIS 2.12-Lyon Geographic Information System software.

3.3.2 Bylot Island

Detailed structural mapping of Sermilik Glacier located on Bylot Island was undertaken using Landsat 8 OLI (Operational Land Imager) imagery acquired on 9 August 2013 (*downloaded from* earthexplorer.usgs.gov). 30 metre spatial resolution Red-Green-Blue (RGB) bands were manipulated in ENVI 5.1 spectral image processing and geospatial analysis software to create a true-colour composite image, which was subsequently pan-sharpened to a 15 metre spatial resolution image using the panchromatic band (Figure 3.2).

Interpretation of structures at the surface of Sermilik Glacier from satellite imagery was supplemented with oblique low-level aerial photography of the glacier tongue acquired by M. J. Hambrey in summer 2014.

Figure 3.2. Landsat 8 OLI (Operational Land Imager) imagery of Sermilik Glacier acquired on 9 August 2013 used for detail structural mapping of the glacier.

3.3.3 Antarctica

Mapping of surface features in Antarctica was achieved using optical (MODIS and LIMA) and radar (RADARSAT) satellite imagery (*after* Glasser et al., 2015). A combination of optical and radar imagery was used to maximise the accuracy of mapping, while taking advantage of the different sensor's strengths. Optical imagery sources proved beneficial for identifying structural features on ice shelves, whereas radar imagery enabled tracing of features into the interior of the ice sheet despite the increasing thickness of surface snow cover. The continuity and consistency of

structural features between different imagery sources gave increased confidence that structures were present on the ice sheet and not artefacts of the imagery. Further confidence in the accuracy of the imagery used was provided by observations of extensive blue ice areas in which surface structures can be clearly seen, as well ground observations by M. J. Hambrey in 1995/1996 that verified the surface structures present in the Lambert Glacier System. Differences in the resolution of imagery sources was not an issue for the accuracy of mapping of structural features on this scale as structural features on the Antarctic Ice Sheet are often many hundreds of kilometres long and variations in resolution were too small to affect the accuracy of mapping such large features. The details of each satellite imagery source are included below.

i. The Moderate Resolution Imaging Spectroradiometer (MODIS) Mosaic of Antarctica (MOA) (*available from* nsidc.org/data/moa) (scambos et al., 2007) provides a cloud-free mosaic image of the whole Antarctic Ice Sheet. The mosaic is composed of 260 swaths of both Terra and Aqua MODIS images that provides a grid scale of 125 metres and an estimated resolution of 150 metres. Composite imagery were collected between 20 November 2003 and 29 February 2004. MODIS imagery provided high resolution mapping of structures on ice shelves and their corresponding tributary glaciers (*following* Glasser et al. (2015)).

ii. The Landsat Image Mosaic of Antarctica (LIMA) (*available from* lima.usgs.gov) is a high-resolution true colour mosaic of the Antarctic Ice Sheet. The mosaic is composed of in excess of 1000 Landsat ETM+ images, resulting in a spatial resolution of 30 metres in bands 1 - 6, and 15 metres in the panchromatic band. LIMA imagery supplemented MODIS imagery for the structural mapping of ice shelves and their corresponding tributary glaciers (*following* Glasser et al. (2015)).

iii. RADARSAT imagery (*available from* nsidc.org/data/radarsat/index.html) is a composite radar image of the Antarctic Ice Sheet. RADARSAT imagery has a spatial resolution of 25 metres and proved useful for identifying areas of fast ice flow. Variations in backscatter intensity or 'brightness' of radar returns are very useful for identification of ice stream lateral margins (Ng and King, 2013; Glasser et al., 2015). RADARSAT images were used for the structural mapping of the interior of the Antarctic Ice Sheet and its ice streams because of its ability to view structural features despite substantial surface snow cover (*following* Glasser et al. (2015)).

In addition to the imagery described above, several glaciers/areas of glaciers were structurally mapped using other types of optical imagery, each of which are described in turn below.

Detailed mapping of Hatherton Glacier was conducted using Landsat 7 imagery acquired on 24 December 1999 (*downloaded from* earthexplorer.usgs.gov). The imagery has a spatial resolution of 15 metres and was manipulated as a GeoTIFF.

Detailed mapping of both Taylor Glacier and Ferrar Glacier was conducted using U.S. Geological Survey, Digital Globe, and CNES/Astrium satellite imagery that was collected during December 2013. The imagery was acquired from Google Earth and sourced through QGIS 2.12-Lyon Geographic Information System software.

Detailed structural mapping of crevassed areas on Lambert Glacier was undertaken using Landsat 8 OLI (Operational Land Imager) imagery acquired on 2 November 2014 (*downloaded from* earthexplorer.usgs.gov).

3.3.4 Remotely sensed mapping

Detailed surface mapping of glaciological features from aerial photography and satellite imagery was conducted in ESRI ArcMap 10.1 Geographical Information System software or QGIS 2.12-Lyon Geographic Information System software. Mapped

features included the on-screen digitisation of glacier outlines, areas of supraglacial debris and snow cover, as well as various glaciological structures. Glaciological features were identified using criteria outlined by Goodsell et al. (2005b) and Jennings et al. (2014) and adapted for this study (as shown in Table 3.1). Structures that were identified and mapped in Svalbard from aerial photography were verified in a field campaign during the summer of 2013.

3.4 Field-based structural observations

Field-based structural observations and measurements have been an important source of structural information since the rejuvenation of interest in structural glaciology in the early 1960s (*e.g.* Schwarzacher and Untersteiner, 1953; Allen et al., 1960; Meier, 1960; Hambrey, 1976a, 1976b; Milnes and Hambrey, 1976; Hambrey and Milnes, 1977, Hambrey et al., 1980; Hambrey et al., 1999, 2005; Goodsell et al., 2005b; Roberson, 2008; Jennings et al., 2014). Observations and measurements in the field are important for ascertaining the three-dimensional characteristics of glacier structures that cannot be deduced from remotely sensed data. They are also important for documenting other small-scale structural characteristics such as crystallographic descriptions that cannot be ascertained by other means. The methods used for general glacier-wide structural measurements and detailed small-scale structure specific observations are discussed in turn below.

3.4.1 Glacier-wide structural observations

Structures were identified in the field according to their dimensions, orientation and cross-cutting relationships following the criteria outlined by Goodsell et al. (2005b) and Jennings et al. (2014) (Table 3.1). Transects across the glacier (approximately perpendicular to flow) were used to measure the three-dimensional characteristics and orientation of structures. The start and end locations of each transect were recorded using a Garmin eTrex 30 handheld GPS (Global Positioning System) with a horizontal accuracy of ± 15 metres, with distances along each transect paced-out

relative to the starting location (after a standard pace length had been measured). The three-dimensional characteristics of structures were measured using a compass/clinometer (with an accuracy of ± 1°). The following attributes of each structure was recorded: length, shape, dip orientation, dip angle, whether the structure was open or closed, any evidence of displacement, ice-crystal size and shape, ice colour, debris content and size, debris colour, and lithology. The dip of planar structures was measured by inserting an ice axe parallel along the plane (when possible) and reading the dip angle by aligning a compass/clinometer along the ice axe shaft. When it was not possible to insert an ice axe into a structure, excavation of the structure allowed the ice axe to be inserted and the dip read by using a compass/clinometer as described above. By recording these data for a number of transects along the length of the glacier, the overall glacier structure can be deduced. Furthermore, the sequential development of structures could be determined and described from the upper reaches of the glacier to the snout using conventional structural geological notation (*see section 3.2.1*) (Hambrey and Lawson, 2000; Goodsell et al., 2005b, Roberson, 2008; Appleby et al., 2010; Jennings et al., 2014).

3.4.2 Detailed ice facies logging

Areas of glaciological structural interest were identified and located using a handheld GPS unit (details of GPS unit above). Detailed logging of surface ice facies was conducted along approximate flow lines to identify change in ice facies in response to flow. Depending on the structures present at each log site, logs ranged from several metres up to *c*. 15 metres in length. Structures were identified in the field according to their dimensions, orientation, cross-cutting relationships and their ice facies following Goodsell et al. (2005b) and Jennings et al. (2014). Areas of debris cover or supraglacial mud patches were investigated by firstly cleaning the debris from the ice surface to reveal the ice structures below (Figure 3.3). Supraglacial debris cover commonly protects the underlying ice from ablation and etching out of ice crystals, which enabled detailed structural characteristics to be observed. A 30 metre tape measure was laid perpendicular to flow along the length of the log, and the up-glacier direction in

Figure 3.3. 'Cleaning' a supraglacial mud patch on the surface of Austre Brøggerbreen to reveal the underlying ice structures. Photograph courtesy of M. J. Hambrey.

relation to the log was noted. Where applicable an overview sketch of the structures present in the log was drawn along with corresponding interpretation. Furthermore, photographs of the log and any specific structures of particular interest were taken for subsequent reference. Detailed logging of the ice facies was used to record the thicknesses (to millimetre accuracy), dip angle, ice type, bubble content, morphology, debris content, cross-cutting relationships and sequential order of ice layers. Prominent ice layers of different facies were sampled for stable isotope analysis along the length of the log to enable accurate identification of ice sample locations, ice characteristics and surrounding morphology (*see section 3.5* for further details).

3.5 Stable isotopic sampling

Stable isotope analysis was first introduced into glaciology in the 1950's (*e.g.* Epstein, 1956; Epstein and Sharp, 1959). Since then co-isotopic analysis of glacier ice using both oxygen and hydrogen ratios has become an important tool for differentiating between ice types with different origins (*e.g.* Glasser and Hambrey, 2002; Hubbard et al., 2004), especially with regard to basal ice facies (Hubbard and Sharp, 1995; Knight, 1997).

Water molecules comprise two hydrogen atoms and one oxygen atom. Both hydrogen and oxygen always contain the same number of protons in their nuclei; however, the number of neutrons can vary. Oxygen has three isotopes with atomic masses of 16, 17, and 18 (^{16}O, ^{17}O, ^{18}O), and hydrogen has two naturally occurring isotopes with atomic masses of 1 and 2 (^{1}H, ^{2}H - which is also known as deuterium, D). As a result, water molecules can have different atomic masses; therefore, water and ice can have varying isotopic signatures depending on the different proportions of oxygen and hydrogen isotopes (Knight, 1997; Benn and Evans, 2010). The concentration of isotopes contained within a sample is compared against a standard, usually Standard Mean Ocean Water (SMOW), with known isotopic values. The isotopic signature of a sample is measured as the ratio of heavy isotopes to light isotopes ($^{18}O/^{16}O$ and D/H) in comparison to SMOW, which is displayed as $\delta^{18}O$ or δD (Equation 3.1 and 3.2).

(*Equation 3.1*)

$$\delta^{18}O = \left\{ \frac{\frac{^{18}O}{^{16}O}[sample] - \frac{^{18}O}{^{16}O}[SMOW]}{\frac{^{18}O}{^{16}O}[SMOW]} \right\} \times 1000$$

(*Equation 3.2*)

$$\delta D = \left\{ \frac{\frac{D}{H}[sample] - \frac{D}{H}[SMOW]}{\frac{D}{H}[SMOW]} \right\} \times 1000$$

δ values are given in parts per thousand (‰) with positive δ values indicating a sample that is enriched in heavy isotopes in comparison to SMOW, and conversely negative values indicate isotopically lighter samples in comparison to SMOW. The concentration of different isotopes is dependent upon different circumstances, which allows the origin and history of ice and water to be inferred from its corresponding isotopic composition. As a result of different isotopic weights, water molecules have different physical properties (*e.g.* $H_2{}^{18}O$ is heavier than $H_2{}^{16}O$). This means that during evaporation or freezing isotopic fractionation occurs (*i.e.* the water becomes enriched or depleted in different isotopes depending on their weight, *e.g.* heavier isotopes preferentially freeze first, while lighter isotopes preferentially evaporate first). Using the changes in isotope concentrations it is possible to infer the environment that the ice originates (Knight, 1997).

Stable isotope samples are often taken in combination with detailed ice facies logging so that the ice facies, surrounding structural setting and location are known. This also allows parallel but different ice facies to be sampled in a relatively small area. On occasions where isotope sample are collected away from ice logs, a GPS location is taken for each sample with a handheld GPS unit. Isotope samples are extracted using a 10 millimetre diameter, 200 millimetre long ice screw that is screwed into the selected ice facies (Figure 3.4). The ice screw is inspected before use to ensure that it is clean, and screwed into the ice previous to sampling to ensure no contamination. When sampling, the three-dimensional dip of the ice layer is taken into consideration to mitigate against sampling into a different ice facies. The teeth of the ice screw break down the ice into small chippings or produce a small ice core that collects in the barrel of the screw, which is subsequently collected in two airtight 8 millilitre high-density polyethylene vials (Hubbard and Glasser, 2005). The vials are allowed to melt in the shade before being transferred into one vial to ensure there is no air space for evaporation to occur (Glasser and Hambrey, 2002). Vials are then stored in a cool environment to further reduce the possibility of evaporation during storage. Once collected, samples are transported to the University of Birmingham's School of Geography, Earth and Environmental Sciences stable-isotope facility (SILLA) for stable isotope (oxygen, $\delta^{18}O$-δD) analysis. Continuous-flow isotope-ratio mass spectrometry

(CF-IRMS) of isotope samples is undertaken using a continuous-flow Isoprime isotope ratio mass spectrometer (IRMS) that permits the analysis of $\delta^{18}O$ and δD in liquids. Samples collected in this study were processed by Dr Ian Boomer under the direction of Professor Ian Fairchild.

Figure 3.4. Isotopic sampling of an ice layer using an ice screw. Photograph courtesy of M. J. Hambrey.

3.6 Sedimentology

The distribution of particle sizes found in different sedimentary deposits can reveal information about the source lithology as well as processes that have acted upon the body of the sediments, such as types of erosion, transport, and deposition. Many studies have attempted to draw direct comparison between particle size distributions

and processes that have acted upon them (*e.g.* Boulton, 1978; Haldorsen, 1981; Drewry, 1986; Gale and Hoare, 1991; Sharp et al., 1994; Hooke and Iverson, 1995; Benn and Gemmell, 2002). However, it is now accepted that it is rarely possible to directly relate the two. Lithological controls dictate variability of grain sizes depending on source material deposition and previous weathering processes, and previous phases of sediment erosion, transport, and deposition can produce biased grain-size distributions in the observed deposit. However, when combined with other sources of evidence, grain-size distributions are useful for interpretation of sediment deposits (Hoey, 2004).

Different sediments contained within ice facies were sampled in the field and transported to the sediment laboratory at Aberystwyth University for further analysis. Sediment sample sites were identified in areas of structural interest which had characteristics which suggested that the sediments and ice facies may have a non-supraglacial origin. Each sample site was located using a handheld GPS unit and described in detail. Sediments were collected from the ice surface, using a palette knife in areas that sediment had melted out of the ice, or using an ice axe to extract sediment-rich ice. Sediment samples were stored and transported in labelled zip-lock plastic bags. Once transported back to the sediment laboratory, ice-sediment samples were transferred into individual trays and allowed to melt at room temperature to release any sediments contained within the ice. When fully melted, sediment samples were dried in an oven at *c*. 40°C (a sufficiently low temperature to ensure that there was no alteration to the sediment grain sizes, especially the clay fraction which is prone to alteration by heat, regardless of the time spent in the oven). All samples were left in the oven until totally dry, which varied between samples depending on the moisture content in each. Once dry, samples were gently disaggregated using a pestle and mortar to ensure grains were not clumped together. Initial disaggregation was preformed using a hard pestle; however, to ensure that no grains were artificially broken up by the process, a rubber pestle was subsequently used to ensure that even the finest grain sizes were thoroughly disaggregated without crushing any particles. Once disaggregated, samples were weighed before being introduced into the top of a clean dry sieve stack consisting of 12 sieves ranging in mesh diameter from -1.5 Φ

(2.828 millimetres) through to 4.0 Φ (0.063 millimetres) in 0.5 Φ increments. All sediments with a diameter less than 4.0 Φ (termed from here on in as the 'pan fraction') were collected in a pan at the base of the sieve stack. Each sieve stack was agitated on a mechanical sieve shaker for 15 minutes to ensure the sample was thoroughly sorted (McManus, 1988), before the sediment retained on each sieve was tipped onto a piece of paper and the sieve cleaned with a nylon brush to remove any trapped particles from the mesh. The sediment collected from each sieve was then measured to an accuracy of 0.001 grams and recorded. The weight of the pan fraction was also measured and retained for further size analysis.

To get a full grain-size distribution for each of the samples, the sediment collected after dry sieving with a diameter less than 4.0 Φ was introduced into a laser granulometer to ascertain the particle size distribution of the pan fraction. The laser granulometer uses laser diffraction to quickly and accurately analyse fine grain-size material (Buurman et al., 1997; Hoey, 2004). As particles pass through the granulometer, the forward scattering of a laser beam passing through the flow of particles enables the back calculation of particle sizes by analysing the resulting diffraction pattern. 0.5 grams of the pan fraction for each sample was weighed and dispersed in 10 millilitres of 0.5% Calgon (weight/volume) in individual beakers. The beakers were placed in an ultrasonic bath for 10 minutes and stirred regularly to ensure that individual particles did not aggregate. A Mastersizer 2000 version 5.60 laser granulometer manufactured by Malvern Instruments Ltd. was used for the analysis, set with a pump speed of 2000 revolutions per minute. Before each analysis was run, the laser granulometer was cleaned by flushing distilled water through the system three times to ensure no sediment remained from previous sample runs. A background water reading was performed before each sample was run with distilled water. Once completed, the sediment sample was stirred to ensure that the sediment was in suspension, and then added into the laser granulometer using a pipette. The laser granulometer took three repeat measurements of each sample's grain-size distribution, before averaging them for the final report. After each sample run, all equipment (*e.g.* pipette) was cleaned with distilled water to ensure no cross contamination of samples.

The analysis of grain-size distributions using dry-sieving and laser granulometer techniques have certain limitations that can introduce errors in the final grain-size data. Dry-sieving is reliant on the principal that particles with a diameter that is equal to or greater than the mesh spacing of a sieve will remain on that sieve after agitation. However, whether a particle will pass through a particular mesh spacing is dependent upon the shape of the particle (*e.g.* a platy particle could pass diagonally through a mesh spacing where a similar sized spherical particle could not) (*see* McManus, 1988). Consequently, whether a particle will pass through a certain mesh spacing is dependent upon both the shape and dimensions of the smallest cross-sectional area. Furthermore, the shape of a particle also influences the probability of that particle passing through a sieve mesh, with more spherical particles being more likely to pass through the sieve, whereas non-spherical particles are less likely to pass through the sieve (Matthews, 1991). A further complicating factor is the combining of sieve and laser granulometer data. In several of the graphs displaying the combined data from both techniques, an anomalously high peak occurs at the 4.0 Φ (0.063 millimetres) grain-size class, which coincides at the overlap between measurement techniques. The cause of this peak is not directly known; however, it is likely to be a combination of the insufficient disaggregation of sediment samples combined with particles passing through sieve meshes as a consequence of their shape. However, despite the necessity for caution when interpreting combined datasets (*see* Hoey, 2004), it is thought that meaningful conclusions can still be drawn from the grain-size distributions analysed in this way.

To further differentiate between the characteristics of sediment samples, hydrochloric acid was added to a small sample of the pan fraction to identify whether calcium carbonate is present. Samples were treated with 10% (volume/volume) hydrochloric acid by adding several drops of acid to the sample using a pipette. The effervescence of each sample was visibly and auditory assessed, providing an estimated percentage of calcium carbonate present.

For the description of sediments, size terms following Wentworth (1922) are used with Φ and millimetre measurements also stated.

3.7 Data presentation

Initial map production and digitisation was carried out in either ESRI ArcMap 10.1 or QGIS 2.12-Lyon Geographic Information System software using vector drawing tools, with georeferenced data from the field accurately plotted on the map using GPS co-ordinates. Once completed, the map was imported into Inkscape v. 0.91 for further manipulation and final map production.

Detailed log production was initially carried out manually to ensure that the correct scales were used, before being scanned at 800 dots per inch (dpi) resolution and imported into Inkscape v. 0.91 for digitising. Vector drawing tools, colour shading, and shape tools were used to clearly display log data.

All numerical data collected (dry-sieving data, laser granulometer data, oxygen isotope data) were analysed in Microsoft Excel, with subsequent graph production and manipulation also conducted within the same program.

Chapter Four

Ice facies descriptions

4.1 Introduction

As summarised in *section 2.5.1*, several different ice facies are often observed at the surface of valley glaciers. The stratified nature of glacier ice represents the annual layering of snowfall that becomes preserved during firnification (Lewis, 1960; Hambrey, 1976a, 1994; Hambrey and Lawson, 2000), with the different ice facies present reflecting the seasonal variations occurring during initial snowpack formation (Wadham and Nuttall, 2002). The characteristics of each ice facies have been described in many previous studies (*e.g.* Kamb, 1959; Allen et al., 1960; Hambrey, 1976a, 1977a; Goodsell et al., 2005b; Jennings et al., 2014). However, facies are not all consistent, varying between glaciers according to thermal regime. Therefore, for the purpose of this study, the characteristics of each ice facies in the Svalbard glaciers are initially described non-genetically, before the interpretation of each ice facies and its glaciological significance is explained. The following ice facies descriptions are based on the facies schemes of several previous studies (*e.g.* Allen et al., 1960; Hambrey, 1977a; Hambrey and Milnes, 1977; Goodsell et al., 2005b; Jennings et al., 2014); however, they have been refined and expanded on in this chapter to accurately define the ice facies encountered during this study.

4.2 Coarse bubbly ice

Coarse bubbly ice can be separated into two sub-facies depending on the comparative bubble content of individual ice layers. The characteristics of each sub-facies and related interpretations are discussed further below.

4.2.1 Coarse bubbly ice (bubble-rich)

Description

Coarse-grained bubble-rich ice typically found in comparatively thick layers (up to tens of centimetres thick) is generally the most abundant ice type found in valley glaciers. Crystal sizes range from 1 - 5 centimetres with a high concentration of interstitial and inter-crystal bubbles present resulting in a low-density, highly porous ice facies (Figure 4.1). Commonly, bubbles are elongated in one direction. Coarse-grained bubble-rich ice facies tend to form topographic high points on the surface of the glacier, consisting of white ice (when weathered, otherwise it can appear as pale blue ice) that generally has relatively low concentrations of trapped aeolian sediment.

Interpretation

Coarse-grained bubble-rich ice is interpreted to be winter snow accumulation that has undergone partial melt and refreezing during firnification of snow into ice (Wadham and Nuttall, 2002). In the accumulation area, coarse-grained bubble-rich ice layers tend to form irregular but continuous planar structures which tend to plunge gently up-glacier. Large-scale asymmetric folding, commonly with parasitic folds on larger fold limbs occur around flow-parallel fold axes, with the strongest folding coinciding with flow-unit boundaries. In this situation coarse-grained bubble-rich ice layers in continuous arcuate planar structures are contained in primary stratification (S_0) which represents the initial layering of snow and firn preserved during firnification. Initially, sub-horizontal ice layers become increasingly folded as the ice flows from a broad

Figure 4.1. A coarse-grained bubble-rich ice crystal. Note the high concentration of interstitial bubbles present in this type of ice facies. The a-axis length of the crystal is approximately 5 centimetres.

accumulation area in to a comparatively narrow glacier tongue (Hambrey et al., 2005; Jennings et al., 2014). Further down-glacier, coarse-grained bubble-rich layers often form steeply dipping longitudinal planar structures. As described above, coarse-grained bubble-rich ice represents the winter accumulation of snow preserved during its transition into glacier ice. Once the initially sub-horizontal layers get advected down-glacier, they become increasingly folded and re-orientated into steeply dipping longitudinal planar structures (longitudinal foliation (S_1)) (Hambrey et al., 2005; Jennings et al., 2014).

4.2.2 Coarse bubbly ice (bubble-poor)

Description

Coarse-grained ice with a comparatively lower concentration of bubbles is commonly found alongside coarse-grained bubble-rich ice layers. The boundary between each sub-facies can either be sharply defined by bubble content, or transitional with bubble content gradually changing in concentration between each sub-facies. Coarse-grained bubble-poor ice can form comparatively thick layers (up to tens of centimetres thick); however, this ice facies is generally less abundant than coarse-grained bubble-rich ice. Crystal sizes are also very similar to the coarse-grained bubble-rich ice facies attaining crystal size diameters of 1 – 5 centimetres. This ice facies also tends to form topographic high-points on the surface of the glacier, consisting of white ice that generally has relatively low concentrations of trapped aeolian sediment.

Interpretation

Coarse bubbly ice with a comparatively lower concentration of bubbles is interpreted to have originated from superimposed ice. The white appearance of the ice in contrast to different types of superimposed ice (usually blue in colour) suggests that this ice type developed during the early melt period where melt and refreezing occurs over short time periods (Wadham and Nuttall, 2002). At the surface of the glacier, coarse-grained bubble-poor ice often has a smooth surface crust that reflects subaerial melting or sublimation and refreezing (Wadham and Nuttall, 2002). As for coarse-grained bubble-rich ice, coarse-grained bubble-poor ice forms irregular but continuous planar structures which plunge gently up glacier in the accumulation area. This reflects primary stratification (S_0) which develops as the initial snowpack is transformed into glacier ice (Hambrey et al., 2005). Further down-glacier, coarse-grained bubble-poor ice forms steeply dipping longitudinal structures, as primary stratification (S_0) becomes increasingly folded and re-orientated into longitudinal foliation (S_1) (Hambrey et al., 2005; Jennings et al., 2014).

4.3 Coarse clear ice

Description

Coarse-grained bubble-deficient ice commonly forms clear blue layers on the surface of the glacier. Despite being less abundant that the coarse bubbly ice facies, coarse clear ice can form comparatively thick layers (up to tens of centimetres thick). Crystal sizes range from 1 – 15 centimetres with a low concentration of interstitial and inter-crystal bubbles present resulting in a high-density, impermeable ice facies. However, occasional bubbles present in the ice facies can be elongated in one direction. Coarse clear ice tends to form topographic low points on the glacier surface, where meltwater runoff and aeolian sediments can collect.

Interpretation

Coarse clear ice is interpreted to be the product of slush and meltwater refreezing at the base of the snowpack. Melt from the surface of the snowpack percolates down until it reaches the impermeable glacier surface. The meltwater fills any pore-spacing at the snowpack base forcing out any trapped air that would otherwise form bubbles during firnification. Refreezing of this layer develops a bubble-deficient, clear blue ice layer that is usually overlain by coarse bubbly ice. As for the coarse bubbly ice facies, coarse clear ice layers can be seen in the accumulation area of a glacier as primary stratification (S_0), irregular but continuous planar structures which plunge gently up glacier. It is also evident lower down the glacier as longitudinal foliation (S_1) as steeply dipping longitudinal structures (Hambrey et al., 2005; Jennings et al., 2014). However, coarse clear ice facies can be observed in other structural contexts. It is common for crevasses and crystal quirks to fill with meltwater, which when frozen forms discontinuous lenses of coarse clear ice. It is often easy to differentiate between the coarse clear ice in primary stratification and longitudinal foliation from that of healed crevasse traces and crystal quirks for a number of reasons. The cross-cutting nature of the different structures helps identify the different structures from one another. However, from a crystallographic perspective, coarse clear ice crystals that develop in

crevasses or crystal quirks form perpendicular to the edge of the structure, developing a suture where they join, whereas this is not the case for snowpack-derived coarse clear ice. Coarse clear ice is often observed in basal ice where regelation has added refrozen water to the base of the glacier. This type of ice facies is often distinguishable from other coarse clear ice facies as the ice tends to have high concentrations of disseminated mud (*see* Hubbard et al., 2009).

4.4 Fine ice

Description

Fine-grained white ice is the least abundant ice facies found in the Svalbard valley glaciers. Ice crystal diameters rarely exceed *c*. 5 millimetres, and consist of rounded bubble-deficient ice crystals (Figure 4.2). Individual ice crystals are not well amalgamated with one-another (when weathered at the surface of a glacier), therefore fine white ice layers tend to have a 'sugary' texture with a lot of interstitial pore-space that is often saturated during the summer months with meltwater. These layers often form topographic lows on the glacier surface, acting as sediment traps for aeolian sediment. It is common for fine ice layers to be comparatively narrow (sub-centimetre); however, in places they can form layers up to tens of centimetres in thickness.

Interpretation

Unlike coarse bubbly and coarse clear ice facies, fine ice is not observed in primary stratification (S_0); however, it is observed in longitudinal foliation (S_1) in the ablation area. As fine ice layers are not present in initial snowpack formation, it is inferred that they are most likely formed by crystallographic modification of existing ice layers by simple shear (Jennings et al., 2014). The occurrence of most fine ice layers in close proximity to flow unit boundaries further supports this conclusion as simple shear is

Figure 4.2. Fine-grained white ice crystals. Note the small (*c.* 5 millimetres) diameter and rounded nature of individual crystals. Also note the lack of interstitial bubbles.

greater where two flow units converge (Hambrey and Milnes, 1977; Hambrey and Müller, 1978; Hambrey et al., 2005).

4.5 Foliated ice

Foliated ice is characterised by pervasive and typically discontinuous planar structures, defined by variations in ice facies, ice crystal size, crystal geometry, bubble concentrations, bubble distribution, and bubble shape (*see section 2.5.2.2*) (Allen et al., 1960; Hambrey, 1975, 1976a, b, 1977a, Hambrey and Milnes, 1977; Hambrey and Lawson, 2000; Hudleston, 2015). The 'strength' of foliation is highly variable, ranging from weakly foliated ice that is commonly defined by bubble concentrations arranged in stringers of bubbles (linear trains of bubbles that are commonly one bubble wide)

contained within one ice facies, to strongly foliated ice that is defined by variations in ice facies with well-defined boundaries (Figure 4.3). Typically, strongly foliated ice consists of thin layers of alternating ice types with near vertical dip angles, whereas weakly foliated ice is much more subtle being defined on a much finer scale by bubble distribution.

Figure 4.3. Strongly foliated ice at the surface of Pedersenbreen, Svalbard. Note the thin layers of alternating ice facies with sharply defined boundaries and steep dip angles. Photograph courtesy of M. J. Hambrey.

Chapter Five

Austre Brøggerbreen

5.1 Introduction

The overall aim of this chapter is to document the structural characteristics of Austre Brøggerbreen at a range of scales, and to demonstrate that individual flow units have unique structural assemblages and evolutions. To achieve this a number of techniques including; mapping of surface structures from aerial imagery, glacier-wide three-dimensional structural measurements, detailed ice facies logs, stable isotopic analysis and sedimentological analysis are utilised. For a detailed description of the techniques employed, please refer to 'Methods' in *Chapter Three*.

The specific objectives of this chapter are:

i. To map the surface of Austre Brøggerbreen using a combination of aerial imagery and field-based measurements.

ii. To determine if Austre Brøggerbreen was once more dynamic during the Neoglacial maxima (*c*. 1900 AD).

iii. To test the hypothesis stating that flow units are unique and mutually exclusive from one another (*i.e.* if flow units can be treated as individual systems that do not interact with one-another) (Jennings et al. 2014).

iv. To test the hypothesis stating that longitudinal foliation has a part-basal origin and that, in part, debris entrainment is structurally controlled (Hambrey and Glasser, 2003).

For a brief overview of Austre Brøggerbreen and the previous research conducted on the glacier, refer to the 'Study-site descriptions' in *section 2.6*.

Austre Brøggerbreen is composed of six major flow units (labelled Flow Unit 1 to 6), with Flow Units 2 and 5 further sub-divided into three and two sub-flow units respectively (Figure 5.1). Each sub-flow unit originates in a separate sub-accumulation area, the consequence of which influences the structural characteristics and evolution of their corresponding flow unit. The structural evolution of each sub-flow unit will be discussed in turn below.

5.2 Structural evolution of individual flow units

Each flow unit on Austre Brøggerbreen has different structures, structural evolution and sequential order of structure formation. For each individual flow unit, the sequential order of structure formation is described using standard geological structural notation (discussed in detail in the 'Methods' in *Chapter Three*). The structural attributes of each flow unit are summarised in Table 5.1 Flow units are labelled starting from the true-left of the glacier working towards the true-right (Figure 5.1). Flow unit descriptions also follow this order.

5.2.1 Flow Unit 1

The first structure observed in the upper reaches of Flow Unit 1 is primary stratification (S_0) (Figure 5.2), which subsequently evolves into longitudinal foliation (S_1) in the upper middle reaches of the flow unit. Longitudinal foliation is most

FIGURE 5.1 - ABB MAIN STRUCTURAL MAP - PLEASE SEE APPENDIX

Table 5.1. Summary of the sequential structural evolution of each flow unit on Austre Brøggerbreen. Key located below main table (note that the colours are related to the colours that represent each structure on the main structural map, Figure 5.1.) (Jennings et al., 2015).

Order of formation	Flow Unit 1	Flow Unit 2			Flow Unit 3	Flow Unit 4	Flow Unit 5		Flow Unit 6
		A	B	C			A	B	
1									
2									
3									
4									
5									

Key	
	Primary stratification
	Water-healed crevasses
	Longitudinal foliation
	First, second and third generation crevasse traces respectively

pronounced at the flow unit boundaries, and is strongest on the true-right of the flow unit where it abuts Flow Unit 2a. A third suite of structures also develop in the upper middle reaches of the glacier. Transverse crevasse traces (S_2) form linear features that cross-cut the whole width of the flow unit and cross the flow unit boundary with Flow Unit 2a. The crevasse traces become increasingly arcuate down-glacier; however, they are not as strongly deformed as some suites of crevasse traces in other flow units.

5.2.2 Flow Unit 2a

The accumulation area of Flow Unit 2a is dominated by primary stratification (S_0) that gets folded within a comparatively short distance (*c.* 750 metres) down-glacier. Water-healed crevasses (S_1) are also found high in the accumulation area, which are visible as comparatively broad blue linear features that form transverse to flow (Figure 5.2). Water-healed crevasses (S_1) do not persist down-glacier and die-out in a relatively short distance. Even though there is comparatively strong longitudinal foliation associated with both boundaries of Flow Unit 2a, it is not actively forming within the flow unit. The longitudinal foliation at each boundary is the result of Flow Unit 2a

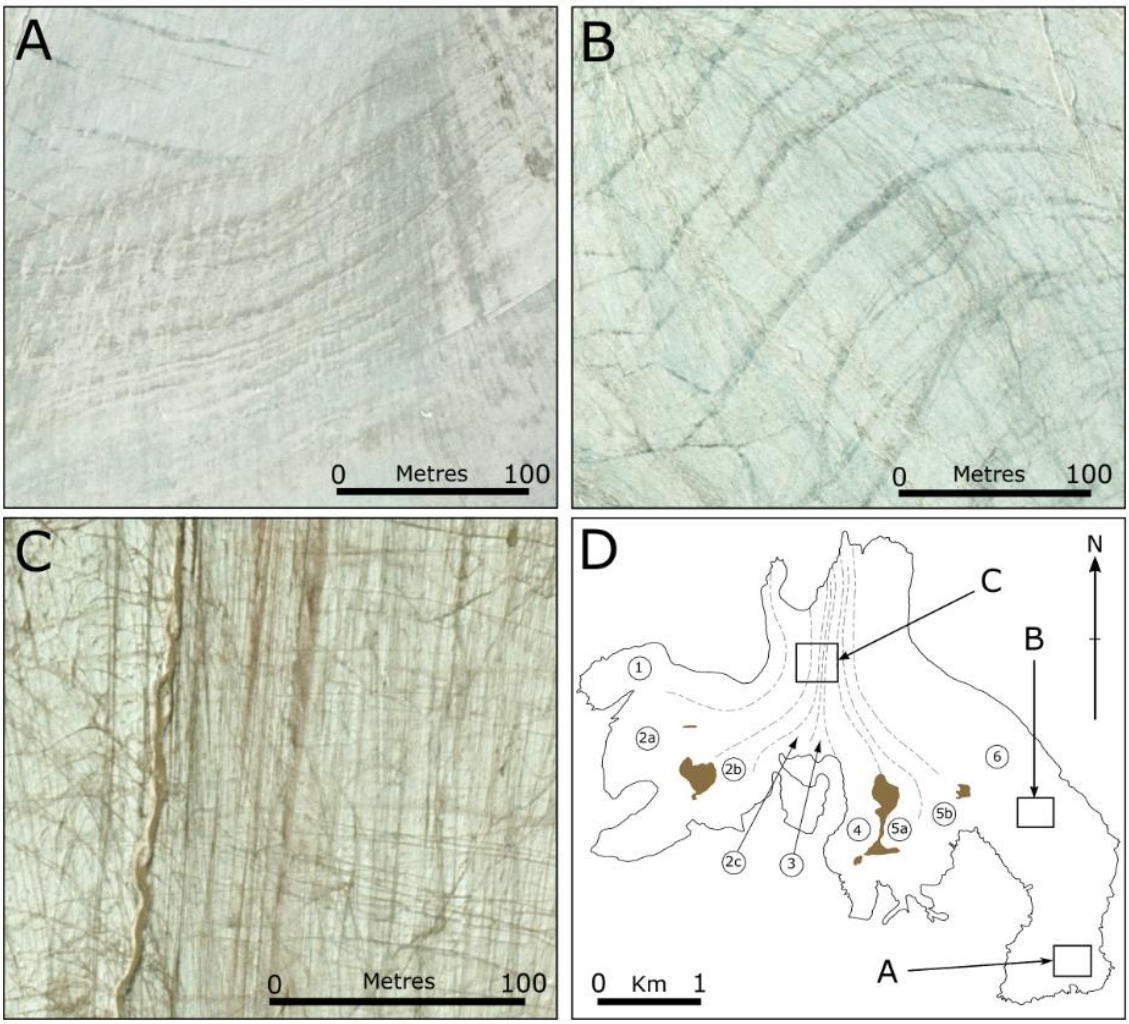

Figure 5.2. Aerial photographs of some major structural features on Austre Brøggerbreen: (A) primary stratification (S_0), parallel and continuous layering running approximately from left to right of the image; (B) water-healed crevasses (S_2), comparatively thick dark blue arcuate features; (C) longitudinal foliation (S_4), thin long linear traces running from the bottom to the top of the image; (D) flow unit map of Austre Brøggerbreen showing the different flow units along with the location of image A-C (Jennings et al., 2015).

interacting with neighbouring flow units. Flow Unit 2a also has 3 suites of crevasse traces. Each generation of crevasse traces has a different origin, morphology and evolutionary history. The first suite of crevasse traces (S_2) develops in the accumulation area of the flow unit, near to the true-left flow-unit boundary (boundary with Flow Unit 2b). Initially transverse to flow, S_2 fractures become increasingly rotated down-glacier in an anti-clockwise direction. Rotation of S_2 is sufficient to almost rotate the fractures parallel to flow when nearing the terminus of the glacier.

The second generation of crevasse traces (S_3) develop in the middle reaches of the glacier, and not only cross-cut the whole breadth of Flow Unit 2a, but also cross-cuts Flow Unit 2b, and the upper section of Flow Unit 2c. S_3 fractures evolve differently from S_2 fractures, becoming slightly arcuate as they travel down-glacier, plus they develop in clusters of fractures that are separated by comparatively fracture-free ice. The final generation of crevasse traces (S_4) develops near to the terminus of the glacier. S_4 fractures cross-cut the whole width of Flow Unit 2a, as well as Flow Units 2b, 2c, 3 and 4. These crevasse traces are oriented transverse to flow and are slightly arcuate down-glacier.

5.2.3 Flow Unit 2b

The first structure evident in the upper reaches of Flow Unit 2b is primary stratification (S_0). However, the primary stratification (S_0) becomes transposed into longitudinal foliation (S_1) (Figure 5.2) in a relatively short distance (*c*. 600 metres) down-glacier. The whole width of the flow unit is dominated by longitudinal foliation (S_1); however, it is strongest on the true-left of the flow unit, especially at the boundary with Flow Unit 2c. Clusters of crevasse traces (S_2) develop in the upper middle reaches of the flow unit (the same fracture set as S_2 in Flow Unit 2a), which are primarily concentrated on the true-right of the flow unit and become increasingly arcuate down-glacier. A second suite of crevasse traces (S_3) form near to the terminus of the glacier (the same fracture set as S_4 in Flow Unit 2a), and remain transverse to flow.

5.2.4 Flow Unit 2c

Primary stratification (S_0) in the accumulation basin of Flow Unit 2c evolves into longitudinal foliation (S_1), which is strongest at the boundaries of the flow unit. Two suites of crevasse traces can be found in the flow unit. The first set of fractures (S_2) are exclusively found clustered in the upper-middle section of the flow unit and are linear features oriented transverse to flow (the same fracture set as S_3 in Flow Unit 2a). The second fracture set (S_3) develops relatively far down the glacier tongue (*c*. 300 metres

up-glacier from the terminus), forming linear crevasse traces oriented transverse to flow that are in distinct clusters (the same fracture set as S_4 in Flow Unit 2a).

5.2.5 Flow Unit 3

The accumulation area of Flow Unit 3 is dominated by the transposition of primary stratification (S_0) into longitudinal foliation (S_1). The rest of the flow unit is mainly composed of longitudinal foliation (S_1), which is strongest at both of the flow unit boundaries. In the lower reaches of the flow unit there are two cross-cutting fracture sets, the first of which (S_2) cross-cuts the flow unit perpendicular to flow (the same fracture set as S_4 in Flow Unit 2a). The second fracture set (S_3) develops near to the terminus and is oriented obliquely up-glacier to fracture set S_2.

5.2.6 Flow Unit 4

The first structure observed in the accumulation basin of Flow Unit 4 is primary stratification (S_0). Down-glacier of the primary stratification, transverse fractures (S_1) develop on the true-right of the flow unit. This suite of crevasse traces (S_1) is composed of approximately equally spaced (*c*. 25 metres apart) fractures that are contained wholly in Flow Unit 4, and persist from the upper accumulation area to the glacier terminus. As the fractures travel down-glacier they become increasingly arcuate but remain symmetrical, ultimately becoming very tight similar folds towards the terminus (Figure 5.3). In the middle-reaches of the flow unit, longitudinal foliation (S_2) forms, that is particularly strong at the boundary with Flow Unit 3. In the lower section of the flow unit, two suites of fractures are present. The first set (S_3) comprises linear transverse fractures that form in clusters (the same fracture set as S_4 in Flow Unit 2a). The second fracture set (S_4) develops slightly further down-glacier near to the terminus (the same fracture set as S_3 in Flow Unit 3), oriented obliquely up-glacier from the previous fracture set.

Figure 5.3. View up-glacier of the boundary between Flow Units 4 and 5a. Note the longitudinal foliation in the foreground. Person shown to indicate scale. Photograph taken during summer 2013, and provided courtesy of M. J. Hambrey.

5.2.7 Flow Unit 5a

Primary stratification (S_0) in the upper accumulation area of Flow Unit 5a becomes increasingly folded down-glacier, eventually transposing into longitudinal foliation (S_1). Flow Unit 5a is a particularly narrow flow unit and longitudinal foliation (S_1) is the dominant structure, becoming strongest at the boundary with Flow Unit 4 towards the terminus (Figure 5.3). Crevasse traces are not a prominent feature in Flow Unit 5a; however, some fractures (S_2) derived from Flow Unit 5b extend into the true-right of the flow unit. Some further minor fractures (S_3) occur near the terminus where a spatially limited cluster of fractures obliquely cross-cuts the flow unit (the same fracture set as S_3 in Flow Unit 3).

5.2.8 Flow Unit 5b

Primary stratification (S_0) in the upper reaches of Flow Unit 5b becomes transposed into longitudinal foliation (S_1) in a comparatively short distance (*c*. 500 metres),

especially at the flow-unit boundaries. Also high in the accumulation basin, regularly spaced transverse fractures (S_2) develop, initially on the true-right of the flow unit, but becoming increasingly dominant in the centre of the flow unit down-glacier. This fracture set (S_2) also becomes increasingly rotated down-glacier in an anti-clockwise direction until becoming almost longitudinally oriented at the terminus. A second set of fractures (S_3) also appears in the upper-middle reaches of the flow unit, forming on the true-right. However, the fractures quickly die-out after formation. Near the terminus of the glacier, a third set of crevasse traces (S_4) also cross-cut the flow unit obliquely up-glacier (the same fracture set as S_3 in Flow Unit 3).

5.2.9 Flow Unit 6

The upper basin of Flow Unit 6 is dominated by primary stratification (S_0) that becomes cross-cut by water-healed crevasses (S_1) (Figure 5.2). Both S_0 and S_1 structures become increasingly arcuate down-glacier, until in the middle-reaches of Flow Unit 6, water-healed crevasses (S_1) die-out. In the upper-middle-reaches of the flow unit, longitudinal foliation (S_2) can be found developing at the flow unit's boundaries, and is particularly strong with the boundary with Flow Unit 5b. Two suites of fractures are present in Flow Unit 6. The first fracture set (S_3) develops in the middle-reaches of the flow unit, forming regularly spaced linear fractures oriented transverse to flow that become increasingly clustered and arcuate down-glacier. The second fracture set (S_4) forms close to the terminus and cross-cuts the flow unit obliquely up-glacier (the same fracture set as S_3 in Flow Unit 3).

5.3 Detailed ice facies log descriptions

A total of five detailed ice facies logs were taken on Austre Brøggerbreen to document the surface variations in ice facies. Logs are ordered from up-glacier to down-glacier and taken at locations along a single flowline, approximately following the boundary between Flow Units 5a and 5b, with the highest up-glacier log located in the middle-reaches of the glacier (Figure 5.4). Log sizes range from 1.7 to 15.0 metres depending

on the sections of ice facies exposed at the surface of the glacier at each selected site. A brief description of each log is discussed below; however, for more detail please refer to the drawn logs (Figure 5.5).

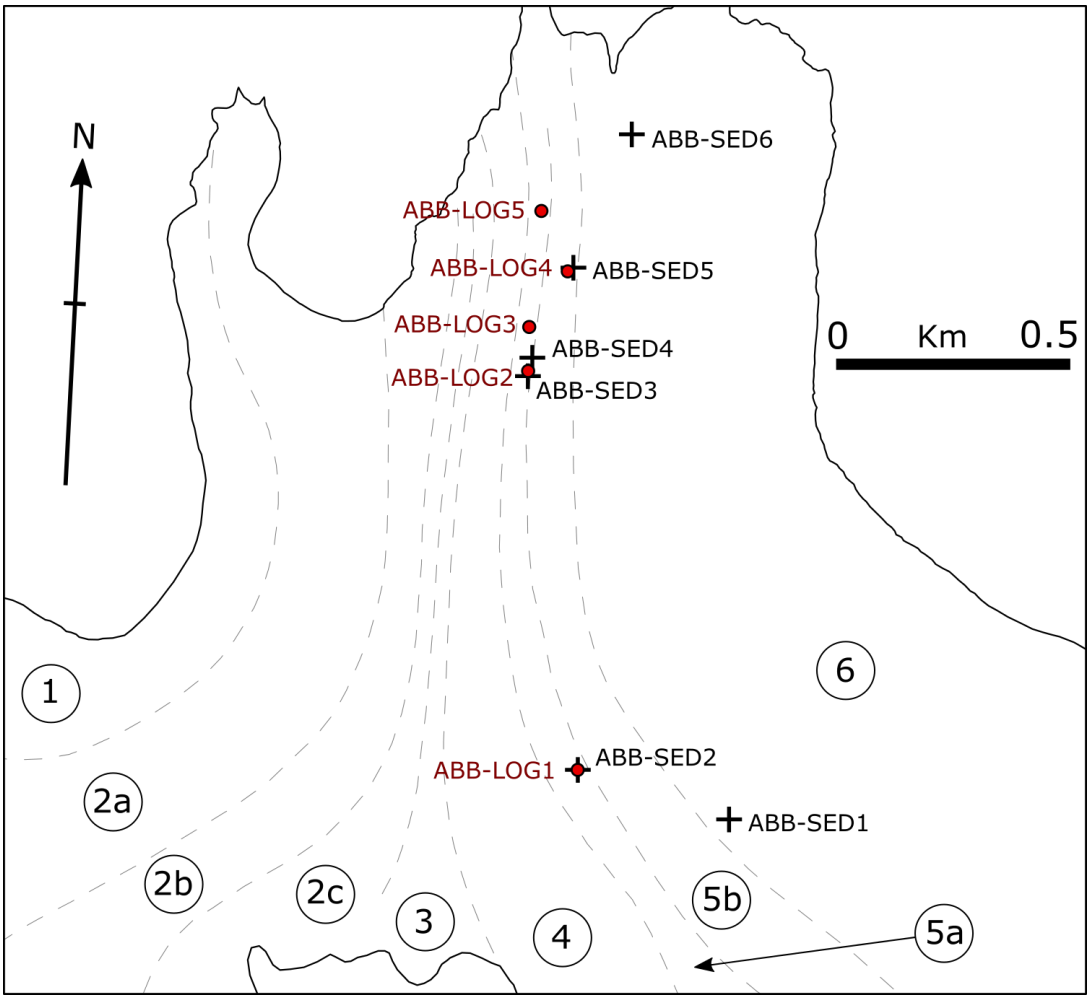

Figure 5.4. Flow unit map of the snout of Austre Brøggerbreen showing the location of the detailed ice facies logs (red circles with red log identification numbers), and the sediment samples (black crosses with black sediment identification numbers).

5.3.1 ABB-LOG1 – 78.89203°N, 11.82353°E

ABB-LOG1 (Figure 5.5) is the highest up-glacier log collected in this study on Austre Brøggerbreen, and measures 15.0 metres in length. The log is dominated by alternating layers of coarse bubbly and fine ice with occasional comparatively thin (*c.* 1 centimetre thick) layers of coarse clear ice. Ice layers are moderate to steeply dipping (60° - 90°), with numerous cross-cutting fractures. Cross-cutting fractures often consist

FIGURE 5.5 - ABB COMBINED DETAILED LOGS - PLEASE SEE APPENDIX

of thin traces with no evidence of ice crystal growth within the fracture, or slightly wider fractures that are healed by coarse clear ice crystals. Infrequent coarse clear ice lenses are found in some fine ice layers, with strongly folded coarse bubbly layers contained in fine ice layers suggesting strong deformation. All fine ice layers are strongly foliated, while coarse bubbly layers are less so, with moderate or weak foliation evident.

5.3.2 ABB-LOG2 – 78.89967°N, 11.81638°E

ABB-LOG2 (Figure 5.5) is 3.0 metres long cross-cutting the apex of a debris ridge on the surface of Austre Brøggerbreen. The log is dominated by coarse clear ice and coarse bubbly ice with infrequent thin fine ice layers. All layers are steeply dipping with many ice layers containing stringers of bubbles and mud clots oriented parallel to the ice layer (Figure 5.6). Most layers are weakly foliated with occasional strongly foliated layers. At the 1.8 metre mark a comparatively thin debris septum containing Neoproterozoic psammite clasts (fine sand to cobble size, with occasional boulders) held in interstitial ice (Figure 5.7), is the source of debris for the debris ridge. Clasts are mainly sub-angular in roundness with long axes (*a*-axes) aligned roughly parallel to ice layers and foliation.

5.3.3 ABB-LOG3 – 78.90052°N, 11.81625°E

ABB-LOG3 (Figure 5.5) is 4.4 metres in length and is almost exclusively composed of strongly foliated coarse bubbly ice. Infrequent thin fine ice layers sometimes contain debris or disseminated muds. All ice layers and foliation are steeply dipping (> 70°), which are cross-cut by several shallower angled fractures. Fracture planes are often defined by bubble planes and sediment content. Folded ice layers are uncommon; however, a strongly folded thin layer defined by disseminated muds at *c*. 3.0 metres with isoclinal folds demonstrates axial planar foliation parallel to the fold hinge (Figure 5.8).

Figure 5.6. Steeply dipping coarse clear ice facies with thin layers of disseminated muds and stringers of bubbles orientated parallel to foliation. Photograph taken at log location ABB-LOG2.

Figure 5.7. A comparatively thin, steeply dipping debris septum containing Neoproterozoic psammite clasts. Note the mainly sub-angular clasts (ranging from fine sand to cobble size) with long axes orientated parallel to foliation. Photograph courtesy of M. J. Hambrey.

5.3.4 ABB-LOG4 – 78.90163°N, 11.81981°E

ABB-LOG4 (Figure 5.5) was located directly below several moulins located in the lower-reaches of the glacier, 1 metre east of a minor orange/cream weathered debris ridge

consisting of psammite clasts. The log is 1.7 metres in length and comprises numerous layers of coarse bubbly, coarse clear and fine ice that are comparatively steeply dipping. Several coarse bubbly and fine ice layers are foliated with disseminated muds which vary in colour from red to brown. Several coarse clear ice lenses can be found in a coarse bubbly ice layer at *c*. 0.25 metres with a further strongly folded coarse clear ice layer located at *c*. 0.8 metres (Figure 5.9).

Figure 5.8. A thin folded layer defined by disseminated muds demonstrating an axial planar relationship with longitudinal foliation (foliation runs from the bottom to the top of the image).

Figure 5.9. Alternating layers of steeply dipping coarse bubbly, coarse clear, and fine-grained ice with disseminated multi-coloured muds. Isotope sampling locations indicated by 'V' markers. Ice screw for scale.

5.3.5 ABB-LOG5 – 78.90277°N, 11.81684°E

ABB-LOG5 (Figure 5.5) is 1.8 metres in length and is the furthest down-glacier log taken on Austre Brøggerbreen. The log was located near to the apex of a prominent moraine of Neoproterozoic schist on the snout of the glacier, and is mainly composed of fine ice separated by comparatively thin layers of coarse clear ice. All ice layers are steeply dipping (> 75°) and many ice layers are foliated, with several fine ice layers contain various types of greenish or reddish muds.

5.3.6 Summary of detailed log descriptions

Each log taken on Austre Brøggerbreen is structurally unique. Even though every log contains a variety of ice types, the percentage of each ice facies varies significantly (Figure 5.10). However, the logs are similar in having moderately to steeply dipping ice layers, as well as containing fine ice facies which are not observed in initial snowpack formation (*see* Wadham and Nuttall, 2002; Jennings et al., 2014). The steeply dipping

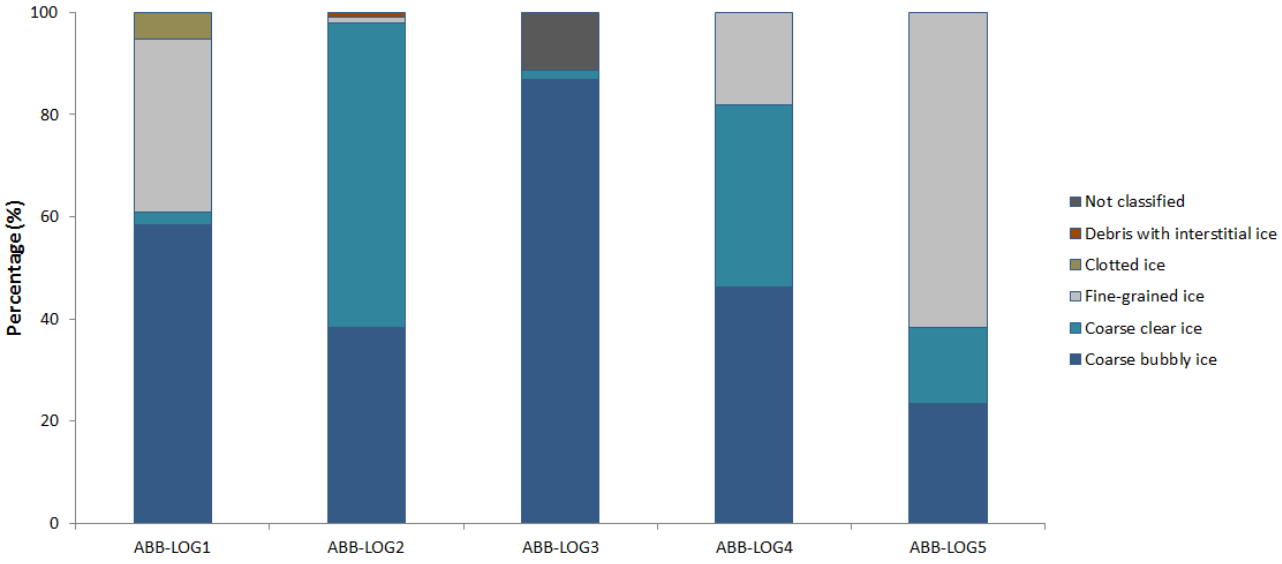

Figure 5.10. Graph showing the percentage of each ice facies present in the detailed ice logs collected on Austre Brøggerbreen.

ice layers demonstrate how primary stratification has become strongly folded and re-orientated as it travels down-glacier, with changes in the percentage of different ice

types reflecting the spatial and temporal variability of ice formation and evolution. Crystal modification of ice to form a fine ice facies combined with varying strengths of foliation observed suggests that the ice described has undergone strong deformation and simple shear as a result of differential flow at a flow unit boundary.

5.4 Stable isotope analysis

A total of 27 isotopic samples were collected from the surface of Austre Brøggerbreen. The majority of isotopic sample locations coincided with the detailed ice facies logs (described above) to ensure that the surrounding structural context of each sample was recorded. In addition to the spatial location of individual isotopic samples, the type of ice sampled was recorded for each to enable any differences between ice facies to be identified. Four classes of ice facies, including coarse bubbly ice, coarse clear ice, fine-grained ice, and clotted ice, were sampled on Austre Brøggerbreen and analysed for $\delta^{18}O$ and δD values (values summarised in Table 5.2).

Table 5.2. Table showing the mean $\delta^{18}O$ and δD values for isotope samples of varying ice facies collected at the surface of Austre Brøggerbreen. Note *n* refers to the number of samples and σ is the standard deviation.

		$\delta^{18}O$ (‰)		δD (‰)	
Ice facies	***n***	**Mean**	σ	**Mean**	σ
Coarse bubbly ice	11	-12.04	0.81	-84.01	5.62
Coarse clear ice	9	-11.56	0.84	-80.63	5.75
Fine-grained ice	3	-11.02	0.63	-77.52	3.70
Clotted ice	3	-10.98	0.72	-77.50	4.96

5.5 Sedimentology

Six supraglacial sediment samples were obtained from Austre Brøggerbreen, most of which were collected in relation to the detailed ice facies logs to ensure that the

surrounding structural context of the sediment was recorded (Figure 5.4). Sediment samples not correlated to a detailed ice facies log were located using a handheld GPS unit, and the glaciological setting described. Sediment samples are ordered from up-glacier to down-glacier and are described in relation to log locations. A brief description of each sample is discussed below, but for more detailed information refer to the raw sediment data and combined sediment graphs (Figure 5.11).

5.5.1 ABB-SED1 - 78.89123°N, 11.83892°E

ABB-SED1 is located up-glacier of ABB-LOG1 in a *c*. 1 metre wide zone of sediment laden coarse bubbly and coarse clear ice surrounded by foliated coarse bubbly ice. The sediment laden ice facies is strongly foliated and consists of clotted ice with millimetre-scale clots of brown mud disseminated throughout (Figure 5.12). Discontinuous sub-centimetre veins of coarse clear ice contain fewer mud clots that cross-cut the foliated clotted ice facies obliquely.

The grainsize distribution histogram for ABB-SED1 (Figure 5.11) shows a large peak at the 4 Φ (0.063 millimetres) size fraction. Even though there are some limited amounts of coarse sands present, the majority of sediment contained in the sample is within the very fine sand, silt and clay size classes. The amount of calcium carbonate contained within the sample as confirmed by effervescence is classed as 'very slightly calcareous' with a calcium carbonate concentration of 0.5%.

5.5.2 ABB-SED2 – 78.89203°N, 11.82353°E

ABB-SED2 is located near to ABB-LOG1 in an area of strong deformation consisting primarily of alternating coarse bubbly layers with moderate to weak foliation, and fine ice/clotted ice layers with strong foliation (Figure 5.13). Two types of sediment are present at ABB-LOG1; reddish fine-grained sediment and brown fine-grained sediment, both of which are probably derived from different lithologies and highlight different ice structures.

FIGURE 5.11 - ABB COMBINED SEDIMENT GRAPHS – PLEASE SEE APPENDIX

The grainsize distribution histogram for ABB-SED2 (Figure 5.11) has a bimodal distribution with distinct peaks occurring at 3 Φ (0.125 millimetres) and 7.5 Φ (0.00539 millimetres), illustrating larger concentrations of very fine sand and very fine silt size fractions within the sample. The amount of calcium carbonate contained within the sample as confirmed by effervescence is classed as 'non-calcareous' with a calcium carbonate concentration of 0 - 0.1%.

Figure 5.12. Clotted ice facies at the surface of Austre Brøggerbreen. Note the millimetre-scale clots that are disseminated throughout the ice facies, with discontinuous sub-centimetre veins of coarse clear ice cutting through the clotted ice. Photograph courtesy of M. J. Hambrey.

Figure 5.13. Strongly foliated fine-grained ice that contains brown fine-grained sediment, separated by weakly foliated coarse bubbly ice. Note the strongly folded fracture cross-cutting both ice facies that contains reddish fine-grained sediments.

5.5.3 ABB-SED3 - 78.89957°N, 11.81638°E

ABB-SED3 is located just up-glacier of ABB-LOG2 in an area where a number of englacial debris packages emerge at the surface of the glacier to form ice-cored debris ridges. Debris ridges are oriented longitudinally, parallel to local foliation, and consist of a range of sediment/clast sizes from clay through to cobble size particles.

The grainsize distribution histogram for ABB-SED3 (Figure 5.11) has a bimodal distribution with peaks occurring at *c*. 1 Φ (0.5 millimetres) and 7 Φ (0.007832 millimetres). This sample contains concentrations of medium to very fine sand, silt and clay size fractions; however, with a slightly larger peak in the slit fraction (*c*. 7 Φ). The amount of calcium carbonate contained within the sample as confirmed by effervescence is classed as 'non-calcareous' with a calcium carbonate concentration of 0 - 0.1%.

5.5.4 ABB-SED4 - 78.89993°N, 11.81672°E

ABB-SED4 is located near to ABB-LOG2 where the fold hinge of a folded sediment laden ice facies crops out at the surface of the glacier (Figure 5.14 and 5.15) *c*. 4 metres east of the apex of an emerging longitudinal debris ridge. The sediment disseminated throughout the ice layer varies in colour from greenish to reddish-brown.

The grainsize distribution histogram for ABB-SED4 (Figure 5.11) has a slightly bimodal distribution with a leaser peak occurring at *c*. 2 Φ (0.25 millimetres) and a larger peak at *c*. 6 Φ (0.015659 millimetres). In addition to this, a further peak that does not fit into the bimodal distribution occurs at 4 Φ (0.063 millimetres). As for previous samples, ABB-SED4 has high concentrations of medium sand particles through to clay particles. The amount of calcium carbonate contained within the sample as confirmed by effervescence is classed as 'non-calcareous' with a calcium carbonate concentration of 0 - 0.1%.

Figure 5.14. A fold hinge of sediment-rich ice cropping out at the surface of Austre Brøggerbreen. Photograph courtesy of M. J. Hambrey.

Figure 5.15. Strongly foliated sediment laden ice facies with disseminated multi-coloured muds. Photograph courtesy of M. J. Hambrey.

5.5.5 ABB-SED5 - 78.90171°N, 11.82035°E

ABB-SED5 is located next to ABB-LOG4 in an area of alternating ice types with varying amounts entrained sediments (Figure 5.16). Reddish and brown sediment types were visible, probably indicating two different lithological sources, contained within

Figure 5.16. Alternating layers of thin and strongly foliated ice types with varying amounts of disseminated reddish and brown muds. Photograph courtesy of M. J. Hambrey.

millimetre-scale clots of fine-grained sediment. Infrequent cobble size clasts contained in the ice have *a*-axis orientations parallel to ice layers.

The grainsize distribution histogram for ABB-SED5 (Figure 5.11) has a bimodal trend with peaks occurring at *c*. 1 Φ (0.5 millimetres) and *7* Φ (0.005539 millimetres). As is the case for ABB-SED 4, an additional peak that does not fit into the bimodal distribution occurs at 4 Φ (0.063 millimetres); however, this peak is much more dominant. The amount of calcium carbonate contained within the sample as confirmed by effervescence is classed as 'slightly calcareous' with a calcium carbonate concentration of 2%.

5.5.6 ABB-SED6 - 78.90434°N, 11.82547°E

ABB-SED6 is located on the snout of Austre Brøggerbreen, 5 metres up-glacier from the terminus. The sediment sample was extracted from coarse clear ice consisting of

ice crystals with typical diameters of *c*. 10 centimetres, with mud clots reaching *c*. 2 - 3 centimetres in diameter consisting reddish brown sediment.

The grainsize distribution histogram for ABB-SED6 (Figure 5.11) shows a large peak at the 4 Φ (0.063 millimetres) size fraction. The majority of sediment in the sample are contained within the medium sand through to medium/fine silt size fractions. The amount of calcium carbonate contained within the sample as confirmed by effervescence is classed as 'very calcareous' with a calcium carbonate concentration of 10%.

5.6 Interpretation and discussion

5.6.1 Glacier-wide structural overview

Like many glaciers in Svalbard, Austre Brøggerbreen has receded and thinned substantially since its maximum extent during the Neoglacial of around 1900 AD. However, this has revealed the internal structure of the glacier in unprecedented detail, acting like a bed-parallel slice through the glacier that allows structures that are not usually visible at the surface of the glacier to be documented.

Unlike many other previously studied glaciers, Austre Brøggerbreen is predominantly covered by fractures that are ubiquitous throughout, from the upper accumulation area to the terminus. Each flow unit has several fracture sets with unique origins and evolutions; however, as the glacier is at present relatively inactive with low flow velocities ranging from 0.5 to 3.0 m a^{-1} (*see* Hagen and Liestøl, 1990; Hagen et al., 1993), the majority of fractures must be relict features. It is therefore likely that the majority of fractures were formed when ice velocities were sufficiently high to induce glacier-wide ice fracturing, most likely during the Neoglacial when the glacier was at its maximum extent (Jennings et al., 2015). The presence of relict fractures across the whole of Austre Brøggerbreen, despite undergoing substantial ablation and surface lowering, suggests that these fractures penetrate to great depths, possibly reaching the glacier bed (*see* Hambrey and Müller, 1978; Jennings et al., 2014; 2015). The great depths to which relict fractures penetrate further suggest that the

glacier must have been substantially more dynamic when they formed to enable the fractures to propagate to that depth.

Contemporary forming structures on Austre Brøggerbreen include primary stratification that undergoes folding and eventual transposition into longitudinal foliation, the formation of spatially limited fractures high in the accumulation area which subsequently heal as they become infilled by meltwater, slush and snow, and ductile modification of pre-existing relict fracture sets. Ductile modification becomes superimposed on passively transported fractures as a result of ice creep; however, ductile deformation is spatially variable and differs between individual flow units.

5.6.2 Origin and structural evolution of flow units

The structural investigation of a temperate Alpine valley glacier (Vadrec del Forno, Switzerland) undertaken by Jennings et al. (2014) yielded a number of unique findings, especially with regard to flow units and how multiple flow units interact. One of the main conclusions made by Jennings et al. (2014) was that flow units originating in their own individual sub-accumulation basins are unique and mutually exclusive from neighbouring flow units. As each sub-accumulation basin has different characteristics (*e.g.* basin size, altitude and snow input), those attributes are reflected in their corresponding flow unit, dictating the structures present, the structural evolutions, and dominance of the flow unit within the whole-glacier system. This study attempts to test the hypothesis of Jennings et al. (2014) to see if it is applicable for a cold-based Arctic glacier.

Glacier-wide structural mapping of Austre Brøggerbreen from aerial photography allowed the identification of different structures, verified by field observations in 2013, and the division of the glacier into discrete flow units using criteria outlined by Goodsell et al. (2005b) and Jennings et al. (2014) (Figure 5.1). As can be seen in *section 5.2* and summarised in Table 5.1, the structural attributes of each flow unit are inherently different from one-another. The different characteristics of each flow unit, including the structures present, number of structures, order of

structure formation and unique structural evolutions indicates that the flow units on Austre Brøggerbreen are unique and mutually exclusive from one-another, as proposed by Jennings et al. (2014) for Vadrec del Forno. Jennings et al. (2014) further suggested that the evolution of structures in discrete flow units differed from one-another, concluding that different types of longitudinal foliation (transposition foliation and axial planar foliation) preferentially formed in flow units with different characteristics. In contrast to Vadrec del Forno, Austre Brøggerbreen is dominated by fractures, not by the formation and evolution of longitudinal foliation. Nevertheless, the different evolutions of passively transported fractures in discrete flow units can be used to infer contrasting flow conditions in different sectors of the glacier. Comparison of the evolution of transverse fracture sets in discrete flow units reveal the unique deformation history and corresponding characteristics of each flow unit. On Austre Brøggerbreen this is especially evident in Flow Units 2a, 4 and 5b, where initially transverse fracture sets contained exclusively in each flow unit undergo different flow histories when transported passively down-glacier (Figure 5.1). The transverse fractures in Flow Unit 4 become increasingly arcuate down-glacier indicating that flow is fastest in the centre of the flow unit, with increased amounts of simple shear at the flow unit's boundaries. However, in Flow Units 2a and 5b, initially transverse fractures remain linear features but become rotated in a clockwise and anticlockwise direction respectively. This suggests that flow is non-uniform in each of the flow units, and is fastest on the true left of Flow Unit 2a, and true right of Flow Unit 5b (Jennings et al., 2015). Regardless of the direction of crevasse rotation, because rotation of initially transverse crevasses is observed, ongoing simple shear at flow unit boundaries can be inferred. This is further supported by the presence of strong longitudinal foliation observed in logs located on a flow unit boundary such as ABB-LOG1. Previous studies have suggested that the strongest longitudinal foliation is found at flow unit boundaries where simple shear is inferred to be greatest (*e.g.* Hambrey et al., 2005; Jennings et al., 2014, 2015). Very strong foliation in ABB-LOG1, combined with the presence of large amounts of fine-grained ice, lends support to this hypothesis as it is likely that fine ice develops as a result of crystallographic modification of existing ice layers by simple shear (Jennings et al., 2014).

5.6.3 Sedimentological evidence for the origin and evolution of longitudinal foliation

Sediment pathways through glaciers and the manner in which debris becomes entrained and is transported has been an area of research that has received an increasing amount of interest over the last two decades. It has become apparent that sediment transport through glaciers is more complex than previously thought, and that glacier structure plays an important controlling role. Structural analysis of glacial sediments has already been successfully applied to a number of valley glaciers in Svalbard (*e.g.* Bennett et al., 1996; Hambrey et al., 1996, 1999, 2005; Boulton et al., 1999; Hambrey and Glasser, 2003; Hubbard et al., 2004), and structural controls on debris transport in temperate valley glaciers has also been receiving an increasing amount of attention (*e.g.* Eyles and Rogerson, 1978; Goodsell et al., 2005a, b; Roberson, 2008; Appleby et al., 2010; Jennings et al., 2014). Unlike previous studies that have generally undertaken sedimentological analysis to understand how debris becomes entrained and is subsequently transported through an ice mass, this study attempts to also use sedimentological analysis to infer the formation mechanism and evolution of longitudinal foliation. By identifying areas of structurally interesting ice that appeared to have 'basal' characteristics, it was hoped that evidence could be collected to test Hambrey and Glasser's (2003) model of a part-basal origin of foliation and structurally controlled debris entrainment in glaciers. To do this, detailed structural and sedimentological investigation of Austre Brøggerbreen was undertaken along an approximate flowline at a flow-unit boundary (boundary between Flow Units 5a and 5b).

Debris entrained in a glacier can originate from a number of different source locations, such as rockfall/avalanche from precipitous head- and side-walls, or from entrainment at the glacier bed. Once entrained on the surface of the glacier or within the body of the ice mass, the debris can be transported through different pathways (supraglacially, englacially, or subglacially). Englacially and subglacially transported material can subsequently re-emerge at the surface of the glacier as a result of several processes such as ablation/surface lowering, folding of internal layering, and thrusting of debris up through the ice mass (*e.g.* Hambrey et al., 1999, 2005; Goodsell et al., 2002, 2005b; Herbst et al., 2006; Swift et al., 2006). By looking at the characteristics of

debris that has been transported and re-emerged at the surface of the glacier, it is possible to discern the origin of the debris and identify its transport pathway through the glacier. All of the sediment samples collected on Austre Brøggerbreen in areas with 'basal' characteristics primarily comprise fine sediment fractions (medium sand to clay). The large proportion of fine grain fractions and lack of coarse particles suggests debris is being sorted before or during the process of debris entrainment. The preferential entrainment of fine-grained sediments indicates that debris derived from rockfall/avalanche is unlikely to be the source of the sediments. Rockfall, which comprises a wide range of clast sizes, can become entrained in an ice mass as it accumulates on the surface of a glacier and becomes buried by snow (Drewry, 1986; Benn and Evans, 2010). Even though some limited weathering can occur on the surface of the glacier, it is not able to substantially erode large clasts. Once buried by snow, the eventual diagenesis of snow into glacier ice entrains the debris in primary stratification. Folding of the primary stratification and the englacial debris package can cause limited crushing of particles as clast interact (Jennings et al., 2014); however, as large boulders are infrequently transported at higher levels in a glacier it is unlikely that large amounts of debris can be substantially altered by crushing to form a fine grain-size distribution (Boulton, 1978). Dunning et al. (2015) demonstrated that rockfall deposits that become entrained into glacier ice are well preserved, conserving the characteristics of the rockfall debris despite being englacially transported. As a result, debris depleted in coarse grain fractions and enriched in fine fractions are more likely to be derived from the glacier bed rather than debris transported at higher levels in the glacier (Boulton, 1978). At the bed of a glacier, the velocity of debris particles in traction is reduced below the velocity of the surrounding ice as a result of friction against the bed. This reduction in velocity increases the number of particle collisions that take place in the basal ice, which is further enhanced by plastic flow around obstacles and pressure melting/regelation that causes particles to frequently become in contact with the glacier bed (Boulton, 1978). The grainsize distributions of the supraglacial sediment samples collected from Austre Brøggerbreen (Figure 5.11) resemble the distributions for terminal grades in tills. Terminal grades reflect the action of crushing and abrasion that breakdown larger rocks to form sand and silt size fractions, a process that is common at the bed of a glacier. Pure crushing causes rock

disintegration along crystal boundaries to form sand-sized particles, whereas abrasion produces cracks across mineral grains resulting in silt-sized particles. Despite the different formation processes for sand and silt size fractions, both are regarded as components that are resistant to further glacial comminution (Dreimanis and Vagners, 1971; Haldorsen, 1981). However, even though basal transport of debris can produce sufficient amounts of fine grain sediments, basal debris is not exclusively fine-grained material and usually comprises a wide particle size distribution. Therefore, another mechanism that preferentially entrains only fine debris particles must have been active during entrainment. Furthermore, a mechanism to elevate basal debris to the surface of the glacier is also necessary. Several debris entrainment mechanisms are known to occur at the bed of a glacier including the incorporation of debris as a result of regelation/freezing processes, the formation of basal crevasses, or by thrusting (Alley et al., 1997). However, in the case of many of these processes, the entrained debris would be a non-sorted diamicton which contains a wide range of clast sizes. Processes such as thrusting can also be eliminated as no evidence of thrusting was found on Austre Brøggerbreen. It is therefore more likely that the origin of the entrained fine sediments is from suspended sediment contained in the basal hydrological system, as larger clasts cannot be held in suspension. This is further supported as differences in the calcium carbonate concentration between samples suggest a basal hydrological origin for the sediment. As samples were collected along an approximate flowline, it would be expected to find similar lithologies (with similar concentrations of calcium carbonate) along the length of the flowline. However, this is not the case, indicating that there is some mixing of sediments that are derived from different lithologies. Mixing of sediments from different source areas is most likely to occur at the glacier bed as sediments transported by the basal hydrological system combine. Furthermore, the concentration of calcium carbonate in samples located further down-glacier (*e.g.* ABB-SED5 and ABB-SED6) is higher, which would be expected for sediments transported in the basal hydrological system as mixing of sediment from different sources is more likely down-glacier.

Sediment carried in suspension at the glacier bed can become regelated to the basal zone of the glacier, forming fine-grained debris-rich ice layers. This process has

been documented in previous studies (*e.g.* Souchez and Lorrain, 1987; Hubbard and Sharp, 1993, 1995), forming ice facies known as regelation ice. Regelation ice is often observed with closely spaced laminae *c*. 0.1 - 1.0 millimetre in thickness, composed of alternating clear and debris-rich ice which represents individual freezing events (Lawson et al., 1998; Benn and Evans, 2010). However, on Austre Brøggerbreen, no laminated ice was observed, and sediment samples were collected near to sediment-rich clotted ice facies. An alternate process which has been suggested as the formation mechanism of clotted ice is glaciohydraulic supercooling (Lawson et al., 1998; Cook et al., 2006). It has been argued that the freezing of supercooled water can form ice with clots containing silt-sized debris; however, other studies have suggested that the process forms stratified basal ice layers that can reach up to *c*. 10 metres in thickness (*see* Lawson et al., 1998). Nevertheless, because clotted ice has been observed in a variety of environments, it has been suggested that it might just form when turbid water undergoes bulk freezing (Knight, 1994; Christofferssen et al., 2006; Benn and Evans, 2010). Regardless of the exact formation process, the sediment sampled at the surface of Austre Brøggerbreen has, most likely, a basal glaciofluvial origin. Once the fine-grained sediment is entrained in the glacier, the basal ice layer becomes folded upwards at flow unit boundaries as a result of lateral compression, as suggested by Hambrey and Glasser (2003). Ice flow from a wide accumulation area into a comparatively narrow tongue folds the initially bed-parallel ice layers, elevating sediment-rich basal ice layers higher in the glacier. This process is most pronounced at flow unit boundaries where greater amounts of simple shear are inferred. As a result, basal ice layers can become sufficiently folded and elevated within the glacier at flow unit boundaries to become exposed at the surface of the glacier by ablation and surface lowering. Isotopic sampling of different ice facies at the surface of Austre Brøggerbreen supports this conclusion to some degree. Mean $\delta^{18}O$ and δD values show an enrichment of heavy isotopes in ice facies that are not observed in initial snowpack formation, suggesting that clotted ice facies probably form as a result of refreezing at the glacier bed (Hubbard and Sharp, 1995). However, the low number of isotope samples collected in this study means that isotopic values are not significantly different from one-another; therefore, a larger sampling campaign is necessary to draw more meaningful conclusions.

For the above hypothesis, regarding the entrainment of fine-grained sediment at the bed of Austre Brøggerbreen and subsequent elevation to the surface of the glacier by folding, it is necessary for water to be present at the glacier bed. It is known that Austre Brøggerbreen at present is predominantly cold-based (Hagen and Sætrang, 1991; Björnsson et al., 1996; Stuart et al., 2003); however, it is unlikely that it was always so. The dominance of fracture sets preserved all over the surface of the glacier (including high in the accumulation area) suggests that Austre Brøggerbreen was substantially more dynamic during Neoglacial time when the glacier was thicker and more extensive (Garwood and Gregory, 1898). This implies that the glacier must have had a polythermal basal regime during this time to enable such widespread fracturing; therefore, water would have been present at the bed of the glacier in the past. The ongoing change from polythermal to cold-based thermal regimes since Neoglacial time has been suggested for neighbouring glaciers Midtre and Austre Lovénbreen by Glasser and Hambrey (2001), a process which would have also occurred for Austre Brøggerbreen as the glacier receded and down-wasted. The implication of this is that the entrainment of fine-sediments is a relict process that occurred during the past when Austre Brøggerbreen had a polythermal thermal regime. Subsequent folding elevated the sediment-rich basal layer through the glacier, eventually becoming exposed at the surface as a result of ablation and surface lowering. The folding of ice layers and related elevation of sediment-rich basal ice is possible within a glacier with a cold thermal regime; therefore, despite the sediment entrainment process being relict in Austre Brøggerbreen, the folding and associated formation of strong longitudinal foliation maybe still ongoing. Even though this may be an important entrainment process in polythermal glaciers, it is not likely to be common in temperate glaciers as basal melt rates are too high to allow substantial basal regelation of sediment-rich water.

5.6.4 Origin and evolution of crevasse traces and related fracture-derived longitudinal foliation

As mentioned above, Austre Brøggerbreen is unique when compared with other structurally studied glaciers as it is dominated by fractures. Previous structural studies have illustrated that the evolution of primary stratification into longitudinal foliation (either transposed foliation or axial planar foliation) is one of the dominant processes occurring in valley glaciers, regardless of glacier size, geographical location, or thermal regime (*e.g*. Allen et al., 1960; Hambrey and Milnes, 1977; Hooke and Hudleston, 1978; Hambrey et al., 1980, 2005; Goodsell et al., 2005b, Jennings et al., 2014, 2015; Hudleston, 2015). Even though both transposition and axial planar foliation were documented on Austre Brøggerbreen, the main process evident on the glacier is ductile modification of pre-existing fracture sets. In two cases, reorientation of initially transverse fracture sets (Flow Units 4 and 5b) has been sufficient to develop a fracture-derived longitudinal foliation that has not been observed in previous structural studies (Jennings et al., 2015). Even though a fracture-derived longitudinal foliation has not been previously observed on other glaciers, it is worth noting that arcuate foliation (also called transverse foliation) is also a fracture-derived foliation (*see* Allen et al., 1960; Ragan, 1969; Hambrey and Milnes, 1977; Hambrey et al., 1980; Goodsell et al., 2002); however, it typically develops at the base of an icefall and is oriented transverse to ice flow. On Austre Brøggerbreen, fracture-derived longitudinal foliation is most discernible at flow-unit boundaries where the cumulative effect of simple shear is inferred to be greater, allowing sufficient rotation of initially transverse fractures into longitudinal orientations.

5.7 Summary

i. In contrast to previously studied Arctic valley glaciers, Austre Brøggerbreen is dominated by fractures and not by the evolution of primary stratification into longitudinal foliation.

ii. As Austre Brøggerbreen is relatively inactive at present, the majority of fractures are interpreted as relict features. This suggests that the glacier must have been substantially more dynamic in the past, most likely during the Neoglacial, to enable glacier-wide fracturing.

iii. Ductile modification of relict fracture sets contained within discrete flow units demonstrate unique structural evolutions, suggesting that flow units are unique and independent from one-another.

iv. The rotation of relict transverse fracture sets by ductile deformation has developed a fracture-derived longitudinal foliation that has not been observed in previous structural studies.

v. The preferential entrainment of fine-grained sediment contained within clotted ice facies suggests that sediment-rich water has undergone freezing at the bed of the glacier. Consequently, it is inferred that Austre Brøggerbreen must have been polythermal in the past.

vi. The presence of clotted ice at the surface of Austre Brøggerbreen suggests that basal ice has been folded and elevated through the ice mass at flow unit boundaries as a result of lateral compression, as suggested by Hambrey and Glasser (2003).

Chapter Six

Midtre Lovénbreen, Austre Lovénbreen, and Pedersenbreen

6.1 Introduction

The aim of this chapter is to investigate the structural characteristics of three glaciers (Midtre Lovénbreen, Austre Lovénbreen, Pedersenbreen) in Svalbard at a variety of scales to demonstrate that the formation and evolution of structures is variable depending on the characteristics of the flow units they are contained within. Each of the three glaciers are located on Brøggerhalvøya to the east of Austre Brøggerbreen, and are similar to one another as they are north-flowing valley glaciers that comprise multiple accumulation basins that merge into comparatively narrow glacier tongues. It is hoped that the comparison of three geometrically similar glaciers will enable the evaluation of the role of flow units for dictating structural characteristics of glaciers. To examine the structural characteristics of each of the glaciers a range of techniques are employed including; mapping of surface structures from aerial photography and satellite imagery, glacier-wide three-dimensional structural measurements, detailed ice facies logs, stable isotopic analysis and sedimentological analysis, which are described in detail in *Chapter Three*.

The specific objectives of this chapter are:

i. To map the surface of Midtre Lovénbreen, Austre Lovénbreen, and Pedersenbreen using a combination of aerial photography, satellite imagery, and field-based measurements.

ii. To define the flow units in each glacier, characterise their boundaries, and evaluate the evolution of structures within them, to test if flow units are mutually exclusive with regard to the structures present, and that each flow unit evolves in a unique manner (Jennings et al., 2014).

iii. To determine how longitudinal foliation and associated structures form and evolve in three geometrically similar Svalbard valley glaciers.

6.2 Midtre Lovénbreen

6.2.1 Introduction

Midtre Lovénbreen is one of the best studied glaciers in the world, and along with Austre Brøggerbreen, has the longest record of mass balance monitoring in Svalbard. Furthermore, Midtre Lovénbreen has previously been structurally studied (*e.g.* Hambrey et al., 1997; Hambrey and Glasser, 2003; Hambrey et al., 2005; Roberson and Hubbard, 2010) providing a good foundation for further structural work; however, it is worth noting that the glacier has substantially receded and down-wasted since the last structural study. The comparatively simple geometry of the glacier, the geometrical similarity between it and its neighbouring glaciers (Austre Lovénbreen, Pedersenbreen), and the previous structural studies conducted on the glacier, makes Midtre Lovénbreen an ideal case study for assessing the role of flow units for structural formation and evolution, especially with regard to the development of longitudinal foliation. For more detail about Midtre Lovénbreen and the previous research conducted on the glacier, please refer to the 'Study-site descriptions' in *section 2.6*.

FIGURE 6.1 - MLB MAIN STRUCTURAL MAP – PLEASE SEE APPENDIX

Table 6.1. Summary of the sequential structural evolution of each flow unit on Midtre Lovénbreen. Key located below main table (note that the colours are related to the colours that represent each structure on the main structural map, Figure 6.1.).

Order of formation	Flow Unit 1	Flow Unit 2	Flow Unit 3		Flow Unit 4
			A	B	
1					
2					
3					
4					

Key	
	Primary stratification
	Longitudinal foliation
	First, second and third generation crevasse traces respectively

Midtre Lovénbreen is composed of four major flow units (labelled Flow Units 1 to 4), with Flow Unit 3 further divided into two sub-flow units (Figure 6.1). As for other glaciers described in this study, each flow unit of Midtre Lovénbreen originates in a separate accumulation basin that dictates the structural characteristics and evolution of each flow unit. The structural evolution of each sub-flow unit will be discussed in turn below.

6.2.2 Structural evolution of individual flow units

The large-scale structural mapping of Midtre Lovénbreen is based on aerial photography collected in summer 2004 (refer to 'Methods' in *Chapter Three* for further details). Hambrey et al. (2005) also structurally mapped Midtre Lovénbreen from aerial photography collected in 1995; however, during the decade between the

acquisition of both sets of imagery, Midtre Lovénbreen underwent extensive amounts of ablation and surface lowering. As a result, the structures visible in each study are different from one another and represent two different snapshots in time from the structural history of the glacier. Therefore it is worth noting the conclusions of both studies may differ from each other.

The sequential order of structure formation is described for each sub-flow unit on Midtre Lovénbreen using geological structural notation. The structural attributes of each sub-flow unit are summarised in Table 6.1. Flow units are labelled starting from the true-left of the glacier working towards the true-right (Figure 6.1). Flow unit descriptions also follow this order. When the aerial photographs were acquired of Midtre Lovénbreen in summer 2004 the upper basins of the glacier were snow-covered, hiding some of the structures present in the upper accumulation area. Open fractures are visible even in snow covered areas allowing structural mapping of this feature; however, structures such as primary stratification cannot be traced above the snowline. Despite this, when describing the sequential order of structures on Midtre Lovénbreen it is assumed that primary stratification is the first structure to develop. This assumption is inferred on a number of observations:

i. Primary stratification is widely observed at the snowline on Midtre Lovénbreen having undergone very little folding and reorientation, indicating that primary stratification is actively forming on Midtre Lovénbreen in the upper accumulation basins.

ii. Primary stratification is the pervasive layering formed by the diagenesis of snow into glacier ice, and therefore represents the 'building blocks' of the glacier. Consequently, it is impossible for other structures to predate the formation of primary stratification on Midtre Lovénbreen.

6.2.2.1 Flow Unit 1

Primary stratification (S_0) in Flow Unit 1 forms in the upper accumulation area and persists into the middle reaches of the flow unit, becoming increasingly arcuate down-glacier. Transverse crevasses (S_1) also quickly develop in the accumulation area of the flow unit, but die-out relatively quickly in the accumulation area. Some limited longitudinal foliation (S_2) is evident on the true left of the flow unit, near to the lateral margin, but quickly dies out. Arcuate crevasse traces (S_3) (convex down-glacier) start to develop in the lower-middle-reaches of the flow unit, becoming increasingly numerous and cross-cutting towards the snout of the glacier.

6.2.2.2 Flow Unit 2

The first structure found in the upper accumulation area of Flow Unit 2 is primary stratification (S_0), which becomes increasingly folded as it is transported down-glacier, remaining until the lower middle reaches of the flow unit. Transverse crevasses (S_1) are also present in the upper accumulation area of Flow Unit 2, however, they do not persist lower down the glacier. Some limited longitudinal foliation (S_2) is evident in the upper reaches of the flow unit at the boundary with Flow Unit 3a, but is more extensive at the boundary between the two flow units on the lower reaches of the glacier. Arcuate crevasse traces (S_3) develop towards the snout of the glacier.

6.2.2.3 Flow Unit 3a

Primary stratification (S_0) in the upper accumulation basin of Flow Unit 3a is less dominant than in other flow units, quickly becoming folded down-glacier. The dominant structures in the accumulation basin are transverse crevasses (S_1); however, despite being numerous in the upper reaches of the flow unit, transverse crevasses do not persist down-glacier. Some limited areas of longitudinal foliation (S_2) are present high in the flow unit and near to the snout of the glacier at the boundary with Flow Unit 2; however, the strongest longitudinal foliation can be found at the boundary with

Flow unit 3a. Arcuate fractures (S_3) develop on the snout of the glacier, becoming increasingly numerous and cross-cutting towards the terminus.

6.2.2.4 Flow Unit 3b

As is the case for Flow Unit 3a, primary stratification (S_0) is spatially limited in the accumulation area of Flow Unit 3b. Furthermore, only a small number of transverse crevasses (S_1) are present in the flow unit. In contrast to all other flow units on Midtre Lovénbreen, Flow Unit 3b is dominated by very strong longitudinal foliation (S_2) which develops in the lower accumulation area and remains the dominant structure until the terminus of the glacier. Arcuate crevasse traces (S_3) also develop relatively high up-glacier in comparison with other flow units, forming in the middle reaches of the glacier, yet are also less numerous than in other flow units.

6.2.2.5 Flow Unit 4

Primary stratification (S_0) in the accumulation area becomes increasingly folded down-glacier. Spatially limited transverse crevasses (S_1) in the flow unit are confined to the upper slopes of the accumulation area, and cease to exist further down-glacier. Some spatially limited longitudinal foliation (S_2) is present on the true right of the flow unit, near to the lateral margin, and also near to the terminus of the glacier. As for Flow Unit 3b, arcuate crevasse traces (S_3) develop in the middle reaches of the flow unit, but are not as numerous as in other flow units on Midtre Lovénbreen.

6.2.3 Detailed ice facies log descriptions

Two detailed ice facies logs were taken on Midtre Lovénbreen. Both logs were taken on the true left of the glacier in Flow Unit 1, and are ordered from up-glacier to down-glacier (Figure 6.2). A brief description of each log is discussed below; however, for more detail please refer to the drawn logs (Figure 6.3).

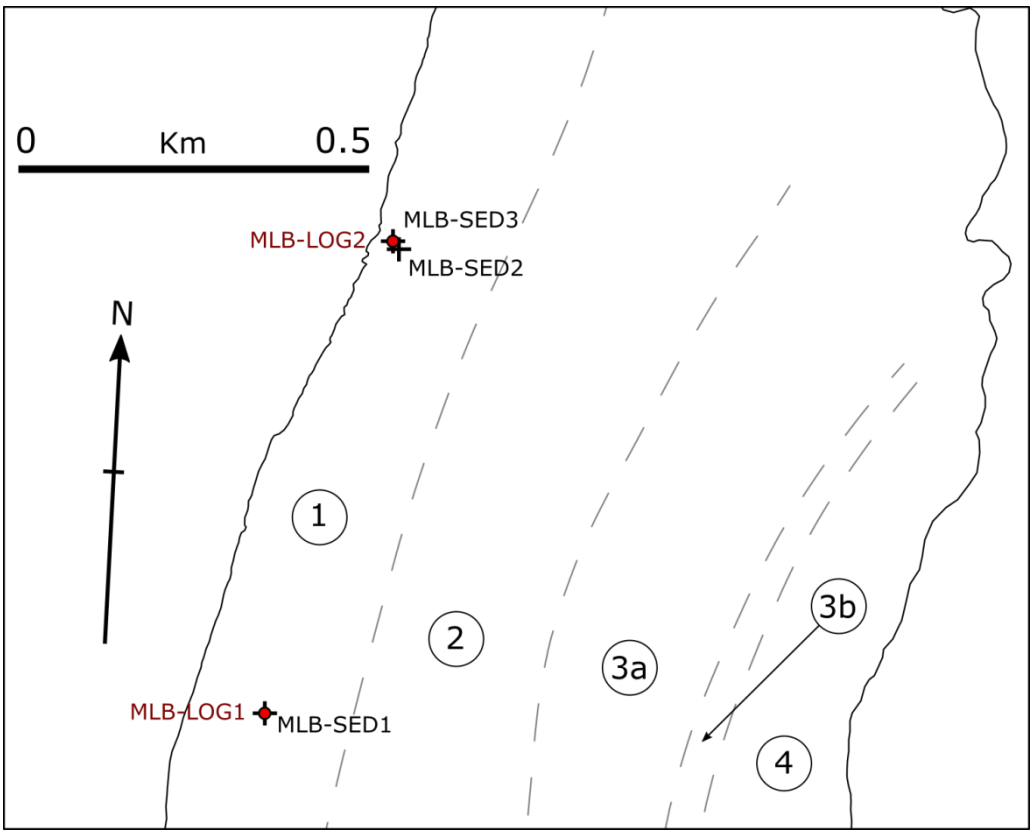

Figure 6.2. Flow unit map of the snout of Midtre Lovénbreen showing the location of the detailed ice facies logs (red circles with red log identification numbers), and the sediment samples (black crosses with black sediment identification numbers).

6.2.3.1 MLB-LOG1 – 78.88520°N, 12.03073°E

MLB-LOG1 (Figure 6.3) is the furthest up-glacier log taken on Midtre Lovénbreen, located in the middle reaches of the glacier near to the true-left lateral margin. The log is 2.1 metres long and primarily dominated by fine and coarse clear ice facies. Distinct groupings of ice facies alternate between non-foliated and strongly foliated ice, with moderate to steep dip angles (60° - 90°). Some fine ice layers contain mud clots, with evidence at *c*. 1.3 metres of minor folding and boudinage (Figure 6.4), suggesting a shear zone.

FIGURE 6.3 - MLB COMBINED DETAILED LOGS – PLEASE SEE APPENDIX

Figure 6.4. Fine alternating layers of coarse clear and clotted ice facies that show evidence of minor folding and boudinage. Photograph courtesy of M. J. Hambrey.

6.2.3.2 MLB-LOG2 – 78.89133°N, 12.03766°E

MLB-LOG2 (Figure 6.3) is located down-glacier of MLB-LOG1 on the snout of Midtre Lovénbreen, situated on the true-left of the glacier near to the lateral margin. The log is 2.4 metres in length and primarily dominated by coarse bubbly ice facies with some thin coarse clear and fine ice layers that have varying strengths of foliation. All ice layers are moderately dipping (55° - 80°) and varying concentrations of mud clots are common in fine ice layers.

6.2.4 Stable isotope analysis

A total of twelve isotopic samples were collected from the surface of Midtre Lovénbreen. The majority of isotopic sample locations coincided with the detailed ice facies logs (described above) to ensure that the surrounding structural context of each

sample was recorded. In addition to the spatial location of individual isotopic samples, the type of ice sampled was recorded for each to enable any differences between ice facies to be identified. Four classes of ice facies, including coarse bubbly ice, coarse clear ice, fine-grained ice, and coarse clear/fine ice, were sampled on Midtre Lovénbreen and analysed for $\delta^{18}O$ and δD values (values summarised in Table 6.2).

Table 6.2. Table showing the mean $\delta^{18}O$ and δD values for isotope samples of varying ice facies collected at the surface of Midtre Lovénbreen. Note *n* refers to the number of samples and σ is the standard deviation.

		$\delta^{18}O$ (‰)		δD (‰)	
Ice facies	***n***	**Mean**	**σ**	**Mean**	**σ**
Coarse bubbly ice	6	-12.62	0.50	-88.06	3.62
Coarse clear ice	2	-11.92	0.43	-83.04	1.57
Fine-grained ice	1	-11.64		-81.12	
Coarse clear ice/ fine-grained ice	3	-11.92	0.27	-84.27	1.42

6.2.5 Sedimentology

Three supraglacial sediment samples were obtained from Midtre Lovénbreen to provide insight into the origins of the structures within the ice mass by providing information on sediment entrainment processes and transport history. The majority of samples were collected in relation to the detailed ice facies logs to ensure that the surrounding structural context of the sediment was recorded (Figure 6.2). Sediment samples not correlated to a detailed ice facies log were located using a handheld GPS unit, and the glaciological setting described. Sediment samples are ordered from up-glacier to down-glacier and are described in relation to log locations. A brief description of each sample is provided below, but for more detailed information refer to the raw sediment data and combined sediment graphs (Figure 6.5).

FIGURE 6.5 - MLB COMBINED SEDIMENT GRAPHS – PLEASE SEE APPENDIX

6.2.5.1 MLB-SED1 – 78.88520°N, 12.03073°E

MLB-SED1 is located near to MLB-LOG1 on the true-left of the glacier (Flow Unit 1), in an area of an obliquely oriented fracture system dominated by fine and course clear ice facies. Distinct groupings of ice facies alternate between non-foliated and strongly foliated, with several layers containing light brown/sandy coloured mud clots. Sediment sampled from this location was collected from the surface of the glacier where mud clots had melted out of underlying clotted ice layers.

The grainsize distribution histogram for MLB-SED1 (Figure 6.5) has a bimodal distribution with distinct peaks occurring at 4 Φ (0.063 millimetres) and 7 Φ (0.007832 millimetres). Even though there is a limited amount of coarse sand present, the bulk of sediment contained in the sample is within the very fine sand, silt and clay size classes. The amount of calcium carbonate contained within the sample as confirmed by effervescence is classed as 'non-calcareous' with a calcium carbonate concentration of 0 - 0.1%.

6.2.5.2 MLB-SED2 – 78.89123°N, 12.03808°E

MLB-SED2 is located near to MLB-LOG2, *c*. 12 metres towards the centre of the glacier from the log, in a comparatively narrow zone (up to *c*. 42 centimetres wide) of fine ice containing light brown mud clots (Figure 6.6). The fine ice layer pinches out *c*. 2 metres up-glacier of the sample location to form a fracture trace between coarse bubbly and coarse clear ice layers. The fine ice layer is strongly foliated with a moderate dip angle of 59°. The sediment sampled from this location was collected from the surface of the glacier where mud clots had melted out of the underlying fine ice layer.

The grainsize distribution histogram for MLB-SED2 (Figure 6.5) has a slightly bimodal distribution with peaks occurring at 1 Φ (0.5 millimetres) and 6 Φ (0.015659 millimetres). A further large peak occurs at 4 Φ (0.063 millimetres). As for previous samples, MLB-SED2 has high concentrations of medium sand particles through to clay particles. The amount of calcium carbonate contained within the sample as confirmed

by effervescence is classed as 'non-calcareous' with a calcium carbonate concentration of 0 - 0.1%.

Figure 6.6. Sediment-rich fine-grained ice cropping out at the surface of Midtre Lovénbreen.

6.2.5.3 MLB-SED3 – 78.89133°N, 12.03766°E

MLB-SED3 is located next to MLB-LOG2 on the true-left of the glacier, *c*. 860 metres up-glacier from the terminus. The area primarily comprises coarse bubbly ice; however, comparatively steeply dipping (*c*. 76°) fine and coarse clear ice faces contain varying quantities of light sandy coloured mud clots. The sediment sample was collected from the surface of the glacier where mud clots had melted out of the underlying ice layers to form a supraglacial sediment deposit.

The grainsize distribution histogram for MLB-SED3 (Figure 6.5) shows a large peak at the 4 Φ (0.063 millimetres) size fraction. Even though there is a limited amount of medium to fine sand present, the bulk of sediment contained in the sample is within

the very fine sand, silt and clay size classes. The amount of calcium carbonate contained within the sample as confirmed by effervescence is classed as 'non-calcareous' with a calcium carbonate concentration of 0 - 0.1%.

6.2.6 Interpretation and discussion

6.2.6.1 Glacier-wide structural overview

Like a number of other temperate and polythermal valley glaciers (*e.g.* Goodsell et al., 2005b; Hambrey et al., 2005; Jennings et al., 2014), Midtre Lovénbreen is dominated by the evolution of primary stratification into longitudinal foliation. Glacier ice that forms from the diagenesis of snow and superimposed ice preserves the snowpack's horizontal layering (Wadham and Nuttall, 2002). As ice flows from a wide accumulation area into a comparatively narrow tongue, the layering (primary stratification) becomes folded as a result of lateral compression and longitudinal extension, eventually transposing the primary stratification into longitudinal foliation (Hambrey et al., 1999). As previously suggested by Hambrey and Glasser (2003), this process is most evident on Midtre Lovénbreen at its flow unit boundaries where there is inferred greater amounts of simple shear. This is especially evident at the boundaries between Flow Units 3a, 3b and 4 where there is very strong longitudinal foliation (Figure 6.1). Even though not observed in this study, it is worth noting that both Hambrey et al. (2005) and Roberson and Hubbard (2010) documented axial planar foliation in the centre of flow units. Hambrey et al. (2005) observed that the majority of longitudinal foliation cuts across primary stratification in a similar manner to slaty cleavage found in folded sedimentary rocks, concluding that a different mechanism from the transposition of pre-existing structures was responsible for the formation of longitudinal foliation in Midtre Lovénbreen. However, the exact mechanism for the formation of axial planar foliation is still unknown (Hambrey and Lawson, 2000).

Arcuate fractures located on the snout of Midtre Lovénbreen have previously been interpreted as thrusts by Hambrey et al. (2005), a conclusion further supported by Roberson and Hubbard (2010). Thrusts have been inferred in many glaciers and are

especially common in polythermal glaciers (*e.g.* Hambrey and Dowdeswell, 1997; Glasser et al., 1998; Hambrey et al., 1999; Murray et al., 2000). For Midtre Lovénbreen, Hambrey et al. (2005) presented a range of evidence to support their hypothesis that the arcuate fractures on the snout of the glacier were indeed thrusts. The exclusive presence of the arcuate fractures on the snout of the glacier, as illustrated by the glacier-wide structural mapping (Figure 6.1), to some degree supports this conclusion. Thrusting is hypothesised to occur in polythermal glaciers when warm-based ice overrides ice that is frozen to the bed at the snout of the glacier (*see* Hambrey et al., 1999; Rippin et al., 2003; King et al., 2008). This would explain why arcuate fractures are only observed towards the snout of the glacier. Hambrey et al. (2005) also suggested that these features may be relict from when the glacier was much thicker during Neoglacial time. However, a study undertaken on Storglaciären by Moore et al. (2010) questioned the plausibility of thrusting in glacier ice, and Moore (2014) further concluded that thrusting is improbable except when pre-existing structural weaknesses are oriented in a favourable orientation for slip to occur along the fracture.

6.2.6.2 Origin and structural evolution of flow units

Despite each flow unit on Midtre Lovénbreen having a similar dominant structural evolution (*i.e.* the transposition of primary stratification into longitudinal foliation), differences in the structural characteristics of individual flow units, and the distance down-glacier that structures are preserved (*e.g.* primary stratification) or form (*e.g.* longitudinal foliation) (Figure 6.1 and Table 6.1), demonstrates that each flow unit is unique and mutually exclusive from one-another, as previously suggested by Jennings et al. (2014). As a result, it is possible to treat individual flow units as separate and mutually exclusive systems (*i.e.* individual systems that are adjacent to one-another but do not interact with each other). The characteristics of each sub-accumulation basin dictate the inputs for its corresponding flow unit, determining the dominance of the flow unit within the whole-glacier system. Furthermore, the location of the flow

unit dictates the stress regimes experienced, which in turn controls the location that structures form and how those structures evolve.

6.2.6.3 Sedimentological evidence of structural processes

As is the case for Austre Brøggerbreen (*see section 5.7.3*), all the sediment samples collected on the surface of Midtre Lovénbreen primarily comprise fine sediment fractions (medium sand to clay) (Figure 6.5) that resemble the distribution of terminal grades in subglacial tills (Dreimanis and Vagners, 1971; Haldorsen, 1981). As previously explained in *section 5.7.3*, the exclusive entrainment of fine-grained sediment is indicative of entrainment at the bed of the glacier as sediment-rich water freezes. In contrast to Austre Brøggerbreen, ice facies at the surface of Midtre Lovénbreen do not appear to have differing isotopic signatures (Table 6.2) (as would be expected between meteoric and basally derived ice facies); yet, this is most likely a result of the limited number of samples collected. Despite the lack of isotopic evidence, a similar process is inferred to that at Austre Brøggerbreen; however, unlike Austre Brøggerbreen, it is possible that entrainment in this manner is still occurring in Midtre Lovénbreen as it is still a polythermal glacier (Björnsson et al., 1996; King et al., 2008). Regardless of the exact entrainment mechanism, basal sediments have been elevated through the ice mass, ultimately becoming exposed at the surface of the glacier. Even though foliated ice facies were observed in both of the detailed ice facies logs collected on Midtre Lovénbreen (Figure 6.3), observations from the field raise doubts as to whether the sediment-rich ice was elevated by a similar mechanism as proposed for Austre Brøggerbreen (*see section 5.7.3*). The sediment-rich ice sampled appeared to be derived from longitudinal fractures that originated on the true-left margin of the glacier. Initially transverse fractures become rotated in an anti-clockwise direction down-glacier, eventually becoming approximately longitudinally orientated. If the origin of the basal debris is fracture-derived, the fractures must propagate to the bed of the glacier. If this is the case, it differs from the structural description of Midtre Lovénbreen provided by Hambrey et al. (2005), who only observed axial planar foliation at flow unit boundaries. As a result of the longitudinal orientation, the

fractures appear to be geometrically similar to the fracture-derived longitudinal foliation as described for Austre Brøggerbreen (*see section 5.7.4*). Therefore, the observations of this study combined with those of Hambrey et al. (2005) suggest that longitudinal foliation in Midtre Lovénbreen has multiple origins.

6.2.7 Summary

i. Midtre Lovénbreen is structurally dominated by the evolution of primary stratification into longitudinal foliation, with the strongest longitudinal foliation occurring at flow unit boundaries.

ii. Despite similar structural assemblages occurring within each flow unit, differences between the formation and evolution of structures in separate flow units suggests that they are unique and independent of one-another.

iii. Sediment samples collected from the surface of Midtre Lovénbreen demonstrate 'basal' characteristics; however, in contrast to Austre Brøggerbreen, the sediment appears to originate from longitudinal fractures.

iv. The exact mechanisms for entrainment and transport of sediment-rich ice from the bed of the glacier to the surface are unknown. Further study, including detailed structural and sedimentological analysis is required to better understand the formation and evolution of longitudinal fractures in Midtre Lovénbreen, and to suggest mechanisms for how sediment-rich ice becomes entrained in fractures at the glacier bed.

6.3 Austre Lovénbreen

6.3.1 Introduction

In comparison to its neighbouring glacier Midtre Lovénbreen, Austre Lovénbreen is a comparatively poorly studied glacier; however, it has previously received some limited structural attention (*see* Hambrey et al., 1999; Glasser and Hambrey, 2001; Midgley et al., 2013). Presented in this section is the first glacier-wide structural study of Austre Lovénbreen, comprising structural mapping from aerial photography and satellite imagery, and detailed ice facies logging. Austre Lovénbreen is geometrically similar to Midtre Lovénbreen, and is also considered to be polythermal based on ground penetrating radar data collected in 2010 (Saintenoy et al., 2013). However, it is worth noting that in contrast to Midtre Lovénbreen, the glacier is predominantly frozen to the bed with warm-based ice restricted to the thickest areas of the glacier. As is the case for many glaciers in Svalbard, Austre Lovénbreen has receded and thinned substantially since its Neoglacial maxima (*c*. 1900 AD), and its terminus has receded by *c*. 400 metres in the last 50 years (Friedt et al., 2012). The similarities between Austre Lovénbreen and Midtre Lovénbreen combined with the limited amount of previous structural studies, makes Austre Lovénbreen an ideal glacier to structurally compare with its neighbouring glaciers. For a more in-depth overview of Austre Lovénbreen and the previous research conducted on the glacier, refer to the 'Study-site descriptions' in *section 2.6*.

Austre Lovénbreen is composed of four major flow units (labelled Flow Unit 1 to 4), with Flow Unit 4 further sub-divided into two sub-flow units (Figure 6.7). The structural details of each sub-flow unit are discussed in turn below.

6.3.2 Structural evolution of individual flow units

The main glacier-wide structural map of Austre Lovénbreen is based on aerial photography collected in summer 2003 and Google Earth satellite imagery collected in summer 2011 (refer to 'Methods' in *Chapter Three* for further details). The snout of

FIGURE 6.7 - ALB MAIN STRUCTURAL MAP – PLEASE SEE APPENDIX

Table 6.3. Summary of the sequential structural evolution of each flow unit on Austre Lovénbreen. Key located below main table (note that the colours are related to the colours that represent each structure on the main structural map, Figure 6.7.).

Order of formation	Flow Unit 1	Flow Unit 2	Flow Unit 3	Flow Unit 4	
				A	B
1					
2					
3					
4					

Key	
	Primary stratification
	Longitudinal foliation
	First, second and third generation crevasse traces respectively

Austre Lovénbreen has previously been structurally mapped by Midgley et al. (2013) also using aerial photography collected in 2003, and their mapped area broadly agrees with the mapping undertaken in this study.

The sequential order of structure formation is described for each sub-flow unit on Austre Lovénbreen using geological structural notation. The structural attributes of each sub-flow unit is summarised in Table 6.3. Flow units are labelled starting from the true-left of the glacier working towards the true-right (Figure 6.7). Flow unit descriptions also follow this order. As is the case for other glaciers mapped in this study, when the aerial and satellite images were acquired, the upper accumulation basins of the glacier were snow-covered, obscuring any underlying structures from view (except for open fractures which remained visible despite the snow cover). Primary stratification is assumed to be the first structure to develop in each flow unit even when it is not directly observed on the aerial photography (*see section 6.2.2*).

6.3.2.1 Flow Unit 1

Primary stratification (S_0) forms in the upper accumulation area of Flow Unit 1 and becomes increasingly folded down-glacier, persisting until the confluence of the flow unit with the main trunk of the glacier. Transverse crevasses (S_1) also develop in the upper accumulation area; however, remain largely confined to the true-left lateral margin of the flow unit. Longitudinal foliation (S_2) develops at both lateral margins of the flow unit at the confluence with the main tongue of the glacier; however, is strongest at the boundary between Flow Units 1 and 2, and becomes increasingly strong towards the terminus. Arcuate fractures (S_3) form on the snout of the glacier *c*. 700 metres from the terminus. These fractures are orientated transverse to flow and are slightly arcuate down-glacier.

6.3.2.2 Flow Unit 2

Primary stratification (S_0) develops in the upper accumulation basin of Flow Unit 2; however, it is not observed in the flow unit until the middle-reaches of the glacier where the primary stratification is already strongly folded with flow-parallel fold axes. Spatially limited fracturing (S_1) on the flow unit's true-left lateral margin is also present in the upper accumulation area, yet dies out at the confluence with Flow Unit 1. Strong longitudinal foliation (S_2) develops at the confluence of Flow Unit 1 and 2, persisting until the terminus; however, no longitudinal foliation is evident at the boundary of Flow unit 2 and 3 until within *c*. 500 metres of the terminus of the glacier. Some arcuate fractures (S_3) orientated transverse to flow and slightly arcuate down-glacier develop on the snout of the glacier within *c*. 600 metres of the terminus; however, they are less numerous than those present in Flow Unit 1.

6.3.2.3 Flow Unit 3

The first structure that forms in Flow Unit 3 is primary stratification (S_0), which becomes visible at the confluence of Flow Unit 3 and 4a, but is most evident in the

middle-reaches of the glacier where the primary stratification is strongly folded. Some spatially limited fracturing (S_1) is also present in the upper accumulation area; however, does not persist below the snowline which terminates *c*. 1 kilometre down-glacier from the basin headwall. Longitudinal foliation (S_2) develops at the boundary between Flow Units 3 and 4a, *c*. 800 metres down-glacier from the confluence of the two flow units, and increases in strength towards the snout of the glacier. Arcuate fractures develop *c*. 400 metres up-glacier from the terminus and are orientated transverse to flow and slightly arcuate down-glacier.

6.3.2.4 Flow Unit 4a

Primary stratification (S_0) develops in the upper-reaches of Flow Unit 4a, and becomes strongly folded with flow-parallel fold axes in a comparatively short distance down-glacier (*c*. 800 metres), persisting until the middle-reaches of the glacier. Strong longitudinal foliation (S_1) forms at both lateral margins of the flow unit as well as in the centre of the flow unit *c*. 900 metres down-glacier from the basin headwall. The longitudinal foliation found in the centre of the flow unit has an axial planar relationship with primary stratification, as it is orientated parallel to the fold axes of the primary stratification. The longitudinal foliation becomes increasingly strong down-glacier, eventually dominating the whole flow unit *c*. 1.2 kilometres from the terminus. Arcuate fractures (S_2) develop *c*. 400 metres up-glacier of the terminus, and are orientated transverse to flow and slightly arcuate down-glacier.

6.3.2.5 Flow Unit 4b

Primary stratification (S_0) is inferred to be the first structure that forms in Flow Unit 4b despite only being evident lower down the glacier. Some spatially limited transverse fractures (S_1) are also present in the upper accumulation area, but do not persist lower than *c*. 800 metres below the basin headwall. Longitudinal foliation (S_2) forms comparatively high in the flow unit (*c*. 500 metres below the headwall) on the true-

right margin, and develops within *c*. 900 metres from the headwall at the boundary with Flow Unit 4a. The longitudinal foliation present at the boundary between Flow units 4a and 4b is particularly strong and increases in strength towards the terminus. Arcuate fractures (S_3) develop comparatively high up-glacier in comparison with other flow units on Austre Lovénbreen, forming *c*. 900 metres up-glacier from the terminus. However, as for the previously described flow units, the fractures are orientated transverse to flow and are slightly arcuate down-glacier.

6.3.3 Detailed ice facies log descriptions

A total of seven detailed ice facies logs were taken on Austre Lovénbreen. Logs are ordered from up-glacier to down-glacier and taken at locations along an approximate flowline on the true right of the glacier (approximately at the boundary between Flow

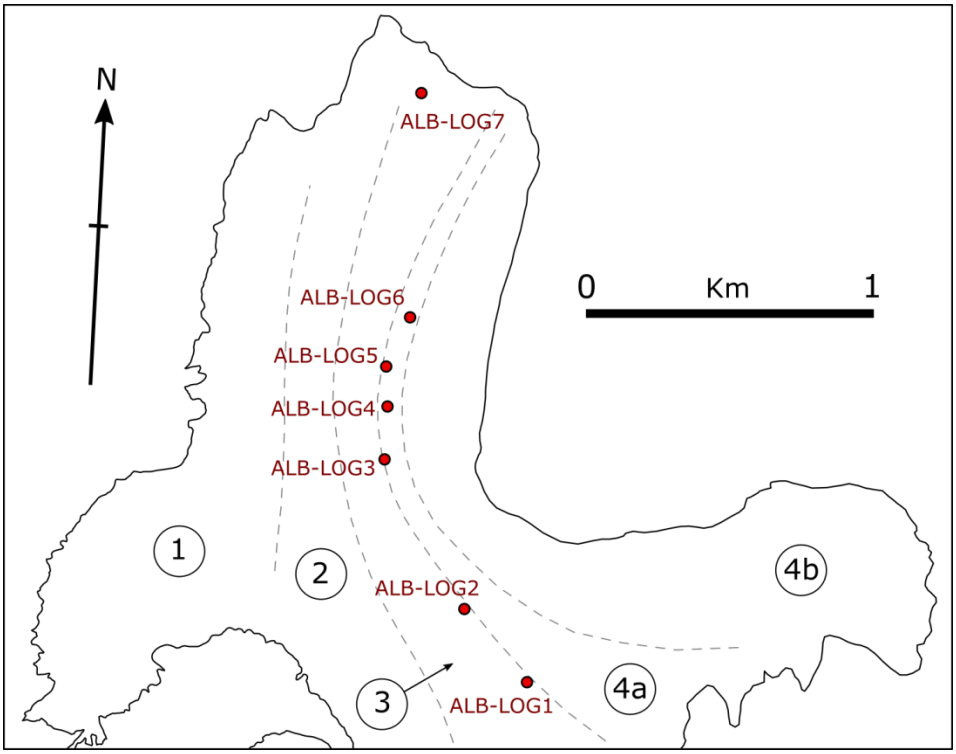

Figure 6.8. Flow unit map of Austre Lovénbreen showing the location of the detailed ice facies logs (red circles with red log identification numbers).

FIGURE 6.9 - ALB COMBINED DETAILED LOGS (Page 1) - PLEASE SEE APPENDIX

FIGURE 6.9 - ALB COMBINED DETAILED LOGS (Page 2) - PLEASE SEE APPENDIX

Unit 3 and 4a), with the highest up-glacier log located in the middle-reaches of the ice mass (Figure 6.8). Log sizes range from 2.2 to 7.6 metres in length depending on the ice sections exposed at the surface of the glacier. A brief description of each log is discussed below; however, for more detail refer to the drawn logs (Figure 6.9).

6.3.3.1 ALB-LOG1 – 78.86855°N, 12.17480°E

ALB-LOG1 (Figure 6.9) is the furthest up-glacier log taken on Austre Lovénbreen, located on the true right of the glacier between Flow Units 3 and 4a. The log is 7.0 metres long and primarily composed of coarse bubbly ice facies with some minor layers of coarse clear ice. Ice layer dip angles are moderate to steep (70° - 85°) with several fine ice and coarse clear ice layers containing varying concentrations of mud clots. Folding of coarse bubbly ice facies, mainly focused at *c*. 3.2 metres, have up-glacier dipping fold axes with low dip angles (5° - 15°). Additionally, many coarse bubbly ice layers are strongly foliated and display an axial planar relationship with folded ice layers.

6.3.3.2 ALB-LOG2 – 78.87075°N, 12.16407°E

ALB-LOG2 (Figure 6.9) was located down-flow of ALB-LOG1 at the boundary between Flow Units 3 and 4a. The log is 3.1 metres in length and mainly consists of coarse bubbly ice with occasional coarse clear and fine ice layers. Dip angles of ice layers are moderate to steep (60° - 85°), with many ice facies having varying strengths of foliation. Some layers are fold limbs, which are part of a larger-scale fold that is not depicted on the log. The only fine ice layer on the log located at *c*. 2 metres was deeply weathered in comparison to other ice facies in the log, and acted as a local supraglacial drainage pathway.

6.3.3.3 ALB-LOG3 – 78.87532°N, 12.14995°E

ALB-LOG3 (Figure 6.9) is 7.6 metres in length and comprises large proportions of coarse bubbly ice, with thin fine and coarse clear ice layers concentrated towards the end of the log. Ice layer dip angles are moderate to steep (75° - 90°) with different ice facies having varying strengths of foliation. Between *c*. 4.6 and 5.8 metres a transverse reverse fault runs parallel along the log. Supraglacial relief along the log was very pronounced between different ice types and reflected a synclinal/ridge structure at the glacier surface.

6.3.3.4 ALB-LOG4 – 78.87698°N, 12.14999°E

ALB-LOG4 (Figure 6.9) is 3.0 metres in length and is composed almost exclusively of coarse bubbly ice with several minor coarse clear ice layers. Ice layer dip angles are moderate (60° - 75°) with only several ice layers having foliation. Folding found at *c*. 0.15 metres is related to a fold hinge not displayed on the log, which has a shallow up-glacier fold axis dip angle (5°). Thin millimetre thick coarse clear ice layers found in coarse bubbly ice layers are common in the log. A cross-cutting crevasse trace composed of a thin coarse clear ice layer located at *c*. 1.6 metres displays an up-glacier dip (56°).

6.3.3.5 ALB-LOG5 – 78.87823°N, 12.14948°E

ALB-LOG5 (Figure 6.9) is located in the middle reaches of Austre Lovénbreen near to a foliation parallel supraglacial stream. The log is 4.6 metres in length and is primarily composed of coarse bubbly and coarse clear ice facies, with occasional thin fine ice layers. Ice layer dip angles are moderate (55° – 70°) with varying amounts of foliation present along the log's length. Some coarse bubbly ice layers have varying concentrations of bubbles. A thin fine ice layer present at *c*. 3.3 metres had a yellowish colouring suggesting the presence of mud in the ice layer. Additionally, at *c*. 4.2 metres there is a layer of anastomosing coarse clear and fine ice layers.

6.3.3.6 ALB-LOG6 – 78.87981°N, 12.15295°E

ALB-LOG6 (Figure 6.9) cross-cuts a section of preserved folded primary stratification in the lower middle reaches of Austre Lovénbreen. The log is 3.0 metres in length and mainly comprises coarse bubbly ice with infrequent coarse clear and fine ice layers. Foliated ice layer dip angles are comparatively steep (> 80°), whereas primary stratification fold limbs tend to have moderate up-glacier dips (30° – 55°). Coarse bubbly layers have varying bubble concentrations, and are occasionally strongly foliated.

6.3.3.7 ALB-LOG7 – 78.88686°N, 12.15302°E

ALB-LOG7 (Figure 6.9) is located towards the terminus of Austre Lovénbreen, and has a length of 2.2 metres. The log is primarily composed of coarse bubbly ice that has varying strengths of foliation, with some layers of coarse clear and fine ice. Ice layers are steeply dipping (> 80°), with synclinal ridges cross-cutting the log at shallower angles (45° – 55°). At *c*. 1.35 to 1.70 metres, alternating layers of coarse clear and fine ice form a substantial layer. In this section the coarse clear layers contain clots of brown coloured mud.

6.3.4 Stable isotope analysis

A total of twenty three isotopic samples were collected from the surface of Austre Lovénbreen. The majority of isotopic sample locations coincided with the detailed ice facies logs (described above) to ensure that the surrounding structural context of each sample was recorded. In addition to the spatial location of individual isotopic samples, the type of ice sampled was recorded for each to enable any differences between ice facies to be identified. Three classes of ice facies, including coarse bubbly ice, coarse clear ice, and coarse clear/fine ice, were sampled on Austre Lovénbreen and analysed for $\delta^{18}O$ and δD values (values summarised in Table 6.4).

Table 6.4. Table showing the mean $\delta^{18}O$ and δD values for isotope samples of varying ice facies collected at the surface of Austre Lovénbreen. Note *n* refers to the number of samples and σ is the standard deviation.

		$\delta^{18}O$ (‰)		δD (‰)	
Ice facies	***n***	**Mean**	**σ**	**Mean**	**σ**
Coarse bubbly ice	12	-12.39	0.71	-86.07	5.07
Coarse clear ice	9	-13.01	2.28	-89.87	15.62
Coarse clear ice/ fine-grained ice	2	-11.42	0.05	-80.33	0.21

6.3.5 Interpretation and discussion

6.3.5.1 Glacier-wide structural overview

As is the case for nearby Midtre Lovénbreen, Austre Lovénbreen is primarily dominated by the evolution of primary stratification into longitudinal foliation. This is most evident at flow unit boundaries where greater amounts of simple shear are inferred. The horizontal layering contained within the snowpack is preserved during the diagenesis of snow into glacier ice, eventually forming primary stratification. The subsequent gravity induced flow of the ice from a wide accumulation area into a comparatively narrow tongue folds the primary stratification as a result of lateral compression and longitudinal extension. This process eventually transposes the primary stratification into longitudinal foliation (Hambrey and Lawson, 2000; Goodsell et al., 2005b; Hambrey et al., 2005; Jennings et al., 2014, 2015), a process that is especially evident at the flow unit boundaries between Flow Units 1 and 2, and at both lateral boundaries of Flow Unit 4a. However, the lack of sediment-rich ice facies and no distinct variations in isotopic signature suggests that no basally derived ice had reached the surface of the glacier in the areas sampled.

The presence of longitudinal foliation in the centre of Flow Unit 4a suggests a further mechanism for the formation of longitudinal foliation on Austre Lovénbreen.

The foliation has an axial planar relationship with the folded primary stratification present in the flow unit, cross-cutting the primary stratification in a geometrically similar fashion to slaty cleavage observed in sedimentary rocks (Hambrey et al., 2005; Jennings et al., 2014). The exact formation mechanism of axial planar foliation is currently unknown (Hambrey and Lawson, 2000); however, Jennings et al. (2014) suggested that axial planar foliation preferentially forms in flow units that have a less pronounced narrowing down-glacier, which allows crystallographic modification of individual ice crystals.

Austre Lovénbreen is thought to be polythermal (Saintenoy et al., 2013) in a similar fashion to nearby Midtre Lovénbreen, and similarly, arcuate fractures are present on the snout of both glaciers. Hambrey et al. (1999) interpreted the arcuate fractures found on the snout of Midtre Lovénbreen as thrusts where warm-based ice found further up-glacier had overridden ice at the terminus of the glacier that was frozen to its bed, a conclusion further supported by Roberson and Hubbard (2010). This hypothesis accounts for why arcuate fractures are exclusively observed at the snout of the glacier. The similar thermal regime and locations of both Austre Lovénbreen and Midtre Lovénbreen suggests that the arcuate fractures observed on the snout of both glaciers may be derived from a similar origin. This would infer that the arcuate fractures observed on the snout of Austre Lovénbreen were also thrusts; however, no evidence to test this hypothesis was collected during this study. Furthermore, the extent of warm-based ice found below Austre Lovénbreen is minimal, and only exists beneath the thickest extents of the glacier. Therefore, it less likely that thrusting could result from warm-based ice overriding ice frozen to the bed at the terminus. The presence of an overdeepening below the glacier that ends *c*. 250 metres before the glacier terminus (*see* Saintenoy et al., 2013) may provide an alternative hypothesis for the origin of thrusts, as reactivation of crevasse traces against a reverse bed slope has been documented in several Alpine valley glaciers (*e.g.* Herbst and Neubauer, 2000; Goodsell et al., 2002, 2005b; Herbst et al., 2006) and in an Icelandic outlet glacier (*e.g.* Swift et al., 2006). However, this hypothesis does not explain the lack of crevasse traces observed up-glacier of the arcuate fractures on the

snout (Figure 6.7). A second hypothesis states that the arcuate fractures are indeed thrusts, but are relict structures from when the glacier was much thicker and when warm-basal conditions were more extensive during the Neoglacial (following a similar hypothesis proposed by Hambrey et al. (2005) for Midtre Lovénbreen). In this case, the thrusts may have originally formed as 'blind thrusts' (*i.e.* thrusts that did not originally reach the surface of the glacier) that have subsequently become exposed at the surface of the glacier as a result of ablation and surface lowering.

6.3.5.2 Origin and structural evolution of flow units

Each of the flow units on Austre Lovénbreen have similar suites of structures that develop in similar sequential orders (Table 6.3). However, the characteristics of each flow unit are inherently different from one-another. The dominance of structures within a flow unit, and the exact distance down-glacier that each type of structure forms and is preserved are unique (Figure 6.7). This suggests, as proposed by Jennings et al. (2014), that individual flow units are unique and mutually exclusive from one-another (*i.e.* can be treated as independent systems). Furthermore, the dominant type of longitudinal foliation found in separate flow units differs. In all flow units, except Flow Unit 4a, longitudinal foliation is transposed from primary stratification. However, in the centre of Flow Unit 4a, longitudinal foliation has an axial planar relationship with primary stratification. This suggests that the type of longitudinal foliation present within a flow unit is location dependent (*i.e.* the type of longitudinal foliation present in a flow unit is dictated by the physical characteristics of that flow unit), an idea first proposed by Jennings et al. (2014) for an Alpine valley glacier (Vadrec del Forno).

6.3.6 Summary

i. The majority of flow units in Austre Lovénbreen are structurally dominated by the evolution of primary stratification into longitudinal

foliation, with the strongest longitudinal foliation occurring at flow unit boundaries.

ii. The dominance of axial planar foliation in the centre of Flow Unit 4a, in contrast to all other flow units in Austre Lovénbreen, suggests that the type of longitudinal foliation that develops in a flow unit is location dependent (*i.e.* the type of longitudinal foliation that develops is dependent on the characteristics of the flow unit it is contained within), confirming the hypothesis proposed by Jennings et al. (2014).

iii. Despite similar structural assemblages occurring within each flow unit, differences between the formation and evolution of structures in separate flow units suggests that they are unique and independent of one-another (*i.e.* they can be treated as individual systems that have little or no interaction between one-another).

iv. The origin of the arcuate fractures observed on the snout of Austre Lovénbreen is unknown. However, it is possible that they are thrusts as has been suggested for nearby Midtre Lovénbreen (*following* Hambrey et al. (2005)); nevertheless, it is doubtful that they are actively forming and they probably represent relict features.

6.4 Pedersenbreen

6.4.1 Introduction

The Svalbard archipelago has one of the highest concentrations of surge-type glaciers in the world (Sevestre and Benn, 2015; Sevestre et al., 2015), with estimates of the amount of surge-type glaciers ranging from 13% to 90% (Hagen et al., 1993; Jiskoot et al., 2000). Surge-type glaciers have received a lot of attention worldwide; however, structural studies of surge-type glaciers are comparatively rare. The most detailed

structural study of foliation in a surge-type glacier was undertaken on Variegated Glacier in Alaska (*see* Lawson et al., 1994; Lawson, 1996), but surge-type glaciers in Svalbard are receiving increasing amounts of structural attention (*e.g.* Hambrey and Dowdeswell, 1997; Fleming et al., 2013; King et al., 2015; Lovell et al., 2015). In contrast to the other Brøggerhalvøya glaciers included in this study, there is structural evidence to suggest that Pedersenbreen has surged in the past. The presence of a looped moraine, formed when a pulse of 'active' ice flows past 'less active' ice, is often used to indicate surge-type behaviour (*e.g.* Meier and Post, 1969; Williams et al., 1991; Dowdeswell and Williams, 1997; Glasser et al., 2004). Evidence from historical photographs shows that a looped moraine was close to the snout of Pedersenbreen during 1897, and that a second looped moraine formed further up-glacier previous to 1966 (this looped moraine is still visible on the surface of the glacier) (Glasser et al., 2004). The two looped moraines demonstrate the periodical advances of ice originating from the glacier's western cirque (Flow Unit 1 in this study) that enters the main trunk of the glacier. The thermal regime of Pedersenbreen is unknown; however, previous studies have assumed that it has a similar regime to Midtre Lovénbreen, with a layer of cold ice covering temperate ice in the accumulation area, and frozen basal conditions in the ablation area (Hagen and Sætrang, 1991; Glasser et al., 2004). The presence of aufeis in the proglacial zone further supports the assumption that Pedersenbreen is polythermal (Bennett et al., 1998; Glasser et al., 2004). Pedersenbreen was selected to be studied for several reasons. Firstly, the geometrical similarity of the glacier with its neighbouring glaciers Midtre Lovénbreen and Austre Lovénbreen offers an interesting comparison, especially as the thermal and flow regimes of each glacier differs from one-another. Secondly, the presence of a surge-loop defined by a medial moraine provides an opportunity to explore flow unit boundary foliation in a surge-type glacier. For a more in-depth overview of Pedersenbreen and the previous research conducted on the glacier, refer to the 'Study-site descriptions' in *section 2.6*.

Pedersenbreen is composed of four major flow units (labelled Flow Unit 1 to 4), with Flow Unit 2 further sub-divided into two sub-flow units (Figure 6.10). As for each

of the glaciers described above, each sub-flow unit in Pedersenbreen originates in a separate sub-accumulation area, the characteristics of which are reflected in the structures and their evolution observed in their corresponding flow unit. The structural evolution of each sub-flow unit is discussed in turn below.

6.4.2 Structural evolution of individual flow units

Glacier-wide mapping of Pedersenbreen was undertaken using Google Earth satellite imagery collected in summer 2011 (refer to 'Methods' in *Chapter Three* for further details). Even though the glacier has received some limited structural attention in the past (*see* Bennett et al., 1996; Glasser et al., 2004), the only mapping conducted on the glacier was of the down-glacier movement and deformation of the looped medial moraine from field and vertical aerial photographs (Glasser et al., 2004).

The sequential order of structure formation is described for each flow unit on Pedersenbreen using geological structural notation, and the structural attributes of each flow unit are summarised in Table 6.5. Flow units are labelled starting from the true-left of the glacier, working towards the true-right (Figure 6.10). Flow unit descriptions also follow this order. As is the case for several of the glaciers described above, the upper basins of Pedersenbreen were snow-covered when the satellite imagery of the glacier was acquired, concealing some of the structures present in the upper accumulation area. Open fractures are visible even in snow-covered areas allowing structural mapping of this feature; however, structures such as primary stratification cannot be traced above the snowline. Despite this, when describing the sequential order of structures on Pedersenbreen it is assumed that primary stratification is the first structure to develop. This assumption is inferred on a number of observations as previously discussed in *section 6.2.2*.

FIGURE 6.10 - PB MAIN STRUCTURAL MAP – PLEASE SEE APPENDIX

6.4.2.1 Flow Unit 1

Primary stratification (S_0) in Flow Unit 1 forms in the upper accumulation area, but is only evident for a short distance below the snowline as it becomes increasingly arcuate down-glacier. A few transverse crevasses (S_1) also form high in the accumulation area; however, they are only evident further down the flow unit on the true-left, dying out as the flow unit joins the main trunk of the glacier. As the flow unit joins the main trunk of the glacier, it becomes dominated by strong longitudinal foliation (S_2). Initially the longitudinal foliation is predominantly found at the lateral margin of the glacier on the true-left of the flow unit; however, longitudinal foliation becomes increasingly evident at the boundary between Flow Unit 1 and Flow Unit 2a. The strongest foliation occurs towards the end of the flow unit at the boundary between Flow Unit 1 and 2a, with the foliation remaining orientated parallel to the looped medial moraine that is present between the two flow units.

6.4.2.2 Flow Unit 2a

The first structure inferred to form in the upper accumulation area of Flow Unit 2a is primary stratification (S_0); however, it is not evident below the snowline. A number of transverse crevasses (S_1) also develop high in the accumulation area but seem to die-out further down-glacier as the flow unit merges with the main trunk of the glacier. Some limited longitudinal foliation (S_2) develops on the true-right of the flow unit just down-glacier of the transverse crevasses; however, it does not become particularly strong until the middle-reaches of the glacier, where longitudinal foliation develops on the true-right and left of the flow unit. Longitudinal foliation in the middle-reaches of the glacier appears more prominent as a result of exploitation by supraglacial streams. The final structures to develop in Flow Unit 2a are arcuate transverse fractures (S_3) which form several hundred metres up-glacier from the snout on the true-left of the flow unit.

Table 6.5. Summary of the sequential structural evolution of each flow unit on Pedersenbreen. Key located below main table (note that the colours are related to the colours that represent each structure on the main structural map, Figure 6.10.).

Order of formation	Flow Unit 1	Flow Unit 2		Flow Unit 3	Flow Unit 4
		A	B		
1					
2					
3					
4					

Key	
	Primary stratification
	Longitudinal foliation
	First, second and third generation crevasse traces respectively

6.4.2.3 Flow Unit 2b

Primary stratification (S_0) develops in the upper accumulation area of Flow Unit 2b and becomes increasingly folded and arcuate down-glacier, dying-out when the flow unit joins the main trunk of the glacier. Transverse crevasses (S_1) also form in the upper accumulation basin but also die-out in a comparatively short distance. Strong longitudinal foliation (S_2) develops at the boundary with Flow Unit 3 when the two flow units merge and persists to the snout of the glacier. Strong longitudinal foliation also develops at the boundary with Flow Unit 2a, but only forms in the middle-reaches of the glacier, before remaining until the snout.

6.4.2.4 Flow Unit 3

As for Flow Unit 2b, primary stratification (S_0) develops in the upper accumulation basin of Flow Unit 3, which becomes arcuate down-glacier. Transverse crevasses (S_1)

also develop in the upper accumulation basin but die-out when the flow unit joins the main glacier trunk. Strong longitudinal foliation (S_2) develops at the boundaries with Flow Units 2b and 4 where all flow units merge into the main trunk of the glacier. The longitudinal foliation at the boundary with Flow Unit 2b persists to the snout of the glacier; however, the longitudinal foliation present at the boundary with Flow Unit 4 becomes obscured by supraglacial debris towards the terminus of the glacier.

6.4.2.5 Flow Unit 4

Primary stratification (S_0) forms in the upper accumulation area of Flow Unit 4, becoming arcuate as it travels down-glacier. Transverse crevasses (S_1) also develop in the upper accumulation area, and persist down-glacier, eventually becoming rotated in a clockwise direction. Longitudinal foliation (S_2) develops at both boundaries of the flow unit; however, it can only be traced to the main trunk of the glacier on the true-right of the flow unit, and to the middle-reaches of the glacier on the true-left of the flow unit as a result of supraglacial debris cover obscuring the surface of the glacier.

6.4.3 Detailed ice facies log descriptions

A total of three detailed ice facies logs were taken on Pedersenbreen to provide insight into the type of structures present at a flow unit boundary in a surge-type glacier, and to document their down-glacier evolution. Logs are ordered from up-glacier to down-glacier and taken at locations along a flowline at the boundary between Flow Units 1 and 2a, located on either side of a surge loop, with the highest up-glacier log located near to the confluence of the two flow units (Figure 6.11). Logs range from 2.0 to 3.0 metres in length. In each of the logs, longitudinal foliation is parallel to the medial moraine. The medial moraine comprises sandy gravel with some boulder size clasts reaching diameters of *c*. 0.5 metres, with clasts angularities predominantly subangular to angular. Rock types include marble, psammite and phyllite, which are derived from a precipitous head-wall above the confluence of Flow Unit 1 and 2a. Near to the

confluence of the two flow units, the medial moraine has no relief and comprises a thin and diffuse supraglacial cover of debris several metres wide; however, the relief of the moraine increases to *c*. 2.0 metres towards the surge loop as a result of debris cover insulating underlying ice. The moraine also becomes wider (up to *c*. 10 metres) down-glacier. A brief description of each log is given below, but for more detailed refer to the drawn logs (Figure 6.12).

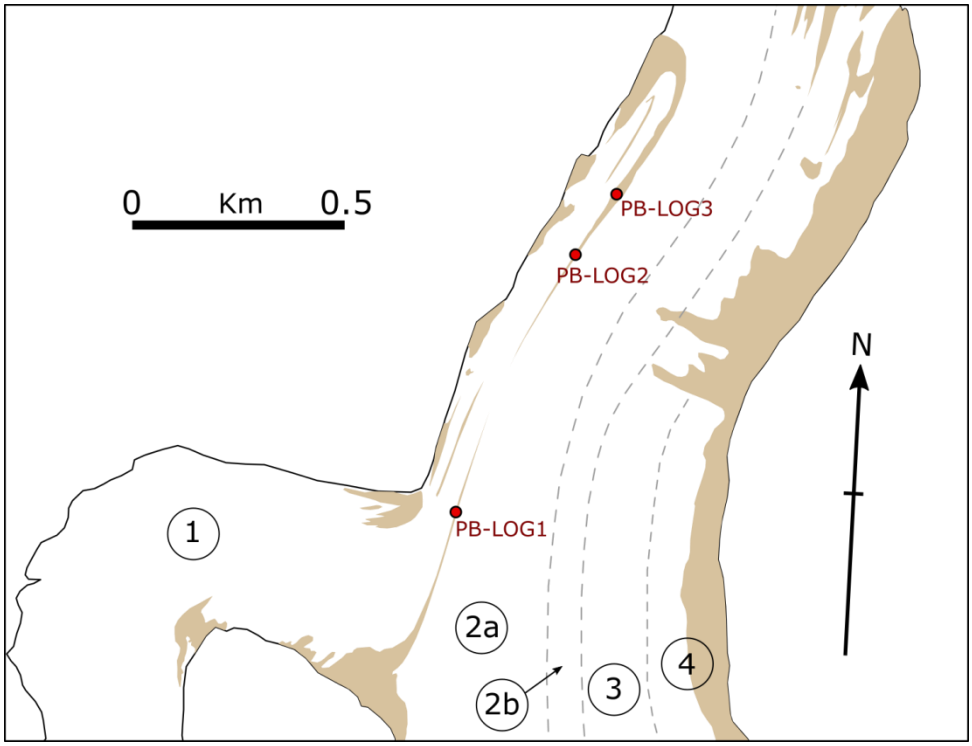

Figure 6.11. Flow unit map of Pedersenbreen showing the location of the detailed ice facies logs (red circles with red log identification numbers).

6.4.3.1 PB-LOG1 – 78.86572°N, 12.27126°E

PB-LOG1 (Figure 6.12) was located near to the start of the medial moraine separating Flow Units 1 and 2a located on either side the surge loop on Pedersenbreen. The medial moraine consisted of marble, psammite and phyllite lithologies, and all supraglacial debris was removed from the surface of the glacier to reveal the underlying ice structures. Despite the substantial amount of supraglacial debris, there was a surprising lack of englacial debris, suggesting that the medial moraine originated

from the peak above the confluence of both flow units. The log is 3.0 metres long and is mainly composed of coarse bubbly ice with frequent comparatively thin coarse clear ice layers. Foliation is common in the log, but with varying strengths between different ice layers. Even though the log details the ice structures present beneath the supraglacial medial moraine, a zone of strong foliation was located several metres away. The only englacial debris observed for PB-LOG1 was located at *c*. 1.5 metres where a coarse clear ice layer contained a thin layer of sandy gravel. An isolated fold hinge with up-glacier dip was also observed at *c*. 1.2 metres.

6.4.3.2 PB-LOG2 – 78.87147°N, 12.28463°E

PB-LOG2 (Figure 6.12) was located down-glacier of PB-LOG1, situated in an area of Pedersenbreen's medial moraine that comprises discontinuous angular supraglacial debris with minor amounts of fine grained debris oriented parallel to longitudinal foliation. The log is 3.0 metres in length and mainly comprises coarse bubbly ice with frequent thin coarse clear ice layers. Foliation strengths vary throughout the log as does the bubble concentrations in different coarse bubbly ice layers. Englacial debris is rarely observed on the log, with only some disseminated muds observed in coarse bubbly ice at *c*. 1.35 metres, and a thin muddy layer at *c*. 1.4 metres. A folded layer of coarse bubbly ice with comparatively fewer bubbles is present at *c*. 1.8 metres.

6.4.3.3 PB-LOG3 – 78.87263°N, 12.28907°E

PB-LOG3 (Figure 6.12) is the furthest down-glacier log taken on Pedersenbreen, located in an area of continuous moraine cover with strong foliation with parallel debris layers. The moraine was *c*. 7.0 metres wide at the logging site, and the log is 2.0 metres long starting at the true left (east) edge of the medial moraine going towards the centre of the moraine. The log is composed primarily of coarse bubbly ice with

FIGURE 6.12 - PB COMBINED DETAILED LOGS – PLEASE SEE APPENDIX

numerous thin coarse clear ice layers. Coarse bubbly ice layers regularly have variations in bubble content and all layers have varying strengths of foliation and moderate dip angles. Unlike the other logs taken on Pedersenbreen, PB-LOG3 has a higher concentration of englacial debris present. Several different ice layers are muddy or have small concentrations of disseminated mud; however, small clasts of angular to subangular pebbles are also found at *c*. 1.2 – 1.5 metres.

6.4.4 Interpretation and discussion

6.4.4.1 Glacier-wide structural overview

Like many other small valley glaciers (*e.g.* Hambrey, 1976b; Goodsell et al., 2005b; Hambrey et al., 2005; Jennings et al., 2014), Pedersenbreen is primarily dominated by the evolution of primary stratification into longitudinal foliation (Figure 6.10). Snow falling in the accumulation area of the glacier becomes buried by subsequent snowfalls and eventually undergoes diagenesis into glacier ice. The layering of the snowpack is preserved during the transition into glacier ice to form primary stratification. As ice flows from a wide accumulation area into a comparatively narrow glacier tongue, primary stratification becomes folded as a result of lateral compression and longitudinal extension, eventually transposing into longitudinal foliation. This process is most evident at flow unit boundaries as suggested by Hambrey and Glasser (2003) as a result of greater amounts of inferred simple shear between flow units. Longitudinal foliation on Pedersenbreen supports this hypothesis as the strongest foliation coincides with the glacier's flow unit boundaries (Figure 6.10). Bennett et al. (1996) noted that near vertical longitudinal foliation orientated parallel to the valley walls was present across the whole snout of the glacier, and that it cross-cut primary stratification. Bennett et al. (1996) also observed that near to the lobe of the surge loop, the longitudinal foliation was diagonally orientated by *c*. 30° as a result of Flow Unit 1 surging into Flow Unit 2a. In this study, no evidence of axial planar foliation was found at the boundary between Flow Unit 1 and 2a, with all longitudinal foliation remaining parallel to the looped medial moraine and not cross-cutting primary

stratification. However, the findings of this study agree with the conclusion of Bennett et al. (1996) that longitudinal foliation near to the lobe of the surge loop (in Flow Unit 2a) is deformed. Furthermore, the lack of axial planar foliation observed in this study does not contradict the findings of Bennett et al. (1996) as detailed structural observations were only made at the boundary between Flow Unit 1 and 2a. It is possible that axial planar foliation may be present elsewhere on the glacier, and was not directly observed in the field, or visible on the satellite imagery used for the glacier-wide structural mapping in this study. It is also worth noting that Bennett et al. (1996) documented extensive fracture sets on Pedersenbreen, stating this as evidence that the glacier was once heavily crevassed (as would be the case in a surge), or that there was extensive thrusting associated with periods of strong longitudinal compression. No extensive fracture sets were directly observed at the boundary between Flow Unit 1 and 2a in this study. As wide-spread fracturing would be expected during a surge, this suggests that the surface fracturing induced in the surge of Flow Unit 1 was comparatively shallow and that subsequent ablation and surface lowering has melted-out the relict features.

6.4.4.2 Origin and structural evolution of flow units

As previously suggested by Jennings et al. (2014) for an Alpine valley glacier, glacier-wide structural mapping of Pedersenbreen indicates that individual flow units are unique and mutually exclusive to one-another. Even though the degree to which flow units differ on Pedersenbreen is not as profound as for other glaciers, it is clear that individual flow units have different structural evolutions, as evidenced by the different locations that each type of structure forms in contrasting flow units (Figure 6.10).

One flow unit that is very different from all the others on Pedersenbreen is Flow Unit 1 (Figure 6.10). It has been suggested by Bennett et al. (1996) and Glasser et al. (2004) that Pedersenbreen is a surge-type glacier currently in its quiescent phase, and that Flow Unit 1 has previously surged into the main trunk of the glacier. This conclusion is supported by the structural mapping that has been undertaken for this

Figure 6.13. Photograph of strong longitudinal foliation present at the boundary between Flow Units 1 and 2a on Pedersenbreen. Note the thin alternating layers of different ice facies with steep dip angles.

study. The presence of a looped medial moraine originating from Flow Unit 1 is indicative of a flow instability (*see* Meier and Post, 1969; Dowdeswell and Williams, 1997), demonstrating that the flow unit once had higher ice-flow velocities during its active-phase. During this active-phase, Flow Unit 1 would have flowed into its less-active neighbouring flow unit and consequently deformed the medial moraine between the two. This conclusion is further supported by the detailed ice facies logs that were undertaken at the boundary between Flow Units 1 and 2a (Figure 6.12). Each of the three logs are dominated by very strong longitudinal foliation (Figure 6.13). This further suggests that Flow Unit 1 surging into Flow Unit 2a, as the difference in ice velocity between both flow units would lead to very high amounts of simple shear at the flow unit boundary which would quickly develop strong longitudinal foliation (*see* Hambrey and Glasser, 2003; Hambrey et al., 2005; Jennings et al., 2014). However, it is not clear if Pedersenbreen is still a surge-type glacier that is currently in its quiescent

phase, or if the glacier is now unable to surge as a result of its continued mass loss and thinning since Neoglacial time (*see* Benn and Evans, 2010; Striberger et al., 2011; Sevestre and Benn, 2015).

6.4.5 Summary

i. Pedersenbreen is structurally dominated by the evolution of primary stratification into longitudinal foliation, with the strongest longitudinal foliation occurring at flow unit boundaries.

ii. The presence of a looped medial moraine suggests that Flow Unit 1 has surged during the past.

iii. The presence of very strong longitudinal foliation at the boundary between Flow Unit 1 and 2a further supports the surge hypothesis as it indicates that high amounts of simple shear as a result of different ice flow velocities occurred between the two flow units.

iv. Longitudinal foliation at the boundary between Flow Unit 1 and 2a is parallel to the medial moraine defined surge loop. The comparative lack of englacial debris observed in the detailed ice facies logs, combined with the thin cover of supraglacial debris near to the confluence of Flow Unit 1 and 2a, and the angular to subangular nature of the clasts, suggest that the medial moraine is primarily composed of debris derived from a precipitous headwall that is transported on the surface of the glacier.

v. The lack of fracture sets observed in Flow Unit 1 and 2a despite the presence of a surge loop suggests that surge-related fracture propagation was relatively shallow, and that subsequent ablation and surface lowering has melted-out any fractures once present.

vi. It is not clear if Pedersenbreen can still be classified as a surge-type glacier in its quiescent phase, or if the glacier is less prone to/no longer has the ability to surge as a result of climate change since Neoglacial time.

Chapter Seven

Sermilik Glacier

7.1 Introduction

The overall aim of this chapter is to 'up-scale' the investigation of longitudinal structures from field-based small valley glaciers to intermediate sized ice masses utilising remote sensing techniques supplemented by ground observations. The structural characteristics of Sermilik Glacier (justification for the selection of glacier below) are assessed using structural mapping techniques from satellite imagery. For a detailed description of the techniques employed, refer to 'Methods' in *Chapter Three*.

The specific objectives of this chapter are:

i. To map the surface of Sermilik Glacier using satellite imagery.

ii. To test the hypothesis of Jennings et al. (2014) stating that flow units are unique and mutually exclusive from one-another, and see if this hypothesis is applicable to intermediate sized ice masses.

iii. To draw parallels between the longitudinal structures observed in small valley glaciers and an intermediate sized ice mass.

Sermilik Glacier has been selected as an ideal case study for 'up-scaling' the investigation of longitudinal structures from small valley glaciers to a larger valley glacier for several reasons:

i. The glacier is a good intermediate size which falls between the field studied valley glaciers in this project and ice streams.

ii. The glacier has multiple accumulation basins (approximately an order of magnitude more than the small valley glaciers in this study) that feed flow units that coalesce into a main glacier trunk.

iii. There is satellite imagery that clearly shows the structure of the glacier for most of the length of the flow units, enabling the glacier's well developed longitudinal structures to be traced high into the accumulation area.

iv. Sermilik Glacier was classified by Dowdeswell et al. (2007) as likely to be a non-surge-type glacier, therefore reducing the complexities of interpreting the formation mechanisms of observed structures.

v. The remotely sensed data and subsequent conclusions can be supplemented and supported by low-level oblique aerial photography of the lower tongue of the glacier.

Sermilik Glacier at present is *c*. 35 kilometres in length with a maximum glacier snout width of *c*. 4 kilometres. The glacier is composed of 21 major accumulation basins (labelled 1 to 21), which are further sub-divided into 45 sub-accumulation basins (Figure 7.1). For a brief overview of Bylot Island and Sermilik Glacier, refer to the 'Study-site descriptions' in *section 2.6*. A detailed description of the techniques employed in this chapter can be found in 'Methods' in *Chapter Three*.

7.2 Glacier-wide structural description

The glacier-wide structural mapping of Sermilik Glacier is based on satellite (Landsat 8 OLI) imagery collected in summer 2013 (refer to 'Methods' in *Chapter Three* for further details), with additional structural observations of the snout made from oblique aerial photographs collected in summer 2015. No structural mapping studies of Sermilik Glacier have previous been undertaken.

As is the case for many valley glaciers, Sermilik Glacier comprises a broad accumulation area consisting of separate accumulation basins that feed into a comparatively narrow tongue. The accumulation area is snow-covered (*c*. 65% of the glacier surface is snow-free); however, as has been the case for the smaller glaciers documented in this study, it is assumed that primary stratification is the first structure to develop. A justification for this assumption on Midtre Lovénbreen can be found in *section 6.2.2*. Even though there is a scale difference between the two glaciers and there is only limited exposure of primary stratification on Sermilik Glacier, the process of ice formation from the diagenesis of snow is consistent at all scales. Therefore, as primary stratification represents the preservation of layering contained in the initial snowpack (*i.e*. the 'building blocks' of the glacier), it is impossible for other structures to predate the formation of primary stratification.

The tongue of Sermilik Glacier is dominated by strong longitudinal structures that become more evident towards the snout. Longitudinal structures are defined by alternating light and dark bands at the surface of the glacier that run parallel to ice flow. Light and dark bands are often several kilometres in length, but can persist for *c*. 10 kilometres, and have widths of *c*. 10 – 50 metres. At the terminus of the glacier the structures become folded (large wavelengths, *c*. 300 – 400 metres; low amplitudes, *c*. 20 – 100 metres), especially where the glacier-width increases slightly towards the snout. Supraglacial debris is orientated parallel to longitudinal structures, and supraglacial streams remain sub-parallel; however, they become increasing sinuous and less constrained by glacier structure down-glacier (observations of supraglacial debris and stream orientations are made from oblique aerial photographs and not

FIGURE 7.1 - SERMILIK GLACIER MAIN STRUCTURAL MAP – PLEASE SEE APPENDIX

from satellite imagery). Few examples of primary stratification, open crevasses, and fracture traces are observed on the satellite imagery; however, this may be a result of the image resolution (15 metres) which is not sufficient to illustrate comparatively narrow structures (< 5 metres in width).

7.3 Interpretation and discussion

As explained in *section 7.2*, the accumulation area of Sermilik Glacier is snow-covered, obscuring the ice structures present in the upper reaches of the glacier. However, it is inferred that primary stratification is the first ice structure to form as a result of the diagenesis of snow into glacier ice. By the time that the surface of the glacier becomes snow-free, there is already strong longitudinal foliation present. Therefore, the formation mechanism of the longitudinal foliation is also concealed by the snow cover in the accumulation area. Even though identifying the exact mechanism of longitudinal foliation formation is not possible (transposition or axial planar foliation), it is possible to discount a fracture-derived formation mechanism as no fractures are evident in the accumulation area or on the tongue of the glacier. Even if the lack of fractures observed on the glacier is an artefact of the image resolution, the lack of sufficiently large fractures to be observed suggests that they are unlikely to be the origin of the longitudinal structures. Regardless of the exact formation process, the development of longitudinal foliation on Sermilik Glacier is consistent with observations taken from other glaciers in this study. Formation by a similar process as has been suggested for smaller glaciers is plausible as longitudinal foliation has been observed to develop within *c*. 500 metres on several glaciers. On Sermilik Glacier, the snow cover conceals a distance of at least *c*. 1 kilometre which is sufficient for longitudinal foliation to develop. Jennings et al. (2014) suggested that the dominant type of longitudinal foliation (transposition or axial planar foliation) present was dependent upon the lateral narrowing of flow units, stating that flow units with a more pronounced narrowing down-glacier preferentially develop transposition foliation. If this hypothesis is correct, it is probable that having 45 individual flow units from 45 sub-accumulation basins that feed in to a narrow tongue (< 4 kilometres in width) would

cause a pronounced narrowing. This infers higher rates of simple shear that would quickly transpose primary stratification into longitudinal foliation. However, further study utilising higher-resolution satellite imagery and ground based measurements would be required to determine if this hypothesis is valid for Sermilik Glacier.

Longitudinal foliation on the tongue of Sermilik Glacier is highlighted by alternating light and dark bands. The differences in colour of individual bands reflect the varying amount of debris/sediment contained in the supraglacial ice. Even though a medial moraine is present on the glacier (Figure 7.2), the remaining bands appear to have varying concentrations of trapped aeolian-derived dust and organic material (Oerlemans et al., 2009; Jennings et al., 2014). Strong longitudinal foliation is revealed at the surface of the glacier as alternating layers of steeply dipping ice facies. Differential ablation of individual ice facies at the surface of the glacier leads to the formation of a ridge/furrow ice surface topography. Furrows act as sediment traps, trapping aeolian fines in the surface ice, which subsequently highlights the ice structure. Some debris revealed at the surface of the glacier may have en- or subglacial origins; however, this is hard to ascertain without field-sampling. Nevertheless, the presence of strong longitudinal foliation on the trunk of the glacier is consistent with the hypothesis of medial moraine formation as suggested by Hambrey and Glasser (2003) whereby folding of englacial and basal ice layers elevates debris that subsequently emerges at the surface of the glacier as a result of ablation and surface lowering.

Unlike for the smaller valley glaciers documented in this study, it does not appear possible to separate the tongue of Sermilik Glacier into individual flow units. This is in part a result of the large number of accumulation basins feeding into the tongue, which is further exacerbated by the resolution of the imagery available for mapping. For example, the image resolution (pixel size) used in this study for Austre Brøggerbeen and Austre Lovénbreen is *c*. 0.25 metres and 0.17 metres respectively, whereas for Sermilik Glacier, the image resolution available is 15 metres (*see sections 3.3.1 and 3.3.2*). The structural complexity resulting from the numerous accumulation basins feeding into the tongue, combined with the coarser imagery used for mapping Sermilik Glacier appears to hinder the identification of flow unit boundaries.

Figure 7.2. Oblique aerial photograph of the medial moraine present on the snout of Sermilik Glacier. Note how the medial moraine is folded towards the snout of the glacier. Photograph courtesy of M. J. Hambrey.

Nevertheless, by taking a section across the snout of the glacier, the number of longitudinal structures present across the whole width of the glacier is approximately 44 features (the number of the features can vary depending on the location of the section across the glacier; however, the location selected was chosen because it provided the clearest view of the longitudinal structures, but also coincided with an area of low deformation to reduce the possibility of longitudinal structures being erroneously counted multiple times). This number coincides with the number of sub-accumulation basins that the glacier has (45 sub-accumulation basins). Observations from oblique aerial photographs (Figure 7.3 and 7.4) illustrates that there is more longitudinal foliation present on the glacier than could be mapped from the available satellite imagery. Consequently, the longitudinal structures mapped from the satellite imagery are most likely to be areas consisting of densely packed strong longitudinal foliation, as opposed to individual longitudinal foliation structures. As previously observed on other glaciers (*e.g.* Allen et al., 1960; Hambrey, 1977a; Hooke and Hudleston, 1978; Hambrey and Milnes, 1977; Hambrey et al., 1980, 1999, 2005; Hambrey and Lawson, 2000; Goodsell et al., 2005b; Roberson, 2008; Appleby et al.,

Figure 7.3. Oblique aerial photograph of the snout of Sermilik Glacier. Note the amount of longitudinal foliation that is not visible on the satellite imagery. Photograph courtesy of M. J. Hambrey.

Figure 7.4. Oblique aerial photograph of the middle-reaches of Sermilik Glacier. Note how longitudinal foliation is grouped into bands that appear comparatively dark. Photograph courtesy of Timothy K, available from: www.panoramio.com/photo/58891606.

2010; Jennings et al., 2014, 2015), and in this study, strong longitudinal foliation coincides with flow unit boundaries. Mapping of smaller valley glaciers in this study has shown that individual longitudinal foliation structures form in distinct bands at flow unit boundaries. Furthermore, it has been demonstrated for the small valley glacier mapped in this study that the number of flow unit boundaries is always one lower than the number of accumulation basins (not including the boundaries at the glacier margins) (Figure 7.5). Therefore, it is hypothesised that the 44 longitudinal structures on Sermilik Glacier are in fact flow unit boundaries consisting of bands of longitudinal

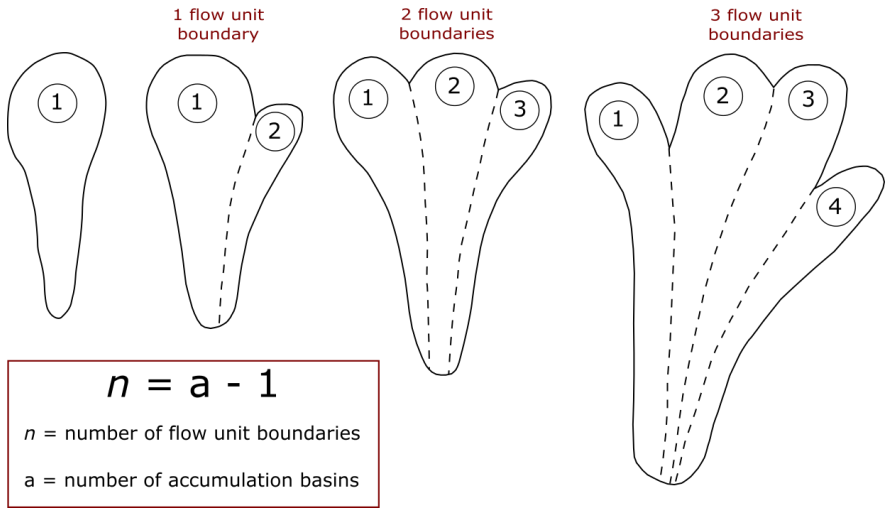

Figure 7.5. Schematic diagram demonstrating that the number of flow unit boundaries present in a glacier (excluding the glacier margins) is dependent upon the number of accumulation basins. Circled numbers indicate accumulation basins and dashed lines represent flow unit boundaries.

foliation. However, because of the amount of flow units, combined with the comparatively low resolution of the satellite imagery, the bands of strong longitudinal foliation appear as individual linear features on the satellite imagery (Figure 7.6). The geometric similarity between longitudinal foliation and flow unit boundaries at different scales suggests that there is 'self-similarity' between the features, and that longitudinal features are 'scale-independent', forming at a range of scales yet appearing geometrically similar.

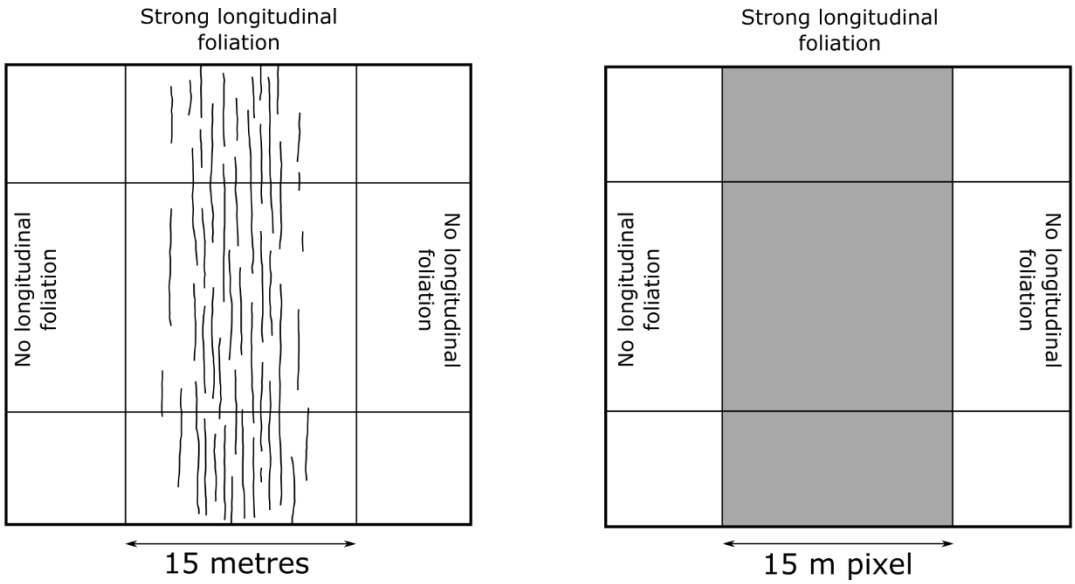

Figure 7.6. Conceptual diagram illustrating how bands composed of anastomosing layers of strong longitudinal foliation can appear as long linear lines on satellite imagery with comparatively low spatial resolution. The square on the left shows strong longitudinal foliation clustered in a band as it would appear at the surface of a glacier. The square on the right demonstrates how the band of longitudinal foliation would appear on a satellite image with a spatial resolution of 15 metres. Note how the longitudinal structures clustered in a band get grouped together in a single pixel on the satellite image to form one linear feature.

On the snout of the glacier some folding of the longitudinal features occurs near to the terminus. This folding is the result of the tongue of the glacier flowing from a topographically confined area on to a non-confined comparatively flat coastal outwash plain. As the lateral margins of the glacier no longer abut against lateral moraines or mountain-sides, the ice begins to spread laterally, resulting in longitudinal compression and lateral extension developing low-amplitude folds with axes transverse to flow. Other glaciers on Bylot Island typically form piedmont lobes when no longer laterally confined (Dowdeswell et al., 2007). In the case of Sermilik Glacier, the ice does not spread laterally to form a characteristic piedmont lobe as it becomes constrained by ice-cored lateral moraines, but does experience sufficient longitudinal compression and lateral extension to distort and fold the initially linear longitudinal structures (Figure 7.1).

7.4 Summary

i. Despite being obscured by snow cover, primary stratification is inferred to be the first structure that forms on Sermilik Glacier.

ii. The exact formation mechanism of the longitudinal structures cannot be observed because of snow cover in the accumulation area. However, the distance from the snow-covered accumulation area to the longitudinal structures is sufficient for the formation of longitudinal foliation, as observed on other glaciers in this study.

iii. Satellite imagery and oblique aerial photographs illustrate that longitudinal foliation on the snout of Sermilik Glacier is highlighted by alternating dark and light bands. The changes in colour are most likely to be the result of varying debris/sediment concentrations in the supraglacial ice. It is not known if the source of the surface debris/sediment is aeolian dust trapped by ice surface topography, or if the debris is sourced from en- or subglacial origins; however, it is likely that the concentration of debris present is directly related to the strength of the longitudinal foliation in that area.

iv. Longitudinal structures on the trunk of Sermilik Glacier are hypothesised to be flow unit boundaries. The presence of 44 longitudinal features on the snout of the glacier coincides with the amount of accumulation basins feeding Sermilik Glacier (45 sub-accumulation basins). Because of the comparatively low resolution of the satellite imagery, it is suggested that bands of strong longitudinal foliation located at flow unit boundaries appear as individual linear features. It is therefore hypothesised that longitudinal structures (*i.e.* longitudinal foliation and flow unit boundaries) have 'self-similarity' and are 'scale-independent', forming geometrically similar features at a range of scales.

v. Folding of linear features on the snout of the glacier is the result of lateral extension and longitudinal compression as the glacier flows from a laterally confined valley into a non-confined outwash plain.

Chapter Eight

Longitudinal flow structures in the Antarctic Ice Sheet

8.1 Introduction

Longitudinal ice-surface structures are commonly found on the Antarctic and Greenland ice sheets, and are most discernible at the surface of fast-flowing ice streams and outlet glaciers (*see section 2.5.6.1*). A wide range of terms have been used to describe these features (*see section 2.5.6.1*); however, in this study, longitudinal surface structures will be referred to as flowlines (*following* Crabtree and Doake, 1980). On the Antarctic Ice Sheet, flowlines originate in the interior, continuing to the periphery of the ice sheet and on to its fringing ice shelves (Reynolds, 1988; Reynolds and Hambrey, 1988; Swithinbank et al., 1988; Hambrey and Dowdeswell, 1994; Fahnestock et al., 2000; Ely and Clark, 2015; Glasser et al., 2015). It is important to understand the origin and evolution of flowlines on ice sheets as they potentially provide important information on past dynamics that is not available by other means of study. However, several hypotheses for the formation of flowlines are currently suggested and no consensus has been reached on the exact process of formation.

The name 'flowline' is derived from the fact that they are often orientated parallel to ice-flow direction and inferred to represent current or relict flow-pathways within an ice sheet (Fahnestock et al., 2000); however, this is not always the case. Flowlines can be found in the accumulation area of ice sheets despite being snow-covered as they are highlighted by variations in surface topography. Furthermore, they are also present in surface ablation areas (blue-ice areas) where they appear to be the

surface expression of three-dimensional longitudinal foliation (Hambrey and Dowdeswell, 1994). Longitudinal features on the surface of ice shelves have been connected with meltwater channels located beneath the shelf; however, these features may or may not be orientated parallel to modern ice-flow direction (Le Brocq et al., 2013; Millgate et al., 2013). Even though there is no general consensus on how flowlines form, several hypotheses have been suggested. Merry and Whillians (1993) suggested that flowlines form as a result of localised high shear strain rates near to the flowline's onset zone. However, Casassa and Brecher (1993) found no velocity variations between adjacent flowlines on Byrd Glacier, indicating that their formation cannot be attributed to shear zones forming at the boundaries of neighbouring flowlines. A further hypothesis suggests that flowlines are formed by the deformation and folding of pre-existing structures (*e.g.* primary stratification) when experiencing lateral compression and longitudinal extension, in much the same way as longitudinal foliation has been observed to form in valley glaciers and ice caps (Hambrey, 1977a; Hooke and Hudleston, 1978). Evidence for this hypothesis has been documented by Hambrey and Dowdeswell (1994) and Glasser et al. (2015). Numerical modelling of ice sheets has demonstrated that longitudinal surface structures can form when fast-flowing ice flows over an undulating bedrock surface. However, for this to be the case there has to be rapid basal sliding and the basal undulations have to have wavelengths that are comparable to the ice thickness to cause an ice-surface expression (Gudmundsson et al., 1998). Glasser and Scambos (2008) inferred that areas with longitudinal ice-surface structures were fast-flowing, whereas areas without these features were slow-flowing. Glasser and Gudmundsson (2012) further concluded that longitudinal ice-surface features form where individual tributary glaciers merge, and down-flow of nunataks as a result of transverse convergence of ice and longitudinal extension. In both cases, flowlines develop in areas of ice acceleration and extensional flow, representing stretching lineations in zones of rapid ice velocities.

As summarised by Glasser et al. (2015), there are three main hypotheses regarding how flowlines form:

i. That they are a macro-scale version of longitudinal foliation as can be seen in small valley glaciers and form in a similar manner. Primary stratification in the interior of the ice sheet becomes folded as it flows from a broad accumulation area into a topographically confined narrow glacier tongue. In this case, flowlines are the surface expression of a three-dimensional structure that forms in response to strong lateral compression and longitudinal extension (Reynolds and Hambrey, 1988; Hambrey and Dowdeswell, 1994). Furthermore, they also develop in the lee of nunataks and at the confluence of tributary glaciers where there is strong convergence and longitudinal extension (Glasser and Gudmundsson, 2012). In all the situations above, flowlines represent the surface expression of a three-dimensional structure.

ii. They form at the confluence of two flow units that are flowing at different velocities, subsequently forming a shear margin at the boundary between the two. If this is the case, flowlines should mainly form at the confluence of glaciers or flow units. They may also represent the surface expression of vertical sheets of differing ice fabrics that develop as a result of shear. In this case, flowlines represent weak bands in the ice sheet where shear aligns ice crystals (Hulbe and Whillans, 1997; Whillans and Van der Veen, 1997).

iii. They are the surface expression of bed topography that has been transmitted to the ice surface in areas of rapid basal sliding and where bed perturbations have wavelengths of a similar length as the overlying ice thickness (Gudmundsson et al., 1998).

The aim of this chapter is to attempt to map and document the structural characteristics of flowlines in the Antarctic Ice sheet. Subsequent comparison with smaller-scaled glaciers observed in this study will allow flowlines to be compared with longitudinal foliation in an attempt to discover if flowlines are a macro-scale longitudinal foliation, as suggested by Reynolds and Hambrey (1988), Hambrey and Dowdeswell (1994) and Glasser et al. (2015). Furthermore, the other hypotheses of flowline formation will be tested to ascertain if they are supported by the structural data collected in this study. For a detailed description of the techniques employed, refer to 'Methods' in *Chapter Three*.

8.2 Study sites and glacier-wide structural descriptions

A number of study sites from various locations around the Antarctic Ice Sheet have been selected to offer a wide range of localities that flowlines form. Furthermore, the study of flowlines in the Antarctic Ice Sheet is conducted at different scales, including large topographically confined glaciers (large-scale valley glaciers) and major ice streams. Two main criteria were prioritised for the selection of study sites.

i. The selection of major ice streams that drain large portions of the ice sheet, which are important for understanding large-scale dynamics.

ii. The selection of representative outlet glaciers that have exposed ice surfaces (blue-ice areas), and therefore can be used to ascertain the validity of the longitudinal foliation hypothesis.

A description of each location studied is discussed in turn below (Figure 8.1), and a brief overview of each glacier can be found in the 'Study-site descriptions' in *section 2.6*.

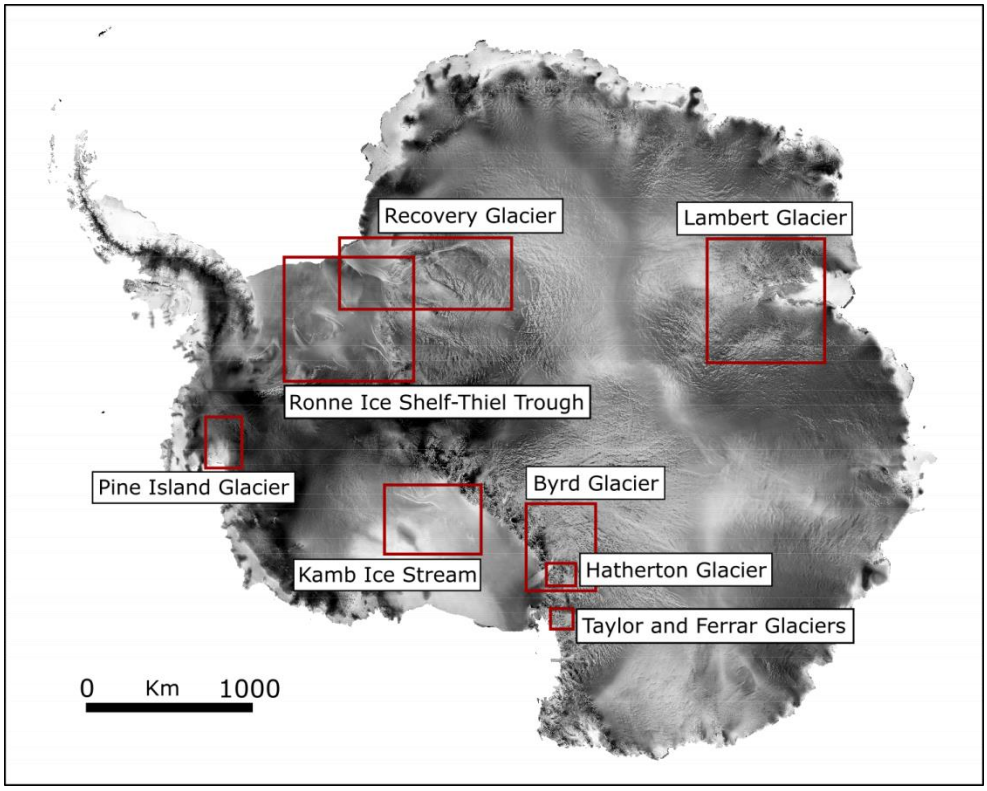

Figure 8.1. Synthetic aperture radar (SAR) imagery of Antarctica showing the location of key areas discussed in this chapter.

The structural mapping of Antarctic glaciers was undertaken using a range of satellite imagery including optical (MODIS, LIMA, ASTER, LANDSAT 8, and Google Earth imagery) and radar (RADARSAT) sensors (please refer to 'Methods' in *Chapter Three* for further details). Longitudinal surface structures (flowlines) are present in the imagery derived from each of the sensors, and are consistent between all optical and radar products, giving confidence that the flowlines visible in the satellite imagery are not an artefact of the imagery. For the mapping of larger-scale glacier systems (*e.g.* Lambert Glacier system) a combination of optical and radar sensors were utilised to enable accurate mapping of flowlines into the interior of the Antarctic Ice Sheet. The use of radar imagery allowed the tracing of flowlines further into the interior than optical imagery as it was able to 'see' the features despite substantial snow-cover. Differences in the image resolution between the satellite sensors had no impact on the accuracy of the mapping, because of the scale of the mapping being undertaken (flowline features often cover many hundreds of kilometres).

Mapping of flowlines on the surface of the Antarctic Ice Sheet was undertaken independently of other maps of Antarctica; however, once completed, the structural maps were compared to velocity and bed topography maps produced for the ice sheet (Figure 8.2). The distribution of flowlines was compared to the velocity map of Antarctica (Rignot et al., 2011), which is a high-resolution digital mosaic of ice flow velocities composed from multiple satellite interferometric synthetic-aperture radar (InSAR) measurements (available from: http://nsidc.org/data/nsidc-0484.html). The distribution of flowlines was also compared to the subglacial topography of Antarctica (BEDMAP-2) (Fretwell et al., 2013).

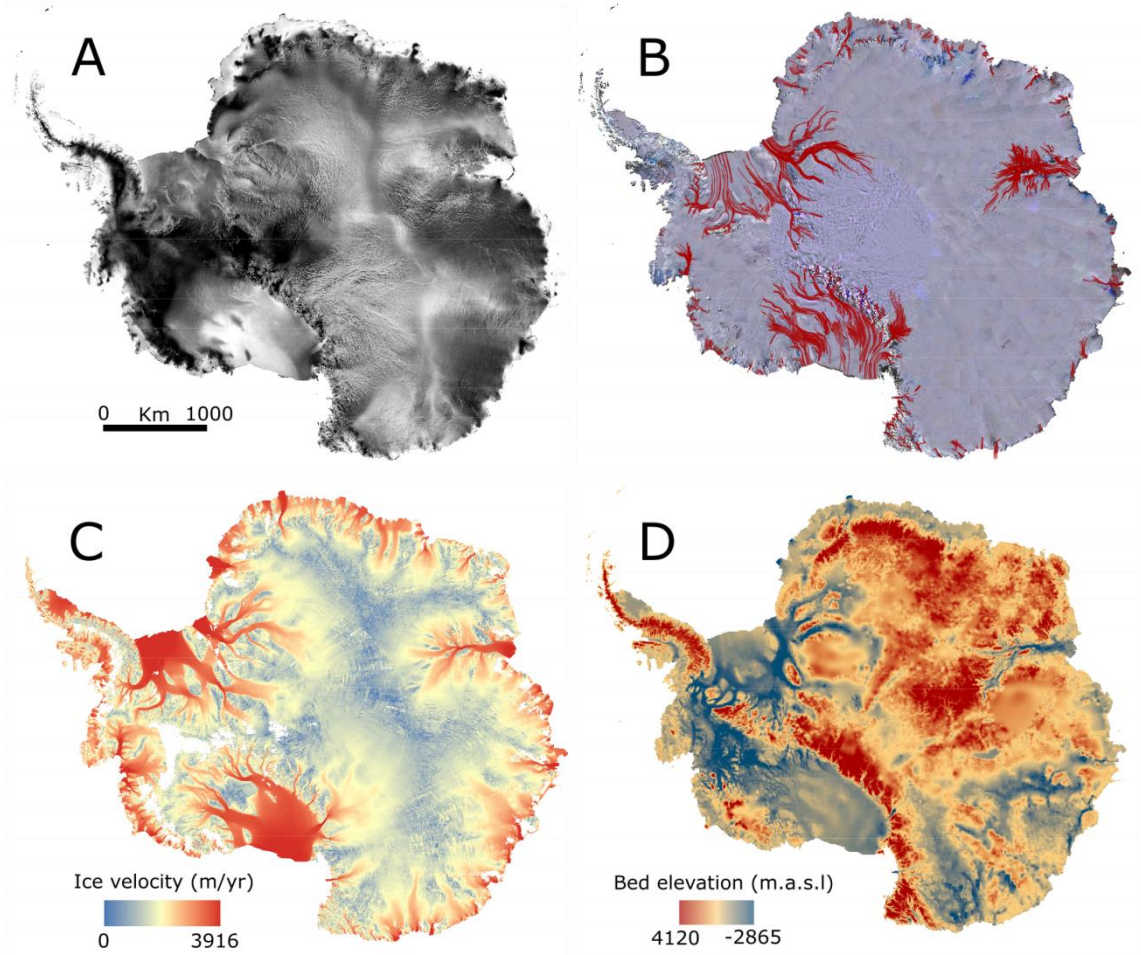

Figure 8.2. Comparison between the distribution of flowlines and other Antarctic data sets: (A) synthetic aperture radar (SAR) imagery showing the surface of the Antarctic Ice Sheet; (B) the continent-wide distribution of flowlines displayed over LIMA imagery, mapping of flowlines undertaken by N. F. Glasser and supplemented by the author; (C) velocity map of Antarctica (Rignot et al., 2011); (D) subglacial topography of Antarctica (Fretwell et al., 2013). Figure made by the author and published in Glasser et al. (2015).

Unlike the other glaciers investigated in this study, the glaciers investigated in Antarctica are not topographically constrained in their accumulation basins. The accumulation area of each glacier is directly sourced from the Antarctic Ice Sheet, with the location of the accumulation area often being dictated by the basal geometry of various sectors of the ice sheet, ice-surface topographic highs such as ice domes, and ice-surface gradients from major ice divides. The two smaller-scale areas investigated in this chapter (Hatherton Glacier and Taylor/Ferrar Glaciers) are topographically constrained in their lower reaches as they flow through mountainous terrain (large-scale valley glaciers). The remaining glaciers are larger-scale ice streams that have onset zones within the interior of the ice sheet and are initially not constrained by topography. The onset zones of ice streams consist of arborescent networks of tributaries that converge into a major outlet ice stream. The lateral boundaries of tributary and main ice stream channels consist of sharp transitions between fast-flowing and comparatively slow-flowing ice that are inferred to be dominated by simple shear. However, some ice streams become topographically confined in their lower-reaches as they flow into large-scale valleys (*e.g.* Lambert Glacier - Amery Ice Shelf system) or when flowing through mountain ranges (*e.g.* Byrd Glacier). Regardless of scale, all the Antarctic glaciers observed in this study are characterised by flow from a very broad accumulation area into a narrow main trunk. Furthermore, almost without exception, all major Antarctic ice streams/glaciers and their tributaries are dominated by flowlines that originate from their onset zones in the interior of the ice sheet and persist down-glacier onto the fringing ice shelves. Flowlines also remain present when traced through crevasse fields and areas of ablation (blue-ice areas) (Glasser et al., 2015).

In this study, unique areas of channellised glacier flow that cannot be defined into individual flow units are referred to as ‘flow areas’. A flow area can be defined as an area of glacier flow that originates from a distinct area. An individual flow area may encompass numerous flow units and accumulation basins/initiation zones; however, it defines a component of flow that is distinct from its neighbouring flow areas. The boundary of flow areas can be defined by tributaries of ice, the presence of flowlines, the presence of strong longitudinal foliation, medial moraines, or by crevasse patterns.

8.2.1 Hatherton Glacier

The accumulation area of Hatherton Glacier is not topographically constrained and comprises a broad expanse of ice that feeds into a comparatively narrow glacier tongue. The glacier becomes topographically constrained when flowing from the accumulation area into the main glacier tongue, as the ice is channelled through the Transantarctic Mountains (Figure 8.3). The accumulation area of the glacier is predominantly snow-covered; however, the surface of the main glacier trunk becomes snow-free (*i.e.* a blue-ice area) once it is topographically constrained. When flowing through the Transantarctic mountains, additional bodies of ice that originate from topographically constrained accumulation basins merge with the main glacier trunk (predominantly on the true-right of the glacier tongue). Each of the topographically constrained accumulation basins are snow-covered; however, the ice surface becomes snow-free before merging with the main glacier trunk. Hatherton Glacier can be divided into four flow areas (labelled Flow Area 1 to 4), with Flow Areas 3 and 4 further divided into two and four sub-flow areas respectively (Figure 8.3). Flow areas are numbered from up-glacier to down-glacier in the order that they join the main trunk of the glacier. All of the flow areas/sub-flow areas defined for Hatherton Glacier contain multiple flow units that originate from multiple accumulation basins. Flow areas are defined by the location of major accumulation areas (distinct areas that encompass multiple accumulation basins), as well as by the presence of medial moraines/flowlines. The tongue of Hatherton Glacier is characterised by the presence of flowlines, some of which are defined by debris which forms medial moraines. Flowlines/medial moraines generally remain parallel to ice flow direction; however, in two cases flowlines/medial moraines are orientated perpendicular to ice flow (Figure 8.3).

8.2.2 Taylor and Ferrar Glaciers

Both the Taylor and Ferrar Glaciers (Figure 8.4) have similar general characteristics, with each having a broad non-topographically confined accumulation basin that feeds into a comparatively narrow glacier tongue. Both accumulation basins are also snow-

FIGURE 8.3 - HATHERTON GLAICER FLOWLINE MAP – PLEASE SEE APPENDIX

FIGURE 8.4 - TAYLOR AND FERRAR GLAICER FLOWLINE MAP – PLEASE SEE APPENDIX

covered; however, the Taylor and Ferrar Glaciers become snow-free (blue-ice areas) and topographically confined when entering into their respective main glacier trunks. When flowing through the Royal Society Range, additional bodies of ice derived from topographically confined accumulation basins join both glaciers, especially so for Ferrar Glacier which has several tributaries join its main trunk at the southern margin of the glacier. For both glaciers, flow areas are numbered from up-glacier to down-glacier in the order that they join the main trunk of their respective glacier.

Taylor Glacier can be divided into three flow areas (labelled Flow Area 1 to 3), with Flow Area 1 further divided into two sub-flow areas (Figure 8.4). Flow areas are defined by the location of major bodies of ice that join the main trunk of Taylor Glacier, as well as by the presence of flowlines on the glacier surface. The main trunk of Taylor Glacier is dominated by the presence of flowlines that generally remain parallel to flow; however, in one case folding of flowlines perpendicular to flow can be seen (Figure 8.4). The majority of the flowlines present on the surface of Taylor Glacier are derived from the interior of the ice sheet, with only a few flowlines forming in the lee of nunataks or at the confluence of tributaries.

Ferrar Glacier can be divided into six flow areas (labelled 1 to 6), with Flow Area 3 further divided into two sub-flow areas (Figure 8.4). The majority of flow areas are defined by tributaries that join the main trunk of Ferrar Glacier. The surface of Ferrar Glacier is dominated by flowlines that are predominantly orientated parallel to ice flow direction. In direct contrast to Taylor Glacier, the majority of flowlines on Ferrar Glacier are derived from the merging of tributary ice masses, or confluence of ice around nunataks.

8.2.3 Lambert Glacier system

The Lambert Glacier system (Figure 8.5) has a very broad arborescent accumulation area that drains a significant proportion of the East Antarctic Ice Sheet. Ice flowing from the surrounding ice sheet drains through the Lambert Graben, eventually becoming the Amery Ice Shelf. Hambrey and Dowdeswell (1994) identified eight

FIGURE 8.5 - LAMBERT GLAICER FLOWLINE MAP – PLEASE SEE APPENDIX

independent ice streams that join the Lambert-Amery Ice Shelf system; however, many of these ice streams flow directly into the Amery Ice Shelf. Therefore, the main upstream components of the Lambert Glacier system comprise the Lambert, Mellor, and Fisher Glaciers, as well as numerous smaller ice masses that flow from the Mawson Escarpment to the east, and the Prince Charles Mountains to the west. The accumulation area of the Lambert Glacier system is predominantly snow-covered; however, at the confluence of the Lambert, Mellor and Fisher Glaciers, wind scour reveals the ice surface, exposing a large blue-ice area that covers the grounded section of the Lambert Glacier system. Despite the snow-cover in the accumulation area, flowlines can be traced deep into the interior of the ice sheet, especially for the Lambert Glacier where flowlines can be traced to within several hundred kilometres of the ice divide. The arborescent network of flowlines converges into the comparatively narrow (*c.* 50 kilometres wide) Lambert Graben where they become topographically confined within the rift valley that is flanked by the Mawson Escarpment and the Prince Charles Mountains. The majority of flowlines that form in the three major ice streams (the Lambert, Mellor, and Fisher Glaciers) develop in the interior of the ice sheet; however, an increasing proportion of flowlines that form in the lee of nunataks are present when the ice approaches the topographic confinement of the Lambert Graben. This is especially the case for smaller glaciers that flow through, or are derived, from the Mawson Escarpment and the Prince Charles Mountains. The Lambert Glacier system can be divided into five flow areas consisting of the main ice streams, Lambert Glacier, Mellor Glacier, Fisher Glacier, ice derived from the Mawson Escarpment, and ice from the Prince Charles Mountains (Figure 8.5).

8.2.4 Recovery Glacier

The accumulation area of Recovery Glacier spans a broad catchment that drains the East Antarctic Ice Sheet. Even though the accumulation area and main trunk of the glacier are not topographically confined, arborescent networks of flowlines converge into comparatively narrow tributaries that eventually form the main trunk of the glacier (Figure 8.6). The whole of Recovery Glacier is snow-covered (including its down-

FIGURE 8.6 - RECOVERY GLAICER FLOWLINE MAP – PLEASE SEE APPENDIX

glacier continuation into the Filchner Ice Shelf); however, despite the snow cover, flowlines can be traced deep into the interior of the ice sheet. The majority of the flowlines present on the surface of the glacier do not form as the result of ice converging around nunataks, but form in the interior of the ice sheet away from nunataks or subglacial mountains. The down-glacier persistence of flowlines varies with many flowlines measuring tens of kilometres in length; however, some flowlines persist for distances in excess of several hundred kilometres. Recovery Glacier can be divided into four flow areas (labelled Flow Area 1 to 4), with Flow Area 1 further divided into two sub-flow areas (Figure 8.6). Flow areas are ordered from up- to down-glacier depending on the order that they join the main glacier trunk, with individual flow areas defined by the presence of flowlines. However, despite originating in the interior of the ice sheet, flow areas comprise multiple flow units.

8.2.5 Pine Island Glacier

Pine Island Glacier (Figure 8.7) has a broad accumulation area defined by a broad arborescent network of flowlines that converge into the main glacier trunk. The comparatively wide accumulation area undergoes a pronounced narrowing into the main glacier trunk; however, the glacier is not topographically confined. Pine Island Glacier is totally snow-covered; nevertheless, flowlines can be traced into the interior of the ice sheet, but unlike for other Antarctic Glaciers in this study, flowlines can only be traced for *c*. 150 kilometres into the interior of the ice sheet. However, it is worth noting that the comparatively short distance that flowlines can be traced on Pine Island Glacier is likely to be a result of an artefact of the satellite imagery used for mapping. There are no notable nunataks present that lead to the formation of flowlines, with the majority of flowlines developing in the interior of the ice sheet. Pine Island Glacier can be separated into three flow areas (labelled Flow Area 1 to 3), with Flow Areas 1 and 2 further divided into two sub-flow areas each (Figure 8.7). Flow areas are labelled from the true-right to the true-left of the glacier, and are defined by the channellisation of flowlines.

FIGURE 8.7 - PINE ISLAND GLAICER FLOWLINE MAP – PLEASE SEE APPENDIX

8.2.6 Byrd Glacier

Byrd Glacier (Figure 8.8) has a broad accumulation area that drains a large catchment that is not topographically confined; however, the glacier undergoes a pronounced narrowing into a topographically controlled fjord flowing through the Transantarctic Mountains. Flowlines on the surface of Byrd Glacier form an arborescent network that becomes channellised into a comparatively narrow glacier trunk (*c*. 20 kilometres). Flowlines originating in the interior of the ice sheet can persist for in excess of several hundred kilometres; however, the glacier has a large proportion of flowlines that extend for much shorter distances and form in the lee of nunataks. The accumulation area of Byrd Glacier is snow-covered; however, when entering the topographically controlled glacier trunk, the ice surface becomes wind-scoured and snow-free (blue-ice area) (Figure 8.8). The snow-free main trunk of the glacier reveals the structure of the ice mass which consists of differing flow units that are defined by crevasse sets with different orientations. Byrd Glacier can be separated into five flow areas (labelled Flow Area 1 to 5), with Flow Areas 2 and 3 further divided into two sub-flow areas each (Figure 8.8). Flow areas are labelled from the true-right to the true-left of the glacier, and are defined by the channellisation, length, and formation areas of flowlines. Flow Areas 3a, 3b, and 4 are all predominantly dominated by flowlines that form in the interior of the ice sheet away from nunataks, whereas Flow Areas 1, 2a, 2b, and 5 have a large proportion of flowlines that form in the lee of nunataks.

8.3 Interpretation and discussion

8.3.1 Continent-wide distribution of flowlines

The distribution of flowlines across the Antarctic Ice Sheet is non-uniform, primarily coinciding with the flow from major ice streams (Figure 8.2). The flowlines form arborescent networks initiating in the interior of the ice sheet that become focused in comparatively narrow corridors of ice as tributaries coalesce down-glacier. They can be traced for great distances that can be in excess of a thousand kilometres, and remain

FIGURE 8.8 - BYRD GLAICER FLOWLINE MAP – PLEASE SEE APPENDIX

present as ice streams flow into ice shelves. The presence of flowlines correlates well with ice flow velocities, typically being located in areas with velocities greater than *c*. 15 m a^{-1} or originating in areas of high shear strain (Figure 8.2). High flow velocities and flowlines also coincide with basal topography, having preferential alignment over deep subglacial troughs (Figure 8.2) (Glasser et al., 2015). Flowlines are also evident in the lee of nunataks where converging tributaries experience strong transverse convergence and concomitant longitudinal extension (Glasser and Gudmundsson, 2012). However, away from fast-flowing ice streams, flowlines are entirely absent in areas of slow ice flow velocities (Glasser et al., 2015). The correlation between fast ice flow velocities, deep subglacial troughs, and the presence of flowlines, suggests that flowlines are organised into channels of rapid ice flow (ice streams), which are in turn strongly steered by the underlying subglacial topography. Interestingly, the presence of deep subglacial troughs owe their existence to fast-flowing ice that has excavated them (*e.g.* the Lambert Glacier system drains into a deep glacially-excavated tectonic rift that has been exploited by three major ice streams – Lambert Glacier, Fisher Glacier, and Mellor Glacier). It is therefore apparent, that fast ice flow must have remained in the same location for an extended period of time to enable large over-deepened troughs to develop. This inference is supported by geological and stratigraphic evidence that suggests that the Lambert Graben (the tectonic rift that the Lambert Glacier system drains through) has provided an outlet for ice flow from the interior since the formation of the ice sheet in late Eocene or early Oligocene time (Barron et al., 1991; Hambrey and McKelvey, 2000; O'Brien et al., 2001; Taylor et al., 2004).

8.3.2. Flowlines as three-dimensional structures

In direct contrast to all the other glaciers investigated in this study, the majority of the Antarctic Ice Sheet is covered by snow. Even though optical and radar satellite imagery can depict flowlines despite the substantial surface snow-cover, the ice surface of the ice sheet can only be directly viewed in several locations. Areas of net ablation (usually dominated by sublimation or wind-scour) allow areas of bare ice to be exposed (blue-

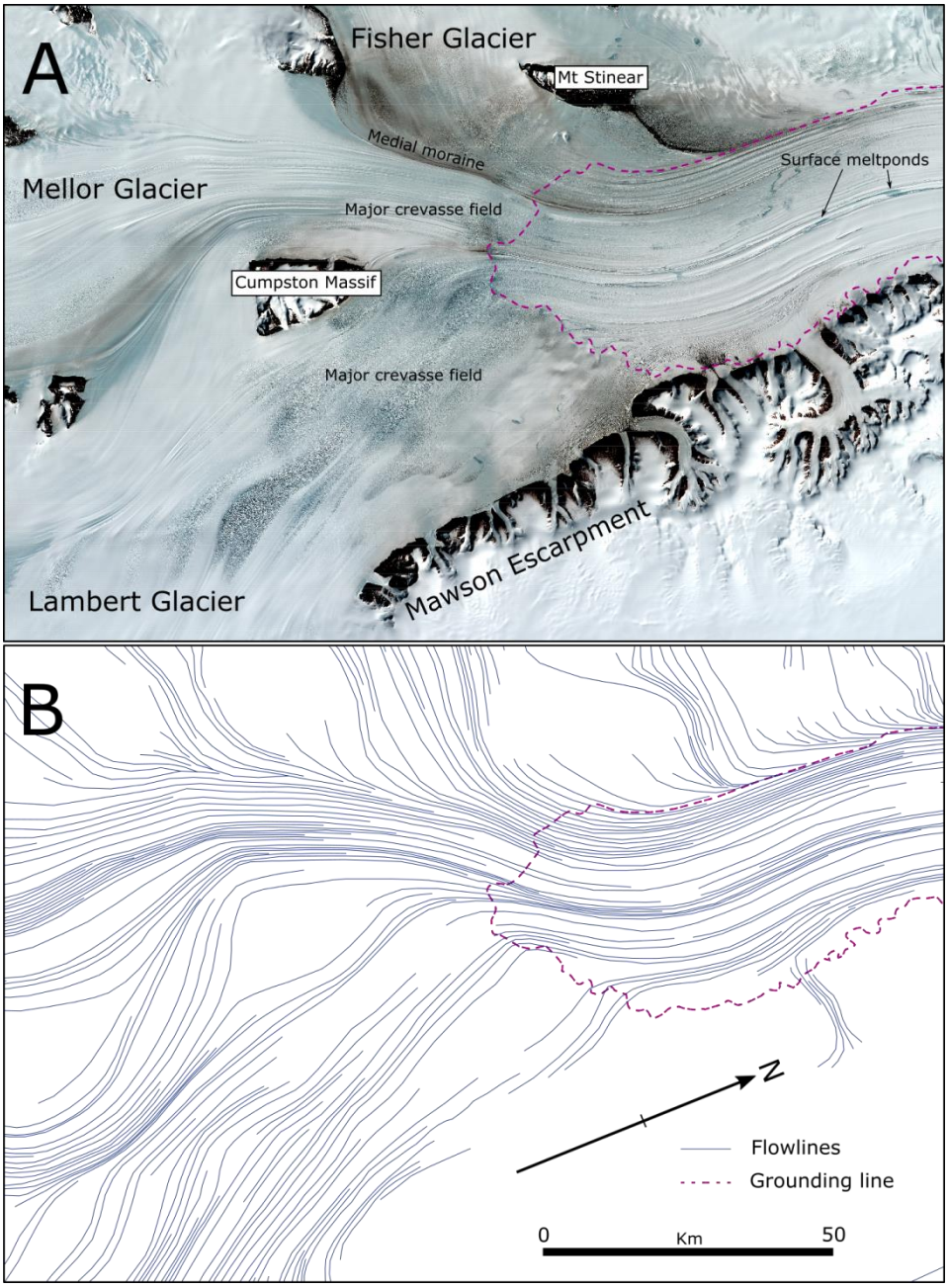

Figure 8.9. The confluence of the Lambert, Mellor, and Fisher Glaciers as they flow into the Lambert Graben: (A) Landsat 7 image; (B) flowline map illustrating their down-glacier persistence despite travelling through blue-ice areas and major crevasse fields. Figure made by the author and published in Glasser et al. (2015).

ice areas). For the smaller-scale Antarctic glaciers investigated in this study (Hatherton and Taylor/Ferrar Glaciers), sublimation keeps the main trunk of the glaciers snow-free, allowing the ice surface to be seen (Figure 8.3). This is also the case for sections of larger ice streams (*e.g.* Byrd Glacier and the Lambert Glacier system). In all of the

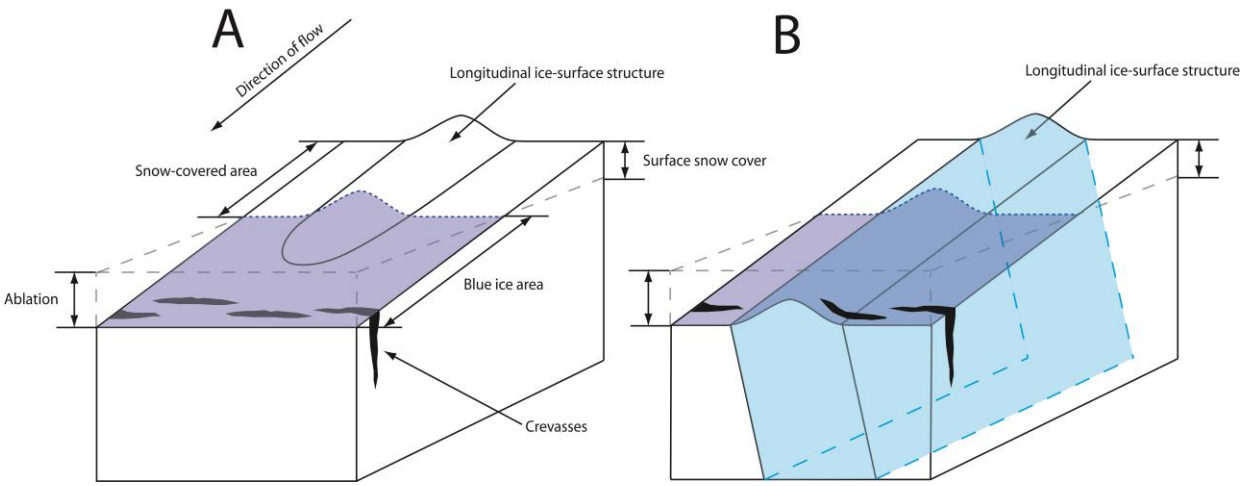

Figure 8.10. Conceptual diagram illustrating the expected down-glacier changes in (A) a two-dimensional and (B) a three-dimensional structure when passing through a blue-ice area. Note that a two-dimensional feature would meltout when advected through an area of net ablation, whereas a three-dimensional structure could survive. Figure made by the author and published in Glasser et al. (2015).

above cases, flowlines can be traced through crevassed areas and through areas of surface ablation (Figure 8.9). Gudmundsson et al. (1998) hypothesised that flowlines are the surface expression of bed topography that is transmitted to the surface of the ice sheet in areas of rapid basal sliding. This hypothesis states that flowlines are surface-only features (two-dimensional features) that manifest as ice-surface lineations. In this case the ice surrounding and underlying the flowline would consist of the same ice facies as of that comprising the surface lineation. However, as flowlines have been observed persisting through extensive blue-ice areas (*e.g.* the middle-reaches of the Lambert Glacier system), it is unlikely that a two-dimensional surface features would be able to persist for such long distances while experiencing extensive ablation and surface lowering (Figure 8.10). Furthermore, this hypothesis is unable to explain the formation of flowlines in the lee of nunataks. These observations suggest that this hypothesis is unlikely to be correct, and further indicates that flowlines are not two-dimensional surface structures, but are three-dimensional features that can persist through areas of ablation, despite substantial surface lowering (Figure 8.10) (Glasser et al., 2015).

8.3.3 Flowline formation along flow unit boundaries

Flowlines develop in many geographical settings and the locations in which they form can be generalised into three basic situations:

i. Formation in the interior of the ice sheet at the boundary between areas of ice experiencing differential flow.

ii. Formation at the boundary between fast-flowing ice and slow-flowing ice, usually found at the lateral margins of ice streams.

iii. Formation in the lee of nunataks where two tributary glaciers coalesce.

The remaining flowline formation hypotheses, as summarised by Glasser et al. (2015), consider flowlines to be three-dimensional structures that form as a result of simple shear. Simple shear develops in all the above scenarios at the boundary between neighbouring parcels of ice travelling at different velocities or where they coalesce. As the tributaries or zones of ice with different ice flow velocities can be considered mutually exclusive before they coalesce, they can be defined as separate flow units, as is the case in small valley glaciers (*e.g.* Hambrey and Milnes, 1977; Hambrey and Müller, 1978; Hambrey and Lawson, 2000; Jennings et al., 2014; 2015). Consequently, flowlines can be defined as features that form and evolve at and along flow unit boundaries. The occurrence of simple shear at flow unit boundaries is well documented in smaller ice masses and has been previously described for many valley glaciers in this study and elsewhere (*e.g.* Hambrey and Milnes, 1977; Hambrey and Müller, 1978; Hambrey et al., 1999, 2005; Goodsell et al., 2005b; Roberson, 2008; Appleby et al., 2010; Jennings et al., 2014, 2015). This study has also demonstrated that flow units exist for a wide range ice masses regardless of scale (*see Chapter Seven*); therefore, it is highly likely that flow in an ice sheet or ice stream is organised into mutually exclusive flow units that coalesce down-glacier. Evidence for this can be

seen on the eastern margin of the Lambert Glacier where comparatively small valley glaciers flow off the Mawson Escarpment and join the main trunk of the Lambert Glacier. Flow units originating from the comparatively small glaciers can be observed becoming flowlines once they join the main trunk of the ice stream (Figure 8.9).

8.3.4 The down-glacier persistence of flowlines

The longevity and down-glacier persistence of flowlines is surprising as they have been traced for distances in excess of a thousand kilometres (Glasser et al., 2015). For this reason, it is important to understand if flowlines actively form along their entire length, or if they only form in their initiation zones. The importance of making this distinction is to be able to make meaningful conclusions about their dynamic significance, especially for inferring past flow dynamics. However, the origin and formation mechanism of flowlines has been highly debated over the past three decades. Raymond (1996) suggested that flowlines represent 'shear zones' within individual flow units; however, Casassa and Brecher (1993) did not find any velocity differences across the boundary of flowlines on Byrd Glacier, and further concluded that simple shear between the flowlines could not explain their down-glacier persistence. In a similar study investigating the incremental strain occurring across a flow unit boundary of two merging tributaries in a smaller valley glacier, Hambrey and Milnes (1977) attempted to reveal the relationship between longitudinal foliation (the structure defining the flow unit boundary) and incremental strain. However, the relationship between the two did not remain constant down-glacier. Once longitudinal foliation developed in the upper reaches of the glacier, the ice subsequently flowed through different stress regimes, with the longitudinal foliation being transported as a passive marker (*e.g.* Lawson, 1996). This finding was further supported by observations from White Glacier (Axel Heiberg Island, Northwest Territories, Canada) where no relationship between longitudinal foliation on the snout of the glacier and localised strain-rate was found (Hambrey and Müller, 1978). Therefore, measurements of incremental strain can only be related to longitudinal foliation where the structure is actively forming. It is possible that this is the case for the formation of flowlines in ice

streams and would explain why Casassa and Brecher (1993) did not find any velocity variations for a lateral profile across flowlines on Byrd Glacier. Conversely, Merry and Whillans (1993) concluded that flowlines form near to their onset zones in localised areas of high shear strain, a finding that has been observed for longitudinal foliation in small valley glaciers in previous studies (*e.g.* Hambrey and Milnes, 1977; Hambrey and Müller, 1978) and in this study. This hypothesis suggests that flowlines are passively transported down-glacier after their initial formation. This to some degree is supported by observations from the now-stagnant Kamb Ice Stream (formerly known as Ice Stream C) (Bindschadler and Vornberger, 1998; Fahnestock et al., 2000; Hulbe and Fahnestock, 2007; Catania et al., 2012; Glasser et al., 2015) and the Bungenstock Ice Rise (Siegert et al., 2013; Glasser et al., 2015). Periodic variations in the discharge from the Siple Coast ice streams into the Ross Ice Shelf have been well documented (Fahnestock et al., 2000; Hulbe and Fahnestock, 2007; Catania et al., 2012). Each of the ice streams have flowline structures; however, the Kamb Ice Stream (Ice Stream C) has strongly distorted flowlines that are folded and are no longer parallel to ice flow (towards the Ross Ice Shelf) (Figure 8.11). Present day ice flow velocity in the Kamb Ice Stream is negligible (Rignot et al., 2011), as the ice stream began to stagnate *c*. 150 years ago (Retzlaff and Bentley, 1993; Jacobel et al., 1996; Engelhardt and Kamb, 2013). Folded surface structures have been interpreted as flowlines inherited from when the ice stream was active that have subsequently become deformed as ice velocities substantially dropped (Fahnestock et al., 2000; Hulbe and Fahnestock, 2007; Catania et al., 2012; Glasser et al., 2015). Therefore, as flowline structures remain visible, despite substantial deformation in a no longer active ice stream, it suggests that flowlines must form further up-glacier and remain as passive markers on the surface of the ice sheet as they travel down-glacier, as opposed to actively forming along the entire length of the flowline (Glasser et al., 2015). An analogy of this process has been observed in surge-type valley glaciers where longitudinal foliation and medial moraines become buckled and folded as a result of the glacier switching between active and quiescent phases (Lawson et al., 1994; Lawson, 1996). It is therefore likely that the flowline structures in the Kamb Ice Stream formed much higher up-glacier and were then passively transported down-glacier when the ice stream was still active, to subsequently become deformed as a result of a switch in flow behaviour. This process

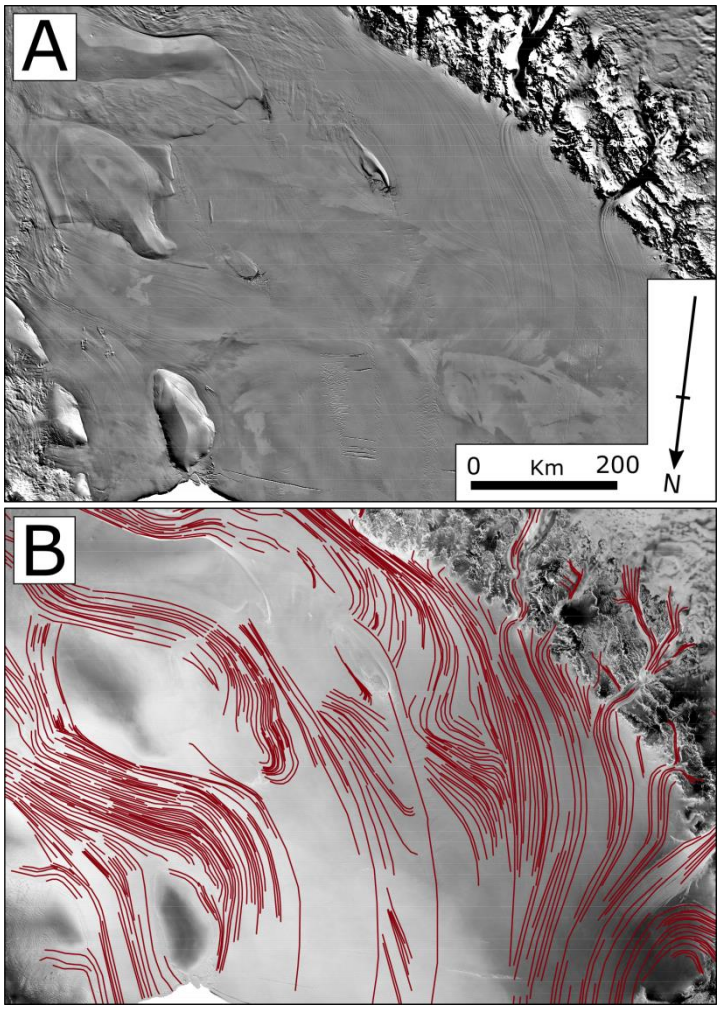

Figure 8.11. Distorted flowlines at the surface of the Kamb Ice Stream: (A) MODIS imagery of the surface of the Kamb Ice Stream; (B) mapped flowlines illustrating their distorted nature. Flowlines mapped by N. F. Glasser.

is similar to surge-type flow observed in smaller ice masses but occurs on much longer timescales (Glasser et al., 2015). Another location that illustrates the longevity of flowlines regardless of current ice flow conditions is on the Bungenstock Ice Rise, located in the Ronne Ice Shelf-Thiel Trough area (Figure 8.12) (Siegert et al., 2013; Glasser et al., 2015). As previously mentioned, ice streams reside in deep subglacial troughs that drain the ice sheet. Siegert et al. (2013) described the large-scale configuration of the Ronne Ice Shelf-Thiel Trough area, noting that flowlines reside in areas of fast flow channelled through deep subglacial troughs. However, even though the Möller and Institute ice streams have flowlines present, the Thiel Trough is predominantly devoid of flowlines despite being a deep subglacial feature (Figure

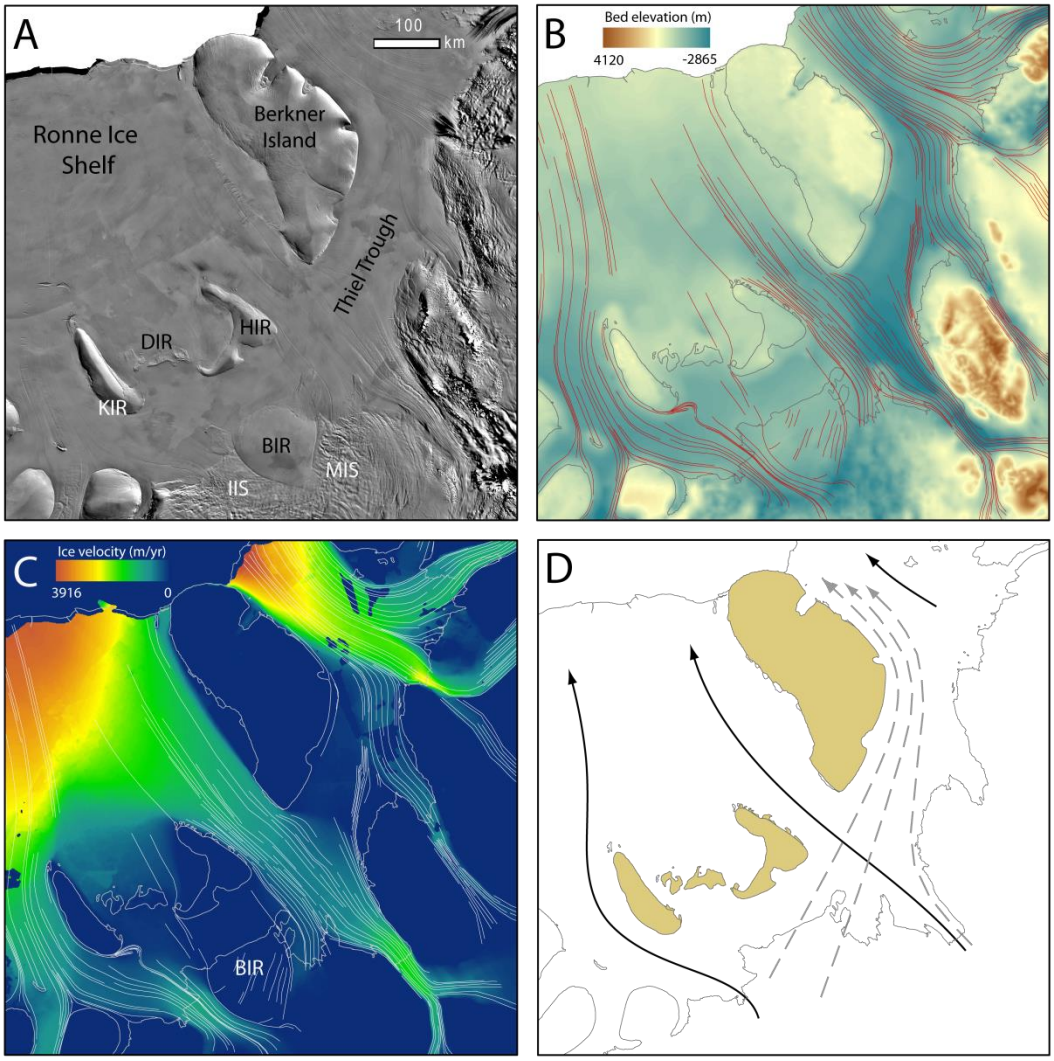

Figure 8.12. Maps of the Ronne Ice Shelf-Thiel Trough area: (A) surface of the ice sheet/ice shelf with location names. HIR: Henry Ice Rise; DIR: Doake Ice Rumples; KIR: Korff Ice Rise; BIR: Bungenstock Ice Rise; IIS: Institute Ice Stream; MIS: Möller Ice stream. (B) Flowlines superimposed on BEDMAP-2 (Fretwell et al., 2013). Note the lack of flowlines in the Thiel Trough and the presence of flowlines in its up-glacier continuation at the Bungenstock Ice Rise. (C) Flowlines superimposed on ice flow velocities from the MEASURES project (Rignot et al., 2011). Inferred ice flow switch from an initial configuration flowing through the Thiel Trough (dashed lines and arrows), followed by contemporary ice flow towards the Ronne Ice Shelf (solid lines and arrows). Figure made by the author and published in Glasser et al. (2015).

8.12). Furthermore, ice flow velocities are comparatively low through the trough, raising questions about how the subglacial trough formed (Figure 8.12). The Bungenstock Ice Rise is the up-stream continuation of the Thiel Trough, and despite also having low ice flow velocities, the ice rise has flowlines orientated parallel to the

Thiel Trough (Figure 8.12). The presence of a deep subglacial trough aligned with flowlines in an area of negligible ice flow suggests that in the past ice flow initially crossed the Bungenstock Ice Rise and drained through the Thiel Trough, before switching towards the Ronne Ice Shelf (Figure 8.12) (Glasser et al., 2015). This conclusion is supported by radar studies conducted by Siegert et al. (2013) who suggested that buckled internal layers in the Bungenstock Ice Rise indicated a significant and recent change in ice flow configuration in the area. The preservation of flowlines on the Bungenstock Ice Rise despite a significant switch in regional ice flow configuration further supports the hypothesis that once formed flowlines are passive markers that get transported down-glacier. Furthermore, the presences of flowlines in areas of negligible flow (*e.g.* the Kamb Ice Stream and the Bungenstock Ice Rise) illustrates that flowlines have great preservation potential as long as there are no active processes over printing them. The comparative lack of deformed flowlines on the Antarctic Ice Sheet further supports the conclusion that the location of major ice streams in Antarctica have remained in the same locations for extended periods of time (at least the residence time for ice travelling the length of the flowlines).

8.3.5 Flowline formation mechanisms

Even though it has been demonstrated that flowlines only form at their onset zones and develop along flow unit boundaries that are experiencing pronounced amounts of simple shear, several hypotheses still remain regarding their formation. The remaining hypotheses concerning the formation of flowlines suggest that they are the surface expression of longitudinal foliation (Reynolds and Hambrey, 1988; Hambrey and Dowdeswell, 1994), or are formed at the boundary between two flow units, reflecting the surface expression of vertical sheets of ice fabrics derived from simple shear (Hulbe and Whillans, 1997; Whillans and Van der Veen, 1997). Each of these hypotheses will be discussed in turn below.

8.3.5.1 Flowlines as macro-scale longitudinal foliation

Longitudinal foliation is well documented in smaller scale ice masses; however, it has received comparatively little attention at ice sheet scale. The hypothesis states that lateral compression and longitudinal extension folds initially horizontal ice layers when flowing from a wide accumulation basin into a comparatively narrow tongue, and that flowlines are the surface expression of this folding, *i.e.* are the surface expression of (i) fold axes where folding is tight; (ii) transposition along fold limbs; (iii) axial planar foliation. This process has been well documented in temperate and polythermal glaciers (*e.g.* Hambrey and Milnes, 1977; Hambrey and Müller, 1978; Hambrey and Glasser, 2003; Goodsell et al., 2005b; Hambrey et al., 2005; Roberson, 2008; Appleby et al., 2010; Jennings et al., 2014, 2015). It is also recognised in valley glaciers that simple shear is important for the development of longitudinal foliation, and that the strongest longitudinal foliation develops at flow unit boundaries were simple shear is inferred to be greatest. Hambrey (1991) and Hambrey and Dowdeswell (1994) both studied the structures of the ablation-dominated middle-reaches of the Lambert Glacier system and concluded that flowlines are indeed a three-dimensional structure that is the surface expression of pervasive longitudinal foliation. Their conclusion was supported by ground observations of longitudinal foliation adjacent to the Fisher Massif (Figure 8.13), a nunatak on the western flank of the glacier system (Glasser et al., 2015). The continuity of longitudinal foliation exposed in blue-ice areas with flowlines in snow-covered areas and on ice shelves up- and down-glacier (Figure 8.9) demonstrates that longitudinal foliation and flowlines are intrinsically related. The formation of flowlines on the leeward side of nunataks also supports the hypothesis that flowlines are the surface expression of a three-dimensional structure that is defined by longitudinal foliation. When tributaries of ice (flow units) that are separated by a nunatak coalesce down-glacier, they develop a three-dimensional suture (often defined by a medial moraine) where the two ice masses merge (Glasser and Gudmundsson, 2012). This process is very similar to the joining of two flow units in a valley glacier that originate in separate accumulations basins, which leads to the formation of a medial moraine at the boundary between the two (Hambrey and

Figure 8.13. Foliation observed at the western margin of the Lambert Glacier-Amery Ice Shelf system adjacent to the Fisher Massif in East Antarctica: (A) oblique aerial photograph showing the surface expression of longitudinal foliation running parallel to a medial moraine; (B) ground photograph showing the near-vertical longitudinal foliation that is visible as a result of differential weathering of contrasting ice facies. Photographs courtesy of M. J. Hambrey and published in Glasser et al. (2015).

Glasser, 2003), a mechanism that has been well documented in this study as well as previous studies. In a similar manner as for small valley glaciers, it is inferred that the zone between two merging tributary glaciers (flow units) would be dominated by simple shear, and as a result would develop strong longitudinal foliation. However, the majority of flowlines form much further into the interior of the Antarctic Ice Sheet with

nunataks primarily confined to a zone around the periphery of the ice sheet and in the Transantarctic Mountains; therefore, a large proportion of flowlines and flow units must develop in a different way. In direct contrast to valley glaciers, the initiation zones of ice streams in the interior of the ice sheet (main accumulation area) are not constrained by topography and therefore are not separated into individual accumulation basins by mountainous terrain. Ice discharging from ice streams is derived from large-scale drainage basins separated by ice divides (Rignot et al., 2011); however, ice divides only determine the large-scale drainage area for each ice stream and do not determine the location of flow units within the area being drained. Individual flow units in the interior of the ice sheet are constrained by slower moving ice, often with velocity differences that are separated by orders of magnitude (Figure 8.2). The most striking example of this can be observed at the lateral margins of ice streams where fast-moving ice abuts against ice with negligible ice flow velocity. At these boundaries there is high shear strain resulting from the pronounced difference in flow unit velocities. Flow units also form in areas dominated by high ice velocities. Fast ice flow is spatially variable and in the interior of the ice sheet forms arborescent networks divided by areas of comparatively slower moving ice. Fast-flowing ice constrained by comparatively slower moving ice acts in a similar way to the constraining headwalls in valley glaciers that divide individual flow units. As a consequence, flow units develop in the interior of the ice sheet, each having different characteristics and flow velocities. When these flow units begin to coalesce down-glacier, shear strain develops at the flow unit boundaries, resulting in the formation of longitudinal foliation. However, the exact formation mechanism for the longitudinal foliation (transposition or axial planar foliation) is currently unknown, but it is likely that a combination of the two processes is active, as has been observed in small temperate and polythermal valley glaciers (*e.g.* Jennings et al., 2014, 2015). The main controls for the spatial variability of ice flow velocities in the interior of the ice sheet are likely to be related to subglacial topography and bed conditions (Glasser et al., 2015).

There is strong evidence to suggest that flowlines are the surface expression of longitudinal foliation. This theory is supported by ground observations and is

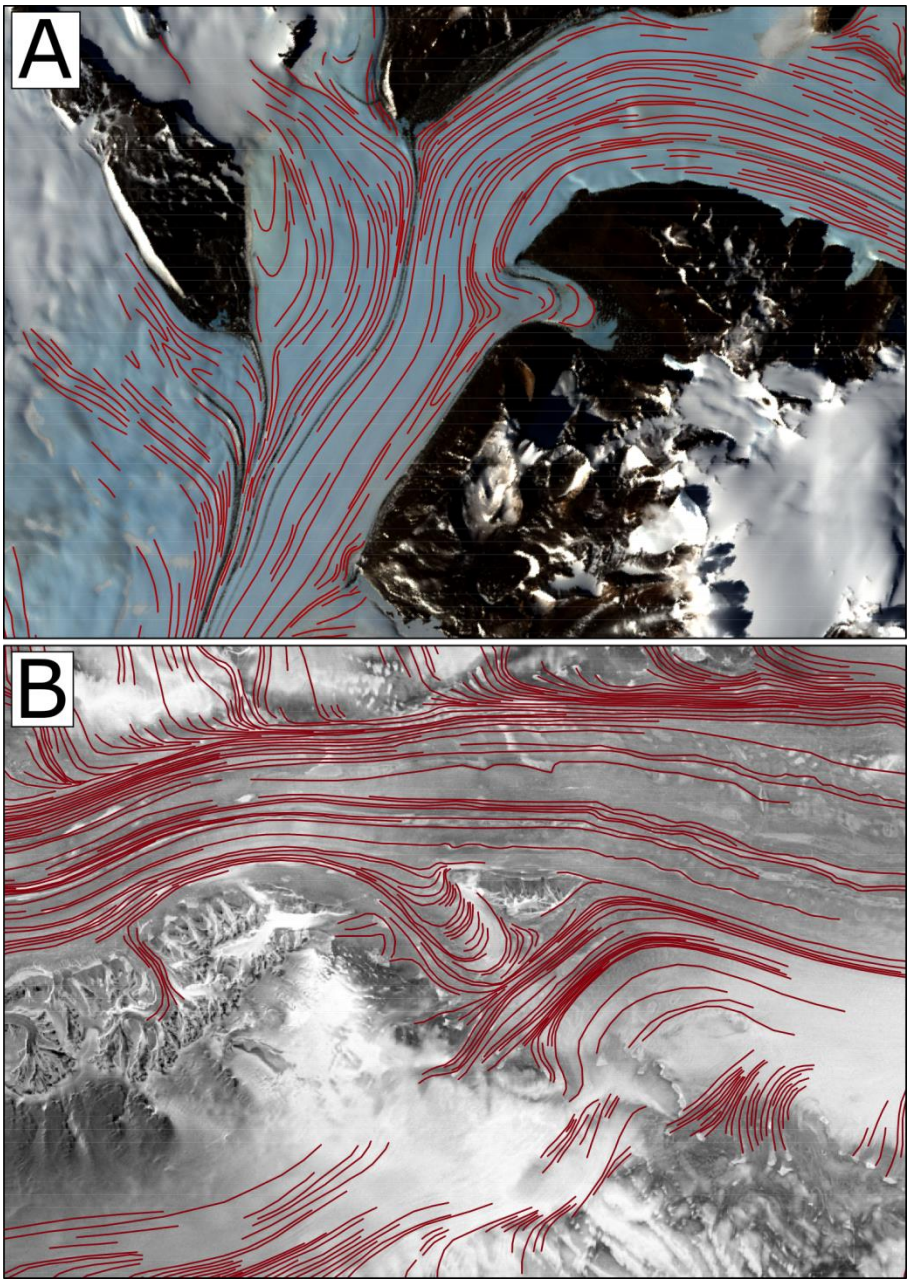

Figure 8.14. Examples of flowlines in an active ice stream and glacier that are not parallel to ice flow direction: (A) Hatherton Glacier with mapped flowlines displayed over a GeoTiff image. Note the flowlines in the centre of the image that are perpendicular to flow when flowing into an embayment. Ice flow from the top of the image to the bottom; (B) Lambert Glacier with mapped flowlines displayed over synthetic aperture radar imagery. Note the flowlines in the centre of the image that are perpendicular to flow. Ice flow direction from the left to the right of the image. Detailed flowline mapping undertaken by the author.

applicable in numerous situations and locations (*i.e.* it adequately describes how flowlines develop in the interior of the ice sheet, as well has how flowlines form in the lee of nunataks). Furthermore, longitudinal foliation has been shown to be an important and widespread structure that is present in ice masses of all scales; therefore, it is probable that it would also be present at ice sheet scale. Despite their name, it has been demonstrated that flowlines do not always remain parallel to flow. In the case of the Kamb Ice Stream, the folding of flowlines is analogous to folding of longitudinal foliation in surge-type valley glaciers when switching from active to quiescent phases. However, there are also examples of flowlines in active ice streams and glaciers that are not parallel to flow (Figure 8.14). In these situations, the non-parallel nature of flowlines with flow direction is analogous to the deformation of longitudinal foliation in valley glaciers when it is passively transported into different stress regimes (*e.g.* as has been observed on the snout of Sermilik Glacier in this study, *see Chapter Seven*). The organisation of strong longitudinal foliation into elongated bands that develop at flow unit boundaries is a characteristic that is common at all glacier scales. However, the identification of longitudinal foliation structures in large-scale ice masses is complicated by the resolution of the satellite imagery used for mapping glaciers of this scale. The relatively coarse resolution of the imagery (≥ 15 metres per pixel) means that areas of strong longitudinal foliation get grouped into thin linear lines (*see Chapter Seven*). This demonstrates geometric self-replication of longitudinal flow structures at varying scales (*i.e.* despite existing at different scales, longitudinal foliation, flow unit boundaries, and flowlines appear geometrically similar) (Figure 8.15).

8.3.5.2 Flowlines as the surface expression of simple shear

Simple shear derived from the merging of two glacier tributaries (flow units) has been suggested as a mechanism for the formation of flowlines. In this case, simple shear derived from differential flow combined with lateral compression would be acting throughout the depth of the ice mass. As a result, realignment of ice crystals develops weak bands of near-vertical ice facies that differ from the surrounding ice (Hulbe and

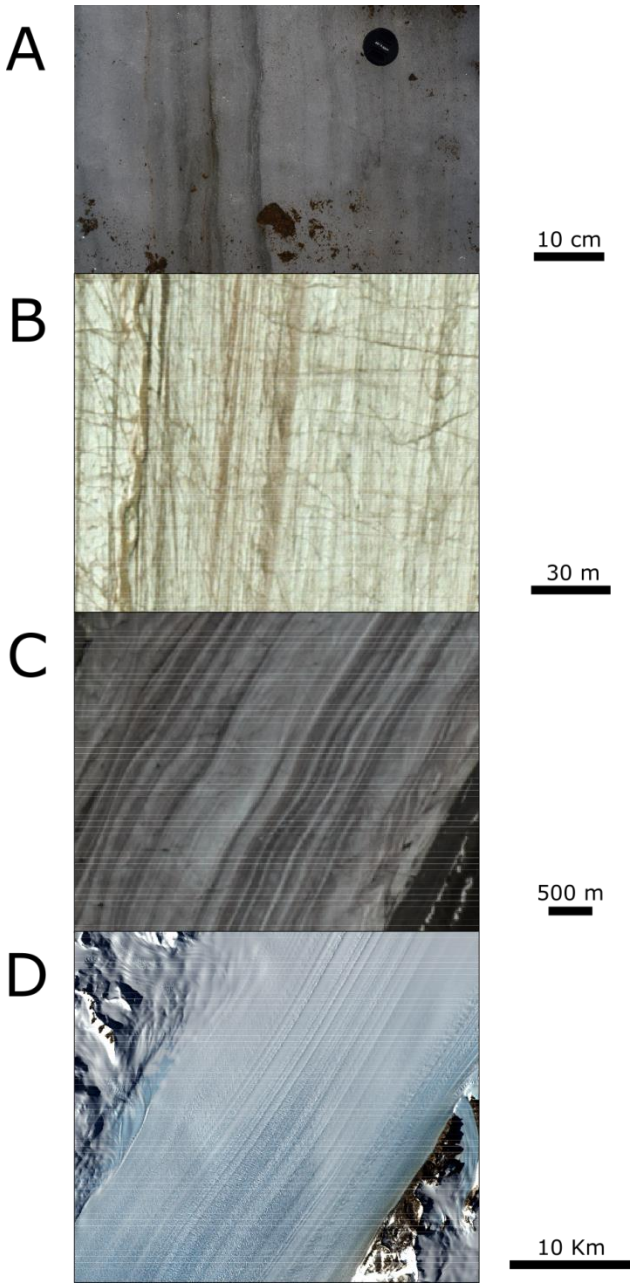

Figure 8.15. Figure illustrating the geometric similarity between longitudinal foliation, flow unit boundaries, and flowlines despite existing at different scales: (A) centimetre to metre scale longitudinal foliation at the surface of Pedersenbreen, Svalbard. Photograph courtesy of M. J. Hambrey; (B) metre to tens of metres scale longitudinal foliation at the surface of Austre Brøggerbreen, Svalbard; (C) tens to hundreds of metres scale flow unit boundaries at the surface of Sermilik Glacier, Bylot Island, Canada; (D) hundreds of metres to kilometres scale flowlines at the surface of Byrd Glacier, Antarctica.

Whillans, 1997). It is therefore expected that these bands of weak ice facies should form where flow units coalesce. It is possible that differential flow between the

merging flow units would cease almost immediately down-glacier; however, differential flow may persist for short distances (Glasser et al., 2015). As previously discussed, it is likely that the structure initially forms before subsequently being transported passively down-glacier. Hulbe and Whillans (1997) studied a section of Whillans Ice Stream (formerly Ice Stream B) and observed deformation in two narrow bands. Hulbe and Whillans (1997) concluded that these narrow bands were areas of

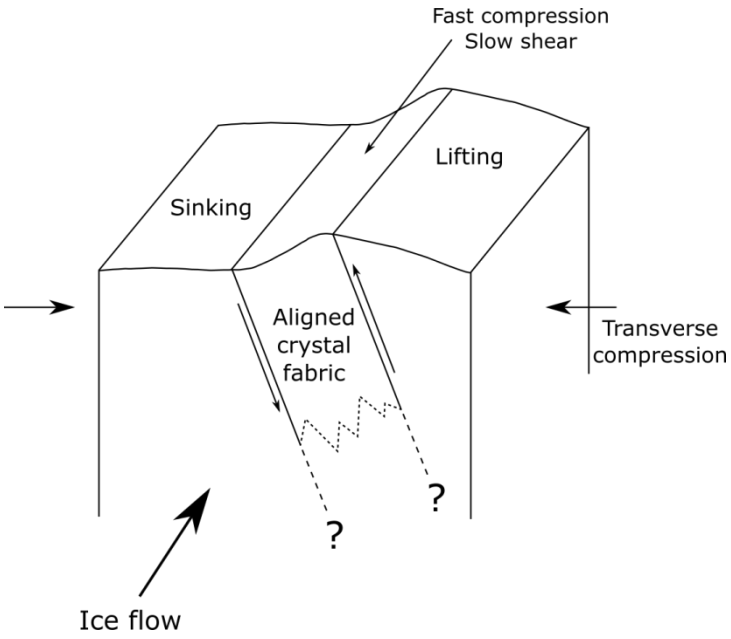

Figure 8.16. Conceptual diagram adapted from Hulbe and Whillans (1997) showing a band of aligned crystal ice facies that acts as a weak layer when experiencing transverse compression. As a result, the compression causes the upper block to rise upwards in comparison to the lower block.

near-vertical weak ice layers that from in response to transverse compression and were also linked to the supraglacial topography of the ice stream. It was proposed that strong transverse compression and slow lateral shearing resulted in blocks of ice moving upward in relation to one-another in a similar fashion as the displacement experienced by lithospheric blocks in a reverse fault (Figure 8.16) (Hulbe and Whillans, 1997). Even though this hypothesis can describe the formation of flowlines in the centre of an ice stream, it does not sufficiently describe the formation of flowlines in the lee of nunataks. Flowlines forming in the lee of nunataks develop instantaneously

when the two flow units coalesce. However, the development of a weak band of ice in the lee of a nunatak would not form instantaneously, but a certain amount of distance down-glacier would be required for the ice crystals to align. This suggests that the alignment of ice crystals in weak bands of ice cannot provided a unified hypothesis for flowline formation in every topographic situation. However, the three-dimensional characteristics of these features lend support to this hypothesis for the formation of flowlines in the interior of the ice sheet. Nevertheless, further detailed field investigations would be needed to ascertain the behaviour of ice crystals at a crystallographic-scale to establish the validity of this hypothesis.

8.4 Summary

i. Flowlines form arborescent networks in the interior of the ice sheet that become focused in comparatively narrow corridors of ice that are preferentially located over deep subglacial troughs in areas of fast-flow ice.

ii. The persistence of flowlines through areas of net ablation (blue-ice areas) and crevasse fields suggests that they are three-dimensional structures as opposed to two-dimensional surface structures.

iii. Flowlines form in three general situations: (i) in the interior of the ice sheet at the boundary between areas of ice experiencing differential flow; (ii) at the lateral margins of ice streams at the boundary between fast and slow moving ice; (iii) in the lee of nunataks at the confluence of tributaries.

iv. The down-glacier persistence of flowlines even in situations where ice flow has stagnated, suggests that flowlines form in their initiation zones and not along the entire length of the flowline (*i.e.* flowlines are passively translated from their initiation zones, and may not be subsequently modified by flow).

v. Flowlines develop in response to simple shear acting along flow unit boundaries.

vi. There is strong evidence to suggest that flowlines are the surface expression of a 'macro-scale' longitudinal foliation, which can explain the formation of flowlines in different topographic situations.

Chapter Nine

Discussion

9.1 Introduction

The aim of this chapter is to provide a general discussion about the formation and evolution of longitudinal foliation in ice masses of various scales. The topics covered are synthesised from the preceding chapters, enabling evidence to be drawn and compared from a wide range of glaciers with contrasting scales, locations, and characteristics. In contrast to the preceding chapters where individual glaciers were analysed and discussed in comparative isolation from one-another, this discussion amalgamates the evidence collected from a range of glaciers that vary in scale and geographical location in an attempt to 'upscale' the field-based structural findings from small valley glaciers to much larger ice masses. Thus deductions can be made about the structural composition of large-scale glaciers that are usually impractical for structural field studies as a consequence of their size or remote location. This chapter also aims to discuss the various testable hypotheses that have been identified in this study (explained in relation to the 'Specific objectives of this thesis' in *section 2.7* and summarised in italics in the relevant sections below).

9.2 Origin of foliation in valley glaciers

Hypothesis: Flow units are mutually exclusive with regard to the structures present, and that each flow unit evolves in a unique manner, as proposed by the author from investigations on a Swiss Alpine glacier (Jennings et al., 2014).

The existence of transposition- and axial planar foliation has been well documented in both alpine and Arctic valley glaciers (*e.g.* Allen et al., 1960; Lawson, 1990; Pfeffer, 1992; Lawson et al., 1994; Hambrey et al., 1999, 2005; Hambrey and Glasser, 2003; Goodsell et al., 2005a, b; Roberson, 2008; Appleby et al., 2010; Jennings et al., 2014, 2015). It has been suggested that the formation of these two types of longitudinal foliation is spatially variable, and depends on the characteristics of individual flow units and the deviatoric stresses present (Jennings et al., 2014). It has been demonstrated in this study as well as in previous studies that the strongest longitudinal foliation is preferentially located at flow unit boundaries. Evidence for this can be seen in the structural maps, three-dimensional measurements, and ice facies logs produced for the small-scale valley glaciers investigated in this study (Austre Brøggerbreen, Midtre Lovénbreen, Austre Lovénbreen, and Pedersenbreen, *see Chapters Five and Six*). Furthermore, it is evident from structural mapping of the small-scale valley glaciers in this study, that strong and steeply dipping longitudinal foliation develops in bands at flow unit boundaries (Figures 5.1, 6.1, 6.7, and 6.10). It has previously been inferred that the occurrence of strong longitudinal foliation at flow unit boundaries is the result of simple shear (*i.e.* simple shear created at the boundary between two merging flow units that are experiencing differential flow). However, studies that have taken velocity measurements across a flow unit boundary have struggled to provide evidence for this theory (*see* Hambrey et al., 1980; Hambrey and Lawson, 2000). The structural mapping of Austre Brøggerbreen not only demonstrates that flow units are unique, reflecting the characteristics of their corresponding accumulation basins, but also illustrates the presence of simple shear that is spatially variable within the glacier. The down-glacier evolution of transverse fracture sets contained in different flow units provided evidence that flow units not only experience differential flow in comparison with

neighbouring flow units, but also differential flow within individual flow unit systems. This is especially evident on Austre Brøggerbreen in Flow Units 2a, 4, and 5b where initially transverse suites of crevasse traces undergo unique and contrasting down-glacier evolutions (Figure 5.1). In Flow Unit 4 the transverse fractures become increasingly arcuate down-glacier, indicating that ice velocity is greatest in the centre of the flow unit and slower at the lateral margins. In contrast, the transverse fractures in Flow Units 2a and 5b remain comparatively linear features but become rotated down-glacier. Fractures in Flow Unit 2a rotate in a clockwise direction while fractures in Flow Unit 5b rotate in an anticlockwise direction, suggesting that ice flow is fastest on the true-left and true-right of each flow unit respectively (Jennings et al., 2015). It is generally expected that the fastest ice flow velocities found in a glacier are located along the centreline of the glacier tongue, away from the drag created at the lateral margins of the glacier or the glacier bed; however, the ductile deformation of structures in Austre Brøggerbreen demonstrates that this is not the case. The reorientation of fractures in Flow Units 2a and 5b highlights that ice flow velocities along the centre line of the glacier tongue are slower than ice flow velocities found towards both lateral margins. This conclusion is supported by the geometry of the glacier. Flow units on the true-left and true-right of the glacier have much larger accumulation basins feeding them than the flow units forming the centre of the glacier; therefore, the driving stresses on the true-left and true-right of the glacier are much greater than in the centre of the glacier. Consequently, ice flow velocities are greater away from the centre line of the glacier tongue. The reorientation of these fracture sets not only demonstrates that ice flow velocities are non-uniform across the breadth of the glacier, but also illustrates the differences between individual flow units within the same ice mass. The characteristics and dominance of individual flow units within the whole-glacier system is dictated by the size and characteristics of their corresponding accumulation basin, and not necessarily by the location of the flow unit within the whole-glacier system. Furthermore, ice flow within the main glacier trunk (when all the constituent flow units have merged) may not be as homogeneous as previously assumed, resulting in the formation of simple shear at flow unit boundaries that subsequently leads to the development of strong longitudinal foliation.

9.3 Role of foliation in debris entrainment

The entrainment, transportation, and subsequent deposition of debris within a glacier system is a topic that has received a large amount of attention. Since the late 1960s, it has been widely recognised that both high- and low-level debris-entrainment processes play an important role in dictating the characteristics of glacial sediments (*e.g.* Boulton, 1967, 1970, 1978; Eyles and Rogerson, 1978; Small et al., 1979; Sollid et al., 1994). However, until recently the influence that ice structure has on debris entrainment and transport has received comparatively little attention (Hambrey and Lawson, 2000). Recent research has focused on the structural controls of debris transport in high-Arctic polythermal and cold-based glaciers, which has highlighted the importance of folding, foliation, and thrusting for debris transport in these types of glacier (*e.g.* Bennett et al., 1996; Hambrey et al., 1996, 1999, 2005; Boulton et al., 1999; Hambrey and Glasser, 2003; Hubbard et al., 2004). More recent studies have also applied these techniques to address the structural controls on debris transport in temperate valley glaciers (*e.g.* Eyles and Rogerson, 1978; Goodsell et al., 2005a, b; Roberson, 2008; Appleby et al., 2010; Jennings et al., 2014). From all of these studies, a complex image has emerged of how structure influences debris in ice masses and to what degree structure acts as a control. For example, Jennings et al. (2014) found no correlation between ice structure and major debris entrainment for a temperate alpine valley glacier, whereas the majority of studies conducted in Svalbard on polythermal and cold-based glaciers have highlighted the importance of folding and foliation for debris entrainment (Bennett et al., 1996; Hambrey et al., 1996, 1999, 2005; Boulton et al., 1999; Hambrey and Glasser, 2003; Hubbard et al., 2004). The main types of debris entrainment involving ice deformation, as summarised by Hambrey et al. (1999), are:

i. Debris entrainment at the base of a glacier.

ii. The incorporation of rockfall debris at the surface of the glacier within primary stratification.

iii. The incorporation of supraglacial and basal debris within longitudinal foliation.

iv. The incorporation of basal debris by thrusting.

v. The incorporation of basal debris as a result of recumbent folding.

vi. The ingestion of supraglacial debris, and possibly basal debris, by crevasses.

As this study is primarily concerned with longitudinal foliation, the main modes of debris entrainment that are related to foliation formation and evolution are discussed below. The two main modes of foliation-related debris entrainment have been identified by previous studies in Svalbard polythermal and cold-based glaciers are:

i. Folding and reorientation of angular rockfall debris that becomes incorporated and entrained at the surface of the glacier by the stratified sequence of snow, firn, and superimposed ice as it undergoes diagenesis into glacier ice. As the debris becomes buried and subsequently transported through an englacial pathway, the flow of ice from a broad accumulation area into a comparatively narrow tongue folds the initially horizontal primary stratification (the stratified sequence of glacier ice that has enveloped the rockfall debris) (Hambrey et al., 1999). Folding is most intense at the lateral margins of the glacier and at flow unit boundaries, coinciding with areas of high cumulative shear strain that is often associated with axial planar foliation (Hambrey et al., 1999, 2005; Hambrey and Glasser, 2003; Jennings et al., 2015), which concentrates englacial debris at these localities. Ablation and surface-lowering further down-glacier re-exposes the debris at the surface of the glacier, often

forming flow-parallel lines of debris that represent the hinges of folds (Hambrey and Lawson, 2000).

ii. The incorporation of both supraglacial and basally derived debris within longitudinal foliation. The entrainment of debris at the base of a glacier has long been recognised as an important mechanism for sediment transport in glacier systems, with several pioneering studies having been conducted on Svalbard valley glaciers (Garwood and Gregory, 1898; Boulton, 1967, 1970). Subsequent research has identified a complex array of ice and debris facies that can be found in the basal ice layers of temperate and polythermal glaciers (Hubbard and Sharp, 1989; Knight, 1997; Lawson et al., 1998; Hubbard et al., 2009). The structural complexity of the basal zone has received comparatively little attention; however, one notable exception is a study examining the fjord-terminating cliff of the surge-type glacier Tunabreen in Svalbard (Fleming et al., 2013). Intense folding that is focused at flow unit boundaries and at the glacier lateral margins elevates basal ice facies through the ice mass, which subsequently becomes exposed at the surface of the glacier by ablation and surface lowering. Basal ice that has been elevated into an englacial position can also be revealed near to the snout of the glacier where it also becomes exposed by ablation. The mechanism by which debris contained within strong longitudinal foliation becoming exposed at the surface of a glacier is similar to that explained above for the incorporation of rockfall debris. However, in this case, entrainment processes acting at the glacier bed involving both the basal ice zone and the underlying deformable bed material dictate the amount and type of debris that is entrained (Hambrey et al., 1999). Building from these earlier conclusions, Hambrey and Glasser (2003) developed their model of medial moraine genesis as a result of folding and foliation development.

It is worth noting that several other hypotheses and conceptual models for debris entrainment and medial moraine formation have been suggested for glaciers in other regions. Each of these models is capable of explaining the entrainment of debris that subsequently re-emerges at the surface of the glacier, and each is briefly discussed below.

It has been suggested that medial moraines can form in the ablation areas of glaciers as debris from medial debris septa becomes exposed and accumulates at the surface of the glacier as a result of ablation and surface-lowering. Several mechanisms have been suggested for the initial formation of debris septa depending on the origin of the debris. Debris-rich basal ice that is initially parallel to the bed of the glacier can be elevated from the bed by ice flow around bedrock obstructions or at the confluence of flow units to form a debris septum (Boulton, 1978; Eyles and Rogerson, 1978; Boulton and Eyles, 1979; Vere and Benn, 1989). Even though a debris septum formed by a bedrock obstruction or by the confluence of flow units in the accumulation area of a glacier may not extend to the surface of the glacier, it can subsequently be revealed by ablation. However, debris septa formed by the confluence of flow units in the ablation area will usually extend from the glacier bed to the surface (Benn and Evans, 2010). Alternatively, medial moraines can form down-glacier of persistent sources of supraglacial debris that are transported down-glacier along the same flow-pathway (Small et al., 1979; Gomez and Small, 1985; Small, 1987). In contrast to debris septa that are derived from debris-rich basal ice that are usually contained in sharply defined bands (Vere and Benn, 1989), this type of debris septa is not necessarily sharply defined and may consist of several individual debris bands that group together (Gomez and Small, 1985; Small, 1987).

Numerous medial moraines are present on the surface of Austre Brøggerbreen, all of which have unique characteristics depending on their location and origin (*e.g.* debris content, height, length, width, initiation point, persistence). The sediment-laden ice facies found at the boundary between Flow Units 5a and 5b on Austre Brøggerbreen is interpreted as clotted ice. Clotted ice consists of clear, bubble-free ice that contains 'clots' of sediment dispersed through the ice facies. The preferential entrainment of fine-grained sediment suggests that clotted ice originates from the

freezing of turbid water, either as supercooled slity water freezes, or as turbid water undergoing bulk freezing (Knight, 1994; Christofferssen et al., 2006; Benn and Evans, 2010). Regardless of the exact process, the wide-spread freezing of sediment-rich water can only occur at the glacier bed, suggesting that clotted ice has a basal origin. Therefore, a mechanism by which sediment-rich basal ice can be elevated through the ice mass must be occurring. The clotted ice facies found at the surface of Austre Brøggerbreen coincides with an area of strong longitudinal foliation associated with the boundary between Flow Units 5a and 5b. Sediment-rich ice facies that initially form parallel to the glacier bed can be re-orientated and elevated through the ice mass as a debris septum to eventually become exposed at the surface of the glacier by ablation (Boulton, 1978; Eyles and Rogerson, 1978; Boulton and Eyles, 1979; Vere and Benn, 1989). However, this mechanism does not explain the presence of strong longitudinal foliation that is associated with the clotted ice facies. It is therefore more likely that basal ice facies are elevated through Austre Brøggerbreen as a result of folding and longitudinal foliation development at flow unit boundaries, as suggested by Hambrey and Glasser (2003). This model sufficiently explains how sediment-rich ice becomes exposed at the surface of the glacier as well as the development of the associated longitudinal foliation.

The findings of this study agree with the majority of previous studies that have been conducted on Svalbard polythermal glaciers (*e.g.* Bennett et al., 1996; Hambrey et al., 1996, 1999, 2005; Boulton et al., 1999; Hambrey and Glasser, 2003; Hubbard et al., 2004) that suggest englacial and subglacial debris can be elevated to the surface of glaciers by folding and longitudinal foliation formation. However, the application of this debris entrainment and medial moraine formation hypothesis to different types of glacier (*e.g.* temperate glaciers) is slightly more problematic. Even though studies in the European Alps have identified medial moraines that form or are influenced by folding and longitudinal foliation development (*e.g.* Goodsell et al., 2005a, b; Roberson, 2008; Jennings et al., 2014), the incorporation of basal ice facies into the body of the glacier has been questioned by Jennings et al. (2014). The latter authors concluded that the folding of sediment-rich basal ice facies, and therefore the entrainment of basal sediments, into an englacial position is highly dependent on basal

melting rates in temperate valley glaciers. Regardless of this, the wide-spread nature of longitudinal foliation structures in ice masses of all scales suggests that foliation-related debris entrainment may be an important mechanism for debris input into glaciers.

9.4 Significance of fractures

Hypothesis: Longitudinal foliation evolves either through the process of transposition from earlier layering (stratification or crevasse traces) or as an axial planar structure related to folding with flow-parallel axes (Hambrey and Lawson, 2000; Hambrey and Glasser, 2003).

Structural mapping of the small Svalbard valley glaciers in this study has revealed that widespread fracturing is common in all the glaciers. This is especially evident on Austre Brøggerbreen where closed fractures (crevasse traces) originate high in the accumulation area and persist to the terminus (Figure 5.1). All the flow units on Austre Brøggerbreen are dominated by suites of fractures, and the persistence of fractures to the terminus despite undergoing substantial ablation and surface-lowering suggests that they penetrate to great depths, possibly reaching the bed (Hambrey and Müller, 1978; Jennings et al., 2014). Crevasse traces form in a similar manner to open crevasses, developing perpendicular to the direction of maximum tensile stress, and are usually characterised by thin clear ice layers that have crystals orientated normal to the fracture. They may form as continuations of open crevasses, or form as independent structures that are analogous to tensional veins in rocks (Hambrey and Lawson, 2000; Jennings et al., 2015). The comparative lack of open crevasses and high proportion of crevasse traces suggests that the latter process is most likely to be the process of formation for the majority of fractures in Austre Brøggerbreen. However, regardless of the exact process, the existence of abundant fractures in a relatively inactive glacier suggests that the fracture sets are relict features that formed when the glacier was much more active, probably during its last advance in the Neoglacial (*c.*

1900) (Jennings et al., 2015). The inferences that can be made from the presence of the fractures in Austre Brøggerbreen are not just confined to their initial formation (*i.e.* process of formation, depth of fracture propagation), but can also inform us about subsequent ice flow within the glacier. Post-formation ductile deformation of fractures allows the ice flow conditions to be inferred for the whole-glacier system as well as for individual flow units, enabling the differences between flow units to be deduced (*see section 5.2*).

A new fracture-derived longitudinal foliation that has not previously been described for any other glacier was identified on Austre Brøggerbreen (Jennings et al., 2015). The high concentration of closed fractures (crevasse traces) present at the surface of the glacier that subsequently underwent ductile modification enabled the formation of the new fracture-derived foliation. An analogy of fracture-derived longitudinal foliation is fracture-derived transverse foliation (also known as arcuate foliation) that is commonly found in valley glaciers. Transverse foliation develops below ice falls as transverse crevasse traces pass in to a longitudinally compressive stress regime, which amplifies the layering in a visually similar manner akin to sets of nested spoons (Allen et al., 1960; Ragan, 1969; Hambrey and Milnes, 1977; Lawson, 1996; Hambrey and Lawson, 2000). In contrast to longitudinal foliation, transverse foliation develops in a pure shear regime where the foliation forms normal to the maximum compressive strain-rate. As a consequence, the amount of cumulative strain required to form strong transverse foliation is much less than that necessary to form strong longitudinal foliation (Hambrey and Milnes, 1977; Hambrey et al., 1980). Conversely, the fracture-derived longitudinal foliation observed on Austre Brøggerbreen does not form at the base of an ice fall; however, it does develop from initially transverse fractures that have formed in the accumulation area of the glacier. Ductile modification of transverse fractures, especially in strong simple shear stress regimes that are usually found near to flow unit boundaries, re-orientates the fractures into a longitudinal orientation. This is particularly evident on Austre Brøggerbreen in Flow Unit 4 where initially transverse fractures become increasingly arcuate down-glacier (Figure 5.1). As the centre of the flow unit experiences pure shear, resulting in the increasingly arcuate modification of fractures down-glacier, the

lateral margins of the flow unit experience simple shear, rotating the limbs of the now arcuate fractures into longitudinal orientations. The importance of understanding the formation of fracture-derived longitudinal foliation is to aid the inference of past glacier dynamics. In much the same way that the initial formation of the fractures in Austre Brøggerbreen suggests that the glacier was once much more dynamic, probably during the glacier's last advance during the Neoglacial, subsequent ductile deformation and development of a fracture-derived longitudinal foliation can inform us about glacier dynamics since Neoglacial time. As the original geometry of the fractures can be observed (*i.e.* the fractures initially form as transverse crevasse traces in the upper accumulation area) and because the fractures act as passive markers once they have been formed, it is possible to deduce the ice flow dynamics and stress regimes present in individual flow units by observing the change in fracture orientation and shape.

In Midtre Lovénbreen, there is evidence to suggest that fractures are important features for debris entrainment. Sediment-rich ice found at the surface of the glacier seems to originate in longitudinal fractures located on the true-left margin of the glacier. The characteristics of the sediment suggest a basal origin, which implies that the fractures must propagate to the bed of the glacier to enable sufficient amounts of basal sediments to be entrained. Furthermore, the exclusive entrainment of fine-grained sediment suggests that the mechanism for sediment entrainment is from the refreezing of sediment-rich water at the glacier bed. Interestingly, the sediment laden longitudinal fractures found in Midtre Lovénbreen originate from the rotation of transverse fractures found further up-glacier; therefore, these structures appear to be geometrically similar to the fracture-derived longitudinal foliation that has been described for Austre Brøggerbreen. If this is the case, it raises questions about the entrainment potential of fracture-derived longitudinal foliation. The persistence of fractures in Austre Brøggerbreen, which survive from the accumulation area to the snout of the glacier despite undergoing substantial ablation and surface lowering, suggests that they penetrate to great depths, possibly reaching the bed. Also, fine-grained sediment exposed at the surface of Austre Brøggerbreen suggests that sediment-rich water has in the past refrozen to the bed of the glacier. These two factors imply that entrainment of debris at the base of Austre Brøggerbreen by

fracture-derived longitudinal foliation may be an important entrainment mechanism that has yet to be revealed at the surface of the glacier.

The dominance of fractures in the Svalbard valley glaciers investigated in this study is surprising considering the current relative inactivity of the glaciers. It is therefore inferred that the majority of fractures present are relict fracture sets originating from when the glaciers were much more extensive and active during the Neoglacial. However, an exception to the assumption that the majority of fractures on a Svalbard valley glacier date back to the Neoglacial is when a glacier surges. Svalbard has a comparatively high proportion of surge-type glaciers in comparison with other glacierised environments in the world (Sevestre and Benn, 2015; Sevestre et al., 2015), with estimated percentages of Svalbard surge-type glaciers ranging from 13% to 90% (Hagen et al., 1993; Jiskoot et al., 2000). The only known surge-type glacier investigated in this study is Pedersenbreen, where it has been shown by previous studies that Flow Unit 1 has surged into the main trunk of the glacier on several occasions in the past (Bennett et al., 1998; Glasser et al., 2004). Several previous studies have stated that it is possible to identify surge-type glaciers from their structural features such as looped medial moraines which are characteristic of pulses of faster-moving ice flowing into surrounding slower-moving ice (Meier and Post, 1969; Dowdeswell and Williams, 1997). Heavy surface crevassing during the active phase of a surge is also a common structural phenomenon; however, crevassing alone is not a definitive sign of surge-type activity (Lawson et al., 1994; Lawson, 1996). Nevertheless, the high proportion of surface fractures on glaciers such as Austre Brøggerbreen, especially when the fractures are ubiquitous across the entire surface of the glacier, indicates that ice flow velocities were once substantially higher than at present. As there is such a high concentration of surge-type glaciers in Svalbard (Hagen et al., 1993; Jiskoot et al., 2000; Sevestre and Benn, 2015; Sevestre et al., 2015), it raises the question if it is possible for a glacier to have surged in the past, yet not leave any characteristic structural signs that indicate former surge-type behaviour. This notion is supported by the observed surge of Comforlessbreen that is located to the south-east of Austre Brøggerbreen. Even though Comfortlessbreen was originally suspected of being a surge-type glacier by Croot (1988), no traditionally accepted signs

of former surge-type behaviour were evident (King et al., 2015). The lack of surge behaviour indicators led Jiskoot et al. (2000) to remove Comfortlessbreen from earlier lists of known or suspected surge-type glaciers, before the glacier's most recent surge between 2002 and 2009 (King et al., 2015). Therefore, it is possible that the highly fractured nature of glaciers such as Austre Brøggerbreen may be attributed to former surge-type behaviour that left no other structural signs. However, the lack of any other evidence, combined with the current inactivity of the glacier makes it highly unlikely that the glacier now has the ability to surge, making proving or disproving this hypothesis improbable. Furthermore, in the case of Pedersenbreen and Comfortlessbreen (prior to its most recent surge), which are both known to be surge-type glaciers, few fractures were present on the surface of either glacier (Figure 6.10) (*see section 6.4.4.1* and King et al., 2015). As a high degree of surface-fracturing is associated with the active-phase of surging, the lack of fractures suggests that fracture propagation depths were probably relatively shallow, meaning that ablation and pronounced surface-lowering could melt-out the surge-related fractures. As it has been demonstrated that the fractures in Austre Brøggerbreen propagate to great depths and possibly even reach the bed of the glacier (Jennings et al., 2015), this may suggest that the formation of the fractures in Austre Brøggerbreen are in fact not surge-related.

9.5 Impact of surging on glacier structure

Even though surge-type glaciers have been extensively studied in numerous locations around the world, the structural characteristics of surge-type glaciers have received comparatively little attention. In a unique study, the formation and evolution of foliation in a surge-type glacier was investigated on Variegated Glacier by Lawson et al. (1994) and Lawson (1996). More recently, Svalbard surge-type glaciers have been receiving increasing amounts of attention, especially with regard the glacier structure (*e.g.* Hambrey and Dowdeswell, 1997; Fleming et al., 2013; King et al., 2015; Lovell et al., 2015). These studies have revealed a complex array of structures and a variety of structural assemblages that are associated with surge-type glaciers. However, it has

also been demonstrated on Variegated Glacier in Alaska (*see* Lawson et al., 1994, Lawson, 1996; Sharp et al., 1994) and on Hessbreen in Svalbard (*see* Hambrey and Dowdeswell, 1997) that distinct suites of structures could be identified as either quiescent-phase or surge-phase structures. The conclusion of these studies suggested that structures formed during the quiescent-phase predominantly consisted of ductile structures, whereas structures formed during the surge-phase mainly comprised brittle structures (Lawson et al., 1994, Lawson, 1996; Sharp et al., 1994; Hambrey and Dowdeswell, 1997). Therefore, by identifying unique suites of ductile and brittle structures, it has been possible to deduce a quiescent- and surge-phase chronology for both Variegated Glacier and Hessbreen. However, even though Variegated Glacier is characterised by short-lived surge-phases separated by decade-long quiescent-phases, it has been demonstrated that the very large cumulative strains accumulated over many surge cycles can be over-printed by subsequent background strain-rates (Lawson et al., 2000). In other words, for surge-type glaciers with complex strain-rate histories, the structural effects of major deformational events (surge-phases) can be 'undone' by subsequent quiescent phase deformation (Lawson et al., 2000).

In contrast to the surge-type glaciers discussed above, Pedersenbreen did not surge in its entirety, but had an individual flow unit (Flow Unit 1) surge into the main trunk of the glacier. As a consequence, the glacier-wide structure of Pedersenbreen is not dominated by surge-phase related structures. The main surge-phase-related structures are contained within Flow Unit 1, whereas the remaining flow units have structural assemblages similar to other non-surge-type polythermal glaciers found in Svalbard (Figure 6.10). When regarding the structural assemblage of Flow Unit 1, it is not possible to conclusively say if the flow unit's surge-phase-related structures are becoming over-printed by subsequent quiescent-phase ductile deformation as suggested by Lawson et al. (2000). However, the subdued nature of the surge-related structures contained within the flow unit at present (*e.g.* the lack of surface-fracturing still evident), combined with the length of time since the last surge phase (prior to 1966, *see* Glasser et al., 2004), means that it is probable that ductile deformation within the flow unit is over-printing any structures developed during its last surge. Unlike Variegated Glacier and Hessbreen, as only one flow unit (Flow Unit 1) surged

into the main trunk of Pedersenbreen, structures that formed along the boundary between Flow Unit 1 and 2a did so at the boundary between a surging ice mass and a non-surging ice mass. As the two flow units were experiencing substantially differential ice flow velocities, the interaction between the two flow units resulted in enhanced amounts of simple shear at the flow unit boundary. The structural evidence for increased amounts of simple shear can be seen at the flow unit boundary as strong longitudinal foliation. Even though the initiation of brittle fractures or the reactivation of pre-existing fractures may have occurred in response to strong differential flow between Flow Units 1 and 2a (as would be expected during a surge-phase), strong longitudinal foliation suggests that ductile deformation also played an important role.

9.6 The occurrence of foliation in larger-scale ice masses

Hypothesis: Longitudinal flow structures in a large valley glacier containing numerous accumulation basins are dominate by flow-unit boundaries and provide the location for the development of pervasive longitudinal foliation.

Hypothesis: Flowlines in the Antarctic Ice Sheet are a macro-scale version of longitudinal foliation and form in a similar manner as can be seen in small valley glaciers. Furthermore, they also develop in the lee of nunataks and at the confluence of tributary glaciers where there is strong convergence and longitudinal extension. In all the situations above, flowlines represent the surface expression of a three-dimensional structure (Reynolds and Hambrey, 1988; Hambrey and Dowdeswell, 1994; Glasser and Gudmundsson, 2012).

The occurrence of longitudinal foliation in comparatively small-scale valley glaciers has been well documented in this study, and by previous studies from glaciers situated all around the world (*e.g.* European Alps – Hambrey and Milnes, 1975, 1977; Hambrey, 1977a; Hambrey et al., 1980; Goodsell et al., 2002, 2005a, b; Roberson, 2008; Jennings

et al., 2014. Svalbard – Hambrey and Dowdeswell, 1997; Hambrey et al., 1999, 2005; Glasser and Hambrey, 2001; Roberson and Hubbard, 2010; Fleming et al., 2013; Jennings et al., 2015; King et al., 2015; Lovell et al., 2015. Norway – Hambrey, 1976a, b. Canada – Meier, 1960; Hambrey and Müller, 1978; Hooke and Hudleston, 1978. USA – Allen et al., 1960; Lawson, 1996. New Zealand – Appleby et al., 2010). These studies not only demonstrate the global occurrence of longitudinal foliation in valley glaciers, but also show that longitudinal foliation forms in all types of glacier (temperate, polythermal, and cold-based glaciers). However, longitudinal foliation is not just confined to comparatively small-scale valley glaciers, but also forms in ice masses of all scales. In this study, structural mapping of Sermilik Glacier in Arctic Canada (Figure 7.1), as well as for Hatherton Glacier (Figure 8.3), Taylor Glacier, and Ferrar Glacier (Figure 8.4) in Antarctica have demonstrated that large-scale valley glaciers also develop longitudinal foliation. Furthermore, structural mapping and photographic evidence of blue-ice areas at the surface of Antarctic ice streams (*e.g.* Lambert Glacier system, Byrd Glacier) have confirmed the presence of longitudinal foliation at the largest scale of glacier. This conclusion confirms the findings of previous pioneering studies that examined the structure of various large-scale glaciers and ice shelves in Antarctica (*e.g.* Reynolds, 1988; Reynolds and Hambrey, 1988; Hambrey, 1991; Hambrey and Dowdeswell, 1994; Glasser and Gudmundsson, 2012; Ely and Clark, 2015; Glasser et al., 2015).

The occurrence of longitudinal foliation in large-scale ice masses is not surprising when the physical properties of longitudinal foliation formation and evolution are considered. The two main types of longitudinal foliation that are abundantly found in small valley glaciers are transposition foliation and axial planar foliation. In the case of transposition foliation, the planar layering observed as longitudinal foliation originates from the preservation of snow layers that undergo diagenesis into glacier ice to form primary stratification. Subsequent folding and reorientation of these originally horizontal layers as a result of ice flowing from a broad accumulation area into a comparatively narrow glacier tongue re-orientates the layering into steeply dipping planar structures that are longitudinally orientated. However, the physical properties of the resulting longitudinal foliation are broadly

controlled by the characteristics of the primary stratification from which it evolved (*i.e.* factors such as the thickness of snow layers once they undergo diagenesis into glacier ice). Similarly, axial planar foliation is thought to form in response to crystallographic modification and reorientation in response to shear stresses. As a consequence, the characteristics of the resulting longitudinal foliation are dependent upon factors such as ice crystal size, bubble content, and the amount of cumulative strain a parcel of ice has experienced. All of the controlling factors for the characteristics of both transposition- and axial planar foliation are broadly similar in ice masses of all scales (*i.e.* snow layer thicknesses (centimetres to metres thick) or ice crystal sizes (millimetres to centimetres in diameter) are approximately similar in all ice masses). Consequently, because the factors controlling longitudinal foliation formation and evolution are not only present in ice masses of all scales, but are also broadly similar, the universal development of longitudinal foliation in all types of ice mass is highly likely. A further implication of this is that longitudinal foliation is most likely to be a 'scale-independent' structure, reflecting the fact that its size is dependent on factors that are not necessarily linked to the size of the ice mass in which it is contained (*i.e.* longitudinal foliation as a structure will be approximately the same size regardless of the size of the ice mass in which it is contained).

As is the case for small valley glaciers, the development of longitudinal foliation in larger-scale ice masses is primarily focused at flow unit boundaries where higher amounts of cumulative strain are inferred. However, evidence collected in this study, primarily from Sermilik Glacier (*see Chapter Seven*), suggests that the linear longitudinal structures that are observed on the surface of the glacier from satellite imagery or aerial photography may not directly be longitudinal foliation structures. When dealing with satellite imagery or aerial photography of large-scale ice masses, the spatial resolution of the image (*i.e.* the size of each pixel) is much coarser (*i.e.* has larger pixel sizes) than is usually used for smaller ice masses. As a consequence, the imagery is not able to distinguish ice structures that are smaller than the spatial resolution of the imagery (*e.g.* if the imagery has a spatial resolution of 15 metres, it is not possible to identify features that are < 15 metres on the imagery). As has been discussed above, longitudinal foliation can be considered to be a 'scale-independent'

structure that is approximately similar in size regardless of the scale of the ice mass. Therefore, even though large valley glaciers like Sermilik Glacier are much larger than small valley glaciers like Midtre Lovénbreen, the longitudinal foliation present in both ice masses will be approximately comparable in scale. As the spatial resolution of the imagery used to structurally map Sermilik Glacier in this study is 15 metres, the longitudinal features present at the surface of the glacier cannot be longitudinal foliation structures. However, structural mapping of small valley glaciers in this study (Austre Brøggerbreen, Midtre Lovénbreen, Austre Lovénbreen, and Pedersenbreen) that uses imagery with a much higher spatial resolution has demonstrated that strong longitudinal foliation develops in bands that are located at flow unit boundaries. It is therefore probable that longitudinal foliation in larger-scale ice masses also develops in bands at flow unit boundaries. However, when longitudinal foliation in large valley glaciers is viewed from satellite imagery or aerial photography with a comparatively low spatial resolution (*e.g.* 15 metres or greater pixel sizing), the longitudinal structures will be grouped together and appear as individual longitudinal linear features located at flow unit boundaries (Figure 7.6). This explains why the linear features mapped on Sermilik Glacier persist for such long distances (> 5 kilometres), while it is rare to observe longitudinal foliation structures that extend for distances in excess of several tens of metres in the field (Hambrey, 1977a). Furthermore, the number of longitudinal structures observed across the tongue of Sermilik Glacier (*c*. 44 individual structures) coincides with the expected number of flow unit boundaries that would originate from a glacier with 45 sub-accumulation basins (*see Chapter Seven*) (Figure 7.5).

The longevity of longitudinal structures has also been observed in other large valley glaciers in this study (*e.g.* Hatherton Glacier, Taylor Glacier, Ferrar Glacier), and the persistence of flowlines in much larger ice masses has been commented on by previous studies (*e.g.* Ely and Clark, 2015; Glasser et al., 2015). Therefore, by 'up-scaling' this conclusion it is probable that flowlines in the Antarctic Ice Sheet represent flow unit boundaries that are defined by bands of longitudinal foliation that are visible as linear features on satellite imagery and aerial photography. Some evidence to support this conclusion can be seen in the large valley glaciers and ice streams in

Antarctica. Ground observations in Antarctica have already confirmed the occurrence of longitudinal foliation at some locations around the margins of the ice sheet, most notably at the western margin of the Lambert Glacier System, adjacent to the Fisher Massif (Figure 8.13) (Glasser et al., 2015). The structural mapping of several large valley glaciers in Antarctica with snow-free surfaces (blue-ice areas) have shown the presence of linear ice structures that are consistent up- and down-glacier with snow-covered flowlines. Furthermore, the persistence of flowlines through areas of net ablation demonstrates the three-dimensional nature of the structures (Figure 8.10). The formation of medial moraines in the lee of nunataks or at the confluence of tributary glaciers has also been shown in both large-scale valley glaciers (Hatherton Glacier) and ice streams (Lambert Glacier System). This is consistent with the formation of medial moraines in small valley glaciers, and agrees with the Hambrey and Glasser (2003) model of medial moraine formation. However, it can be argued that other medial moraine forming hypotheses can also explain medial moraines in large-scale ice masses (*e.g.* Boulton, 1978; Eyles and Rogerson, 1978; Boulton and Eyles, 1979; Vere and Benn, 1989). Even though this maybe the case, the debris septa model of medial moraine formation is unable to explain the formation of flowlines at the confluence of tributary glaciers when no medial moraine develops, or when flowlines form in the interior of the ice sheet when no nunataks or subglacial obstructions are present. Conversely, the Hambrey and Glasser (2003) model of medial moraine formation by folding and longitudinal foliation development can explain the formation of flowlines even when a medial moraine does not form as longitudinal foliation will develop regardless of debris content along the length of a flow unit boundary. If this is the case, bands of longitudinal foliation forming at flow unit boundaries in Antarctic glaciers and ice streams appear as linear flowlines because of the comparatively coarse image resolution in comparison to the width of individual longitudinal foliation structures.

If flowlines are assumed to be the surface expression of three-dimensional longitudinal foliation that develops at flow unit boundaries, the channels of ice separated by the flowlines (flow unit boundaries) must be considered as individual flow units. The structural investigation of a small Alpine valley glacier undertaken by

Jennings et al. (2014) concluded that individual flow units can be regarded as mutually exclusive systems that are unique from their neighbouring flow units. Jennings et al. (2015) further expanded on this concept while studying a small cold-based valley glacier in Svalbard, by identifying different suites of relict fracture sets contained within adjacent flow units that had experienced different structural evolutions. Jennings et al. (2015) therefore concluded that each flow unit in Austre Brøggerbreen was unique, and that they had each been subjected to very different flow histories and dynamics despite being part of the same small valley glacier. If flow units in small valley glaciers are structurally and dynamically different from one another, it would be expected that flow units in much larger Antarctic glaciers would behave in a similar manner and would also be structurally distinct. Observations of the snow-free main glacier trunk of Byrd Glacier as the glacier flows through the Transantarctic Mountains show numerous flowlines running parallel to flow direction, despite this section of Byrd Glacier being highly crevassed. However, the orientations of crevasses across the width of the glacier are not consistent. Crevasses contained in individual channels of ice that are separated by flowlines (*i.e.* crevasses contained in individual flow units) have different orientations in relation to crevasses contained in other adjacent flow units (Figure 9.1). Another example of this can be seen in the Lambert Glacier as the glacier becomes topographically confined when entering the Lambert Graben. As the Lambert Glacier enters the Lambert Graben an extensive crevasse field develops. Flowlines are observed to persist along the length of the Lambert Glacier despite travelling through areas of net surface ablation (blue-ice areas) and through crevasse fields. As has been described above for Byrd Glacier, Lambert Glacier has suites of crevasses separated by flowlines that have different orientations from crevasses contained in adjacent flow units, despite being contained within the same crevasse field (Figure 9.2). These observations from two of the largest ice streams in Antarctica appear to show similar behaviour to that described for Austre Brøggerbreen (Jennings et al., 2015). Different channels of ice separated by flowlines contain suits of crevasses with orientations that differ to crevasse sets contained in adjacent channels of ice. Therefore, it is not only probable that these channels of ice are, in fact, unique flow units separated by flowlines that are in turn flow unit boundaries, but also that individual flow units have experienced differential flow dynamics from one-another

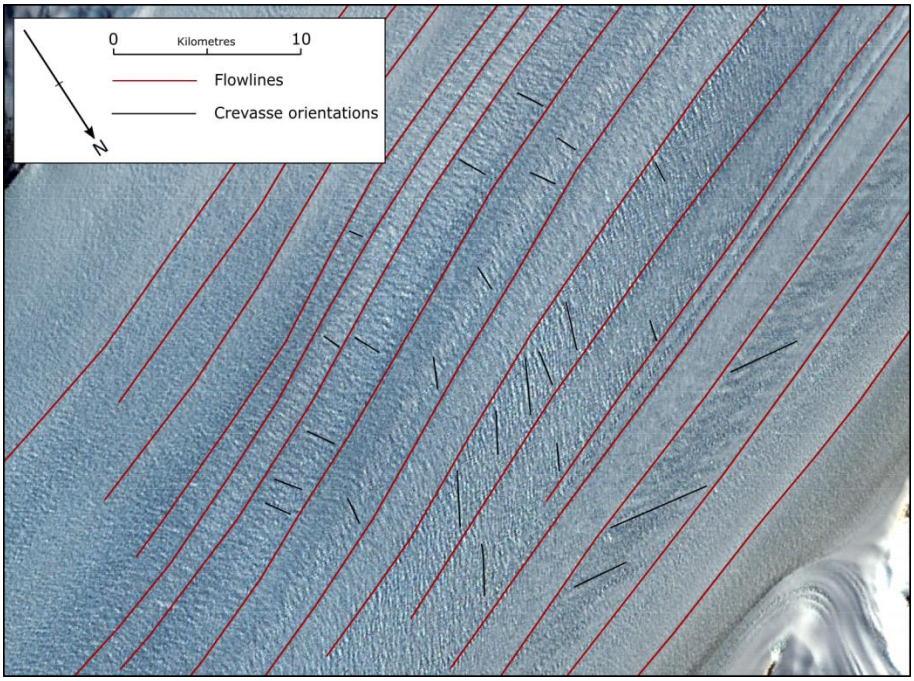

Figure 9.1. Image of the blue-ice area of Byrd Glacier as it passes through the Transantarctic Mountains. Note how flowlines persist through the blue-ice area. Also note that crevasse orientations between flowlines vary.

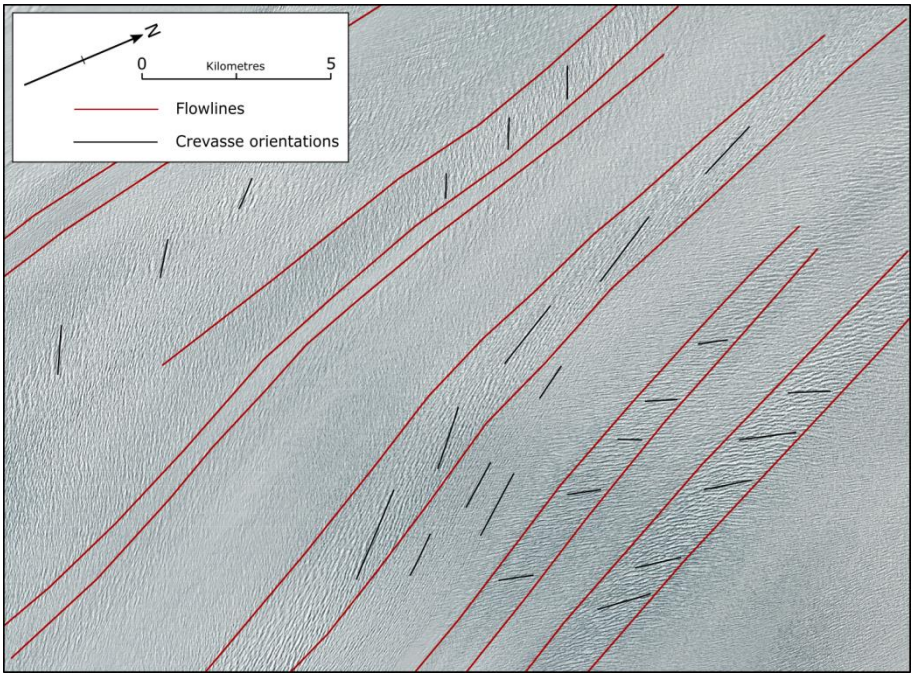

Figure 9.2. Landsat 7 image of the middle-reaches of the Lambert Glacier as it enters the Lambert Graben. Note how crevasse orientations between flowlines differ.

despite being contained within the same ice stream. This concept has also been applied to palaeo-ice streams where narrow corridors of preserved crevasse squeeze ridges have been identified as flow units that have experience differential flow (Evans et al., 2016).

The origin of flow units within topographically confined small- and large-scale glaciers is comparatively easy to identify as they often originate in their own topographically defined accumulation basin, subsequently merging with adjacent flow units as they join the main trunk of the glacier. Similarly, much larger ice streams can also have flow units that originate in topographically confined accumulation basins (*e.g.* flow units that originate as smaller topographically confined glaciers that subsequently join the main trunk of Byrd Glacier as it flows through the Transantarctic Mountains). It is also easy to understand the origin of flow units that develop in ice streams as ice flow is separated around nunataks. However, the up-glacier persistence of many Antarctic flowlines indicates that the majority of flow units contained within large-scale ice streams originate in the interior of the ice sheet. It is therefore not possible for these flow units to develop in the same way as is observed in topographically confined glaciers as there are no topographic controls that dictate the size, nature, and location of the accumulation basins associated with each flow unit. Regardless of this fact, it has been shown above that flow units in both Lambert Glacier and Byrd Glacier behave in a similar manner to those described for Austre Brøggerbreen (*see* Jennings et al., 2015). Even though flow units originating in the interior of the Antarctic Ice Sheet are not topographically confined, their similar behaviour when compared to smaller topographically confined valley glaciers suggests that their formation mechanism is similar.

One of the main definitions of a flow unit can be considered to be ‘a channel of ice flow that differs from its surroundings’. A flow unit originating in a topographically confined basin is theoretically different from the basin as it is undergoing flow, whereas the constraining bedrock basin is stationary. Similarly, parallel flow units can often be separated from one-another based on their differential flow and dynamics. These principles also apply to flow units originating in the interior of an ice sheet. Flow units in the interior of the ice sheet can be simply defined as ‘channels of ice flow that

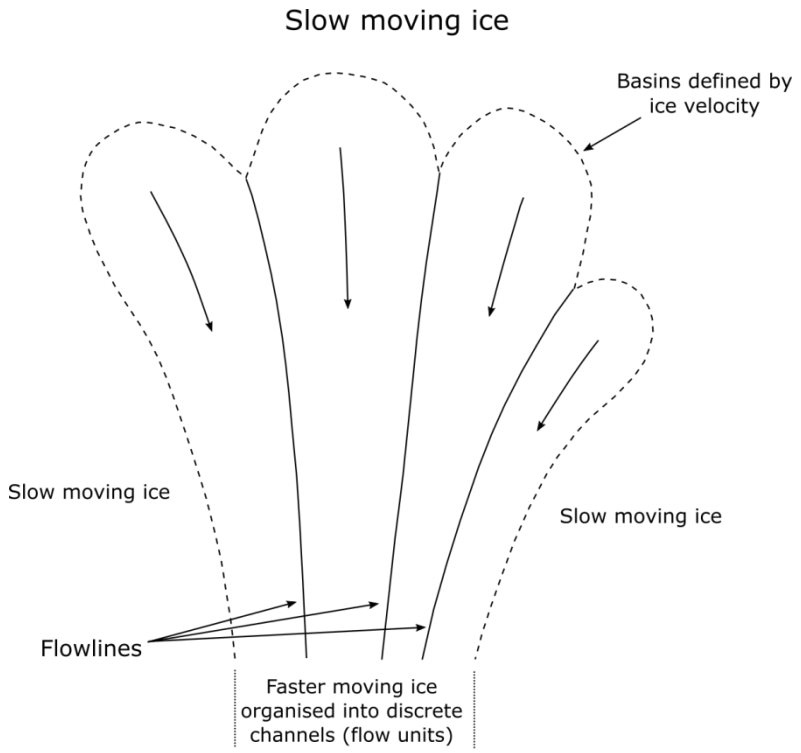

Figure 9.3. Conceptual diagram illustrating how flow units form in the interior of an ice sheet. In contrast to valley glaciers that have accumulation basins defined by topography that constrain the ice mass, accumulation basins in ice sheets are constrained by slower-moving or near stagnant ice. Zones of faster moving ice in the interior of the ice sheet (*i.e.* the onset zone of an ice stream) become organised into channels (flow units) originating from sub-accumulation basins. Differences in ice flow velocities between adjacent flow units lead to the formation of flowlines at flow unit boundaries that are composed of longitudinal foliation.

experience differential flow in comparison to surrounding ice'. Therefore, the mechanism of flow unit formation in the interior of the Antarctic Ice Sheet is comparable to flow unit formation in topographically confined valley glaciers. The initiation zones of flow units in the interior of the ice sheet are also constrained by a basin; however, in contrast to valley glaciers that have stationary bedrock basins, a flow unit's basin is defined by slow-moving ice in the interior of an ice sheet (Figure 9.3). Consequently, instead of having topography as the main controlling factor that defines the basins that flow units originate in (as is the case in valley glaciers), several controls, including basal topography, bed conditions, and ice surface topography, dictate the location and characteristics of flow units within an ice sheet. As a result, each flow unit is unique as it reflects the characteristics of their onset zones (*i.e.*

reflects the characteristics of its accumulation basin), in much the same way that has been observed in small valley glaciers. Even though longitudinal foliation that defines the boundaries of flow units can be considered as a scale-independent structure (*i.e.* it is a similar size of structure regardless of glacier scale), flow units have to be regarded as scale-dependent features (*i.e.* flow units reach much greater sizes in larger ice masses). However, their behaviour is similar regardless of scale (*i.e.* flow units in small valley glaciers behave in a similar manner to much larger flow units in ice sheets).

The lack of direct observations of longitudinal foliation in ice streams and ice sheets can, in part, be explained by the remote and inaccessible nature of ice sheets, which when combined with the scale of ice sheets, makes field observations impractical. Furthermore, snow-cover on the surface of the Antarctic Ice Sheet limits remote sensing of the ice surface to spatially limited blue-ice areas. However, despite the numerous radar studies that have been conducted at locations all over the Antarctic Ice Sheet (*e.g.* Conway et al., 2002; Campbell et al., 2008; Ross et al., 2011; Siegert et al., 2013; Martín et al., 2014), a consensus on the internal ice structure of the ice sheet has yet to be reached. Several reasons for the current lack of radar evidence include the use of frequencies required to observe the ice sheet bed which are not ideal for observing internal ice layering, the inability for radar equipment to easily identify near vertical ice structures, and many studies using longitudinal radar profiles when transverse profiles are more informative for identifying ice structures. Furthermore, direct ground observations of ice surface structures at radar sites are non-existent because radar equipment is either airborne or towed behind a snowmobile where a surface covering of snow is required.

9.7 The structural and dynamic significance of flowlines

The observation and structural mapping of longitudinal foliation in comparatively small valley glaciers has been used in previous studies to deduce the past ice flow dynamics of glaciers (*e.g.* Clarke, 1991; Lawson, 1996; Goodsell et al., 2005b; Hambrey et al., 2005; Jennings et al., 2015). Therefore, if flowlines represent flow unit boundaries that are defined by longitudinal foliation, conclusions about the past dynamics of the

Antarctic Ice Sheet can be inferred. However, for large areas of the Antarctic Ice Sheet, only flowlines can be observed as linear features, and longitudinal foliation cannot be directly observed as a result of snow-cover or satellite image/aerial photography spatial resolution. Nevertheless, meaningful observations and conclusions can still be drawn from the structural observation of flowlines. As flowlines are preferentially located over subglacial troughs in zones of accelerating ice flow, the velocity configuration of the Antarctic Ice Sheet can be inferred from observing flowlines. This enables the flow configuration of the ice sheet to be inferred for the residence time of the ice flowing along the length of the flowlines (Glasser et al., 2015). This is potentially an important source of information regarding past ice sheet configuration and dynamics as no centennial to millennial ice velocity or dynamic records are available. Direct velocity measurements of the Antarctic Ice Sheet using satellite observations has only been available for the past 50 years (Bindschadler and Vornberger, 1998; Rignot and Kanagaratnam, 2006; Rignot et al., 2008), whereas field-based velocity data sets are spatially and temporally limited. Also, it has only been in recent years that InSAR velocity data has been used to deduce the contemporary velocity field of the Antarctic Ice Sheet (Bamber et al., 2000; Rignot and Kanagaratnam, 2006; Rignot et al., 2011). The structural analysis of flowlines have been able to provide an estimate of how long the configuration of the main fast-flowing ice streams have remained in the same location, coming to the conclusion that the main ice-flow configuration of the Antarctic Ice Sheet has remained largely similar for the last several hundred years, and possibly even since the end of the last glacial cycle and throughout the Holocene (Glasser et al., 2015). Furthermore, the residence time of a parcel of ice flowing along individual flowlines for Lambert Glacier, Recovery Glacier, Byrd Glacier, and Pine Island Glacier have been deduced by integrating modern ice flow velocities along their length, suggesting that ice might take anywhere between approximately 2,500 to 18,500 years to travel through the length of these glacier systems (Glasser et al., 2015).

The identification of areas in which flowlines have become distorted have indicated zones of the Antarctic Ice Sheet that have experienced a switch in ice flow behaviour (*see section 8.3.4*; Fahnestock et al., 2000; Siegert et al., 2013; Glasser et al., 2015). The Kamb Ice Stream and the Bungenstock Ice Rise are two main areas that

demonstrate that flowlines keep a record of ice dynamic switches (*see section 8.3.4*), and further adds confidence that the main flow configuration of the fast flowing sectors of the Antarctic Ice Sheet have remained constant for the ice residence times of the glaciers (Glasser et al., 2015).

As well as flowlines recording past ice flow dynamics (as explained above for identifying areas where ice flow has switched) flowlines can also provide insight into the current flow dynamics of glaciers. Examples of active ice areas that have flowlines orientated perpendicular to ice flow (*e.g.* Lambert Glacier, Hatherton Glacier, Taylor Glacier, *see Chapter Eight*) (Figure 8.14) demonstrate that flowlines are not always parallel to ice flow (*i.e.* a flow pathway); however, they can provide important information about current flow dynamics. Longitudinal foliation in small valley glaciers has been used in part to help identify polyphase deformation (Hambrey and Lawson, 2000). Structural analysis enables different stress regimes to be located that help identify where structures are actively forming and where they are transported as passive markers. Similar techniques can be applied to flowlines in much larger ice masses to help deduce their flow dynamics, which in turn can be used to improve ice flow models. Previous studies that have used flowlines as indicators of switching on and off of ice streams (*e.g.* Fahnestock et al., 2000) have only considered flowlines as passively advected markers. However, their conclusions can be made more rigorous if flowlines are assumed to be the surface representation of longitudinal foliation, enabling polyphase deformation and different stress regimes to be identified.

9.8 Future work

As has been discussed previously, there is still uncertainty with regard to the formation of longitudinal foliation in valley glaciers (especially the formation mechanism of axial planar foliation), as well as how flowlines form and develop in much larger ice masses. Several avenues of further work would be useful for trying to address these questions, as well as improving our knowledge of structures within ice sheets.

The occurrence of longitudinal foliation in small valley glaciers has been well documented at the intermediate- (field-based measurements) and large (glacier-wide) scales. However, very little work with regard to longitudinal foliation has been undertaken at the crystallographic scale. In an attempt to document the evolution of longitudinal foliation at the smallest scale, crystallographic analysis of foliated ice would provide valuable information about the modification of ice crystals in response to shear stresses. Documenting the crystallographic evolution of longitudinal foliation would not only improve our understanding of the formation and evolution of axial planar foliation, but would enable the comparison of longitudinal foliation formation for glaciers of all scales. As has been discussed above, longitudinal foliation is hypothesised to be scale-independent (*i.e.* is a similar size in glaciers of all scales because the controlling factors on the characteristics of longitudinal foliation are factors such as snow thickness and ice crystal size), therefore, crystallographic analysis enables ice masses of all sizes to be compared to test this hypothesis. Furthermore, it enables ice crystals from flowlines to be compared to ice crystals from longitudinal foliation derived in small valley glaciers to ascertain whether they share a common process of formation.

The absence of direct field measurements, especially three-dimensional measurements, of large-scale Antarctic glaciers and ice streams makes the comparison of structures found in small valley glaciers and ice sheets problematic. Field structural analysis of snow-free blue-ice areas in Antarctica would provide an important missing link for understanding the three-dimensional nature of flowlines and structures found in large-scale glaciers and ice streams. Undertaking a number of transverse structural transects at points along a flowline would prove particularly fruitful as it would enable the three-dimensional structural evolution of the flowline to be seen along its length, as well as identifying if longitudinal foliation was present. Additionally, it would enable the direct comparison of flowline structural evolution in large-scale ice masses to flow unit boundary structural evolution in small-scale valley glaciers, enabling the flow unit boundary hypothesis about flowlines to be tested at a variety of scales (*e.g.* large-scale, small-scale, crystallographic-scale). The addition of radar studies utilising equipment specifically adapted for the identification of three-dimensional ice

structures at depth (*i.e.* utilising frequencies specifically for identifying internal layering, taking multiple transverse transects along the length of a flowline, correlating the radar transects with surface ice structure measurements in blue-ice areas) would further enhance our understanding of the internal structure of large-scale ice masses. Sufficient collection of field data from Antarctic ice streams/glaciers would not only prove invaluable for comparing to structural data collected from much smaller ice masses, but would also be an invaluable tool for integrating into and constraining ice sheet models. This would not only improve the accuracy of ice sheet models by providing detailed structural and ice dynamic information, but would also allow more accurate ice flow predictions to be made for different applied climate scenarios.

Several studies have applied strain analysis to small-scale valley glaciers in an attempt to understand the formation and evolution of ice structures; however, this has only been applied to a limited number of glaciers (*e.g.* Goodsell et al., 2005b; Hambrey et al., 2005). By increasing the number of studies that incorporate strain analysis of valley glaciers and larger-scale glaciers, it would be possible to compare strain in different scales of glaciers to see if the conditions for longitudinal foliation formation and flowline formation are similar. Furthermore, to date, studies analysing cumulative strain in relation to ice structures have only been considered in two-dimensions. The use of three-dimensional strain analysis (*e.g.* Hubbard et al., 1998) for understanding cumulative strain in ice masses would further improve our understanding of the formation and evolution of different ice structures. By applying two- and three-dimensional techniques, utilising feature-tracking or interferometry, to ice sheet scale studies, there is a great deal of potential for improving ice-flow modelling. The incorporation of these data into models not only enables a more accurate understanding of the conditions required for different ice structures to form and evolve, but improves our understanding of past ice sheet dynamics.

Chapter Ten

Conclusions

This chapter provides a brief summary of the conclusions and key findings of this study. The overall aim of this study was to examine how longitudinal foliation develops in glaciers and ice sheets in a wide range of topographic, climatic, and dynamic settings. These conclusions are structured chronologically, initially summarising the main observations when considering longitudinal foliation in valley glaciers, before detailing the key findings from 'up-scaling' these observations to larger valley glaciers and Antarctic ice streams.

i. Detailed structural mapping of several small-scale valley glaciers has revealed that strong longitudinal foliation develops in concentrated bands at flow unit boundaries as a result of enhanced simple shear.

ii. A fracture-derived longitudinal foliation that has not been previously described for any other glacier has been identified on Austre Brøggerbreen. Relict transverse fracture sets become increasingly re-orientated by ductile flow in simple shear flow regimes until they become longitudinally orientated.

iii. Flow units can be regarded as mutually exclusive (*i.e.* each is unique and can be treated as a separate and independent system), containing unique structural assemblages and experiencing differential flow from neighbouring flow units, as suggested by Jennings et al. (2014). The characteristics of individual

accumulation basins are reflected in their corresponding flow unit, influencing the structures present and their down-glacier evolutions.

iv. The structures present at the surface of several small valley glaciers have been used to infer past ice flow dynamics, as was proposed by Hambrey et al. (2005). This study has shown that structures can potentially record the flow behaviour of a glacier for the residence time of the ice within the glacier system.

v. The number of longitudinal ice-surface structures observed for a large-scale valley glacier (Sermilik Glacier, Bylot Island, Canada) strongly correlates with the number of flow unit boundaries expected to be present when considering the number of sub-accumulation basins in the accumulation area of the glacier. Additionally, 'up-scaling' of field-based structural observations from small valley glaciers, combined with low-level oblique aerial photography, also suggests that longitudinal ice-surface structures present at the surface of Sermilik Glacier are the surface representation of flow unit boundaries. Flow unit boundaries are defined by bands of strong, steeply dipping, longitudinal foliation that appear as linear surface features as a consequence of the comparatively poor spatial resolution of the satellite imagery used to structurally map the glacier.

vi. The persistence of flowlines in the Antarctic Ice Sheet through areas of crevassing and net ablation (blue-ice areas) suggests that flowlines are the surface representation of a three-dimensional structure, as has been observed at the surface of the Lambert Glacier – Amery Ice Shelf system, Byrd Glacier, Hatherton Glacier, and Taylor Glacier. It is therefore inferred that flowlines in the Antarctic Ice Sheet are the surface expression of flow unit boundaries composed of bands of steeply dipping longitudinal foliation. Even though other formation hypotheses could not be conclusively disproved in this study, a longitudinal foliation hypothesis is best able to explain the development of flowlines in all topographic situations.

vii. The survival and deformation of flowlines in areas of ice flow stagnation (*e.g.* the Kamb Ice Stream) indicates that flowlines form in their initiation zones and not

along their entire length. Furthermore, these areas demonstrate that flowlines record past ice-flow dynamics and switches in ice flow.

viii. It has been demonstrated that structural observations from small-scale valley glacier can be 'up-scaled' to much larger ice masses. These findings therefore demonstrate the potential for inferring past ice-flow dynamics from the structural analysis of ice sheets.

References

Allen, C. R., W. B. Kamb, M. F. Meier, and R. P. Sharp (1960), Structure of the lower Blue Glacier, Washington, *Journal of Geology*, **68**, 601-625.

Alley, R. B., K. M. Cuffey, E. B. Evenson, J. C. Strasser, D. E. Lawson, and G. J. Larson (1997), How glaciers entrain and transport basal sediments: physical constraints, *Quaternary Science Reviews*, **16**, 1017-1038.

Alley, R. B., T. K. Dupont, B. R. Parizek, and S. Anandakrishnan (2005), Access of surface meltwater to beds of sub-freezing glaciers: preliminary insights, *Annals of Glaciology*, **40**, 8-14.

Andrews, J. T. (2002), Glaciers of Baffin Island, in *Satellite Image Atlas of Glaciers of the World*, edited by R. S. Williams and J. G. Ferrigno, U. S. Geological Survey Professional Paper, 1386-J: 165-198.

Appleby, J. R., M. S. Brook, S. S. Vale, and A. M. MacDonald-Creevey (2010), Structural glaciology of a temperate maritime glacier: Lower Fox Glacier, New Zealand, *Geografiska Annaler*, **92**(A), 451-467.

Bamber, J. L., R. B. Alley, and I. Joughin (2007), Rapid response of modern day ice sheets to external forcing, *Earth and Planetary Science Letters*, **257**, 1-13.

Bamber, J. L., D. G. Vaughan, and I. Joughin (2000), Widespread complex flow in the interior of the Antarctic Ice Sheet, *Science*, **287**, 1248-1250.

Barron, J. B., J. Anderson, J. G. Bauldauf, and B. L. Larsen (1991), *Proceedings of the Ocean Drilling Program, Scientific results*, Volume 119, College Station, Texas, Ocean Drilling Program.

Benn, D. I., and D. J. A. Evans (2010), *Glaciers and Glaciation*, Hodder Education, London.

Benn, D. I., and A. M. D. Gemmell (2002), Fractal dimensions of diamictic particle-size distributions: Simulations and evaluation, *Geological Society of America Bulletin*, **114**(5), 528-532.

Benn, D. I., J. Gulley, A. Luckman, A. Adamek, and P. S. Glowacki (2009), Englacial drainage systems formed by hydrologically driven crevasse propagation, *Journal of Glaciology*, **55**(191), 513-523.

Benn, D. I., C. R. Warren, and R. H. Mottram (2007), Calving processes and the dynamics of calving glaciers, *Earth-Science Reviews*, **82**, 143-179.

Bennett, M. R., M. J. Hambrey, D. Huddart, and J. F. Ghienne (1996), Moraine development at the high-Arctic valley glacier Pedersenbreen, Svalbard, *Geografiska Annaler Series A, Physical Geography*, **78**(4), 209-222.

Bennett, M. R., D. Huddart, M. J. Hambrey, and J. F. Ghienne (1998), Modification of braided outwash surfaces by aufeis: an example from Pedersenbreen, Svalbard, *Zeitschrift für Geomorphologie*, **42**(1), 1-20.

Bincschadler, R. A. (2006), The environment and evolution of the West Antarctic ice sheet: setting the stage, *Philosophical Transactions of the Royal Society*, **A**(364), 1583-1605.

Bindschadler, R., and P. Vornberger (1998), Changes in the West Antarctic Ice Sheet since 1963 from declassified satellite photography, *Science*, **279**(5351), 689-692.

Björnsson, H., Y. Gjessing, S. –E. Hamran, J. O. Hagen, O. Liestøl, F. Pálsson, and B. Erlingsson (1996), The thermal regime of sub-polar glaciers mapped by multi-frequency radio-echo sounding, *Journal of Glaciology*, **42**(140), 23-32.

Boon, S., and M. Sharp (2003), The role of hydrologically-driven ice fracture in drainage system evolution on an Arctic glacier, *Geophysical Research Letters*, **30**(18), doi: 10.1029/2003GL018034.

Boulton, G. S. (1967), The development of a complex supraglacial moraine at the margin of Sørbreen, Ny Friesland, Vestspitzbergen, *Journal of Glaciology*, **6**, 717-736.

Boulton, G. S. (1970), On the origin and transport of englacial debris in Svalbard glaciers, *Journal of Glaciology*, **9**, 213-229.

Boulton, G. S. (1978), Boulder shapes and grain size distributions of debris as indicators of transport paths through a glacier and till genesis, *Sedimentology*, **25**, 773-799.

Boulton, G. S., and N. Eyles (1979), Sedimentation by valley glaciers: a model and genetic classification, in *Moraines and Varves*, edited by C. Schlüchter, Balkema, Rotterdam.

Boulton, G. S., J. J. M. van der Meer, D. J. Beets, K. J. Hart, and G. H. J. Ruegg (1999), The sedimentary and structural evolution of a recent push moraine complex: Holmströmbreen, Spitsbergen, *Quaternary Science Reviews*, **18**, 339-371.

Brecher, H. H. (1982), Photographic determination of surface velocities and elevations on Byrd Glacier, *Antarctic Journal of the United States*, **17**(5), 79-81.

Buurman, P., T. Paper, and C. C. Muggler (1997), Laser-grain size determination in soil genetic studies: 1 Practical problems, *Soil Science*, **162**, 211-218.

Campbell, I., R. Jacobel, B. Welch, and R. Pettersson (2008), The evolution of surface flow stripes and stratigraphic folds within Kamb Ice Stream: why don't they match?, *Journal of Glaciology*, **54**(186), 421-427.

Campbell, S., S. Roy, K. Kreutz, S. A. Arcone, E. C. Osterberg, and P. Koons (2013), Strain-rate estimates for crevasse formation at an alpine ice divide: Mount Hunter, Alaska, *Annals of Glaciology*, **54**, doi: 10.3189/2013AoG63A266.

Casassa, G., and H. H. Brecher (1993), Relief and decay of flow stripes on Byrd Glacier, Antarctica, *Annals of Glaciology*, **17**, 255-261.

Catania, G., C. Hulbe, H. Conway, T. A. Scambos, and C. F. Raymond (2012), Variability in the mass flux of the Ross ice streams, West Antarctica, over the last millennium, *Journal of Glaciology*, **58**, 741-752.

Christoffersen, P., S. Tulaczyk, F. D. Carsey, and A. E. Behar (2006), A quantitative framework for interpretation of basal ice facies formed by ice accretion over subglacial sediment, *Journal of Geophysical Research*, **111**, F01017, doi: 10.1029/2005JF000363.

Clarke, G. K. C., and E. W. Blake (1991), Geometric and thermal evolution of a surge-type glacier in its quiescent state, Trapridge Glacier, Yukon Territory, Canada 1969-89, *Journal of Glaciology*, **37**, 158-169.

Clarke, T. S. (1991), Glacier dynamics in the Susitna River basin, Alaska, U.S.A., *Journal of Glaciology*, **37**, 97-106.

Clarke, T. S., C. Liu, N. E. Lord, and C. R. Bentley (2000), Evidence for a recently abandoned shear margin adjacent to Ice Stream B2, Antarctica, from ice-penetrating radar measurements, *Journal of Geophysical Research*, **105**, 13409-13422.

Conway, H., G. Catania, C. F. Raymond, A. M. Gades, T. A. Scambos, and H. Engelhardt (2002), Switch of flow direction in an Antarctic ice stream, *Nature*, **419**, 465-467.

Cook, S. J., R. I. Waller, and P. G. Knight (2006), Glaciohydraulic supercooling: the process and its significance, *Progress in Physical Geography*, **30**(5), 577-588.

Copland, L., M. Sharp, and J. A. Dowdeswell (2003), The distribution and flow characteristics of surge-type glaciers in the Canadian High Arctic, *Annals of Glaciology*, **36**, 73-81.

Crabtree, R. D., and C. S. M. Doake (1980), Flow lines on Antarctic ice shelves, *Polar Record*, **20**, 31-37.

Croot, D. G. (1988), Glaciotectonics and surging glaciers: a correlation based on Vestspitsbergen, Svalbard, Norway, in *Glaciotectonics: Forms and Processes*, edited by D. G. Croot, Balkema, Rotterdam.

Cuffey, K. M., and W. S. B. Paterson (2010), *The Physics of Glaciers*, Elsevier, Oxford.

Cunningham, J., and E. D. Waddington (1990), Boudinage: a source of stratigraphic disturbance in glacial ice in central Greenland, *Journal of Glaciology*, **36**(124), 269-272.

Das, S., I. Joughin, M. Behn, I. Howat, M. King, D. Lizarralde, and M. Bhatia (2008), Fracture propagation to the base of the Greenland Ice Sheet during supraglacial lake drainage, *Science*, **320**, 778-781.

Dowdeswell, E. K., J. A. Dowdeswell, and F. Cawkwell (2007), On the glaciers of Bylot Island, Nunavut, Arctic Canada, *Arctic, Antarctic and Alpine Research*, **39**(3), 402-411.

Dowdeswell, J. A., and M. Williams (1997), Surge-type glaciers in the Russian High Arctic identified from digital satellite imagery, *Journal of Glaciology*, **43**, 489-494.

Doyle, S. H., A. L. Hubbard, C. F. Dow, G. A. Jones, A. Fitzpatrick, A. Gusmeroli, B. Kulessa, K. Lindback, R. Pettersson, and J. E. Box (2013), Ice tectonic deformation during the rapid in situ drainage of a supraglacial lake on the Greenland Ice Sheet, *The Cryosphere*, **7**, 129-140.

Dreimanis, A., and U. J. Vagners (1971), Bimodal distribution of rock and mineral fragments in basal tills, *Till*, 237-250.

Drewry, D. J. (1972), A quantitative assessment of dirt-cone dynamics, *Journal of Glaciology*, **11**(63), 431-446.

Drewry, D. J. (1986), *Glacial geologic processes*, Arnold, London.

Drewry, D. J., S. R. Jordan, E. Jankowski (1982), Measured properties of the Antarctic ice sheet: surface configuration, ice thickness, volume and bedrock characteristics, *Annals of Glaciology*, **3**, 83-91.

Driscoll, F. G. (1980), Formation of the Neoglacial surge moraines of the Klutlan Glacier, Yukon Territory, Canada, *Quaternary Research*, **14**, 19-30.

Dunning, S. A., N. J. Rosser, S. T. McColl, and N. V. Rezichenko (2015), Rapid sequestration of rock avalanche deposits within glaciers, *Nature Communications*, **6**(7964), doi: 10.1038/ncomms8964.

Durney, D. W., and J. G. Ramsey (1973), Incremental strains measured by syntectonic crystal growths, in *Gravity and Tectonics*, edited by K. A. De Jong, and R. Scholten, Wiley, New York.

Ely, J. C., and C. D. Clark (2015), Flow-stripes and foliations of the Antarctic ice sheet, *Journal of Maps*, **2015**, 1-11.

Engelhardt, H., and B. Kamb (2013), Kamb Ice Stream flow history and surge potential, *Annals of Glaciology*, **54**, 287-298.

Ensminger, S. L., R. B. Alley, E. B. Evenson, D. E. Lawson, and G. J. Larson (2001), Basal-crevasse-fill origin of laminated debris bands at Matanuska Glacier, Alaska, USA, *Journal of Glaciology*, **47**(158), 412-422.

Epstein, S. (1956), *Variation of the O^{18}/O^{16} Ratio of Freshwater and Ice*, Publication 400, U.S National Academy of Sciences.

Epstein, S., and R. P. Sharp (1959), Oxygen isotope variations in the Malaspina and Saskatchewan glaciers, *Journal of Geology*, **67**, 88-102.

Etzelmüller, B., and J. Sollid (1996), Long-term mass balance of selected polythermal glaciers on Spitsbergen Svalbard, *Norsk Geografisk Tidsskrift – Norwegian Journal of Geography*, **50**(1), 55-66.

Evans, D. J. A. (1989), Apron entrainment at the margins of sub-polar glaciers, northwest Ellesmere Island, Canadian high arctic, *Journal of Glaciology*, **35**, 317-324.

Evans, D. J. A. (2003), *Glacial Landsystems*, Arnold, London.

Evans, D. J. A., and B. R. Rea (1999), Geomorphology and sedimentology of surging glaciers: a landsystems approach, *Annals of Glaciology*, **28**, 75-82.

Evans, D. J. A., and B. R. Rea (2003), Surging glacier landsystem, in *Glacial Landsystems*, edited by D. J. A. Evans, Arnold, London.

Evans, D. J. A., D. R. Twigg, B. R. Rea, and M. Shand (2007), Surficial geology and geomorphology of the Bruarjökull surging glacier landsystem, *Journal of Maps*, **2007**, 349-367.

Evans, D. J. A., R. D. Storrar, and B. R. Rea (2016), Crevasse-squeeze ridge corridors: Diagnostic features of late-stage palaeo-ice stream activity, *Geomorphology*, **258**, 40-50.

Eyles, N., and R. J. Rogerson (1978), A framework for the investigation of medial moraine formation: Austerdalsbreen, Norway and Berenden Glacier, British Columbia, Canada, *Journal of Glaciology*, **20**, 99 – 113.

Fahnestock, M., and J. Bamber (2001), Morphology and surface characteristics of the West Antarctic ice sheet, in *The West Antarctic Ice Sheet: Behavior and Envrionment*, edited by R. B. Alley, and R. A. Bindschadler, American Geophysical Union, Antarctici Research Series, vol. 77, 13-27.

Fahnestock, M. A., T. A. Scambos, R. A. Bindschadler, and G. Kvaran (2000), A millennium of variable ice flow recorded by the Ross Ice Shelf, Antarctica, *Journal of Glaciology*, **46**, 652–664.

Fitzsimons, S., N. Webb, S. Mager, S. MacDonell, R. Lorrain, and D. Samyn (2008), Mechanisms of basal ice formation in polar glaciers: An evaluation of the apron entrainment model, *Journal of Geophysical Research: Earth Surface*, **113**(F2), doi: 10.1029/2006JF000698.

Fleming, E., H. Lovell, C. Stevenson, M. Petronis, D. Benn, M. Hambrey, and I. J. Fairchild (2013), Magnetic fabrics in the basal ice of a surge-type glacier, *Journal of Geophysical Research, Earth Surface*, **118**, 1–16, doi: 10.1002/jgrf.20144.

Forbes, J. D. (1900), Travels through the Alps, Adam and Charles Black, London.

Forster, R. R., E. Rignot, B. L. Isacks, and K. C. Jezek (1999), Interferometric radar observations of Glaciares Europa and Penguin, Hielo Patagónico Sur, Chile, *Journal of Glaciology*, **45**, 325-337.

Fossen, H. (2010), *Structural Geology*, Cambridge University Press, Cambridge.

Fountain, A. G., and J. Walder (1998), Water flow through temperate glaciers, *Reviews of Geophysics*, **36**, 299-328.

Fountain, A. G., R. W. Jacobel, R. Schlichting, and P. Jansson (2005a), Fractures as the main pathways of water flow in temperate glaciers, *Letters to Nature*, **433**, 618-621.

Fountain, A. G., R. B. Schlichting, P. Jansson, and R. W. Jacobel (2005b), Observations of englacial water passages: a fracture-dominated system, *Annals of Glaciology*, **40**, 25-30.

Fretwell, P., H. D. Pritchard, D. G. Vaughan, J. L. Bamber, N. E. Barrand, R. Bell, C. Bianchi, R. G. Bingham, D. D. Blankenship, G. Casassa, G. Catania, D. Callens, H. Conway, A. J. Cook, H. F. J. Corr, D. Damaske, V. Damm, F. Ferraccioli, R. Forsberg, S. Fujita, Y. Gim, P. Gogineni, J. A. Griggs, R. C. A. Hindmarsh, P. Holmlund, J. W. Holt, R. W. Jacobel, A. Jenkins, W. Jokat, T. Jordan, E. C. King, J. Kohler, W. Krabill, M. Riger-Kusk, K. A. Langley, G. Leitchenkov, C. Leuschen, B. P. Luyendyk, K. Matsuoka, J. Mouginot, F. O. Nitsche, Y. Nogi, O. A. Nost, S. V. Popov, E. Rignot, D. M. Rippin, A.

Rivera, J. Roberts, N. Ross, M. J. Siegert, A. M. Smith, D. Steinhage, M. Studinger, B. Sun, B. K. Tinto, B. C. Welch, D. Wilson, D. A. Young, C. Xiangbin, and A. Zirizzotti (2013), Bedmap2: improved ice bed, surface and thickness datasets for Antarctica, *The Cryosphere*, **7**, 375-393, doi: 10.5194/tc-7-375-2013.

Fricker, H. A., R. C. Warner, and I. Allison (2000), Mass balance of the Lambert Glacier-Amery Ice Shelf system, East Antarctica: a comparison of computed balance fluxes and measured fluxes, *Journal of Glaciology*, **46**(155), 561-570.

Friedt, J. –M., F. Tolle, É. Bernard, M. Griselin, D. Laffly, and C. Marlin (2012), Assessing the relevance of digital elevation models to evaluate glacier mass balance: application to Austre Lovénbreen (Spitsbergen, 79^{o}N), *Polar Record*, **48**(244), 2-10.

Gale, S. J., and P. G. Hoare (1991), *Quaternary sediments: Petrographic methods for the study of unlithified rocks*, Wiley, New York.

Gardner, A., G. Moholdt, A. Arendt, and B. Wouters (2012), Accelerated contributions of Canada's Baffin and Bylot Island glaciers to sea level rise over the past half century, *The Cryosphere*, **6**, 1103-1125.

Gardner, A. S., G. Moholdt, B. Wouters, G. J. Wolken, D. O. Burgess, M. J. Sharp, J. G. Cogley, C. Braun, and C. Labine (2011), Sharply increased mass loss from glaciers and ice caps in the Canadian Arctic Archipelago, *Nature*, **473**, 357-360, doi: 10.1038/nature10089.

Garwood, E. J., and J. W. Gregory (1898), Contribution to the glacial geology of Spitsbergen, *Quarterly Journal of the Geological Society of London*, **54**, 197-225.

Glasser, N. F., and G. H. Gudmundsson (2012), Longitudinal surface structures (flowstripes) on Antarctic glaciers, *The Cryosphere*, **6**, 383-391.

Glasser, N. F., and M. J. Hambrey (2001), Styles of sedimentation beneath Svalbard valley glaciers under changing dynamic and thermal regimes, *Journal of the Geological Society, London*, **158**, 697-707.

Glasser, N. F., and M. J. Hambrey (2002), Sedimentary facies and landform genesis at a temperate outlet glacier: Soler Glacier, North Patagonian Icefield, *Sedimentology*, **49**, 43–64.

Glasser, N. F., and T. A. Scambos (2008), A structural glaciological analysis of the 2002 Larsen B Ice Shelf collapse, *Journal of Glaciology*, **54**, 3-16.

Glasser, N. F., S. J. Coulson, I. D. Hodkinson, and N. R. Webb (2004), Photographic evidence of the return period of a Svalbard surge-type glacier: a tributary of Pedersenbreen, Kongsfjord, *Journal of Glaciology*, **50**(169), 307-308.

Glasser, N. F., M. J. Hambrey, K. R. Crawford, M. R. Bennett, and D. Huddart (1998), The structural glaciology of Kongsvegen, Svalbard, and its role in landform genesis, *Journal of Glaciology*, **44**, 136-148.

Glasser, N. F., M. J. Hambrey, L. Etienne, P. Jansson, and R. Pettersson (2003), The origin and significance of debris-charged ridges at the surface of Storglaciären, northern Sweden, *Geografiska Annaler*, **85**(A), 127-147.

Glasser, N. F., T. A. Scambos, J. Bohlander, M. Truffer, E. Pettit, and B. J. Davies (2011), From ice-shelf tributary to tidewater glacier: continued rapid recession, acceleration and thinning of Rohss Glacier following the 1995 collapse of the Prince Gustav Ice Shelf, Antarctic Peninsula, *Journal of Glaciology*, **57**, 397-406.

Glasser, N. F., S. J. A. Jennings, M. J. Hambrey, and B. Hubbard (2015), Origin and dynamic significance of longitudinal structures (“flow stripes”) in the Antarctic Ice Sheet, *Earth Surface Dynamics*, **3**, 239-249.

Glen, J. W. (1955), The creep of polycrystalline ice, *Proceedings of the Royal Society London, Series A*, **228**, 519-538.

Goldthwait, R. P. (1951), Development of end moraines in east-central Baffin Island, *Journal of Geology*, **59**, 567-577.

Gomez, B., and R. J. Small (1985), Medial moraines of the Haut Glacier d'Arolla, Valais, Switzerland: debris supply and implications for moraine formation, *Journal of Glaciology*, **31**, 303-307.

Goodsell, B., M. J. Hambrey, and N. F. Glasser (2002), Formation of band ogives and associated structures at Bas Glacier d'Arolla, Valais, Switzerland, *Journal of Glaciology*, **48**, 287-300.

Goodsell, B., M. J. Hambrey, and N. F. Glasser (2005a), Debris transport in a temperate valley glacier: Haut Glacier d'Arolla, Valais, Switzerland, *Journal of Glaciology*, **51**, 139-146.

Goodsell, B., M. J. Hambrey, N. F. Glasser, P. Nienow, and D. Mair (2005b), The structural glaciology of a temperate valley glacier: Haut Glacier d'Arolla, Valais, Switzerland, *Arctic, Antarctic and Alpine Research*, **37**, 218-232.

Google Earth (2016), Available through: http://www.google.com/earth/index.html.

Gow, A. J. (1972), Glaciological investigations of Antarctica, *Antarctic Journal of the United States*, **7**, 100-101.

Gray, M. B., and G. Mitra (1993), Migration of deformation fronts during progressive deformation: evidence from detailed structural studies in the Pennsylvania Anthracite region, USA, *Journal of Structural Geology*, **15**, 435-449.

Gudmundsson, G. H., C. F. Raymond, and R. Bindschadler (1998), The origin and longevity of flow-stripes on Antarctic ice streams, *Annals of Glaciology*, **27**, 145-152.

Gulley, J. (2009), Structural control of englacial conduits in the temperate Matanuska Glacier, Alaska, USA, *Journal of Glaciology*, **55**(192), 681-690.

Gulley, J., and D. I. Benn (2007), Structural control of englacial drainage systems in Himalayan debris-covered glaciers, *Journal of Glaciology*, **53**(182), 399-412.

Gulley, J. D., D. I. Benn, D. Muller (2009a), A cut-and-closure origin from englacial conduits in uncrevassed regions of polythermal glaciers, *Journal of Glaciology*, **55**, 66-80.

Gulley, J., D. I. Benn, L. Screaton, and J. Martin (2009b), Mechanisms of englacial conduit formation and implications for subglacial recharge, *Quaternary Science Reviews*, **28**, 1984-1999.

Hagen, J. O., and O. Liestøl (1990), Long-term glacier mass-balance investigations in Svalbard, *Annals of glaciology*, **14**, 102-106.

Hagen, J. O., O. Liestøl, E. Roland, and T. Jørgensen (1993), *Glacier atlas of Svalbard and Jan Mayen*, Oslo, Norsk Polarinstitutt.

Hagen, J. O., and A. Sætrang (1991), Radio-echo soundings of sub-polar glaciers with low-frequency radar, *Polar Research*, **9**(1), 99-107.

Haldorsen, S. (1981), Grain-size distribution of subglacial till and its relation to subglacial crushing and abrasion, *Boreas*, **10**, 91-105.

Hamberg, A. (1894), En resa til norra Ishafet sommaren 1892, *ymer*, **14**, 25-61.

Hambrey, M. J. (1975), The origin of foliation in glaciers: evidence from some Norwegian examples, *Journal of Glaciology*, **14**, 181-185.

Hambrey, M. J. (1976a), Debris, bubble and crystal fabric characteristics of foliated glacier ice, Charles Rabots Bre, Okstindan, Norway, *Arctic and Alpine Research*, **8**, 49-60.

Hambrey, M. J. (1976b), Structure of the glacier Charles Rabots Bre, Norway, *Geological Society of America Bulletin*, **87**, 1629-1637.

Hambrey, M. J. (1977a), Foliation, minor folds and strain in glacier ice, *Tectonophysics*, **39**, 397-416.

Hambrey, M. J. (1977b), Supraglacial drainage and its relationship to structure with particular reference to Charles Rabots Bre, Okstindan, Norway, *Norsk Geogrrafisk Tidsskrift*, **31**, 69-77.

Hambrey, M. J. (1991), Structure and dynamics of the Lambert Glacier-Amery Ice Shelf system: implications for the origin of Prydz Bay sediments, in *Proceedings of the Ocean Drilling Program, Sci. Results,* edited by Barron, J., Larsen, B. et al., Vol. 119, College Station, Texas, pp. 61-76.

Hambrey, M. J. (1994), *Glacial Environments*, UCL Press, London.

Hambrey, M. J., and J. A. Dowdeswell (1994), Flow regime of the Lambert Glacier-Amery Ice Shelf system, Antarctica: structural evidence from Landsat imagery, *Annals of Glaciology*, **20**, 401-406.

Hambrey, M. J., and J. A. Dowdeswell (1997), Structural evolution of a surge-type polythermal glacier: Hessbreen, Svalbard, *Annals of Glaciology*, **24**, 375-381.

Hambrey, M. J., and N. F. Glasser (2003), The role of folding and foliation development in the genesis of medial moraines: examples from Svalbard Glaciers, *Journal of Geology*, **111**, 471-485.

Hambrey, M. J., and W. Lawson (2000), Structural styles and deformation fields in glaciers: a review, in *Deformation of Glacial Materials*, edited by A. J. Maltman, B. Hubbard, and M. J. Hambrey, Geological Society London Special Publications, **176**, 59-83.

Hambrey, M. J., and B. McKelvey (2000), Major Neogene fluctuations of the East Antarctic ice sheet: Stratigraphic evidence from the Lambert Glacier region, *Geology*, **28**, 887-890.

Hambrey, M. J., and A. G. Milnes (1975), Boudinage in glacier ice – some examples, *Journal of Glaciology*, **14**, 383-393.

Hambrey, M. J., and A. G. Milnes (1977), Structural geology of an Alpine glacier (Griesgletscher, Valais, Switzerland), *Eclogae Geologicae Helvetia*, **70**, 667-684.

Hambrey, M. J., and F. Müller (1978), Structures and ice deformation in the White Glacier, Axel Heiberg Island, North West Territories, Canada, *Journal of Glaciology*, **20**, 41-66.

Hambrey, M. J., A. G. Milnes, and H. Siegenthaler (1980), Dynamics and structure of Griesgletscher, Switzerland, *Journal of Glaciology,* **25**, 215-228.

Hambrey, M. J., J. A. Dowdeswell, T. Murray, and P. R. Porter (1996), Thrusting and debris-entraient in a surging glacier, Bakaninbreen, Svalbard, *Annals of Glaciology*, **22**, 241-248.

Hambrey, M. J., D. Huddart, M. R. Bennett, and N. F. Glasser (1997), Genesis of 'hummocky moraines' by thrusting in glacier ice: evidence from Svalbard and Britain, *Journal of the Geological Society, London*, **154**, 623-632.

Hambrey, M. J., M. R. Bennett, J. A. Dowdeswell, N. F. Glasser, and D. Huddart (1999), Debris entrainment and transfer in polythermal valley glaciers, *Journal of Glaciology*, **45**, 69-86.

Hambrey, M. J., T. Murray, N. F. Glasser, A. Hubbard, B. Hubbard, G. Stuart, S. Hansen, and J. Kohler (2005), Structure and changing dynamics of a polythermal valley glacier on a centennial timescale: Midre Lovénbreen, Svalbard, *Journal of Geophysical Research*, **110**, R01006, doi: 10.1029/2004JR000128.

Hambrey, M. J., D. J. Quincey, N. F. Glasser, J. M. Reynolds, S. J. Richardson, and S. Clemmens (2008), Sedimentological, geomorphological and dynamic context of debris-mantled glaciers, Mount Everest (Sagarmatha) region, Nepal, *Quaternary Science Reviews*, **27**, 2361-2389.

Hansen, S. (2003), From surge-type to non-surge type glacier behaviour: Midre Lovenbreen, Svalbard, *Annals of Glaciology*, **36**, 97-102.

Harland, W. B. (1997), *The Geology of Svalbard*, Geological Society, Memoirs, **17,** London.

Harper, J. T., N. F. Humphreys, and W. T. Pfeffer (1998), Crevasse patterns and the strain-rate tensor: a high-resolution comparison, *Journal of Glaciology*, **44**, 68-76.

Herbst, P., and F. Neubauer (2000), The Pasterze glacier, Austria: an analogue of an extensional allochthon, in *Deformation of Glacial Materials*, edited by A. J. Maltman, B. Hubbard, and M. J. Hambrey, Geological Society London Special Publications, **176**, 159-168.

Herbst, P., F. Neubauer, and M. P. J. Schöpfer (2006), The development of brittle structures in an alpine valley glacier: Pasterzenkees, Austria, 1887-1997, *Journal of Glaciology*, **52**, 128-136.

Herzfeld, U. C., G. K. C. Clarke, H. Mayer, and R. Greve (2004), Derivation of deformation characteristics in fast-moving glaciers, *Computers and Geosciences*, **30**, 291-302.

Hobbs, B. E., W. D. Means, and P. F. Williams (1976), *An Outline of Structural Geology*, John Wiley and Sons, Chichester.

Hodson, A. J., M. Tranter, J. A. Dowdeswell, A. M. Gurnell, and J. O. Hagen (1997), Glacier thermal regime and suspended-sediment yield: A comparison of two high-Arctic glaciers, *Annals of Glaciology*, **24**, 32-37.

Hoey, T. (2004), The size of sedimentary particles, in *A practical guide to the study of glacial sediments*, edited by D. J. A. Evans, and D. I. Benn, Hodder Education, London.

Hooke, R. LeB., and P. Hudleston (1978), Origin of foliation in glaciers, *Journal of Glaciology*, **20**, 285-299.

Hooke, R. LeB., and N. R. Iverson (1995), Grain-size distribution in deforming subglacial tills: Role of grain fracture, *Geology*, **23**, 57-60.

Hubbard, A., H. Blatter, P. Nienow, D. Mair, and B. Hubbard (1998) Comparison of a three-dimensional model for glacier flow with field data at Haut Glacier d'Arolla, Switzerland, *Journal of Glaciology*, **44**, 368-378.

Hubbard, B., and N. Glasser (2005), *Field techniques in glaciology and glacial geomorphology*, John Wiley and Sons Ltd, Chichester.

Hubbard, B., and M. Sharp (1989), Basal ice formation and deformation: a review, *Progress in Physical Geography*, **13**, 529-558.

Hubbard, B., and M. J. Sharp (1993), Weertman regelation, multiple refreezing effects and the isotopic evolution of the basal ice layer, *Journal of Glaciology*, **39**, 275-291.

Hubbard, B., and M. Sharp (1995), Basal ice facies and their formation in the western Alps, *Arctic and Alpine Research*, **27**(4), 301-310.

Hubbard, B., N. F. Glasser, M. J. Hambrey, and J. Etienne (2004), A sedimentological and isotopic study of the origin of supraglacial debris bands: Kongsfjorden, Svalbard, *Journal of Glaciology*, **50**, 157-170.

Hubbard, B., N. Glasser, M. Hambrey, and J. Etienne (2004), A sedimentological and isotopic investigation of the origin of supraglacial debris bands: Kongsfjorden, Svalbard, *Journal of Glaciology,* **50**, 157-170.

Hubbard, B., S. Cook, and H. Coulson (2009), Basal ice facies: a review and unifying approach, *Quaternary Science Reviews*, **28**, 1956-1969.

Hudleston, P. J. (1976), Recumbent folding in the base of the Barnes Ice Cap, Baffin Island, Northwest Territories, Canada, *Geological Society of America Bulletin*, **87**(12), 1684-1692.

Hudleston, P. J. (1977), Progressive deformation and development of fabrics across zones of shear in glacier ice, in *Energetics of Geological Processes*, edited by S. Saxena, and S. Bhattacharji, Springer-Verlag, New York.

Hudleston, P. J. (1983), Strain patterns in an ice cap and implications for strain variations in shear zones, *Journal of Structural Geology*, **5**, 455-463.

Hudleston, P. J. (1989), The association of folds and veins in shear zones, *Journal of Structural Geology*, **11**, 949-957.

Hudleston, P. J. (1992), A comparison between glacial movement and thrust sheet or nappe emplacement and associated structures, in *Structural Geology of Fold and Thrust Belts*, edited by S. Mitra, G. W. Fisher, O. M. Phillips, S. M. Stanley, and D. F. Strobel, John Hopkins University Press, Baltimore, MD, USA.

Hudleston, P. J. (2015), Structures and fabrics in glacier ice: A review, *Journal of Structural Geology*, **81**, 1-27.

Hudleston, P. J., and R. LeB. Hooke (1980), Cumulative deformation in the Barnes Ice Cap, and implications for the development of foliation, *Tectonophysics*, **66**, 127-146.

Hughes, T. (1998), *Ice Sheets*, Oxford University Press, New York.

Hulbe, C. L., and M. A. Fahnestock (2004), West Antarctic ice-stream discharge variability: mechanism, controls and pattern of grounding-line retreat, *Journal of Glaciology*, **50**, 471-484.

Hulbe, C. L., and M. A. Fahnestock (2007), Century-scale discharge stagnation and reactivation of the Ross ice streams, West Antarctica, *Journal of Geophysical Research*, **112**, F03S27, doi: 10.1029/2006JF000603.

Hulbe, C. L., and I. M. Whillans (1997), Weak bands within Ice Stream B, West Antarctica, *Journal of Glaciology*, **43**, 377–386.

Irvine-Fynn, T. D. L., B. J. Moorman, J. L. M. Williams, and R. S. A. Walter (2006), Seasonal changes in ground-penetrating radar signature observed at a polythermal glacier, Bylot Island, Canada, *Earth Surface Processes and Landforms*, **31**, 892-909.

Jacobel, R. W., T. A. Scambos, and C. R. Raymond (1996), Changes in the configuration of ice stream flow from the West Antarctic Ice Sheet, *Journal of Geophysical Research*, **101**(B3), 5499-5504.

James, T. D., T. Murray, N. E. Barrand, and S. L. Barr (2006), Extracting photogrammetric ground control from lidar DEMs for change detection, *The Photogrammetric Record*, **21**(116), 312-328.

Jenkins, A., P. Dutriux, S. S. Jocobs, S. D. McPhail, J. R. Perrett, A. T. Webb, and D. White (2010), Observations beneath Pine Island Glacier in West Antarctica and implications for its retreat, *Nature Geoscience*, **3**, 468-472.

Jennings, S. J. A., M. J. Hambrey, and N. F. Glasser (2014), Ice flow-unit influence on glacier structure, debris entrainment and transport, *Earth Surface Processes and Landforms*, doi: 10.1002/esp.3521.

Jennings, S. J. A., M. J. Hambrey, N. F. Glasser, T. D. James, and B. Hubbard (2015), A structural glaciological map of Austre Brøggerbreen, northwest Svalbard, *Journal of Maps*, doi: 10.1080/17445647.2015.1076744.

Jezek, K. C. (1999), Glaciological properties of the Antarctic ice sheet from RADARSAT-1 synthetic aperture radar imagery, *Annals of Glaciology*, **29**(1), 286-290.

Jiskoot, H., T. Murray, and P. J. Boyle (2000), Controls on the distribution of surge-type glaciers in Svalbard, *Journal of Glaciology*, **46**, 412-422.

Johnson, J. V., J. W. Staiger (2007), Modeling long-term stability of the Ferrar Glacier, East Antarctica: Implications for interpreting cosmogenic nuclide inheritance, *Journal of Geophysical Research*, **112**, R03S30, doi: 10.1029/2006JF000599.

Joughin, I., J. L Bamber (2005), Thickening of the ice stream catchments feeding the Filchner-Ronne Ice Shelf, Antarctica, *Geophysical Research Letters*, **32**, L17503, doi: 10.1029/2005GL023844.

Kamb, B., C. F. Raymond, W. D. Harrison, H. Engelhardt, K. A. Echelmeyer, N. Humphrey, M. M. Brugman, and T. Pfeffer (1985), Glacier surge mechanism: 1982-1983 surge of Variegated Glacier, Alaska, *Science*, **227**, 469-479.

Kamb, W. B. (1959), Ice petrofabric observations from Blue Glacier, Washington, in relation to theory and experiment, *Journal of Geophysical Research*, **64**, 1891-1909.

Kehle, R. O. (1964), Deformation of the Ross Ice Shelf, Antarctica, *Geological Society of America Bulletin*, **75**, 259-286.

King, E. C., A. M. Smith, T. Murray, and G. W. Stuart (2008), Glacier-bed characteristics of midtre Lovénbreen, Svalbard, from high-resolution seismic and radar surveying, *Journal of Glaciology*, **54**(184), 145-156.

King, O., M. J. Hambrey, T. D. L. Irvine-Fynn, and T. O. Holt (2015), The structural, geometric and volumetric changes of a polythermal Arctic glacier during a surge cycle: Comfortlessbreen, Svalbard, *Earth Surface Processes and Landforms*, doi: 10.1002/esp.3796.

Kirkbride, M. P. (1995), Processes of transportation, in *Modern Glacial Environments: Processes, Dynamics and Sediments. Volume 1. Glacial Environments*, edited by J. Menzies, Butterworth-Heinemann, Oxford.

Klassen, R. A. (1993), Quaternary geology and glacial history of Bylot Island, Northwest Territories, *Geological Survey of Canada, Memoir*, 429-493.

Knight, P. G. (1994), Two-facies interpretation of the basal ice layer of the Greenland ice sheet contributes to a unified model of basal ice formation, *Geology*, **22**, 971-974.

Knight, P. G. (1997), The basal ice layer of glaciers and ice sheets, *Quaternary Science Reviews*, **16**, 975-993.

Kozarski, S., and J. Szupryczynski (1973), Glacial forms and deposits in the Sidujökull deglaciation area, *Geographia Polonica*, **26**, 255-311.

Lawson, D. E., J. C. Strasser, E. B. Evenson, R. B. Alley, and G. J. Larson (1998), Glaciohydraulic supercooling: a freeze-on mechanism to create stratified, debris-rich basal ice: I. Field evidence, *Journal of Glaciology*, **44**, 547-562.

Lawson, W. (1990), *The structural evolution of variegated Glacier, Alaska*, PhD thesis, University of Cambridge, Cambridge.

Lawson, W. (1996), Structural evolution of Variegated Glacier, Alaska, USA, since 1948, *Journal of Glaciology*, **42**, 261-270.

Lawson, W. J., M. J. Sharp, and M. J. Hambrey (1994), The structural geology of a surge-type glacier, *Journal of Structural Geology*, **16**, 1447-1462.

Lawson, W., M. J., Sharp, and M. J. Hambrey (2000), Deformation histories and structural assemblages of glacier ice in a non-steady flow regime, in *Deformation of Glacial Materials*, edited by A. J. Maltman, B. Hubbard, and M. J. Hambrey, Geological Society London Special Publications, **176**, 85-96.

Le Brocq, A. M., N. Ross, J. A. Griggs, R. G. Bingham, H. F. J. Corr, F. Ferraccioli, A. Jenkins, T. A. Jordan, A. J. Payne, D. M. Rippin, and M. J. Siegert (2013), Evidence from ice shelves for channelized meltwater flow beneath the Antarctic Ice Sheet, *Nature Geoscience*, **6**, 945-948.

Lefauconnier, B., and J. O. Hagen (1990), Glaciers and climate in Svalbard: statistical analysis and reconstruction of the Brøgger Glacier mass balance for the last 77 years, *Annals of Glaciology*, **14**, 148-152.

Lenaerts, J. T. M., J. H. van Angelen, M. R. van den Broeke, A. S. Gardner, B. Wouters, and E. van Meijgaard (2013), Irreversible mass loss of Canadian Arctic Archipelago glaciers, *Geophysical Research Letters*, **40**, 870-874.

Lewis, W. V. (1960), *Norwegian cirque glaciers*, Royal Geographical Society Research Series, No. 4.

Liestøl, O. (1988), The glaciers in the Kongsfjorden area, western spitsbergen Svalbard, *Norsk Geografisk Tidsskrift*, **42**, 231-238.

Lovell, H., E. J. Fleming, D. I. Benn, B. Hubbard, S. Lukas, B. R. Rea, R. Noormets, and A. E. Flink (2015), Debris entrainment and landform genesis during tidewater glacier surges, *Journal of Geophysical Research: Earth Surface*, **120**, 1574-1595, doi: 10.1002/2015JF003509.

Lythe, M. B., D. G. Vaughan, and the BEDMAP Consortium (2001), BEDMAP: a new thickness and subglacial topographic model of Antarctica, *Journal of Geophysical Research*, **106**(B6), 11335-11351.

Marmo, B. A., and C. J. L. Wilson (2000), The stress distribution related to the boudinage of a visco-elastic material: examples from a polar outlet glacier, in *Deformation of Glacial Materials*, edited by A. J. Maltman, B. Hubbard, M. J. Hambrey, *Geological Society London Special Publications*, **176**, 115-134.

Martín, C., G. H. Gudmundsson, and E. C. King (2014), Modelling of Kealey Ice Rise, Antarctica, reveals stable ice-flow conditions in East Ellsworth Land over millennia, *Journal of Glaciology*, **60**, 139-146.

Matthews, M. D. (1991), The effect of grain shape and density on size measurement, in *Principles, Methods, and Application of Particle Size Analysis*, edited by J. P. M. Syvitski, Cambridge, CUP, 22-33.

McManus, J. (1988), Grain size determination and interpretation, in *Techniques in sedimentology*, edited by M. Tucker, Blackwell Scientific, Oxford.

Meier, M. F. (1958), The mechanics of crevasse formation, *IASH Publication*, **46** (Symposium at Toronto 1957 – Snow and Ice), 500-508.

Meier, M. F. (1960), *Mode of flow of Saskatchewan Glacier, Alberta*, Canada, US Geological Survey Professional Paper, **351**.

Meier, M. F., and A. Post (1969), What are glacier surges? *Canadian Journal of Earth Sciences*, **6**, 807-817.

Merry, C. J., and I. M. Whillans (1993), Ice-flow features on Ice Stream B, Antarctica, revealed by SPOT HRV imagery, *Journal of Glaciology*, **39**, 515-527.

Mickelson, D. M., and J. M. Berkson (1974), Till ridges presently forming above and below sea level in Wachusett Inlet, Glacier Bay, Alaska, *Geografiska Annaler*, **56**(A), 111-119.

Midgley, N. G., S. J. Cook, D. J. Graham, and T. N. Tonkin (2013), Origin, evolution and dynamic context of a Neoglacial lateral-frontal moraine at Austre Lovénbreen, Svalbard, *Geomorphology*, **198**, 96-106.

Millgate, T., P. R. Holland, A. Jenkins, and H. L. Johnson (2013), The effect of basal channels on oceanic ice-shelf melting, *Journal of Geophysical Research: Oceans*, **118**, 1-14.

Milnes, A. G., and M. J. Hambrey (1976), A method of determining approximate cumulative strains in glacier ice, *Tectonophysics,* **34**, 23-27.

Moore, P. L. (2014), Deformation of debris-ice mixtures, *Reviews in Geophysics*, **52**, 435–467, doi: 10.1002/2014RG000453.

Moore, P. L., N. R. Iverson, and D. Cohen (2010), Conditions for thrust faulting in a glacier, *Journal of Geophysical Research*, **115**, F02005, doi: 10.1029/2009JF001307.

Murray, T., D. L. Gooch, G. W. Stuart (1997), Structures within the surge front at Bakaninbreen, Svalbard, using ground-penetrating radar, *Annals of Glaciology*, **24**, 122-129.

Murray, T., G. W. Stuart, P. J. Miller, J. Woodward, A. M. Smith, P. R. Porter, and H. Jiskoot (2000), Glacier surge propagation by thermal evolution at the bed, *Journal of Geophysical Research*, **105**, 13491-13507.

Nath, P. C., and D. G. Vaughan (2003), Subsurface crevasse formation in glaciers and ice sheets, *Journal of Geophysical Research*, **108**(B1), doi: 10.1029/2001JB000453.

Ng, F., and E. C. King (2013), Formation of RADARSAT backscatter feature and undulating firn stratigraphy at an ice-stream margin, *Annals of Glaciology*, **54**, 90-96.

Nye, J. F. (1952), The mechanics of glacier flow, *Journal of Glaciology*, **2**, 82-93.

Nye, J. F. (1953), The flow law of ice from measurements in glacier tunnels, laboratory experiments, and the Jungfraufirn borehole experiment, *Proceedings of the Royal Society of London*, **219A**, 477-489.

Nye, J. F. (1955), Comments on Dr. Loewe's letter and notes on crevasses, *Journal of Glaciology*, **2**, 512-514.

Nye, J. F. (1957), The distribution of stress and velocity in glaciers and ice sheets, *Proceedings of the Royal Society London*, **239A**, 113-133.

Nye, J. F. (1958), A theory of wave formation in glaciers (Cambridge Austerdalsbre Expedition), *International Association of Scientific Hydrology Publication* **47** (Symposium at Chamonix 1958 – Physics of the Movement of Ice), 139-154.

Nye, J. F. (1959), The deformation of a glacier below an ice fall, *Journal of Glaciology*, **3**, 387-408.

O'Brien, P. E., A. K. Cooper, C. Richter, et al. (2001), *Proceedings of the Ocean Drilling Program, Initial reports*, Volume 188, available at: http://www.odp.tamu.edu/publications/188_IR/188ir.htm.

Oerlemans, J., R. H. Giesen, and M. R. Van Den Broeke (2009), Retreating alpine glaciers: increased melt rates due to accumulation of dust (Vadret da Morteratsch, Switzerland), *Journal of Glaciology*, **55**, 729-736.

Passchier, C. W., and E. Druguet (2002), Numerical modelling of asymmetric boudinage, *Journal of Structural Geology*, **24**, 1789-1803.

Pfeffer, W. T. (1992), Stress-induced foliation in the terminus of the Variegated glacier, USA, formed during the 1982-83 surge, *Journal of Glaciology*, **38**, 213-222.

Phillips, E., A. Finlayson, T. Bradwell, J. Everest, and L. Jones (2014), Structural evolution triggers a dynamic reduction in active glacier length during rapid retreat: Evidence from Falljökull, SE Iceland, *Journal of Geophysical Research: Earth Surface*, **119**, doi: 10.1002/2014JF003165.

Phillips, H. A. (1999), Applications of ERS satellite radar altimetry in the Lambert Glacier-Amery Ice Shelf system, East Antarctica, Ph.D. thesis, University of Tasmania, Tasmania.

Post, A. (1972), Periodic surge origin of folded medial moraines on Bering Piedmont glacier, Alaska, *Journal of Glaciology*, **11**, 219-226.

Post, A., and E. R. LaChapelle (1971), *Glacier Ice*, The Mountaineers and University of Washington Press, Seattle.

Ragan, D. M. (1969), Structures at the base of an icefall, *Journal of Geology*, **77**, 647-667.

Ramsay, J. G. (1967), *Folding and fracturing of rocks*, McGraw-Hill, New York.

Raup, B. H., T. A. Scambos, and T. Haran (2005), Topography of streak-lines on an Antarctic ice shelf from photoclinometry applied to a single Advanced Land Imager (ALI) image, *IEEE Transactions on Geoscience and Remote Sensing*, **43**, 736-742.

Raymond, C. F. (1996), Shear margins in glaciers and ice sheets, *Journal of Glaciology*, **42**, 90-102.

Rea, B. R., and D. J. A. Evans (2011), An assessment of surge-induced crevassing and the formation of crevasse squeeze ridges, *Journal of Geophysical Research*, **116**, F04005, doi: 10.1029/2011JF001970.

Retzlaff, R., and C. R. Bentley (1993), Timing of stagnation of Ice Stream C, West Antarctica, from short pulse radar studies of buried surface crevasses, *Journal of Glaciology*, **39**, 495-506.

Reusch, D., and T. Hughes (2003), Surface "waves" on Byrd Glacier, Antarctica, *Antarctic Science*, **15**(4), 547-555.

Reynolds, J. M. (1988), The structure of the Wordie Ice Shelf, Antarctic Peninsula, *British Antarctic Survey Bulletin*, **80**, 57-64.

Reynolds, J. M., and M. J. Hambrey (1988), The structural glaciology of George VI Ice Shelf, Antarctic Peninsula, *British Antarctic Survey Bulletin*, **79**, 79-95.

Rignot, E., and P. Kanagaratnam (2006), Changes in the velocity structure of the Greenland Ice Sheet, *Science*, **311**, 986-990.

Rignot, E., and R. H. Thomas (2002), Mass balance of polar ice sheets, *Science*, **297**(5586), 1502-1506.

Rignot, E., J. L. Bamber, M. R. Van Den Broeke, C. Davis, Y. H. Li, W. J. Van De Berg, and E. Van Meijgaard (2008), Recent Antarctic ice mass loss from radar interferometry and regional climate modelling, *Nature Geoscience*, **1**, 106-110.

Rignot, E., J. Mouginot, M. Morlighem, H. Seroussi, and B. Scheuchl (2014), Widespread, rapid grounding line retreat of Pine Island, Thwaites, Smith, and Kohler glaciers, West Antarctica, from 1992 to 2011, *Geophysical Research Letters*, **41**, 3502-3509.

Rignot, E., J. Mouginot, and B. Scheuchl (2011), Ice flow of the Antarctic Ice Sheet, *Science*, **333**, 1427-1430, doi: 10.1126/science.1208336.

Roberson, S. (2008), Structural composition and sediment transfer in a composite cirque glacier: Glacier de St. Sorlin, France, *Earth Surface Processes and Landforms*, **33**, 1931-1947.

Roberson, S., and B. Hubbard (2010), Application of borehole optical televiewing to investigating the 3-D structure of glaciers: implications for the formation of longitudinal debris ridges, midre Lovénbreen, Svalbard, *Journal of Glaciology*, **56**(195), 143-156.

Robin, G. de Q. (1974), Depth of water-filled crevasses that are closely spaced, *Journal of Glaciology*, **13**, 543.

Ross, N., M. J. Siegert, J. Woodward, A. M. Smith, H. F. J. Corr, M. J. Bentley, R. A. C. Hindmarsh, E. C. King, and A. Rivera (2011), Holocene stability of the Amundsen-Weddell ice divide, West Antarctica, *Geology*, **39**, 935-938.

Rutishauser, H. (1971), Observations on a surging glacier in East Greenland, *Journal of Glaciology*, **10**, 227-236.

Saintenoy, A., J. –M. Friedt, A. D. Booth, F. Tolle, E. Bernard, D. Laffly, C. Marlin, and M. Griselin (2013), Deriving ice thickness, glacier volume and bedrock morphology of Austre Lovénbreen (Svalbard) using GPR, *Near Surface Geophysics*, **11**(2), 211-225.

Scambos, T. A., T. M. Haran, M. A. Fahnestock, T. H. Painter, and J. A. Bohlander, MODIS-based Mosaic of Antarctica (MOA) data sets: continent-wide surface morphology and snow grain size, *Remote Sensing of the Environment*, **111**, 242-257.

Scambos, T. A., C. Hulbe, M. Fahnestock, and J. Bohlander (2000), The link between climate warming and break-up of ice shelves in the Antarctic Peninsula, *Journal of Glaciology*, **46**(154), 516-530.

Schwarzacher, N., and N. Untersteiner (1953), Zum Problem der Bänderung des Gletschereises, *Sitzungsberichte der Oesterreich Akadamie der Wissenschften Mathem-Naturio*., Klasse Abt. IIa, **162** (1-4), 111-145.

Sevestre, H., and D. I. Benn (2015), Climatic and geometric controls on the global distribution of surge-type glaciers: implications for a unifying model of surging, *Journal of Glaciology*, **61**(228), 646-662.

Sevestre, H., D. I. Benn, N. R. Hulton, and K. Bælum (2015), Thermal structure of Svalbard glaciers and implications for thermal switch models of glacier surging, *Journal of Geophysical Research: Earth Surface*, **120**, 2220-2236, doi: 10.1002/2015JF003517.

Shabtaie, S., and C. R. Bentley (1987), West Antarctic ice streams draining into the Ross Ice Shelf configuration and mass balance, *Journal of Geophysical Research*, **92**, 1311-1336.

Sharp, M. J. (1985), 'Crevasse-fill' ridges: a landform type characteristic of surging glaciers? *Geografiska Annaler*, **67**(A), 213-220.

Sharp, M. J., J. Jouzel, B. Hubbard, and W. Lawson (1994), The character, structure and origin of the basal ice layer of a surge-type glacier, *Journal of Glaciology*, **40**, 327-340.

Sharp, M. J., W. Lawson, R. S. Anderson (1988), Tectonic processes in a surge-type glacier, *Journal of Structural Geology*, **10**, 499-515.

Sharp, R. P. (1958), Malaspina Glacier, Alaska, *Geological Society of America Bulletin*, **69**, 617-646.

Shumskii, P. A. (1964), *Principles of structural glaciology*, Dover Publications Inc., New York.

Siegert, M. J., N. Ross, H. Corr, J. Kingslake, and R. Hindmarsh (2013), Late Holocene ice-flow reconfiguration in the Weddell Sea sector of West Antarctica, *Quaternary Science Reviews*, **78**, 98-107.

Small, R. J. (1987), Englacial and supraglacial sediment: transport and deposition, in *Glaciofluvial Sediment Transfer: An Alpine Perspective*, edited by A. M. Gurnell, and M. J. Clark, Wiley, Chichester.

Small, R. J., M. J. Clarke, and T. J. P. Cawse (1979), The formation of medial moraines on Alpine glaciers, *Journal of Glaciology*, **22**, 43-52.

Sollid, J. L., B. Etzelmüller, G. Vatne, and R. S. Ødeåard (1994), Glacial dynamics, material transfer and sedimentation of Erikbreen and Hannabreen, Liefdefjorden, northern Spitsbergen, *Zeitschrift für Geomorphologie, Supplementband*, **97**, 123-144.

Souchez, R. A. (1967), The formation of shear moraines: an example from south Victoria Land, Antarctica, *Journal of Glaciology*, **6**, 837-843.

Souchez, R. A. (1971), Ice-cored moraines in south-western Ellesmere Island, N.W.T., Canada, *Journal of Glaciology*, **10**, 245-254.

Souchez, R. A., and R. D. Lorrain (1987), The subglacial sediment system, in *Glaciofluvial Sediment Transfer: An Alpine Perspective*, edited by A. M Gurnell and M. J. Clark, Wiley, Chichester.

Spedding, N., and D. J. A. Evans (2002), Sediments and landforms at Kvíárjökull, southeast Iceland: a reappraisal of the glaciated valley landsystem, *Sedimentary Geology*, **149**, 21-42.

Staffelbach, T., B. Stauffer, and H. Oeschger (1988), A detailed analysis of the rapid changes in ice-core parameters during the last ice age, *Annals of Glaciology*, **10**, 167-170.

Stearns, L., and G. Hamilton (2005), A new velocity map for Byrd Glacier, East Antarctica, from sequential ASTER satellite imagery, *Annals of Glaciology*, **41**, 71-76.

Stenborg, T. (1968), Glacier drainage connected with ice structures, *Geografiska Annaler*, **50**(A), 25-53.

Stenborg, T. (1969), Studies of the internal drainage of glaciers, *Geografiska Annaler*, **51**(A), 13-41.

Stenborg, T. (1973), Some viewpoints on the internal drainage of glaciers, in *Hydrology of Glaciers*, IAHS Publication, **95**, 117-129.

Stenoien, M. D., and C. R. Bentley (2000), Pine Island Glacier, Antarctica: A study of the catchment using interferometric synthetic aperture radar measurements and radar altimetry, *Journal of Geophysical Research*, **105**(B9), 21761-21779.

Striberger, J., S. Björck, Í. Ö. Benediktsson, I. Snowball, C. B. Uvo, Ó. Ingólfsson, and K. H. Kjær (2011), Climatic control of the surge periodicity of an Icelandic outlet glacier, *Journal of Quaternary Science*, **26**(6), 561-565.

Stuart, G., T. Murray, N. Gamble, K. Hayes, and A. Hodson (2003), Characterization of englacial channels by ground-penetrating radar: An example from austre Brøggerbreen, Svalbard, *Journal of Geophysical Research: Sold Earth*, **108**(B11), doi: 10.1029/2003JB002435.

Swift, D. A., D. J. A. Evans, and A. E. Fallick (2006), Transverse englacial debris-rich ice bands at Kviarjökull, southeast Iceland, *Quaternary Science Reviews*, **25**, 1708-1718.

Swithinbank, C., K. Brunt, and J. Sievers (1988), A glaciological map of Filchner-Ronne Ice Shelf, Antarctica, *Annals of Glaciology*, **11**, 150-155.

Taylor, J., M. J. Siegert, A. J. Payne, M. J. Hambrey, P. E. O'Brien, A. K. Cooper, and G. Leitchenkov (2004), Topographic controls on post-Oligocene changes in ice-sheet dynamics, Prydz Bay region, East Antarctica, *Geology*, **32**(3), 197-200.

Tyndall, J. (1859), On the veined structure of glaciers, with observations on white seams, air bubbles and dirt bands, *Philosophical Transactions of the Royal Society of London*, **149**, 279-307.

Van der Veen, C. J. (1998a), Fracture mechanics approach to penetration of surface crevasses on glaciers, *Cold Regions Science and Technology*, **27**, 31-47.

Van der Veen, C. J. (1998b), Fracture mechanics approach to penetration of bottom crevasses on glaciers, *Cold Regions Science and Technology*, **27**, 213-223.

Vaughan, D. G. (1993), Relating the occurrence of crevasses to surface strain rates, *Journal of Glaciology*, **39**(132), 255-266.

Vaughan, D. G., H. F. J. Corr, F. Ferraccioli, N. Frearson, A. O'Hare, D. Mach, J. W. Holt, D. D. Blankenship, D. L. Morse, and D. A. Young (2006), New boundary conditions for the West Antarctic ice sheet: Subglacial topography beneath Pine Island Glacier, *Geophysical Research Letters*, **33**(9), L09501, doi: 10.1029/2005GL025588.

Venteris, E. R. (1997), Evidence for bottom crevasse formation on Columbia Glacier, Alaska, in *Calving Glaciers: Report of a Workshop, Feb. 28- March 2, 1997*, edited by C. J. van der Veen, Byrd Polar Research Centre Report No. 15. The Ohio State University, Columbus, Ohio, 181-185.

Vere, D. M., and D. I. Benn (1989), Structure and debris characteristics of medial moraines in Jotunheimen, Norway: implications for moraine classification, *Journal of Glaciology*, **35**, 276-280.

Vornberger, P. L., and I. M. Whillans (1990), Crevasse deformation and examples from Ice Stream B, Antarctica, *Journal of Glaciology*, **36**, 3-10.

Waddington, E. D. (1986), Wave ogives, *Journal of Glaciology*, **32**(112), 325-334.

Waddington, E. D., J. F. Bolzan, and R. B. Alley (2001), Potential for stratigraphic folding near ice-sheet centers, *Journal of Glaciology*, **47**(159), 639-648.

Wadham, J. L., and A. Nuttall (2002), Multiphase formation of superimposed ice during a mass-balance year at a maritime high-Arctic glacier, *Journal of Glaciology*, **48**, 545-551.

Wadham, J., J. Kohler, A. Hubbard, A. Nuttall, and D. Rippin (2006), Superimposed ice regime of a high Arctic glacier inferred using ground-penetrating radar, flow modeling, and ice cores, *Journal of Geophysical Research: Earth Surface*, **111**(F1), doi: 10.1029/2004JF000144.

Weertman, J. (1973), Can a water-filled crevasse reach the bottom surface of a glacier? *IASH Publication*, **95**, 139-145.

Wegmann, C. E. (1963), Tectonic patterns at different levels, *Geology Society of South Africa*, **Annex 66**, 1-73.

Wentworth, C. K. (1922), A scale of grade and class terms for clastic sediments, The *Journal of Geology*, **30**, 377-392.

Whillans, I. M., M. Jackson, and Y-H. Tseng (1993), Velocity pattern in a transect across Ice Stream B, Antarctica, *Journal of Glaciology*, **39**, 562-572.

Whillans, I. M., and van der Veen, C. J. (1997), The role of lateral drag in the dynamics of Ice Stream B, Antarctica, *Journal of Glaciology*, **43**, 231-237.

Williams, R. S., Jr, D. K. Hall, C. S. Benson (1991), Analysis of glacier facies using satellite techniques, *Journal of Glaciology*, **37**(125), 120-128.

Wolf, P. R., and B. A. Dewitt (2000), *Elements of photogrammetry, with applications in GIS (3rd edition)*, McGraw, New York.

Woodward, J., T. Murray, and A. McCaig (2002), Formation and reorientation of structures in the surge-type glacier Kongsvegen, Svalbard, *Journal of Quaternary Science*, **17**, 201-209.

Zawar-reza, P., S. George, B. Storey, and W. Lawson (2010), Summertime boundary layer winds over the Darwin-Hatherton glacier system, Antarctica: observed features and numerical analysis, *Antarctic Science*, **22**(6), 619-632, doi: 10.1017/S0954102010000817.

Zdanowicz, C. M., F. A. Michel, and W. W. Shilts (1996), Basal debris entrainment and transport in glaciers of southwestern Bylot Island, Canadian Arctic, *Annals of Glaciology*, **22**, 107-113.

Appendix

Jennings et al. (2014). Ice flow-unit influence on glacier structure, debris entrainment and transport.

Contribution: Lead author, undertook all data acquisition and structural mapping. Co-authors provided scientific guidance and helped improve the quality of the manuscript.

Jennings et al. (2015). Structural glaciology of Austre Brøggerbreen, northwest Svalbard.

Contribution: Lead author, undertook all data acquisition and structural mapping. Aerial photograph acquisition and processing was undertaken by TDJ. Co-authors provided scientific guidance and helped improve the quality of the manuscript.

Glasser et al. (2015). Origin and dynamic significance of longitudinal structures ("flow stripes") in the Antarctic Ice Sheet.

Contribution: Second author, undertook the majority of the data acquisition, produced all the detailed structural maps, and produced all the figures. Also provided scientific input and editing of the manuscript. Initial concept, continent-wide structural mapping, and manuscript produced by NFG.